

## 7.9 Running Coupling Constant for QCD

The  $Q^2$  behavior of the QCD coupling,  $\alpha_s(Q^2)$ , turns out to be very different to that for  $\alpha(Q^2)$ . The manipulations of the QCD graphs needed for the calculation of  $\alpha_s(Q^2)$  carries over from the discussion of  $\alpha(Q^2)$ . The final answer, (7.57), is therefore also true for  $\alpha_s(Q^2)$ , but there is a crucial difference: the coefficient of  $\log(Q^2/\mu^2)$  is not the same. To determine the coefficient, we must calculate  $I(q^2)$  in QCD. The equivalent of Fig. 7.4 is, in slightly modified symbolic notation,

$$\left[ \begin{array}{c} \text{wavy} \\ \text{line} \end{array} \right] \rightarrow \left[ \begin{array}{c} \text{wavy} \\ \text{line} \end{array} \right] \left\{ 1 - \text{loop } q\bar{q} - \text{loop } T\bar{T} - \text{loop } C\bar{T} + \dots \right\} \quad (7.58)$$

where the extra terms arise from the color self-coupling of the gluons, and where  $C$  and  $T$  stand for “Coulomb” and “transverse” gluons, respectively, see Section 6.13. In the covariant gauge, it can be shown that these QCD diagrams yield the following coefficient of  $\log(Q^2/\mu^2)$ :

$$\frac{\alpha_s(\mu^2)}{4\pi} \left( -\frac{2}{3}n_f - 5 + 16 \right), \quad (7.59)$$

in contrast to the QED coefficient of (7.57),

$$\frac{\alpha(\mu^2)}{4\pi} \left( -\frac{4}{3} \right). \quad (7.60)$$

The consecutive terms in (7.59) represent the contribution of the consecutive loops in (7.58). The first loop is familiar; the gluon can fluctuate into a virtual  $q\bar{q}$  pair, just as a photon can fluctuate into an  $e^+e^-$  pair. There is, however, one loop for each quark flavor; hence,  $- \frac{2}{3}n_f$ , where  $n_f$  is the number of flavors. The QED result, (7.57), was written for one flavor, “ $n_f$ ”  $\rightarrow 1$  (i.e., just the  $e^+e^-$  loop). However, (7.60) is consistent with the first term of (7.59) because there is a factor of 2 mismatch in the definitions of  $\alpha$  and  $\alpha_s$ , see (2.95). The relation between  $\alpha$  and  $\alpha_s$  is discussed in more detail in Sections 10.4 and 10.7. We see that the fermion loops contribute a negative coefficient. So does the loop with two transverse gluons with a coefficient  $-5$ . One can in fact prove a theorem that all these loops have to lead to the same (negative) sign because they are all related to physical cross sections for producing lepton, quark, or gluon pairs. Symbolically,

$$\text{loop} = \left| \text{process} \right|^2 \quad (7.61)$$

for leptons or quarks, and

$$\text{Diagram with three gluons} = \left| \text{Diagram with two gluons} \right|^2 \quad (7.62)$$

for the production of two transverse gluons in, for example,  $q\bar{q} \rightarrow g \rightarrow gg$ . The theorem implies that any state which can be physically produced when the propagator becomes time-like will lead to screening of the charge and hence to a negative coefficient.

How can the third loop in (7.58) violate the theorem and give a coefficient +16 in (7.59)? A clue can be found in the discussion in Section 6.13. There, we saw that the instantaneous Coulomb interaction was associated with the exchange of virtual longitudinal and scalar photons. Such photons are never produced as real physical states since the probability for producing scalar photons cancels that for producing longitudinal photons. In QCD the cancellation is more complicated. It requires the introduction of “ghost” particles to cancel the unphysical polarizations. They can contribute to loops without leading to the production of physical particles. This is how the theorem is sidestepped. The sign of the third loop is not restricted and it is found to be positive. It is not only positive, it is sufficiently large to reverse the overall sign of the coefficient of  $\log(Q^2/\mu^2)$  relative to that in QED. This is related to the fact that there are eight gluons but only three colors of quarks.

Combining (7.59) with (7.57), we obtain the QCD “running coupling constant”

$$\alpha_s(Q^2) = \frac{\alpha_s(\mu^2)}{1 + \frac{\alpha_s(\mu^2)}{12\pi}(33 - 2n_f)\log(Q^2/\mu^2)}. \quad (7.63)$$

Only in a world with more than 16 quark flavors (we are safely below this number at present energies) is the sign of the coefficient the same as in QED, see (7.57). As anticipated in Chapter 1,  $\alpha_s(Q^2)$  decreases with increasing  $Q^2$  and therefore becomes small for short-distance interactions. We say that the theory is “asymptotically free.”

One parameter,  $\mu$ , with the dimensions of mass, remains as a relic of the renormalization. From (7.63) we see that at sufficiently low  $Q^2$ , the effective coupling will become large. It is customary to denote the  $Q^2$  scale at which this happens by  $\Lambda^2$ , where

$$\Lambda^2 = \mu^2 \exp \left[ \frac{-12\pi}{(33 - 2n_f)\alpha_s(\mu^2)} \right]. \quad (7.64)$$

It then follows that (7.63) may be written

$$\alpha_s(Q^2) = \frac{12\pi}{(33 - 2n_f) \log(Q^2/\Lambda^2)} \quad (7.65)$$

For  $Q^2$  values much larger than  $\Lambda^2$ , the effective coupling is small and a perturbative description in terms of quarks and gluons interacting weakly makes sense. For  $Q^2$  of order  $\Lambda^2$ , we cannot make such a picture, since quarks and gluons will arrange themselves into strongly bound clusters, namely, hadrons. Thus, we can think of  $\Lambda$  as marking the boundary between a world of quasi-free quarks and gluons, and the world of pions, protons, and so on. The value of  $\Lambda$  is not predicted by the theory; it is a free parameter to be determined from experiment. We should expect that it is of the order of a typical hadronic mass.

In Chapters 10 and 11, we find indeed that  $\Lambda$  has a value somewhere in the range 0.1 to 0.5 GeV. Thus, for experiments with  $Q^2 = (30 \text{ GeV})^2$ , it follows from (7.65) that  $\alpha_s$  is of order 0.1. We may therefore apply QCD perturbation theory, just as we have done for QED. In the large  $Q^2$  limit, all the quark masses can be neglected, and they contribute no mass scale to QCD. Nevertheless, there is a mass scale,  $\Lambda$ , inherent in the theory which enters through renormalization.

## 7.10 Summary and Comments

We should mention that the story of infinities in field theory does not stop here. We have in particular omitted a discussion of infrared divergences which are connected with the  $Q^2 \rightarrow 0$  limit, namely, the limit of very soft photons. This discussion is postponed until Chapter 11, where it plays a crucial role in the discussion of perturbative QCD.

In this chapter, we have shown how renormalization allows us to compute the physical effects due to the presence of loops in the perturbative expansion of QED (and QCD) amplitudes. The infinities appearing in loop diagrams were a consequence of a naive definition of the electric (or color) charge in the previous chapters. After a proper reparametrization, which takes us from the bare to the physical charge, loops lead to finite and measurable effects. The calculations based on renormalization agree with experiment. The Lamb shift and the anomalous magnetic moment are dramatic illustrations. The loops “dress” the bare leptons so that they no longer appear to be simple point particles. They acquire, for instance, an anomalous magnetic moment like the truly composite neutron and proton, see Chapter 2. A complete calculation of all loops will require a reparametrization of the mass and wavefunction of the particles as well as their charge. The procedure is completely analogous to the one discussed for the charge.

# 8

## The Structure of Hadrons

In Chapters 3 through 7, we have learned how to perform quantitative calculations for the electromagnetic interactions of leptons and quarks. The same techniques will allow us to compute the color interactions of quarks and gluons. There is, however, an immediate problem: experiments to study color (strong) interactions are performed with hadrons (e.g., proton beams or secondary  $\pi$ -beams interacting with nuclear targets), not with the quarks and gluons that are described by quantum field theory. This situation is similar to that encountered in atomic physics where experiments involving complex atoms have to be interpreted through the electromagnetic interactions of the constituent electrons. This analogy reveals the problem: we need to find the “wavefunctions” that describe, for example, a proton in terms of its constituent quarks and gluons. In this chapter, we present an experimental technique that allows us to determine the quark and gluon structure of hadrons; namely the deep inelastic scattering of leptons off hadronic targets. The structure functions so obtained will be presented in Chapter 9. Finally, in Chapters 10 and 11 we reach our goal and translate these quark–gluon QCD calculations into predictions for the results of experiments involving leptons and hadrons.

The discussion will soon reveal that these structure functions are not the static quark wavefunctions introduced in Chapter 2, although they are indirectly related to them.

### 8.1 Probing a Charge Distribution with Electrons. Form Factors

“Photographing” an object by scattering an electron beam off it is a well-proved technique in physics. Suppose we want to determine the charge distribution shown in Fig. 8.1, which could, for example, be the electron cloud of an atom. The procedure is to measure the angular distribution of the scattered electrons and compare it to the (known) cross section for scattering electrons from a point charge, in the form

$$\frac{d\sigma}{d\Omega} = \left( \frac{d\sigma}{d\Omega} \right)_{\text{point}} |F(q)|^2, \quad (8.1)$$

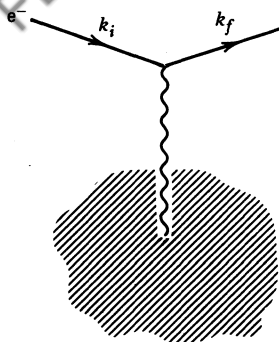


**Fig. 8.1** Lowest-order electron scattering by a charge cloud.

where  $q$  is the momentum transfer between the incident electron and the target,  $q = k_i - k_f$ , see Fig. 8.1. We then attempt to deduce the structure of the target from the form factor  $F(q)$  so determined.

We can gain insight into this technique by first looking at the scattering of unpolarized electrons of energy  $E$  from a static, spinless charge distribution  $Ze \rho(\mathbf{x})$ , normalized so that

$$\int \rho(\mathbf{x}) d^3x = 1. \quad (8.2)$$

For a static target, it is found that the form factor in (8.1) is just the Fourier transform of the charge distribution

$$F(\mathbf{q}) = \int \rho(\mathbf{x}) e^{i\mathbf{q} \cdot \mathbf{x}} d^3x, \quad (8.3)$$

while the reference cross section for a structureless target is

$$\left( \frac{d\sigma}{d\Omega} \right)_{\text{point}} \equiv \left( \frac{d\sigma}{d\Omega} \right)_{\text{Mott}} = \frac{(Z\alpha)^2 E^2}{4k^4 \sin^4 \frac{\theta}{2}} \left( 1 - v^2 \sin^2 \frac{\theta}{2} \right), \quad (8.4)$$

where  $k = |\mathbf{k}_i| = |\mathbf{k}_f|$ ,  $v = k/E$ , and  $\theta$  is the angle through which the electron is scattered.

**EXERCISE 8.1** It is useful practice of the techniques developed in the previous chapters to derive (8.3) and (8.4). We outline the various steps below. The electromagnetic field due to  $Ze \rho(\mathbf{x})$  is  $A^\mu = (\phi, \mathbf{0})$  where, using (6.59),

$$\nabla^2 \phi = -Ze \rho(\mathbf{x}).$$

Use (6.4) and (6.6) to show that the scattering amplitude is (see also Section 7.1)

$$T_{fi} = -i2\pi \delta(E_f - E_i)(-\bar{u}_f \gamma_0 u_i) \int e^{i\mathbf{q} \cdot \mathbf{x}} \phi(\mathbf{x}) d^3x. \quad (8.5)$$

Justify

$$\int e^{i\mathbf{q} \cdot \mathbf{x}} \nabla^2 \phi d^3x = -|\mathbf{q}|^2 \int e^{i\mathbf{q} \cdot \mathbf{x}} \phi d^3x$$

and hence show that the integral in (8.5) is  $Ze F(\mathbf{q})/|\mathbf{q}|^2$ , see (7.9). Following the arguments of Section 4.3, verify that the differential cross section from a fixed target is

$$d\sigma = \frac{|T_{fi}|^2}{T} \frac{d^3k_f}{(2\pi)^3 2E_f} \left( \frac{1}{v^2 2E_i} \right), \quad (8.6)$$

with

$$d^3k_f \delta(E_f - E_i) = kE d\Omega.$$

Summing final, and averaging initial, electron spins give

$$\frac{1}{2} \sum_{s_f, s_i} |\bar{u}_f \gamma_0 u_i|^2 = 4E^2 \left( 1 - v^2 \sin^2 \frac{\theta}{2} \right), \quad (8.7)$$

where  $\theta$  is the angle introduced in Section 7.1. Check this answer with (6.25). Putting all this together yields the advertised result

$$\frac{d\sigma}{d\Omega} = \left( \frac{d\sigma}{d\Omega} \right)_{\text{Mott}} |F(\mathbf{q})|^2,$$

with the form factor given by (8.3).

**EXERCISE 8.2** Show that if the electron beam is replaced by a beam of “point” spinless particles, the only change is that factor (8.7) is replaced by  $4E^2$ . This raises a question: why does the electron spin make no difference in the nonrelativistic limit,  $v \rightarrow 0$ ? The remarks following (6.13) are the clue.

**EXERCISE 8.3** By considering the electron helicity, explain why you would anticipate the  $\cos^2(\theta/2)$  behavior of factor (8.7) in the extreme relativistic limit, see Section 6.6.

By virtue of the normalization condition, (8.2),

$$F(0) \equiv 1. \quad (8.8)$$

If  $|\mathbf{q}|$  is not too large, we can expand the exponential in (8.3), giving

$$\begin{aligned} F(\mathbf{q}) &= \int \left( 1 + i\mathbf{q} \cdot \mathbf{x} - \frac{(\mathbf{q} \cdot \mathbf{x})^2}{2} + \dots \right) \rho(\mathbf{x}) d^3x \\ &= 1 - \frac{1}{6} |\mathbf{q}|^2 \langle r^2 \rangle + \dots, \end{aligned} \quad (8.9)$$

where we have assumed that  $\rho$  is spherically symmetric, that is, a function of  $r \equiv |\mathbf{x}|$  alone. The small-angle scattering therefore just measures the mean square radius  $\langle r^2 \rangle$  of the charge cloud. This is because in the small  $|\mathbf{q}|$  limit the photon in Fig. 8.1 is soft and with its large wavelength can resolve only the size of the charge distribution  $\rho(r)$  and is not sensitive to its detailed structure.

**EXERCISE 8.4** If the charge distribution  $\rho(r)$  has an exponential form,  $e^{-mr}$ , show, using (8.3), that the form factor

$$F(|\mathbf{q}|) = \left( 1 - \frac{q^2}{m^2} \right)^{-2}$$

with  $q^2 = -|\mathbf{q}|^2$ .

## 8.2 Electron-Proton Scattering. Proton Form Factors

The above discussion cannot be applied directly to yield the structure of the proton. First, the proton's magnetic moment is involved in the scattering of the electron, not just its charge. Second, the proton is not static, but will recoil under the electron's bombardment. If, however, the proton were a point charge  $e$  with a Dirac magnetic moment  $e/2M$ , then we already know the answer. We can take over the result for electron-muon scattering, (6.50), and simply replace the mass of the muon by that of the proton:

$$\frac{d\sigma}{d\Omega} \Big|_{\text{lab}} = \left( \frac{\alpha^2}{4E^2 \sin^4 \frac{\theta}{2}} \right) \frac{E'}{E} \left\{ \cos^2 \frac{\theta}{2} - \frac{q^2}{2M^2} \sin^2 \frac{\theta}{2} \right\}, \quad (8.10)$$

where the factor

$$\frac{E'}{E} = \frac{1}{1 + \frac{2E}{M} \sin^2 \frac{\theta}{2}},$$

given by (6.48), arises from the recoil of the target.

Copying the calculation of the electron-muon cross section, the lowest-order amplitude for electron-proton elastic scattering, Fig. 8.2, is given by [see (6.8)]

$$T_{fi} = -i \int j_\mu \left( -\frac{1}{q^2} \right) J^\mu d^4x,$$

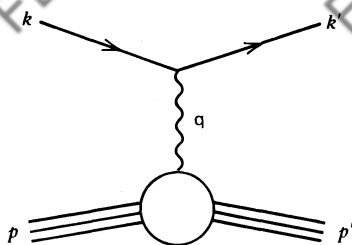


**Fig. 8.2** Lowest-order electron–proton elastic scattering.

where  $q = p' - p$  and the electron and proton transition currents are, respectively,

$$j^\mu = -e \bar{u}(k') \gamma^\mu u(k) e^{i(k'-k)\cdot x} \quad (8.11)$$

$$J^\mu = e \bar{u}(p')[ ] u(p) e^{i(p'-p)\cdot x}, \quad (8.12)$$

see (6.6). Since the proton is an extended structure, we cannot replace the square brackets in (8.12) by  $\gamma^\mu$ , as for point spin- $\frac{1}{2}$  particles in (8.11). But we know that  $J^\mu$  must be a Lorentz four-vector, and so we must use the most general four-vector form that can be constructed from  $p$ ,  $p'$ ,  $q$  and the Dirac  $\gamma$ -matrices sandwiched between  $\bar{u}$  and  $u$ . There are only two independent terms,  $\gamma^\mu$  and  $i\sigma^{\mu\nu}q_\nu$ , and their coefficients are functions of  $q^2$  ( $q^2$  is the only independent scalar variable at the proton vertex). Terms involving  $\gamma^5$  are ruled out by the conservation of parity. Therefore, quite generally, we may write the square bracket of (8.12) in the form

$$[ ] = \left[ F_1(q^2) \gamma^\mu + \frac{\kappa}{2M} F_2(q^2) i\sigma^{\mu\nu} q_\nu \right] \quad (8.13)$$

where  $F_1$  and  $F_2$  are two independent form factors and  $\kappa$  is the anomalous magnetic moment (see Exercise 6.2).

**EXERCISE 8.5** Show that current conservation,  $\partial_\mu J^\mu = 0$ , rules out  $(p - p')^\mu$  as a possible four-vector. Why do we not show a term involving  $(p + p')^\mu$  in (8.13)?

**EXERCISE 8.6** Show that  $p \cdot q$  is not an independent scalar variable by expressing it in terms of the variable  $q^2$ .

For  $q^2 \rightarrow 0$ , that is, when we probe with long-wavelength photons, it does not make any difference that the proton has structure at the order of 1 fermi. We effectively see a particle of charge  $e$  and magnetic moment  $(1 + \kappa)e/2M$ , where  $\kappa$ , the anomalous moment, is measured to be 1.79. The factors in (8.13) must therefore be chosen so that in this limit

$$F_1(0) = 1, \quad F_2(0) = 1. \quad (8.14)$$

The corresponding values for the neutron are  $F_1(0) = 0$ ,  $F_2(0) = 1$ , and experimentally  $\kappa_n = -1.91$ .

If we use (8.13) to calculate the differential cross section for electron–proton elastic scattering, we find an expression similar to (8.10):

$$\frac{d\sigma}{d\Omega} \Big|_{\text{lab}} = \left( \frac{\alpha^2}{4E^2 \sin^4 \frac{\theta}{2}} \right) \frac{E'}{E} \left\{ \left( F_1^2 - \frac{\kappa^2 q^2}{4M^2} F_2^2 \right) \cos^2 \frac{\theta}{2} - \frac{q^2}{2M^2} (F_1 + \kappa F_2)^2 \sin^2 \frac{\theta}{2} \right\}, \quad (8.15)$$

see (6.50). This is known as the Rosenbluth formula. The two form factors,  $F_{1,2}(q^2)$ , parametrize our ignorance of the detailed structure of the proton represented by the blob in Fig. 8.2. These form factors can be determined experimentally by measuring  $d\sigma/d\Omega$  as a function of  $\theta$  and  $q^2$ . Note that if the proton were a point particle like the muon, then  $\kappa = 0$  and  $F_1(q^2) = 1$  for all  $q^2$ , and (8.15) would revert to (8.10).

In practice, it is better to use linear combinations of  $F_{1,2}$ ,

$$\begin{aligned} G_E &\equiv F_1 + \frac{\kappa q^2}{4M^2} F_2 \\ G_M &\equiv F_1 + \kappa F_2, \end{aligned} \quad (8.16)$$

defined so that no interference terms,  $G_E G_M$ , occur in the cross section. Equation (8.15) becomes

$$\frac{d\sigma}{d\Omega} \Big|_{\text{lab}} = \frac{\alpha^2}{4E^2 \sin^4 \frac{\theta}{2}} \frac{E'}{E} \left( \frac{G_E^2 + \tau G_M^2}{1 + \tau} \cos^2 \frac{\theta}{2} + 2\tau G_M^2 \sin^2 \frac{\theta}{2} \right), \quad (8.17)$$

with  $\tau \equiv -q^2/4M^2$ .

Now that interference terms have disappeared, these proton form factors may be regarded as generalizations of the nonrelativistic form factor introduced in Section 8.1, and so it would be nice if we could interpret their Fourier transforms as the charge and magnetic moment distributions of the proton. Unfortunately, the recoil of the proton makes this impossible. However, it is possible to show that the form factors  $G_E(q^2)$  and  $G_M(q^2)$  are closely related to the proton charge and magnetic moment distributions, respectively, in a particular Lorentz frame, called the Breit (or brick wall) frame, defined by  $\mathbf{p}' = -\mathbf{p}$ .

**EXERCISE 8.7** Show that the proton transition current,  $J^\mu(x)$  of (8.12), can be rewritten in the form

$$J^\mu(0) = e \bar{u}(p') \left[ \gamma^\mu (F_1 + \kappa F_2) - \frac{(p^\mu + p'^\mu)}{2M} \kappa F_2 \right] u(p). \quad (8.18)$$

Evaluate  $J^\mu(0) \equiv (\rho, \mathbf{J})$  in the Breit frame ( $\mathbf{p}' = -\mathbf{p}$ ). There is no energy

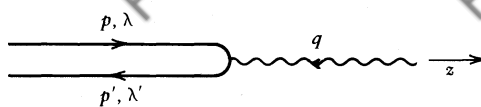


Fig. 8.3 The Breit or brick-wall frame,  $\mathbf{p}' = -\mathbf{p}$ .

transferred to the proton in this frame, and it behaves as if it had bounced off a brick wall, see Fig. 8.3. If the  $z$  axis is chosen along  $\mathbf{p}$  and helicity spinors are used, show that

$$\begin{aligned} \rho &= 2Me G_E(q^2) && \text{for } \lambda = -\lambda', \\ J_1 \pm iJ_2 &= \mp 2|\mathbf{q}|e G_M(q^2) && \text{for } \lambda = \lambda' = \mp \frac{1}{2}, \end{aligned} \quad (8.19)$$

and that all other matrix elements are zero;  $\lambda$  and  $\lambda'$  denote the initial and final proton helicities, respectively. Determine the corresponding values of the helicity of the virtual photon.

In generalizing the form factor of Section 8.1, we have replaced  $F(|\mathbf{q}|)$  by  $F(q^2)$ . However, as long as  $|\mathbf{q}|^2 \ll M^2$ , we can take over the Fourier transform interpretation of Section 8.1.

**EXERCISE 8.8** Show that for  $|\mathbf{q}|^2 \ll M^2$ , the form factors  $G_E$  and  $G_M$  are the Fourier transforms of the proton's charge and magnetic moment distributions, respectively.

$G_E$  and  $G_M$  are referred to as the electric and magnetic form factors, respectively. The data on the angular dependence of  $e\mathbf{p} \rightarrow e\mathbf{p}$  scattering can be used to separate  $G_E, G_M$  at different values of  $q^2$ , see (8.17). The result for  $G_E(q^2)$  is

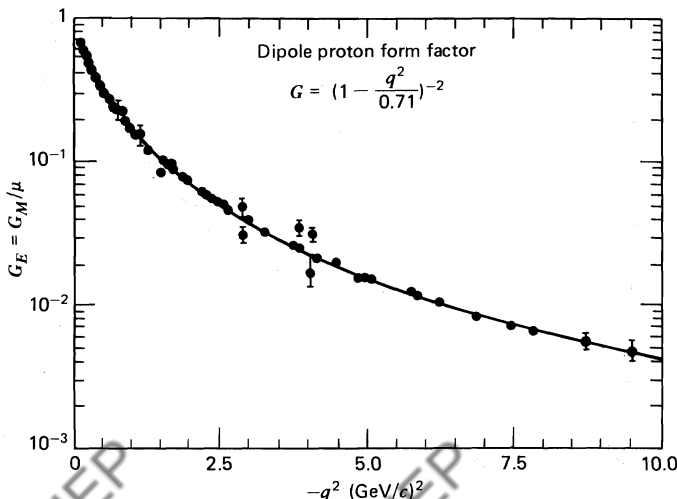


Fig. 8.4 The proton form factors as a function of  $q^2$ .

shown in Fig. 8.4.  $G_M(q^2)$  has the same  $q^2$  dependence. A closer look at Fig. 8.4 reveals that

$$G_E(q^2) \approx \left(1 - \frac{q^2}{0.71}\right)^{-2} \quad (\text{in units of } \text{GeV}^2). \quad (8.20)$$

The behavior for small  $-q^2$  can be used to determine the residual terms in the expansion of (8.9). In particular, the mean square proton charge radius is

$$\langle r^2 \rangle = 6 \left( \frac{dG_E(q^2)}{dq^2} \right)_{q^2=0} = (0.81 \times 10^{-13} \text{ cm})^2. \quad (8.21)$$

The same radius of about 0.8 fm is obtained for the magnetic moment distribution. Using the result of Exercise 8.4, we conclude that the charge distribution of the nucleon has an exponential shape in configuration space.

### 8.3 Inelastic Electron–Proton Scattering $e p \rightarrow e X$

Having measured the size of the proton, one might like to take a more detailed look at its structure by increasing the  $-q^2$  of the photon to give better spatial resolution. This can be done simply by requiring a large energy loss of the bombarding electron. There is, however, a catch: because of the large transfer of energy, the proton will often break up, and the picture of Fig. 8.2 has to be generalized to Fig. 8.5. For modest  $-q^2$ , one might just excite the proton into a  $\Delta$ -state and hence produce an extra  $\pi$ -meson, that is,  $e p \rightarrow e \Delta^+ \rightarrow e p \pi^0$ . In these events, the invariant mass (see Fig. 8.5) is  $W^2 = M_\Delta^2$ . When  $-q^2$  is very large, however, the debris becomes so messy that the initial state proton loses its identity completely and a new formalism must be devised to extract information from the measurements. Figure 8.6 shows the invariant mass distribution. One notices the peak when the proton does not break up ( $W \simeq M$ ) and broader peaks when the target is excited to resonant baryon states. Beyond the resonances, the complicated multiparticle states with large invariant mass result in a smooth distribution in missing mass  $W$ .

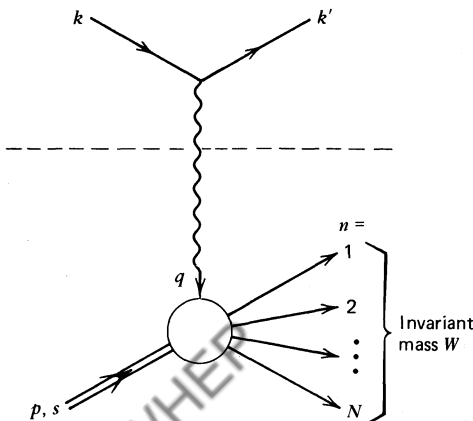
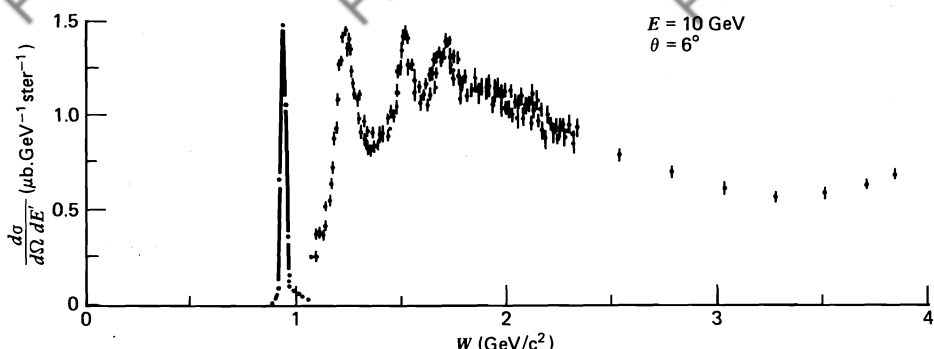


Fig. 8.5 Lowest-order diagram for  $e p \rightarrow e X$ .



**Fig. 8.6** The  $ep \rightarrow eX$  cross section as a function of the missing mass  $W$ . Data are from the Stanford Linear Accelerator. The elastic peak at  $W = M$  has been reduced by a factor of 8.5.

The problem now facing us is illustrated by recalling (8.11), (8.12), and Fig. 8.2. The switch from a muon to a proton target was made by replacing the lepton current  $j^\mu$  ( $\sim \bar{u}\gamma^\mu u$ ) by a proton current  $J^\mu$  ( $\sim \bar{u}\Gamma^\mu u$ ), and the most general form of  $\Gamma^\mu$  was constructed. This is inadequate to describe the inelastic events of Fig. 8.5. Although everything above the dashed line in Fig. 8.5 remains unchanged (a fact which we shall exploit), the final state below it is not a single fermion described by a Dirac “ $\bar{u}$ ” entry in the matrix element or current. Therefore,  $J^\mu$  must have a more complex structure than (8.12). Instead, the expression for the cross section [see (6.18)]

$$d\sigma \sim L_{\mu\nu}^e (L^p)^{\mu\nu} \quad (8.22)$$

is directly generalized to

$$d\sigma \sim L_{\mu\nu}^e W^{\mu\nu}, \quad (8.23)$$

where  $L_{\mu\nu}^e$  represents the lepton tensor of (6.20), since everything in the leptonic part of the diagram above the photon propagator in Fig. 8.5 is left unchanged. The hadronic tensor  $W^{\mu\nu}$  serves to parametrize our total ignorance of the form of the current at the other end of the propagator. The most general form of the tensor  $W^{\mu\nu}$  must now be constructed out of  $g^{\mu\nu}$  and the independent momenta  $p$  and  $q$  ( $p' = p + q$ ).  $\gamma^\mu$  is not included, as we are parametrizing the cross section which is already summed and averaged over spins. We write

$$W^{\mu\nu} = -W_1 g^{\mu\nu} + \frac{W_2}{M^2} p^\mu p^\nu + \frac{W_4}{M^2} q^\mu q^\nu + \frac{W_5}{M^2} (p^\mu q^\nu + q^\mu p^\nu). \quad (8.24)$$

We have omitted antisymmetric contributions to  $W^{\mu\nu}$ , since their contribution to the cross section vanishes after insertion into (8.23) because the tensor  $L_{\mu\nu}^e$  is symmetric. Note the omission of  $W_3$  in our notation; this spot is reserved for a parity-violating structure function when a neutrino beam is substituted for the electron beam, so that the virtual photon probe is replaced by a weak boson; see Perl (1974), Close (1979), or Llewellyn Smith (1972).

**EXERCISE 8.9** Show that indeed  $L_{\mu\nu}^e = L_{\nu\mu}^e$  and that

$$q^\mu L_{\mu\nu}^e = q^\nu L_{\mu\nu}^e = 0. \quad (8.25)$$

**EXERCISE 8.10** Show that current conservation at the hadronic vertex requires

$$q_\mu W^{\mu\nu} = q_\nu W^{\mu\nu} = 0. \quad (8.26)$$

The proof may be left until after (8.39); it follows from  $\partial_\mu \tilde{J}^\mu = 0$ . As a result of (8.26), verify that

$$W_5 = -\frac{p \cdot q}{q^2} W_2,$$

$$W_4 = \left( \frac{p \cdot q}{q^2} \right)^2 W_2 + \frac{M^2}{q^2} W_1.$$

Thus, only two of the four inelastic structure functions of (8.24) are independent; so we may write

$$W^{\mu\nu} = W_1 \left( -g^{\mu\nu} + \frac{q^\mu q^\nu}{q^2} \right) + W_2 \frac{1}{M^2} \left( p^\mu - \frac{p \cdot q}{q^2} q^\mu \right) \left( p^\nu - \frac{p \cdot q}{q^2} q^\nu \right), \quad (8.27)$$

where the  $W_i$ 's are functions of the Lorentz scalar variables that can be constructed from the four-momenta at the hadronic vertex. Unlike elastic scattering, there are two independent variables, and we choose

$$q^2 \quad \text{and} \quad \nu \equiv \frac{p \cdot q}{M}. \quad (8.28)$$

The invariant mass  $W$  of the final hadronic system is related to  $\nu$  and  $q^2$  by

$$W^2 = (p + q)^2 = M^2 + 2M\nu + q^2. \quad (8.29)$$

**EXERCISE 8.11** It is common to replace  $\nu$  and  $q^2$  by the dimensionless variables

$$x = \frac{-q^2}{2p \cdot q} = \frac{-q^2}{2M\nu}, \quad y = \frac{p \cdot q}{p \cdot k}, \quad (8.30)$$

where the four-momenta are shown on Fig. 8.5. Show that the allowed kinematic region for  $e p \rightarrow e X$  is  $0 \leq x \leq 1$  and  $0 \leq y \leq 1$ . Sketch this physical region in the  $\nu, q^2$  plane and check your answer with Fig. 9.3.

**EXERCISE 8.12** Show that in the rest frame of the target proton,

$$\nu = E - E', \quad y = \frac{E - E'}{E},$$

where  $E$  and  $E'$  are the initial and final electron energies, respectively.

Evaluation of the cross section for  $\text{ep} \rightarrow \text{eX}$  is a straightforward repetition of the same calculation for  $\text{e}^-\mu^- \rightarrow \text{e}^-\mu^-$  (or  $\text{ep} \rightarrow \text{ep}$ ) scattering with the substitution of  $W_{\mu\nu}$ , given by (8.27), for  $L_{\mu\nu}^{\text{muon}}$  (or  $L_{\mu\nu}^p$ ). Using the expression (6.25) for  $(L^e)^{\mu\nu}$  and noting (8.25), we find

$$(L^e)^{\mu\nu} W_{\mu\nu} = 4W_1(k \cdot k') + \frac{2W_2}{M^2} [2(p \cdot k)(p \cdot k') - M^2 k \cdot k']. \quad (8.31)$$

In the laboratory frame, this becomes

$$(L^e)^{\mu\nu} W_{\mu\nu} = 4EE' \left\{ \cos^2 \frac{\theta}{2} W_2(\nu, q^2) + \sin^2 \frac{\theta}{2} 2W_1(\nu, q^2) \right\}, \quad (8.32)$$

see (6.44). By including the flux factor, (4.32), and the phase space factor for the outgoing electron, (4.24), we can obtain the inclusive differential cross section for inelastic electron–proton scattering,  $\text{ep} \rightarrow \text{eX}$ ,

$$d\sigma = \frac{1}{4((k \cdot p)^2 - m^2 M^2)^{1/2}} \left\{ \frac{e^4}{q^4} (L^e)^{\mu\nu} W_{\mu\nu} 4\pi M \right\} \frac{d^3 k'}{2E'(2\pi)^3}, \quad (8.33)$$

where  $|\mathcal{M}|^2$  is given by the expression in the braces [recall (6.18)]. The extra factor of  $4\pi M$  arises because we have adopted the standard convention for the normalization of  $W^{\mu\nu}$ . Inserting (8.32) in (8.33) yields

$$\frac{d\sigma}{dE' d\Omega} \Big|_{\text{lab}} = \frac{\alpha^2}{4E^2 \sin^4 \frac{\theta}{2}} \left\{ W_2(\nu, q^2) \cos^2 \frac{\theta}{2} + 2W_1(\nu, q^2) \sin^2 \frac{\theta}{2} \right\},$$

(8.34)

where, as usual, we neglect the mass of the electron.

## 8.4 Summary of the Formalism for Analyzing ep Scattering

Although we have achieved our objective, it is informative to take a second look at the formalism. The final result, (8.34), may be reexpressed in the form

$$\frac{d\sigma}{dE' d\Omega} = \frac{\alpha^2}{q^4} \frac{E'}{E} (L^e)^{\mu\nu} W_{\mu\nu}, \quad (8.35)$$

see (8.32) and (6.44). For comparison, recall the cross section for  $e\mu^- \rightarrow e\mu^-$  scattering, (6.46),

$$d\sigma = \frac{1}{4ME} \frac{d^3 k'}{(2\pi)^3 2E'} \frac{d^3 p'}{(2\pi)^3 2p'_0} \left\{ \frac{e^4}{q^4} (L^e)^{\mu\nu} L_{\mu\nu}^{\text{muon}} \right\} (2\pi)^4 \delta^4(p + q - p'), \quad (8.36)$$

which can also be written in the form (8.35) with

$$W_{\mu\nu} = \frac{1}{4\pi M} \left( \frac{1}{2} \sum_s \sum_{s'} \right) \int \frac{d^3 p'}{(2\pi)^3 2p'_0} \langle p, s | \tilde{J}_\mu^\dagger | p', s' \rangle \times \langle p', s' | \tilde{J}_\nu | p, s \rangle (2\pi)^4 \delta^4(p + q - p') \quad (8.37)$$

where

$$\langle p', s' | \tilde{J}_\nu | p, s \rangle \equiv \bar{u}(s')(p') \gamma_\nu u(s)(p). \quad (8.38)$$

Insertion of (8.37) into (8.35) reproduces (6.49). All we have done is to use a particular regrouping of the factors in our earlier derivation. If we replace (8.38) by  $\bar{u}[\ ]u$  with  $[\ ]$  given by (8.13), then we can recover the result for  $ep \rightarrow ep$  scattering. The reason for all this is to note that  $W_{\mu\nu}$ , for  $ep \rightarrow eX$  is nothing but a generalization of (8.37) to the case where a proton breaks up into many particles in the final hadronic state X. It can be formally written as

$$W_{\mu\nu} = \frac{1}{4\pi M} \sum_N \left( \frac{1}{2} \sum_s \right) \int \prod_{n=1}^N \left( \frac{d^3 p'_n}{2E_n'(2\pi)^3} \right) \sum_{s_n} \langle p, s | \tilde{J}_\mu^\dagger | X \rangle \times \langle X | \tilde{J}_\nu | p, s \rangle (2\pi)^4 \delta^4(p + q - \sum_n p'_n), \quad (8.39)$$

where a sum over all possible many-particle (i.e., N particle) states X is included, see Fig. 8.5.

For future reference, it is useful to make a compendium of our results on form factors. We keep to the laboratory kinematics of Fig. 6.10 and neglect the mass of the electron. For all the reactions, the differential cross section in the energy ( $E'$ ) and angle ( $\theta$ ) of the scattered electron can be written in the form

$$\frac{d\sigma}{dE' d\Omega} = \frac{4\alpha^2 E'^2}{q^4} \left\{ \dots \right\}. \quad (8.40)$$

First, for a muon target of mass  $m$  (or a quark target of mass  $m$  after substitution  $\alpha^2 \rightarrow \alpha^2 e_q^2$  where  $e_q$  is the quark's fractional charge),

$$\{ \quad \}_{e\mu \rightarrow e\mu} = \left( \cos^2 \frac{\theta}{2} - \frac{q^2}{2m^2} \sin^2 \frac{\theta}{2} \right) \delta \left( \nu + \frac{q^2}{2m} \right). \quad (8.41)$$

For elastic scattering from a proton target,

$$\{ \quad \}_{ep \rightarrow ep} = \left( \frac{G_E^2 + \tau G_M^2}{1 + \tau} \cos^2 \frac{\theta}{2} + 2\tau G_M^2 \sin^2 \frac{\theta}{2} \right) \delta \left( \nu + \frac{q^2}{2M} \right), \quad (8.42)$$

where  $\tau = -q^2/4M^2$  and  $M$  is the mass of the proton. Finally, for the case when the proton target is broken up by the bombarding electron,

$$\{ \quad \}_{ep \rightarrow eX} = W_2(\nu, q^2) \cos^2 \frac{\theta}{2} + 2W_1(\nu, q^2) \sin^2 \frac{\theta}{2}. \quad (8.43)$$

Making use of the delta function, (8.41) and (8.42) can be integrated over  $E'$  with the result [see (6.50)]

$$\frac{d\sigma}{d\Omega} = \frac{\alpha^2}{4E^2 \sin^4 \frac{\theta}{2}} \frac{E'}{E} ( \quad ). \quad (8.44)$$

**EXERCISE 8.13** The above results assume (lowest-order) single photon exchange is dominant. If two-photon exchange were significant, convince yourself that the  $e^- p$  and  $e^+ p$  cross sections would not be equal.

## 8.5 Inelastic Electron Scattering as a (Virtual) Photon–Proton Total Cross Section

It is clear from the above discussion that the important issue is what happens below the dashed line in Fig. 8.5, where a (virtual) photon interacts with a proton. The role of the electron beam is simply that it is responsible for the presence of the virtual photon. It is useful to display these facts in our formalism. We start by writing the total cross section for scattering a *real* photon, with energy  $q^0 = \nu \equiv K$  and (transverse) polarization  $\epsilon$ , off the same unpolarized proton target producing two or more final-state particles. Using the Feynman rules and cross section kinematics which we have developed, we obtain

$$\begin{aligned} \sigma^{\text{tot}}(\gamma p \rightarrow X) &= \frac{1}{(2K)(2M)} \sum_N \left( \frac{1}{2} \sum_s \right) \int \prod_{n=1}^N \left( \frac{d^3 p'_n}{2E'_n (2\pi)^3} \right) \\ &\times \sum_{s_n} (2\pi)^4 \delta^4 \left( p + q - \sum_n p'_n \right) \epsilon^{\mu*} \epsilon^\nu e^2 \langle p, s | \tilde{J}_\mu^\dagger | X \rangle \langle X | \tilde{J}_\nu | p, s \rangle, \end{aligned} \quad (8.45)$$

where, as before, a sum over all final states  $X$  is included. If  $W$  is the invariant mass of the final state, then

$$W^2 = (p + q)^2 = M^2 + 2MK. \quad (8.46)$$

We immediately note the striking similarity between (8.45) and the formal expression for  $W_{\mu\nu}$  given by (8.39). Indeed, (8.45) appears to be simply

$$\sigma^{\text{tot}}(\gamma p \rightarrow X) = \frac{4\pi^2\alpha}{K} \epsilon^{\mu*} \epsilon^\nu W_{\mu\nu}. \quad (8.47)$$

However, there is a crucial proviso: for real photons, we must sum only over the two transverse polarizations of the incident photon. On the other hand, to interpret the  $\gamma p \rightarrow eX$  hadronic tensor  $W_{\mu\nu}$  as a photon–proton total cross section, it is vital to remember that the photon is *virtual* and not limited to two polarization states. In fact, the cross section for virtual photons is not a well-defined concept. When  $q^2 = 0$ , the flux factor is the  $4MK$  with  $K = \nu$ ; but for virtual photons ( $q^2 \neq 0$ ), the flux is arbitrary. The conventional choice is to require  $K$  to continue to satisfy (8.46), that is,

$$K = \frac{W^2 - M^2}{2M} = \nu + \frac{q^2}{2M}, \quad (8.48)$$

in the laboratory frame. This is known as the Hand convention. Another possible choice is  $K = |\mathbf{q}|$ .

To complete the interpretation of the structure functions, we must specify the polarization vectors  $\epsilon_\lambda^\mu$  of virtual photons (helicity  $\lambda$ ). We take the  $z$  axis along  $\mathbf{q}$  and use [see (6.92); a further discussion is given in Budner et al. Phys. Rep. C15, 181 (1975)]

$$\lambda = \pm 1: \epsilon_\pm = \mp \sqrt{\tfrac{1}{2}} (0; 1, \pm i, 0), \quad (8.49)$$

$$\lambda = 0: \epsilon_0 = \frac{1}{\sqrt{-q^2}} (\sqrt{\nu^2 - q^2}; 0, 0, \nu). \quad (8.50)$$

**EXERCISE 8.14** Verify that  $\mathbf{q} \cdot \boldsymbol{\epsilon} = 0$  for each  $\lambda$ , and show that, for a spacelike photon ( $q^2 < 0$ ),

$$\sum (-1)^{\lambda+1} \epsilon^{\mu*} \epsilon^\nu = -g^{\mu\nu} + \frac{q^\mu q^\nu}{q^2}, \quad (8.51)$$

where the sum runs over the three polarization states of (8.49) and (8.50).

For  $q^2 > 0$  the factor  $(-1)^{\lambda+1}$  is omitted and the sum (8.51) with  $q^2$  replaced by  $M^2$  is identical to that over the spin states of a massive vector particle, see Section 6.12. see Section 6.12.

We can now evaluate the total cross sections for polarized photons (helicity  $\lambda$ ) interacting with unpolarized protons:

$$\sigma_\lambda^{\text{tot}} = \frac{4\pi^2\alpha}{K} \epsilon_\lambda^{\mu*} \epsilon_\lambda^\nu W_{\mu\nu}. \quad (8.52)$$

Using (8.24) for  $W_{\mu\nu}$ , together with the above polarization vectors, we find that the transverse and longitudinal cross sections are, respectively,

$$\sigma_T \equiv \frac{1}{2} (\sigma_+^{\text{tot}} + \sigma_-^{\text{tot}}) = \frac{4\pi^2\alpha}{K} W_1(\nu, q^2) \quad (8.53)$$

$$\sigma_L \equiv \sigma_0^{\text{tot}} = \frac{4\pi^2\alpha}{K} \left[ \left( 1 - \frac{\nu^2}{q^2} \right) W_2(\nu, q^2) - W_1(\nu, q^2) \right] \quad (8.54)$$

**EXERCISE 8.15** Verify eqs. (8.53) and (8.54). The calculation can be greatly simplified by writing the tensor decomposition for  $W_{\mu\nu}$ , (8.27), in the laboratory frame, where

$$p = (M; 0, 0, 0),$$

$$q = (\nu; 0, 0, \sqrt{\nu^2 - q^2}).$$

**EXERCISE 8.16** Express the  $e p \rightarrow e X$  differential cross section (8.34) in terms of  $\sigma_{T,L}$ . That is, show that

$$\frac{d\sigma}{dE' d\Omega} \Big|_{\text{lab}} = \Gamma(\sigma_T + \epsilon\sigma_L), \quad (8.55)$$

where

$$\Gamma = \frac{\alpha K}{2\pi^2 |q^2|} \frac{E'}{E} \frac{1}{1-\epsilon}, \quad (8.56)$$

$$\epsilon = \left( 1 - 2 \frac{\nu^2 - q^2}{q^2} \tan^2 \frac{\theta}{2} \right)^{-1}. \quad (8.57)$$

**EXERCISE 8.17** The formalism has been set up in such a way that, when  $q^2 \rightarrow 0$ ,

$$\begin{aligned} \sigma_T &\rightarrow \sigma^{\text{tot}}(\gamma p) \\ \sigma_L &\rightarrow 0, \end{aligned} \quad (8.58)$$

where  $\gamma$  is a real photon and  $\sigma^{\text{tot}}(\gamma p)$  is given by (8.45).

Despite its appearance, convince yourself that  $W_{\mu\nu}$  must not be singular at  $q^2 = 0$ . Hence, show that

$$W_2 \rightarrow 0 \quad \text{and} \quad \left( W_1 + \frac{\nu^2}{q^2} W_2 \right) \rightarrow 0 \quad (8.59)$$

as  $q^2 \rightarrow 0$ , and so establish that  $\sigma_L$  vanishes.

Can we extract additional information about the structure of the proton from these complex events where the proton breaks up? Both the structure of the events and their phenomenological interpretation look quite forbidding. The answer to this question is of great importance and is the subject of the next two chapters.

# 9

## Partons

Equipped with the formalism of Chapter 8, we can now turn to the experimental information and ask the question, “Can small-wavelength photons resolve the quarks inside the proton target?”

### 9.1 Bjorken Scaling

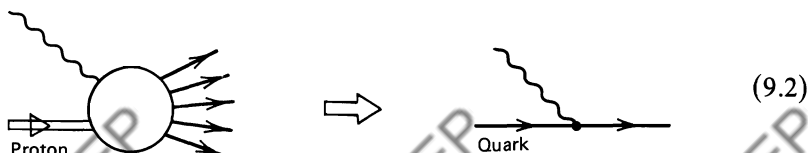
If simple, point-like, spin- $\frac{1}{2}$  quarks reside inside the proton, we should be able to illuminate them with a small-wavelength (large  $-q^2$ ) virtual photon beam (Fig. 9.1). The fact that such photons break up the proton target can be handled by using the inelastic form factors discussed in the previous chapter. The sign that there are structureless particles inside a complex system like a proton is that for small wavelengths, the proton described by (8.43) suddenly starts behaving like a free Dirac particle (a quark) and (8.43) turns into (8.41). The proton structure functions thus become simply

$$2W_1^{\text{point}} = \frac{Q^2}{2m^2} \delta\left(\nu - \frac{Q^2}{2m}\right),$$
$$W_2^{\text{point}} = \delta\left(\nu - \frac{Q^2}{2m}\right). \quad (9.1)$$

For convenience, we have introduced the positive variable

$$Q^2 \equiv -q^2.$$

Here,  $m$  is the quark mass; the “point” notation reminds us the quark is a structureless Dirac particle. Equation (9.1) can be pictured as



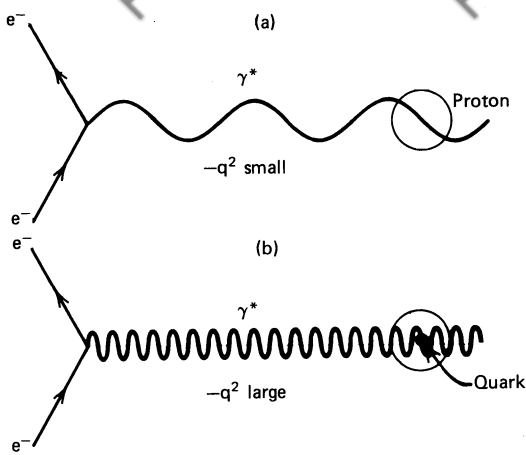


**Fig. 9.1** (a) Elastic  $e p \rightarrow e p$  scattering in which a large-wavelength “photon beam” measures the size of the proton through the elastic form factor analysis. (b) In deep inelastic scattering a short-wavelength “photon beam” resolves the quarks within the proton provided  $\lambda \left( \approx 1/\sqrt{-q^2} \right) \ll 1F$ .

that is, at large  $Q^2$ , *inelastic* electron–proton scattering is viewed simply as *elastic* scattering of the electron on a “free” quark within the proton. Using the identity  $\delta(x/a) = a\delta(x)$ , (9.1) may be rearranged to introduce dimensionless structure functions

$$2mW_1^{\text{point}}(\nu, Q^2) = \frac{Q^2}{2m\nu} \delta\left(1 - \frac{Q^2}{2m\nu}\right),$$

$$\nu W_2^{\text{point}}(\nu, Q^2) = \delta\left(1 - \frac{Q^2}{2m\nu}\right). \quad (9.3)$$

These “point” functions now display the intriguing property that they are only functions of the ratio  $Q^2/2m\nu$  and *not* of  $Q^2$  and  $\nu$  independently. This behavior can be contrasted with that for  $e p$  elastic scattering. For simplicity, set  $\kappa = 0$ , so that  $G_E = G_M \equiv G$ ; then, comparing (8.42) and (8.43), we have

$$W_1^{\text{elastic}} = \frac{Q^2}{4M^2} G^2(Q^2) \delta\left(\nu - \frac{Q^2}{2M}\right),$$

$$W_2^{\text{elastic}} = G^2(Q^2) \delta\left(\nu - \frac{Q^2}{2M}\right). \quad (9.4)$$

In contrast to (9.1), the structure functions of (9.4) contain a form factor  $G(Q^2)$ , and so cannot be rearranged to be functions of a single dimensionless variable. A

mass scale is explicitly present; it is set by the empirical value 0.71 GeV in the dipole formula for  $G(Q^2)$  which reflects the inverse size of the proton, see (8.20). As  $Q^2$  increases above  $(0.71 \text{ GeV})^2$ , the form factor depresses the chance of elastic scattering; the proton is more likely to break up. The point structure functions, on the other hand, depend only on a dimensionless variable  $Q^2/2mv$ , and no scale of mass is present. The mass  $m$  merely serves as a scale for the momenta  $Q^2, v$ .

The discussion can be summarized as follows: if large  $Q^2$  virtual photons resolve “point” constituents inside the proton, then

$$\begin{aligned} MW_1(v, Q^2) &\xrightarrow[\text{large } Q^2]{} F_1(\omega), \\ vW_2(v, Q^2) &\xrightarrow[\text{large } Q^2]{} F_2(\omega), \end{aligned} \quad (9.5)$$

where

$$\omega = \frac{2q \cdot p}{Q^2} = \frac{2Mv}{Q^2}. \quad (9.6)$$

Note that in (9.5) we have changed the scale from what it was in (9.3). We have introduced the proton mass instead of the quark mass to define the dimensionless variable  $\omega$ . The presence of free quarks is signaled by the fact that the inelastic structure functions are independent of  $Q^2$  at a given value of  $\omega$  [see (9.5)]. This is equivalent to the onset of  $\sin^{-4}(\theta/2)$  behavior for large momentum transfers in the Rutherford experiment, which reveals the “point” charge of the nucleus in the atom. A sample of data is shown in Fig. 9.2.  $vW_2$  at  $\omega = 4$  is independent of  $Q^2$ ; the photon is indeed interacting with point-like particles. No form factors, leading to additional  $Q^2$  dependence as in (9.4), are present. Are these particles (called partons by Bjorken) the same as the quarks discovered in the spectroscopy of hadrons (Chapter 2)?

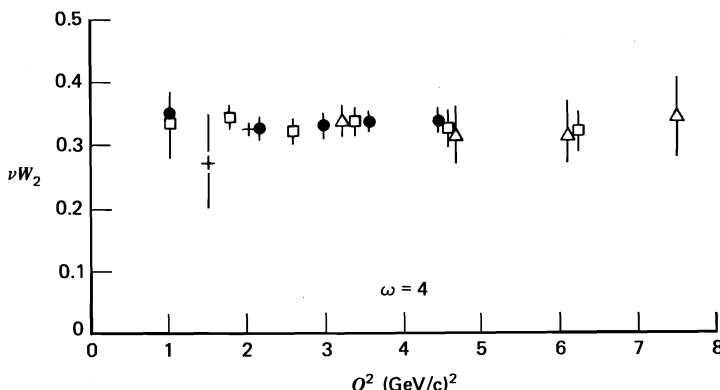


Fig. 9.2 The structure function  $vW_2$  determined by electron–proton scattering as a function of  $Q^2$  for  $\omega = 4$ . Data are from the Stanford Linear Accelerator.

## 9.2 Partons and Bjorken Scaling

Now that scaling is an approximate experimental fact, we attempt to make the identification of (9.2) explicit:

$$= \sum_i \int dx e_i^2 \quad \boxed{E, p \xrightarrow{\text{Proton}} \text{Partons} \xrightarrow{\text{Photon}} xE, xp}$$
(9.7)

Equation (9.7) recognizes the fact that various types of “point” partons make up the proton ( $i = u, d, \dots$ , quarks, with various charges  $e_i$ , as well as gluons; the latter do not interact with the photon, of course). They can each carry a different fraction  $x$  of the parent proton’s momentum and energy. We introduce the parton momentum distribution

$$f_i(x) = \frac{dp_i}{dx} = \frac{dp}{p} \quad \boxed{\text{Proton} \xrightarrow{\text{Photon}} \text{Parton } i \text{ with } xP \text{ and } xp, \text{ others with } (1-x)p}$$
(9.8)

which describes the probability that the struck parton  $i$  carries a fraction  $x$  of the proton’s momentum  $p$ . All the fractions  $x$  have to add up to 1; therefore,

$$\sum_{i'} \int dx x f_{i'}(x) = 1. \quad (9.9)$$

Here,  $i'$  sums over all the partons, not just the charged ones  $i$  which interact with the photon. The kinematics can be summarized as follows:

	Proton	Parton	
	$\downarrow$	$\downarrow$	
Energy	$E$	$xE$	
Momentum	$p_L$	$xp_L$	
	$p_T = 0$	$p_T = 0$	
Mass	$M$	$m = (x^2 E^2 - x^2 p_L^2)^{1/2} = xM.$	

(9.10)

Both the proton and its parton progeny move along the  $z$  axis (i.e.,  $p_T = 0$ ) with longitudinal momenta  $p_L$  and  $xp_L$ . The definition of the reference frame has to be made with more care; we shall return to it later on.

For an electron hitting a parton with momentum fraction  $x$  and unit charge, we see from (9.3) and (9.5) that the dimensionless structure functions are

$$\begin{aligned} F_1(\omega) &= \frac{Q^2}{4mvx} \delta\left(1 - \frac{Q^2}{2mv}\right) = \frac{1}{2x^2\omega} \delta\left(1 - \frac{1}{x\omega}\right), \\ F_2(\omega) &= \delta\left(1 - \frac{Q^2}{2mv}\right) = \delta\left(1 - \frac{1}{x\omega}\right). \end{aligned} \quad (9.11)$$

We have used the kinematics of (9.10);  $\omega$  is the dimensionless variable defined in (9.6). Summing our results for  $F_{1,2}$  for one parton, (9.11), over the partons making up a proton, (9.7) and (9.8), we obtain

$$\begin{aligned} F_2(\omega) &= \sum_i \int dx e_i^2 f_i(x) x \delta\left(x - \frac{1}{\omega}\right), \\ F_1(\omega) &= \frac{\omega}{2} F_2(\omega). \end{aligned} \quad (9.12)$$

It is conventional to redefine  $F_{1,2}(\omega)$  as  $F_{1,2}(x)$  and to express the results in terms of  $x$ . Recalling the identification (9.5), we see that (9.12) become, at large  $Q^2$ ,

$$vW_2(v, Q^2) \rightarrow F_2(x) = \sum_i e_i^2 x f_i(x), \quad (9.13)$$

$$MW_1(v, Q^2) \rightarrow F_1(x) = \frac{1}{2x} F_2(x), \quad (9.14)$$

with

$$x = \frac{1}{\omega} = \frac{Q^2}{2Mv}. \quad (9.15)$$

That is, the momentum fraction is found to be identical to the (dimensionless) kinematic variable  $x$  of the virtual photon that we introduced in Chapter 8; see (8.30). In other words, the virtual photon must have just the right value of the variable  $x$  to be absorbed by a parton with momentum fraction  $x$ . It is the delta function in (9.12) that equates these two distinct physical variables.

The inelastic structure functions  $F_{1,2}$  of (9.13) and (9.14) are functions of only one variable, namely,  $x$ . They are independent of  $Q^2$  at fixed  $x$ . We say they satisfy Bjorken scaling.

**EXERCISE 9.1** Prove that  $0 \leq x \leq 1$ , as it must be if  $x$  represents a momentum fraction; recall Exercise 8.11.

Note that the kinematics, (9.10), are a bit funny. Assigning a variable mass  $xM$  to the parton is of course out of the question. Clearly, if the parton's momentum

is  $xp$ , its energy can only be  $xE$  if we put  $m = M = 0$ . Equivalently, a proton can only emit a parton moving parallel to it ( $p_T = 0$  for both) if they both have zero mass. A corollary to this statement is that if a massive particle decays, there is a nonzero angle between its decay products. We justify our previous calculation by working in a Lorentz frame where

$$|\mathbf{p}| \gg m, M, \quad (9.16)$$

so that all masses can be neglected. In this frame, where the proton is moving with infinite momentum, the kinematics of (9.10) and the structure of  $F_{1,2}(x)$  given by (9.13) and (9.14) become exact. In this frame, relativistic time dilation slows down the rate at which partons interact with one another; that is, during the short time the virtual photon interacts with the quark [see (9.7)], it is essentially a free particle, not interacting with its friends in the proton. We implicitly used this *incoherence* assumption in the derivation of  $F_{1,2}(x)$ ; (9.7) represents an addition of probabilities (not amplitudes) of scattering from *single* free partons. It is the analogue of the impulse approximation in nuclear physics. However, there is a difference. A struck nucleon can escape from the nucleus as a completely free particle, but the struck colored parton has to recombine with the noninteracting spectator partons to form the colorless hadrons into which the proton breaks up. This has to happen with probability 1, because of color confinement (see Chapter 1); and, due to the size of the proton, it requires a much longer time scale than the quick punch the parton receives from the virtual photon. In summary, we argue that in a hard collision, the parton recoils as if it were free enabling the  $e\bar{p} \rightarrow eX$  cross section to be calculated [see (8.43), (9.13), and (9.14)] and that the subsequent confining final state interactions do not affect the result. This picture is valid when both the  $Q^2$  of the virtual photon and the invariant mass of the final-state hadronic system,  $W$ , are large.

**EXERCISE 9.2** Convince yourself that the interaction time is much shorter than the time scale over which the partons inside the target interact with one another. Read the explicit derivation in J. D. Bjorken and E. A. Paschos, *Phys. Rev.* 185, 1975 (1969); see also Perl (1974).

**EXERCISE 9.3** It is helpful to work through an alternative derivation of the parton model result, (9.13)–(9.15), in terms of the invariant variables of (6.29):

$$s = 2k \cdot p, \quad u = -2k' \cdot p, \quad t \equiv -Q^2 = -2k \cdot k',$$

with particle masses neglected. Set the parton momentum  $\hat{p} = xp$ , that is, neglect its component transverse to the proton momentum  $p$ . We outline the steps below. Using the basic idea of (9.7), we can write

$$\left( \frac{d\sigma}{dt du} \right)_{e\bar{p} \rightarrow eX} = \sum_i \int dx f_i(x) \left( \frac{d\sigma}{dt du} \right)_{eq_i \rightarrow eq_i}, \quad (9.17)$$

that is, the  $\text{ep} \rightarrow \text{eX}$  rate is simply the incoherent sum over all the contributing partons. Show that the invariant variables for the parton subprocess are given by

$$\hat{s} = xs, \quad \hat{u} = xu, \quad \hat{t} = t.$$

Use these relations, together with the  $e\mu$  scattering amplitude of (6.30), to show that

$$\left( \frac{d\sigma}{dt du} \right)_{\text{eq}_i \rightarrow \text{eq}_i} = x \frac{d\sigma}{d\hat{t} d\hat{u}} = x \frac{2\pi\alpha^2 e_i^2}{t^2} \left( \frac{s^2 + u^2}{s^2} \right) \delta(t + x(s + u)). \quad (9.18)$$

Now, also express the left-hand side of (9.17) in terms of  $s$ ,  $t$ , and  $u$ . It is simplest to use (8.31). Verify that

$$\left( \frac{d\sigma}{dt du} \right)_{\text{ep} \rightarrow \text{eX}} = \frac{4\pi\alpha^2}{t^2 s^2} \frac{1}{s + u} [(s + u)^2 x F_1 - us F_2], \quad (9.19)$$

where  $F_1 \equiv MW_1$  and  $F_2 \equiv \nu W_2$ . Insert (9.18) and (9.19) into (9.17). Compare coefficients of  $us$  and  $s^2 + u^2$  and so obtain the master formula of the parton model:

$$2x F_1(x) = F_2(x) = \sum_i e_i^2 x f_i(x).$$

As before, we see that  $F_{1,2}$  are functions only of the scaling variable  $x$ , here fixed by the delta function in (9.18):

$$x = \frac{-t}{s + u} = \frac{Q^2}{2M\nu}. \quad (9.20)$$

**EXERCISE 9.4** In Chapter 8, we evaluated the  $\text{ep} \rightarrow \text{eX}$  cross section for the electron to be scattered into the  $dE' d\Omega$  element in the target proton rest frame (the laboratory frame). Show that

$$dE' d\Omega = \frac{\pi}{EE'} dQ^2 d\nu = \frac{2ME}{E'} \pi y dx dy, \quad (9.21)$$

where  $x$  and  $y$  are the dimensionless variables

$$x = \frac{Q^2}{2M\nu}, \quad y = \frac{p \cdot q}{p \cdot k}_{(\text{lab.})} = \frac{\nu}{E}, \quad (9.22)$$

see (8.30). The allowed kinematic region ( $0 \leq x, y \leq 1$ ) is shown in Fig. 9.3.

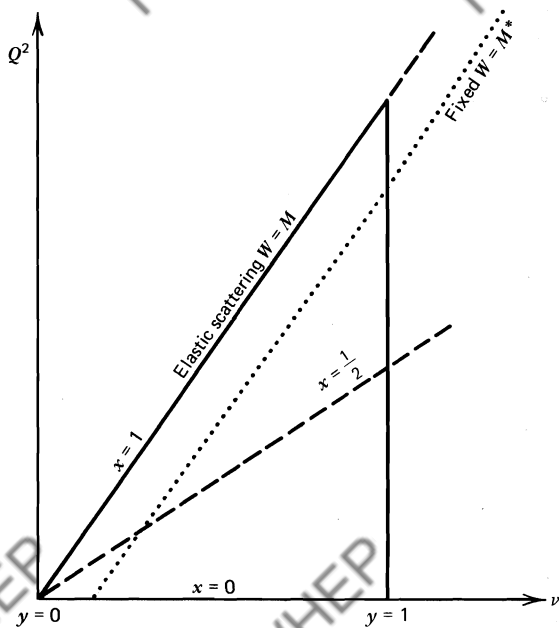


**Fig. 9.3** The triangle is the allowed kinematic region for  $e p \rightarrow e X$ .  $\nu_{\max} = E$  in the laboratory frame.  $W$  is the invariant mass of the hadronic state  $X$ , see (8.29).

Verify that the  $e p \rightarrow e X$  cross section may be written in the invariant form

$$M \nu_{\max} \frac{d\sigma}{dx dy} = \frac{2\pi\alpha^2}{x^2 y^2} \left\{ xy^2 F_1 + \left[ (1-y) - \frac{Mxy}{2\nu_{\max}} \right] F_2 \right\}, \quad (9.23)$$

where  $\nu_{\max} = E$  in the laboratory frame.

**EXERCISE 9.5** Use (9.23) to show that the parton model predicts

$$\left( \frac{d\sigma}{dx dy} \right)_{ep \rightarrow eX} = \frac{2\pi\alpha^2}{Q^4} s [1 + (1-y)^2] \sum_i e_i^2 x f_i(x) \quad (9.24)$$

if particle masses are neglected.

**EXERCISE 9.6** Show that

$$1 - y = \frac{\mathbf{p} \cdot \mathbf{k}'}{\mathbf{p} \cdot \mathbf{k}} \simeq \frac{1}{2}(1 + \cos \theta), \quad (9.25)$$

where  $\theta$  is the scattering angle in the electron-quark center-of-mass frame.

Hence, identify the  $(1 - y)^2$  and 1 terms in (9.24) with scattering between an electron and quark with opposite helicities and with the same helicity, respectively.

The parton model result  $2xF_1 = F_2$  is known as the Callan–Gross relation. It is a consequence of the quarks having spin  $\frac{1}{2}$  and is well borne out by the data.

**EXERCISE 9.7** In the limit  $v, Q^2 \rightarrow \infty$ , with  $x$  fixed, show that the Callan–Gross relation implies that the virtual photon–quark cross sections of (8.53), (8.54) satisfy

$$\frac{\sigma_L}{\sigma_T} \rightarrow 0. \quad (9.26)$$

**EXERCISE 9.8** Starting from (6.51), show that if quarks had spin 0,  $F_2(x)$  would still be given by (9.13) but that  $F_1(x) = 0$  and hence  $\sigma_T = 0$ .

Thus, in contrast to (9.26), spin-0 quarks would yield  $\sigma_T/\sigma_L = 0$ . We can understand this difference by glancing at Fig. 9.4, which shows the head-on collision between the quark and the virtual photon. By conservation of  $J_z$  (with  $z$  along  $\mathbf{p}$ ), we see that a spin-0 quark cannot absorb a photon of helicity  $\lambda = \pm 1$ , so  $\sigma_T = 0$ . Suppose now the quark has spin  $\frac{1}{2}$ . We recall that its helicity is conserved in a high-energy interaction (see Section 6.6). This can only be achieved by a  $\lambda = \pm 1$  photon; hence,  $\sigma_L \rightarrow 0$  in this case.

### 9.3 The Quarks Within the Proton

Does the photon see the proton structure described in Chapter 1, that is, does virtual photon–proton scattering look like Fig. 9.5? Just as measurements of elastic form factors provided us with information on the size of the proton, measurements on the inelastic structure function at large  $Q^2$  reveal the quark structure of the proton. After establishing Bjorken scaling, telling us that the constituents are there, eqs. (9.13) and (9.14) become the tools for extracting further information. The sum in (9.13) runs over the charged partons in the

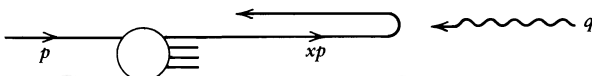
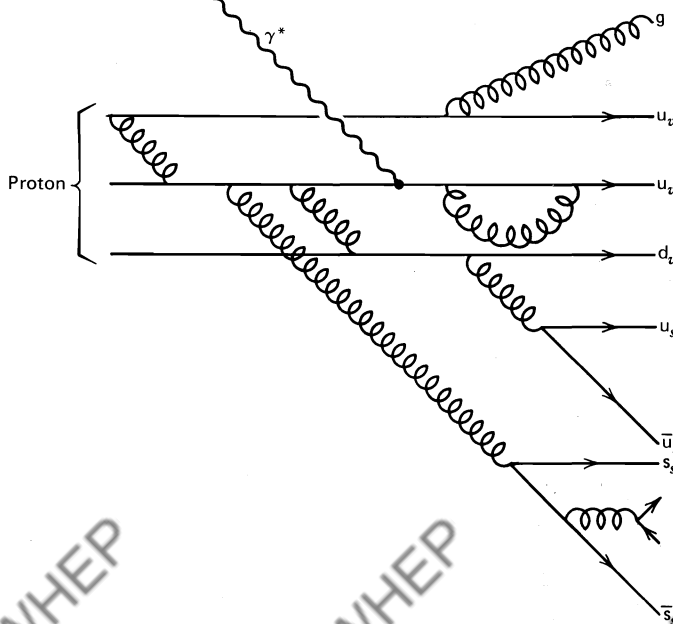


Fig. 9.4 Head-on collision between a constituent quark and the virtual photon.



**Fig. 9.5** A proton made up of valence quarks, gluons, and slow debris consisting of quark-antiquark pairs.

proton:

$$\frac{1}{x} F_2^{ep}(x) = \left(\frac{2}{3}\right)^2 [u^p(x) + \bar{u}^p(x)] + \left(\frac{1}{3}\right)^2 [d^p(x) + \bar{d}^p(x)] + \left(\frac{1}{3}\right)^2 [s^p(x) + \bar{s}^p(x)], \quad (9.27)$$

where  $u^p(x)$  and  $\bar{u}^p(x)$  are the probability distributions of u quarks and antiquarks within the proton. We have neglected the possibility of a sizable presence of charm and heavier quarks inside the proton.

We have six unknown quark structure functions,  $f_i(x)$ . However, the inelastic structure functions for neutrons are experimentally accessible by scattering electrons from a deuterium target. The counterpart to (9.27) is

$$\frac{1}{x} F_2^{en} = \left(\frac{2}{3}\right)^2 [u^n + \bar{u}^n] + \left(\frac{1}{3}\right)^2 [d^n + \bar{d}^n] + \left(\frac{1}{3}\right)^2 [s^n + \bar{s}^n]; \quad (9.28)$$

and as the proton and neutron are members of an isospin doublet, their quark content is related. There are as many u quarks in a proton as d quarks in a

neutron, and so on. So

$$\begin{aligned} u^p(x) &= d^n(x) \equiv u(x), \\ d^p(x) &= u^n(x) \equiv d(x), \\ s^p(x) &= s^n(x) \equiv s(x). \end{aligned} \quad (9.29)$$

**EXERCISE 9.9** Show that the above expressions lead to the bounds

$$\frac{1}{4} \leq \frac{F_2^{en}(x)}{F_2^{ep}(x)} \leq 4$$

whatever the value of  $x$ . The lower (upper) limit would be realized if only u (d) quarks were present in the proton.

Further constraints on the quark structure functions  $f_i(x)$  result from the fact that the quantum numbers of the proton must be exactly those of the uud combination of “valence” quarks of Chapter 2. As shown in Fig. 9.5, we describe the proton as three-constituent or three-valence quarks  $u_v, u_d, u_s$ , accompanied by many quark–antiquark pairs  $u_s\bar{u}_s, d_s\bar{d}_s, s_s\bar{s}_s$ , and so on. These are known as “sea” quarks. If we picture them as being radiated by the valence quarks, as in Fig. 9.5, then as a first approximation we may assume that the three lightest flavor quarks (u, d, s) occur in the “sea” with roughly the same frequency and momentum distribution, and neglect the heavier flavor quark pairs  $c_s\bar{c}_s$ , and so on. This picture of the proton can then be summarized as follows:

$$u_s(x) = \bar{u}_s(x) = d_s(x) = \bar{d}_s(x) = s_s(x) = \bar{s}_s(x) = S(x), \quad (9.30a)$$

$$u(x) = u_v(x) + u_s(x), \quad (9.30b)$$

$$d(x) = d_v(x) + d_s(x), \quad (9.30c)$$

where  $S(x)$  is the sea quark distribution common to all quark flavors. Clearly, the heavier strange quarks are penalized in the radiation process by some threshold suppression so that (9.30a) is only approximately true.

By summing over all contributing partons, we must recover the quantum numbers of the proton: charge 1, baryon number 1, strangeness 0. It follows that

$$\begin{aligned} \int_0^1 [u(x) - \bar{u}(x)] dx &= 2, \\ \int_0^1 [d(x) - \bar{d}(x)] dx &= 1, \\ \int_0^1 [s(x) - \bar{s}(x)] dx &= 0. \end{aligned} \quad (9.31)$$

These sum rules express the requirement that the net number of each kind of valence quark corresponds to the uud combination of constituents discussed in

Chapter 2. Equation (9.31) clearly follows from (9.30) with

$$\begin{aligned} u - \bar{u} &= u - \bar{u}_s = u - u_s = u_v, \\ d - \bar{d} &= d - \bar{d}_s = d - d_s = d_v, \\ s - \bar{s} &= s_s - \bar{s}_s = 0. \end{aligned}$$

Note however that the sum rules are true in any picture where the sea is taken to be made of quark–antiquark pairs, and so does not affect the quantum numbers of the proton, which are exclusively determined by the valence quarks, as expressed by (9.31).

Combining (9.30) with (9.27) and (9.28), we obtain

$$\begin{aligned} \frac{1}{x} F_2^{ep} &= \frac{1}{9} [4u_v + d_v] + \frac{4}{3} S, \\ \frac{1}{x} F_2^{en} &= \frac{1}{9} [u_v + 4d_v] + \frac{4}{3} S, \end{aligned} \quad (9.32)$$

where  $\frac{4}{3}$  is the sum of  $e_i^2$  over the six sea quark distributions. Since gluons create the  $q\bar{q}$  pairs in the sea, we expect  $S(x)$  to have a bremsstrahlung-like spectrum at small  $x$ , so that the number of sea quarks grows logarithmically as  $x \rightarrow 0$  (see Exercise 9.10).

**EXERCISE 9.10** Assume that the virtual photon–proton total cross section of Section 8.5 behaves like a constant as  $x \rightarrow 0$ ,  $v \rightarrow \infty$  for fixed  $Q^2$ , and hence show that

$$f_i(x) \xrightarrow[x \rightarrow 0]{} \frac{1}{x}. \quad (9.33)$$

Thus, we have a logarithmic growth of partons at small  $x$ .

When probing the small-momentum ( $x \approx 0$ ) debris of the proton, we therefore anticipate that the presence of the three valence quarks will be overshadowed by these multiple, low-momentum  $q\bar{q}$  pairs that make up the sea  $S(x)$ . According to (9.32), this means that

$$\frac{F_2^{en}(x)}{F_2^{ep}(x)} \xrightarrow[x \rightarrow 0]{} 1. \quad (9.34)$$

This is indeed the case experimentally, as can be checked from the data in Fig. 9.6. On the other hand, when probing the large-momentum part of the proton structure ( $x \approx 1$ ), the fast-valence quarks  $u_v$ ,  $d_v$  leave little momentum unoccupied for sea pairs. In this limit, the valence quarks dominate in (9.32), and therefore

$$\frac{F_2^{en}(x)}{F_2^{ep}(x)} \xrightarrow[x \rightarrow 1]{} \frac{u_v + 4d_v}{4u_v + d_v}. \quad (9.35)$$

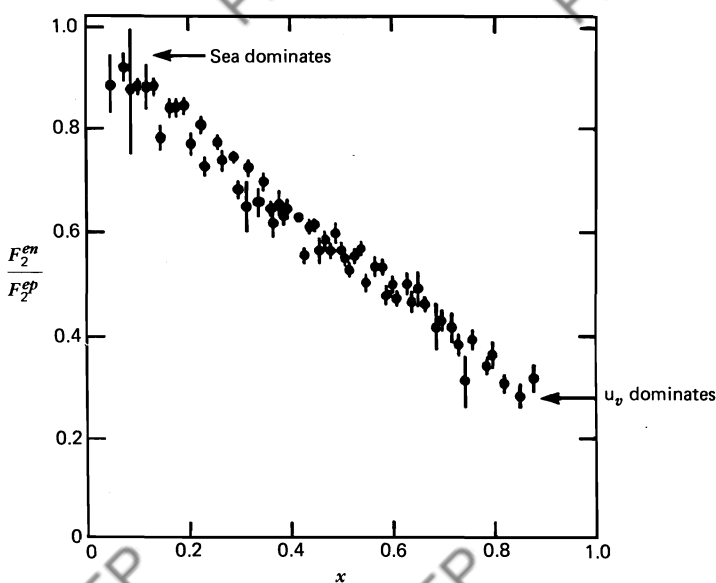


**Fig. 9.6** The ratio  $F_2^{en}/F_2^{ep}$  as a function of  $x$ , measured in deep inelastic scattering. Data are from the Stanford Linear Accelerator.

For the proton, there is evidence that  $u_v \gg d_v$  at large  $x$ , and the ratio (9.35) tends to  $\frac{1}{4}$ , as hinted at in Fig. 9.6.

**EXERCISE 9.11** Discuss, on physical grounds, the behavior of  $f_i(x)$  in the limit as  $x \rightarrow 1$  when parton  $i$  carries all the momentum of the proton. Counting rules have been proposed which argue that

$$f_i(x) \xrightarrow{x \rightarrow 1} (1-x)^{2n_s-1},$$

where  $n_s$  is the number of spectator valence quarks which share between them the residual, vanishingly small momentum of the proton. Contrast the  $x \rightarrow 1$  behavior of  $u^p(x)$  with that of  $u^\pi(x)$ , the u-quark structure function of a  $\pi^+$ -meson.

What should the complete  $F_2(x)$  look like according to our picture of the proton (Fig. 9.5)? Its shape can be guessed by successive approximation; see Fig. 9.7. Figure 9.7 is self-explanatory. The transition from scenario 2 to 3 is of course due to the fact that once the quarks interact, they can redistribute the momenta among themselves, and the sharply defined momentum  $x = \frac{1}{3}$  is washed out, becoming a distribution of momenta peaked around  $x = \frac{1}{3}$ . Data on  $F_2^{ep}(x)$  at large  $Q^2$  do indeed have the general shape of scenario 4 corresponding to Fig. 9.5.

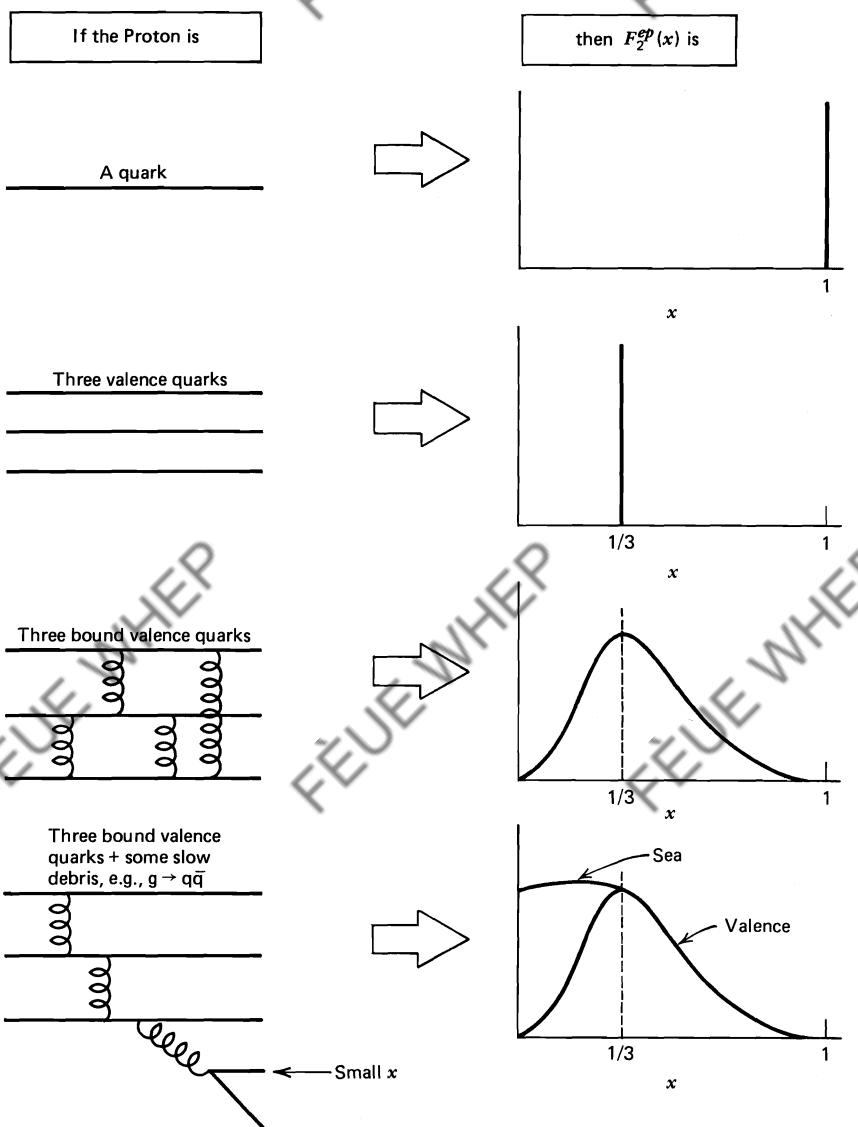


**Fig. 9.7** The structure function pictured corresponding to different compositions assumed for the proton.

However, by subtracting eqs. (9.32),

$$\frac{1}{x} [F_2^{ep}(x) - F_2^{en}(x)] = \frac{1}{3} [u_v(x) - d_v(x)], \quad (9.36)$$

we can observe the valence quarks without their sea quark partners. The result should look like scenario 3 of Fig. 9.7 and should peak around  $\frac{1}{3}$ . It does, as can be seen in Fig. 9.8.

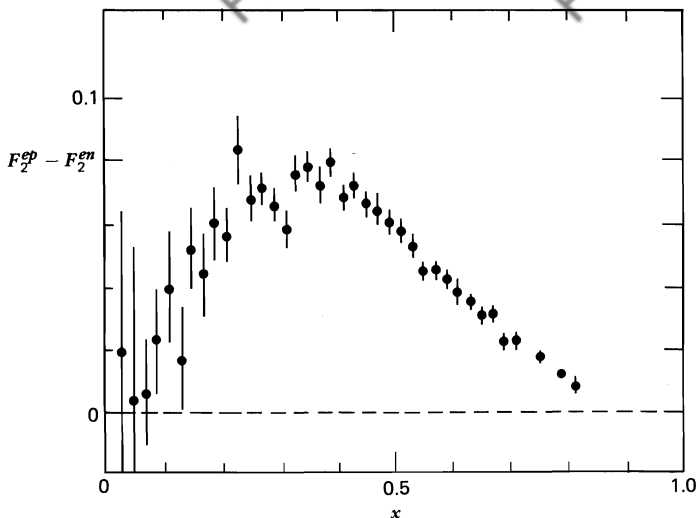


**Fig. 9.8** The difference  $F_2^{ep} - F_2^{en}$  as a function of  $x$ , as measured in deep inelastic scattering. Data are from the Stanford Linear Accelerator.

An alternative phenomenological approach is to parametrize all large  $Q^2$  data on  $F_2^{ep, en}(x)$  in terms of the valence and sea distributions and extract the quark structure functions at each  $x$  subject to the sum rules (9.31). The result of such an analysis is shown in Fig. 9.9. Fig. 9.9a shows the  $\bar{q}$  distribution, which has been subjected also to assumption (9.30). We see how  $u(x) = u_v(x) + u_s(x)$  approaches  $\bar{u}(x)$  at small  $x$  as  $xu_v(x) \rightarrow 0$ . Figure 9.9b displays the general shape of the total valence and sea quark components, corresponding to scenarios 3 and 4 in Fig. 9.7. Note how slow the sea quarks are as compared to their valence partners.

#### 9.4 Where Are the Gluons?

If we sum over the momenta of all the partons, we must reconstruct the total momentum  $p$  of the proton [see (9.8)],

$$\int_0^1 dx (xp)[u + \bar{u} + d + \bar{d} + s + \bar{s}] = p - p_g,$$

or, dividing by  $p$ ,

$$\int_0^1 dx x(u + \bar{u} + d + \bar{d} + s + \bar{s}) = 1 - \varepsilon_g.$$

The momentum fraction  $\varepsilon_g \equiv p_g/p$  carried by the gluons is not directly exposed

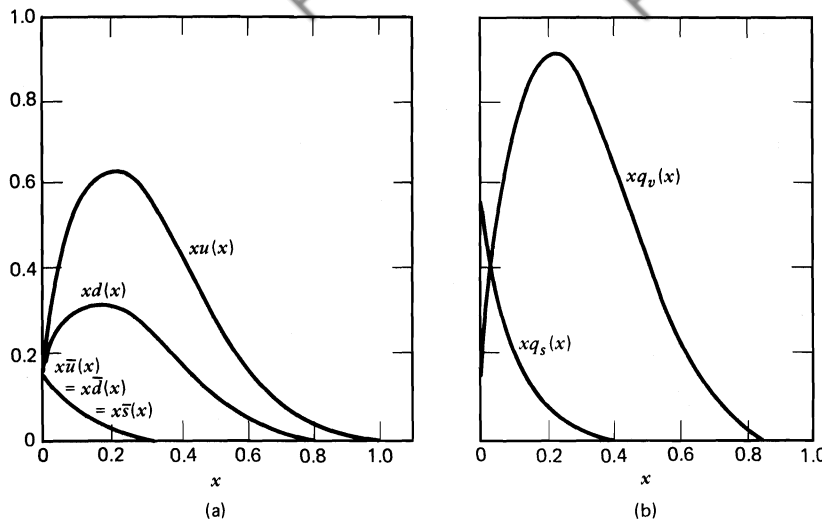


**Fig. 9.9** The quark structure functions extracted from an analysis of deep inelastic scattering data. Figure (b) shows the total valence and sea quark contributions to the structure of the proton.

by the photon probe (since gluons carry no electric charge) and is therefore subtracted from the right-hand side. Integrating over the experimental data on  $F_2^{ep, en}(x)$  gives us the following information:

$$\int dx F_2^{ep}(x) = \frac{4}{9}\epsilon_u + \frac{1}{9}\epsilon_d = 0.18,$$

$$\int dx F_2^{en}(x) = \frac{1}{9}\epsilon_u + \frac{4}{9}\epsilon_d = 0.12, \quad (9.38)$$

where

$$\epsilon_u \equiv \int_0^1 dx x(u + \bar{u})$$

is the momentum carried by u quarks and antiquarks, and similarly for  $\epsilon_d$ . Equation (9.38) follows from (9.27) and (9.28) after neglecting the strange quarks which carry a small fraction of the nucleon's momentum. From (9.37), we have

$$\epsilon_g \simeq 1 - \epsilon_u - \epsilon_d,$$

and on solving (9.38), we obtain

$$\epsilon_u = 0.36, \quad \epsilon_d = 0.18, \quad \epsilon_g = 0.46. \quad (9.39)$$

Hence, the gluons carry about 50% of the momentum, which was unaccounted for by the charged quarks.

In summary, an analysis of data on deep inelastic scattering of leptons by nucleons reveals the presence of point-like Dirac particles inside hadrons through Bjorken scaling. A study of the quantum numbers of these partons allows us to identify them with the quarks introduced in the study of the hadron spectrum in Chapter 2. The momentum distribution of the quarks forces us to the conclusion that a substantial fraction of the proton's momentum is carried by neutral partons, not by quarks. These are the gluons of QCD.

# 10

## Quantum Chromodynamics

### 10.1 The Dual Role of Gluons

We have seen in the previous chapter that deep inelastic scattering measurements actually require the existence of electrically neutral as well as charged constituents of the proton. We concluded that the charged partons could be identified with the colored quarks postulated in Chapter 2 to explain the observed systematics of the hadron spectrum. It is tempting to identify the neutral partons with gluons. Is this identification justified? That is, does experiment actually require the existence of gluons independent of the formal arguments which were the original motivation for postulating their existence?

Recall that the color charge of quarks was originally introduced to remedy a statistics problem in constructing the  $\Delta^{++}$  wavefunction (see Section 2.11). It is interesting to reflect on the fact that although it is economical to associate the same color charge with the charge of the strong interaction and although it is helpful that such a force, mediated by the exchange of gluons, is asymptotically free (see Sections 1.3 and 7.9) so that we can apply perturbation theory, none of these arguments constitutes direct evidence that quantum chromodynamics (QCD) is the correct physical theory.

It is clearly crucial to check that the gluons, introduced in Chapters 1 and 2, can indeed be identified with the neutral partons discovered as “missing momentum” in deep inelastic scattering. Subsequently, we can ask more probing questions and verify that their dynamical properties correspond to those of the carriers of the color force.

In order to proceed, it is not necessary at this stage to formally develop QCD as a color gauge theory. It is sufficient to recall the essential properties of the theory. We have already discussed them in Chapters 1 and 2.

- Quarks carry color as well as electric charge; there are three colors, R, G, and B.
- Color is exchanged by eight bicolored gluons (see Fig. 1.4).
- Color interactions are assumed to be “a copy of electromagnetic interactions.” To be precise, quark–gluon interactions are computed by the rules of QED with the substitution  $\sqrt{\alpha} \rightarrow \sqrt{\alpha_s}$  at each vertex (see Fig. 1.9) and

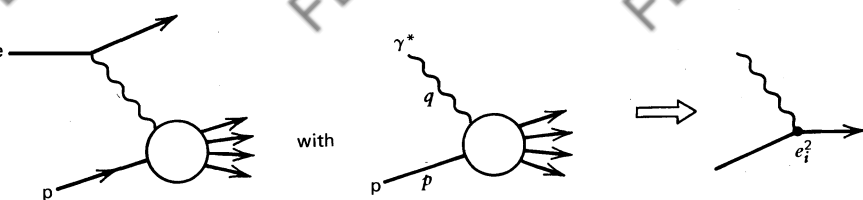


Fig. 10.1 Pictorial representation of the parton model for  $ep \rightarrow eX$ .

the introduction of a color factor, which may be computed by the methods of Section 2.15. That is, the  $q\bar{q}g$  vertex has the same structure as the  $ee\gamma$  vertex. The (eight) gluons are massless and have spin 1.

- Gluons themselves carry color charge, and so they can interact with other gluons. That is, there is a  $ggg$  as well as a  $q\bar{q}g$  vertex in the theory (see Fig. 1.4d).
- At short distances,  $\alpha_s$  is sufficiently small so that we can compute color interactions using the perturbative techniques familiar from QED.

The crucial statement that “color interactions are a copy of electromagnetic interactions” will be given a formal meaning in Chapter 14, where both QED and QCD are shown to be a consequence of local gauge symmetries.

How does the color dynamics of the partons (quarks *and* gluons) affect our discussion of deep inelastic scattering in the two previous chapters? The parton model of Chapter 9, symbolically represented by Fig. 10.1, completely ignores the dynamical role of gluons as the carriers of the strong force associated with colored quarks. We have, for instance, neglected the fact that quarks can radiate gluons. We must therefore allow for the possibility that the quark in Fig. 10.1 may radiate a gluon before or after being struck by the virtual photon,  $\gamma^*$ . These possibilities are shown in Fig. 10.2. Moreover, a gluon constituent in the target can contribute to deep inelastic scattering via  $\gamma^*g \rightarrow q\bar{q}$  pair production as shown in Fig. 10.3. In a computational sense, the processes in Figs. 10.2 and 10.3 are  $O(\alpha\alpha_s)$  contributions to the cross section, whereas the leading contribution in Fig. 10.1 is  $O(\alpha)$ .

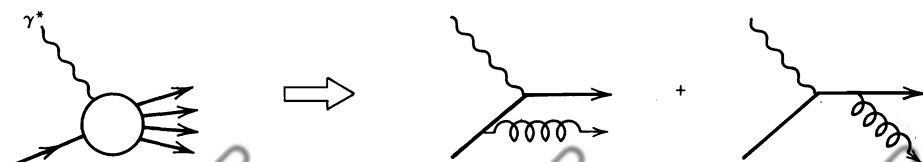
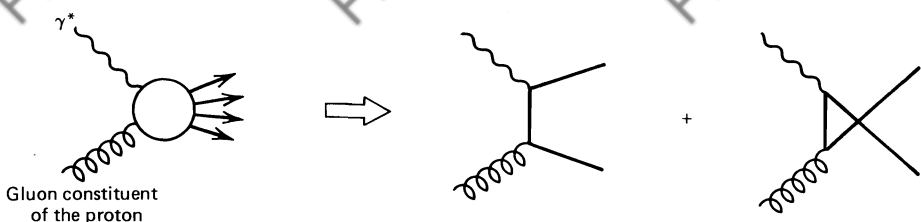


Fig. 10.2  $O(\alpha\alpha_s)$  contributions ( $\gamma^*g \rightarrow q\bar{q}$ ) to  $ep \rightarrow eX$ .



**Fig. 10.3**  $O(\alpha\alpha_s)$  gluon-initiated “hard” scattering contributions ( $\gamma^*g \rightarrow q\bar{q}$ ) to  $e p \rightarrow e X$ .

The inclusion of QCD diagrams of the type shown in Figs. 10.2 and 10.3 has two experimentally observable consequences: (1) the scaling property of the structure functions will no longer be true, and (2) the outgoing quark (and therefore the direction of its hadron jet) will no longer be collinear with the virtual photon. Point (2) is visualized in Fig. 10.4. In the parton model of Chapter 9, final-state hadrons in the jet of the struck quark are produced in the direction of the virtual photon (which is experimentally measured) as sketched in Fig. 10.4a. But if gluons are emitted (Fig. 10.4b), the quark can recoil against a radiated gluon and two jets are produced (indicated by arrows) each of which has a transverse momentum  $p_T$  relative to the virtual photon.

Quark–gluon color theory (QCD) allows us to compute the contribution from the diagrams of Figs. 10.2 and 10.3. Using QCD, we can therefore predict the scaling violations as well as the jet angular distributions relative to the virtual photon. They can then be compared with experiment and so the quark–gluon dynamics can be confronted with data in a quantitative and completely dynamical sense.

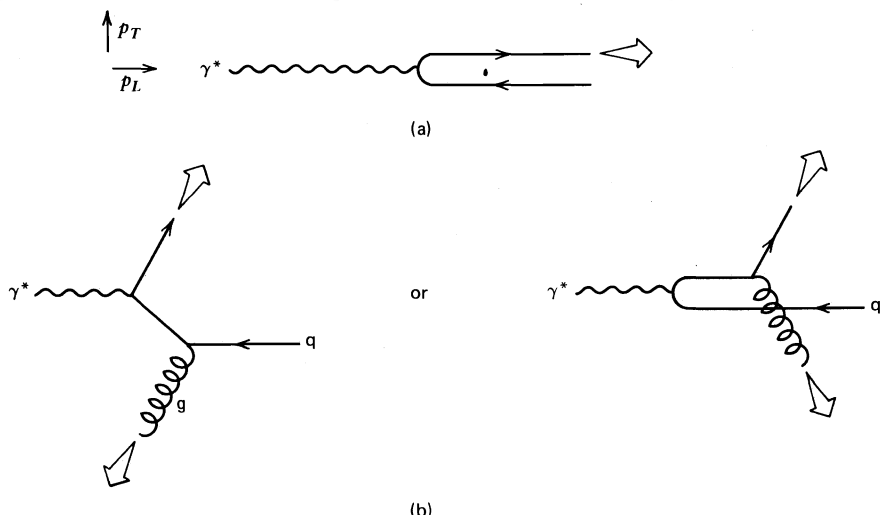


**Fig. 10.4** (a) Parton model diagram for  $\gamma^* q \rightarrow q$ , producing a jet with  $p_T = 0$ .  
 (b) Gluon emission diagrams which produce jets with  $p_T \neq 0$ .

## 10.2 Embedding $\gamma^*$ -Parton Processes in Deep Inelastic Scattering

How do we find the contribution of these  $\gamma^*$ -parton scattering diagrams to the cross section for deep inelastic scattering? A useful starting point is to recall that the  $e p \rightarrow e X$  cross section is given in terms of the structure functions  $W_{1,2}$  or, equivalently,

$$\begin{aligned} F_1 &= M W_1(\nu, Q^2), \\ F_2 &= \nu W_2(\nu, Q^2), \end{aligned} \quad (10.1)$$

see (8.34). Since we are going beyond the parton model, we shall find  $F_{1,2}$  no longer scale; that is, they are functions of both

$$\nu \equiv \frac{p \cdot q}{M} \quad \text{and} \quad Q^2 = -q^2, \quad (10.2)$$

rather than simply the ratio  $x = Q^2/2M\nu$ . In Chapter 8, we interpreted the structure functions in terms of the virtual photon–proton cross sections; see (8.53) and (8.54). In the deep inelastic limit, these relations simplify to

$$2F_1 = \frac{\sigma_T}{\sigma_0} \quad (10.3)$$

$$\frac{F_2}{x} = \frac{\sigma_T + \sigma_L}{\sigma_0} \quad (10.4)$$

where  $\sigma_T$  and  $\sigma_L$  are the  $\gamma^* p$  total cross sections for transverse and longitudinal virtual photons, respectively, and

$$\sigma_0 \equiv \frac{4\pi^2\alpha}{2MK} \simeq \frac{4\pi^2\alpha}{s}. \quad (10.5)$$

**EXERCISE 10.1** Derive (10.3)–(10.5). It is easiest to work in the laboratory frame; the variables are given in Section 6.8. In the deep inelastic limit, the electron beam energy  $E \gg E'$ . Then, as  $\nu^2 \sim E^2$  and  $Q^2 \simeq 4EE'\sin^2(\theta/2)$ , we have  $\nu^2 \gg Q^2$ . We also have introduced the  $\gamma^*$ -proton center-of-mass energy squared:

$$s = (q + p)^2 = M^2 + 2M\nu - Q^2 \simeq 2MK, \quad (10.6)$$

where  $K$  is associated with the  $\gamma^*$ -flux factor of (8.48).

In calculating the  $\gamma^*$ -parton contributions to  $\sigma_T$  and  $\sigma_L$ , we immediately face a problem. Equations (10.3) and (10.4) refer to  $\gamma^*$ -proton and not  $\gamma^*$ -parton cross sections. For example, consider single gluon emission ( $\gamma^* q \rightarrow qg$ ), which is shown

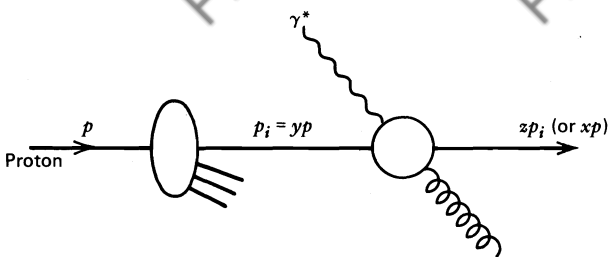


Fig. 10.5 Embedding  $\gamma^* q \rightarrow qg$  in  $\gamma^* p \rightarrow X$ .

in Fig. 10.5. The relation between the two frames is given by

$\gamma^*$ -Proton Frame

$$x = \frac{Q^2}{2p \cdot q}$$

$\gamma^*$ -Parton Frame

$$p_i = yp$$

$$z = \frac{Q^2}{2p_i \cdot q} = \frac{x}{y}$$

Here, we have relied extensively on the fact that both collinear frames move with infinite momentum.

We are now ready to relate cross section ratios in the two systems. For instance, for the ratio (10.3), we have

$$\left( \frac{\sigma_T(x, Q^2)}{\sigma_0} \right)_{\gamma^* p} = \sum_i \int_0^1 dz \int_0^1 dy f_i(y) \delta(x - zy) \left( \frac{\hat{\sigma}_T(z, Q^2)}{\hat{\sigma}_0} \right)_{\gamma^* i} \quad (10.7)$$

where  $f_i(y)$  are the parton structure functions (which give the probability that there is a parton  $i$  carrying a fraction  $y$  of the proton's momentum  $p$ ) and  $\hat{\sigma}_T$  is the cross section for the absorption of a transverse photon of momentum  $q$  by a parton of momentum  $p_i$ ;  $x$  is fixed, and we have to integrate over all  $z, y$  subject to the constraint  $x = zy$ . Using the delta function to perform the  $z$  integration, we obtain

$$\boxed{\left( \frac{\sigma_T(x, Q^2)}{\sigma_0} \right) = \sum_i \int_x^1 \frac{dy}{y} f_i(y) \left( \frac{\hat{\sigma}_T(x/y, Q^2)}{\hat{\sigma}_0} \right).} \quad (10.8)$$

Throughout this chapter, we use  $\hat{\sigma}$ ,  $\hat{s}$ ,  $\hat{t}$ , and so on, to distinguish  $\gamma^*$ -parton quantities from those of the parent process,  $\sigma$ ,  $s$ ,  $t$ , and so on.

### 10.3 The Parton Model Revisited

If all gluon effects were absent, we should be able to recover the parton model result from (10.8). In this case,  $\hat{\sigma}_T$  and  $\hat{\sigma}_L$  are given by the diagram of Fig. 10.1,

$\gamma^*q \rightarrow q$ . If we neglect the mass of the outgoing quark,  $(q + p_i)^2 = 0$ . Hence,

$$z = \frac{Q^2}{2 p_i \cdot q} = 1, \quad (10.9)$$

and  $\hat{\sigma}(z, Q^2)$  is proportional to  $\delta(1 - z)$ .

**EXERCISE 10.2** Show that the parton model diagram, Fig. 10.1, gives

$$\frac{\hat{\sigma}_T(z, Q^2)}{\hat{\sigma}_0} = e_i^2 \delta(1 - z) \quad (10.10)$$

$$\hat{\sigma}_L(z, Q^2) = 0. \quad (10.11)$$

We outline the various stages of the calculation. First, show that for  $\gamma^*(q)q(p) \rightarrow q(p')$ ,

$$\overline{|\mathcal{M}|^2} = 2e_i^2 e^2 p \cdot q, \quad (10.12)$$

where we have averaged over transverse polarization states of the incoming  $\gamma^*$ . From Section 4.3, we have

$$Fd\hat{\sigma}_T = \overline{|\mathcal{M}|^2} (2\pi)^4 \delta^{(4)}(p' - p - q) \frac{d^3 p'}{2p_0'(2\pi)^3}. \quad (10.13)$$

where  $F$  is the  $\gamma^*q$  flux factor. Calculate  $F\hat{\sigma}_T$  by making use of (6.47). Use  $F\hat{\sigma}_0 = 8\pi^2\alpha$ , see (10.5).

To determine the parton model prediction for  $F_2/x$  of (10.4), we input in (10.8) the following cross section ratio for  $\gamma^*q \rightarrow q$ :

$$\frac{1}{\hat{\sigma}_0} (\hat{\sigma}_T + \hat{\sigma}_L) = e_i^2 \delta(1 - z), \quad (10.14)$$

see (10.10) and (10.11). After substitution, we obtain

$$\frac{F_2(x, Q^2)}{x} = \sum_i e_i^2 \int_x^1 \frac{dy}{y} f_i(y) \delta\left(1 - \frac{x}{y}\right) = \sum_i e_i^2 f_i(x). \quad (10.15)$$

An identical expression is found for  $2F_1$ . The parton model results of (9.13) and (9.14) are indeed reproduced.

#### 10.4 The Gluon Emission Cross Section

We are now ready to include the gluon emission diagrams of Fig. 10.2. To calculate  $\gamma^*q \rightarrow qg$ , we take over our results for Compton scattering. In Section

6.14, we evaluated the closely related QED process  $\gamma^*e \rightarrow ye$  and found

$$\overline{|\mathcal{M}|^2} = 32\pi^2\alpha^2 \left( -\frac{u}{s} - \frac{s}{u} + \frac{2tQ^2}{su} \right), \quad (10.16)$$

using for the  $\gamma^*$ -polarization sum  $\sum \epsilon_\mu^* \epsilon_\nu = -g_{\mu\nu}$ , see (6.98). The result for  $\gamma^*q \rightarrow qg$  follows directly on substitution of  $\alpha^2 \rightarrow e_i^2 \alpha \alpha_s$  and insertion of the color factor  $\frac{4}{3}$ , and  $u \leftrightarrow t$  on account of the different ordering of the outgoing particles; so,

$$\overline{|\mathcal{M}|^2} = 32\pi^2 (e_i^2 \alpha \alpha_s) \frac{4}{3} \left( -\frac{\hat{t}}{\hat{s}} - \frac{\hat{s}}{\hat{t}} + \frac{2\hat{u}Q^2}{\hat{s}\hat{t}} \right). \quad (10.17)$$

The invariant variables are denoted  $\hat{s}, \hat{t}, \hat{u}$  to indicate that we are considering a parton subprocess.

The factor  $\frac{4}{3}$  takes into account the summation/averaging over final/initial colors. It can readily be deduced from counting the color lines shown in Fig. 10.6. Each color line can take one of three possible colors, so there are  $(3 \times 3 - 1)$  different configurations, if we subtract the color singlet configuration as explained in Section 2.15. We now average over the three initial quark colors and obtain  $\frac{8}{3}$ . However, this result has to be divided by a factor 2 because of the unfortunate historical definition of  $\alpha_s$  (see Section 2.15).

Most simple QCD diagrams are exactly analogous to QED diagrams, and the QCD cross section is obtained by the replacement

$$\alpha^n \rightarrow C_F \alpha_s^n, \quad (10.18)$$

where  $n$  is the number of quark-gluon (or gluon-gluon) vertices in the diagram. The color factor  $C_F$  is obtained by simply summing and averaging in much the same way as we do for spin. However, without changing the cross section, the color factor can be altered by a redefinition of  $\alpha_s$ . For example,

$$\alpha_s^n C_F \rightarrow (2\alpha_s)^n (C_F/2^n) = (\alpha'_s)^n C'_F. \quad (10.19)$$

The conventional definition of  $\alpha_s$  corresponds to the second convention in (10.19). The final rule to obtain the conventional color factor is simple: “count color on your fingers” and divide the result by  $2^n$ . This is why we divided the color factor  $\frac{8}{3}$  of Fig. 10.6 by  $2^1$ .

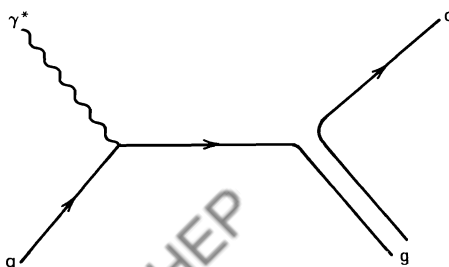


Fig. 10.6 Color lines for  $\gamma^*q \rightarrow qg$ .

Now back to the main problem. In preparation for the calculation of the  $\gamma^* q \rightarrow qg$  cross section from (10.17), we gather together the relevant kinematics.

**EXERCISE 10.3** In the center-of-mass frame of the parton process  $\gamma^* q_1 \rightarrow q_2 g$  of Fig. 10.7, show that

$$\hat{s} = 2k^2 + 2kq_0 - Q^2 = 4k'^2, \quad (10.20)$$

$$\hat{t} = -Q^2 - 2k'q_0 + 2kk'\cos\theta = -2kk'(1 - \cos\theta), \quad (10.21)$$

$$\hat{u} = -2kk'(1 + \cos\theta), \quad (10.22)$$

where  $k, k'$  are the magnitudes of the center-of-mass momenta  $\mathbf{k}, \mathbf{k}'$ . Note that for the virtual photon,  $q_0^2 = k^2 - Q^2$ . A useful result is

$$4kk' = -\hat{t} - \hat{u} = \hat{s} + Q^2. \quad (10.23)$$

The interesting quantity is the transverse momentum of the outgoing quark,  $p_T = k'\sin\theta$ . Show that

$$p_T^2 = \frac{\hat{s}\hat{u}}{(\hat{s} + Q^2)^2} \quad (10.24)$$

or, in the limit of small-angle scattering,  $-\hat{t} \ll \hat{s}$ , that

$$p_T^2 = \frac{\hat{s}(-\hat{t})}{\hat{s} + Q^2}. \quad (10.25)$$

Further, show that for small scattering angles ( $\cos\theta \approx 1$ ),

$$d\Omega = \frac{4\pi}{\hat{s}} dp_T^2. \quad (10.26)$$

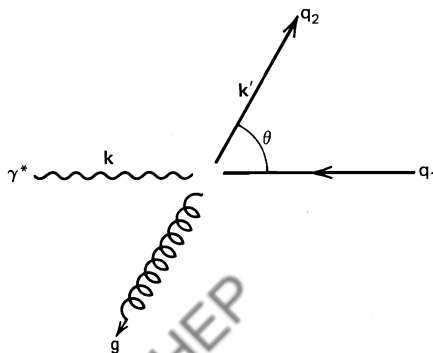


Fig. 10.7 Center-of-mass frame for  $\gamma^* q_1 \rightarrow q_2 g$

It is clear from (10.17) that at high energy ( $\hat{s}$  large), the  $\gamma^*q \rightarrow qg$  cross section peaks as  $-\hat{t} \rightarrow 0$ . Referring back to Fig. 4.8 and the related discussion, we see that this is due to quark exchange in the  $t$  channel. We can therefore approximate the cross section by its forward peak. For forward scattering, we find, from (10.26) and (4.35), that

$$\frac{d\hat{\sigma}}{dp_T^2} \simeq \frac{1}{16\pi\hat{s}^2} |\mathcal{M}|^2. \quad (10.27)$$

**EXERCISE 10.4** Derive (10.27). Make use of (10.26) and (10.20), together with (4.34). Show that the  $\gamma^*q$  flux factor is given by  $2\hat{s}$  using the convention of (8.48).

On substituting (10.17) into (10.27), the  $\gamma^*q \rightarrow qg$  cross section becomes

$$\frac{d\hat{\sigma}}{dp_T^2} \simeq \frac{8\pi e_i^2 \alpha \alpha_s}{3\hat{s}^2} \left( \frac{1}{-\hat{t}} \right) \left[ \hat{s} + \frac{2(\hat{s} + Q^2)Q^2}{\hat{s}} \right], \quad (10.28)$$

where we have used  $-\hat{t} \ll \hat{s}$ . Using (10.25) and

$$z \equiv \frac{Q^2}{2p_i \cdot q} = \frac{Q^2}{(p_i + q)^2 - q^2} = \frac{Q^2}{\hat{s} + Q^2}, \quad (10.29)$$

equation (10.28) can finally be rewritten as

$$\frac{d\hat{\sigma}}{dp_T^2} \simeq e_i^2 \hat{\sigma}_0 \frac{1}{p_T^2} \frac{\alpha_s}{2\pi} P_{qq}(z),$$

(10.30)

where  $\hat{\sigma}_0 = 4\pi^2\alpha/\hat{s}$ , see (10.5), and where

$$P_{qq}(z) = \frac{4}{3} \left( \frac{1+z^2}{1-z} \right) \quad (10.31)$$

represents the probability of a quark emitting a gluon and so becoming a quark with momentum reduced by a fraction  $z$ . The  $z \rightarrow 1$  singularity is associated with the emission of a “soft” massless gluon. It is an example of an infrared divergence (mentioned in Chapter 7). We explain how it is canceled by virtual gluon diagrams in Section 10.8.

The cross section (10.30) is also singular as  $p_T^2 \rightarrow 0$ . Now the diagrams of Figs. 10.1 and 10.3 either do not contribute (remember that for the parton diagram the  $p_T$  of the outgoing parton relative to the virtual photon always vanishes) or are negligible in comparison to  $\gamma^*q \rightarrow qg$  in the limit  $-\hat{t} \ll \hat{s}$ . This is the case for the pair production diagrams of Fig. 10.3. Therefore, in the region  $-\hat{t} \ll \hat{s}$ , (10.30) represents the full  $p_T^2$  distribution of the final-state parton jets.

What is the experimental signature of this result? We refer to Fig. 10.4. The presence of gluon emission is signaled by a quark jet and gluon jet in the final

state, neither of which is moving along the direction of the virtual photon. The transverse momentum  $p_T$  of the jet or of the bremsstrahlung hadrons contained in this jet (see Chapter 1) is nonzero; in fact, we expect the  $p_T$  distribution to be given by (10.30). It has to be embedded into the electron–proton system, using (10.8), exactly as was done for the parton cross section in Section 10.3. Figure 10.8 shows the result of comparing such a calculation with data.

Several remarks about this comparison are in order. The calculation shown in Fig. 10.8 actually includes all diagrams in Figs. 10.1, 10.2, and 10.3, and the limit ( $-t \ll \hat{s}$ ) was not made. Moreover, one has to model the way a quark or gluon fragments into hadrons or, alternatively, one can infer this information from a different experiment. How this is done is explained in the next chapter. What is important is the qualitative observation that hadrons emerge with  $p_T \neq 0$  signaling the presence of gluon emission. In a parton model without gluons, all final-state jets would be collinear with the virtual photon. Their hadron fragments will therefore be nearly collinear with the photon, too, that is, with a spread of  $p_T$  of about 300 MeV as required by the uncertainty principle for confined quarks. This prediction is represented by the dashed line in Fig. 10.8. The data clearly establish an excess of large  $p_T$  hadrons which are the fragments of the quark and gluon jets recoiling against one another.

This “Rutherford experiment of QCD” can be repeated in many disguises such as  $e^+e^- \rightarrow$  hadrons or  $pp \rightarrow$  large- $p_T$  hadrons (see Chapter 1). The ideas and computational techniques are very similar to the example discussed here. Finally, the large  $Q^2$  of the photon guarantees that we are dealing with a short-distance

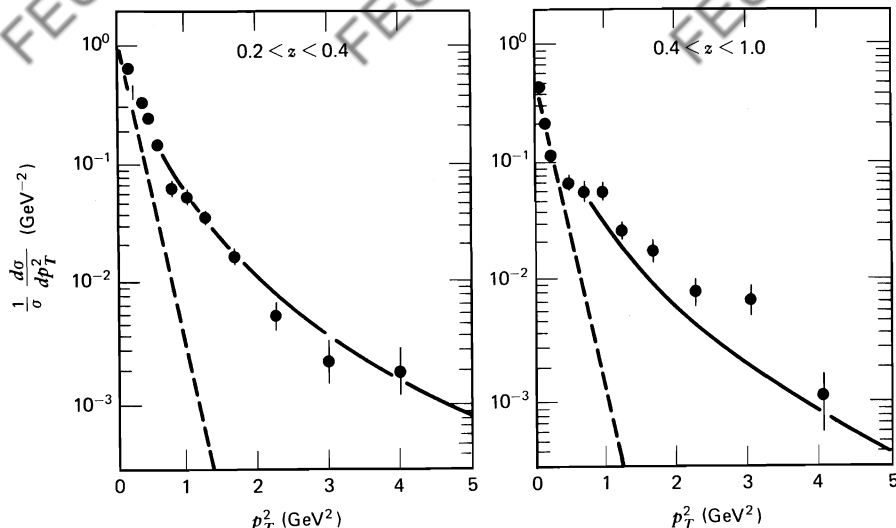


**Fig. 10.8** The  $p_T^2$  distribution of hadrons produced in  $\mu N$  interactions relative to the direction of the virtual photon. The dashed line is the expectation in the absence of gluon emission. Data are from the EMC collaboration at CERN. ( $\mu N$  and  $e N$  interactions give the same curves.)

interaction where  $\alpha_s$  is small (see Chapters 1 and 7). The number of large- $p_T$  hadrons in Fig. 10.8 measures the normalization of the cross section of (10.30), that is, it measures  $\alpha_s(Q^2)$ . At these values of  $Q^2$  the data imply that  $\alpha_s \approx 0.2$ .

### 10.5 Scaling Violations. The Altarelli–Parisi Equation

How does the gluon bremsstrahlung diagram of (10.30) contribute to the structure functions? Recall that the structure functions are related to parton cross sections via (10.8) [and (10.3), (10.4)]. This involves the integrated  $\gamma^*$ -parton cross section. We therefore have to compute

$$\begin{aligned}\hat{\sigma}(\gamma^*q \rightarrow qg) &= \int_{\mu^2}^{\hat{s}/4} dp_T^2 \frac{d\hat{\sigma}}{dp_T^2} \\ &\simeq e_i^2 \hat{\delta}_0 \int_{\mu^2}^{\hat{s}/4} \frac{dp_T^2}{p_T^2} \frac{\alpha_s}{2\pi} P_{qq}(z) \\ &\simeq e_i^2 \hat{\delta}_0 \left( \frac{\alpha_s}{2\pi} P_{qq}(z) \log \frac{Q^2}{\mu^2} \right).\end{aligned}\quad (10.32)$$

**EXERCISE 10.5** Show that the maximal transverse momentum for the two-body interaction  $\gamma^*q \rightarrow qg$  is given by

$$(p_T^2)_{\max} = \frac{\hat{s}}{4} = Q^2 \frac{1-z}{4z}. \quad (10.33)$$

In deriving (10.32), we integrated up to the maximum  $p_T$  of the gluon and then used (10.33) to write  $\log(\hat{s}/4) \simeq \log Q^2$  in the large  $Q^2$  limit. The lower limit  $\mu$  on the transverse momentum is introduced as a cutoff to regularize the divergence when  $p_T^2 \rightarrow 0$ .

Adding  $\hat{\sigma}(\gamma^*q \rightarrow qg)$  to the parton model cross section, (10.14), we find QCD modifies (10.15) to

$$\begin{aligned}\frac{F_2(x, Q^2)}{x} &= \left| \text{Diagram 1} + \text{Diagram 2} + \text{Diagram 3} \right|^2 \\ &= \sum_q e_q^2 \int_x^1 \frac{dy}{y} q(y) \left( \delta\left(1 - \frac{x}{y}\right) + \frac{\alpha_s}{2\pi} P_{qq}\left(\frac{x}{y}\right) \log \frac{Q^2}{\mu^2} \right),\end{aligned}\quad (10.34)$$

where we have introduced the notation that the quark structure function  $q(y) \equiv$

$f_q(y)$ . The presence of the  $\log Q^2$  factor means that the parton model scaling prediction for the structure functions should be violated. That is, in QCD,  $F_2$  is a function of  $Q^2$  as well as of  $x$ , but the variation with  $Q^2$  is only logarithmic. The violation of Bjorken scaling is a signature of gluon emission.

**EXERCISE 10.6** Study the origin of the  $\log Q^2$  term. Recall that the  $\gamma^*q \rightarrow qg$  cross section,  $d\hat{\sigma}/dp_T^2$ , is dominated by the forward peak. The  $t$ -channel quark propagator leads to a factor  $1/p_T^4$ . Show that helicity conservation at the gluon vertex weakens this singularity by introducing a factor  $p_T^2$  in the numerator.

Equation (10.34) may be regarded as the first two terms in a power series in  $\alpha_s$ ;  $\alpha_s$  is a useful expansion parameter at large  $Q^2$  since  $\alpha_s \sim (\log Q^2)^{-1}$ . But comparing the leading and next-order terms in (10.34), we find that the expansion parameter  $\alpha_s$  is multiplied by  $\log Q^2$ . From (7.65), we know that  $\alpha_s(Q^2) \log(Q^2/\mu^2)$  does not vanish at large  $Q^2$ , and so (10.34) does not seem very useful as it stands. How should we proceed? Can we absorb the  $\log Q^2$  term into a modified quark probability distribution? To this end, we rewrite (10.34) in the “parton-like” form

$$\begin{aligned} \frac{F_2(x, Q^2)}{x} &= \sum_q e_q^2 \int_x^1 \frac{dy}{y} (q(y) + \Delta q(y, Q^2)) \delta\left(1 - \frac{x}{y}\right) \\ &= \sum_q e_q^2 (q(x) + \Delta q(x, Q^2)) \end{aligned} \quad (10.35)$$

where

$$\Delta q(x, Q^2) \equiv \frac{\alpha_s}{2\pi} \log\left(\frac{Q^2}{\mu^2}\right) \int_x^1 \frac{dy}{y} q(y) P_{qq}\left(\frac{x}{y}\right). \quad (10.36)$$

The quark densities  $q(x, Q^2)$  now depend on  $Q^2$ . We interpret this as arising from a photon with larger  $Q^2$  probing a wider range of  $p_T^2$  within the proton.

We can picture this as follows. As  $Q^2$  is increased to  $Q^2 \sim Q_0^2$ , say, the photon starts to “see” evidence for the point-like valence quarks within the proton; see Fig. 10.9a. If the quarks were noninteracting, no further structure would be resolved as  $Q^2$  was increased and exact scaling [described by  $q(x)$ ] would set in, and the parton model would be satisfactory. However, QCD predicts that on increasing the resolution ( $Q^2 \gg Q_0^2$ ), we should “see” that each quark is itself surrounded by a cloud of partons. We have calculated one particular diagram, shown in Fig. 10.9b, but there are of course other diagrams with a greater number of partons. The number of resolved partons which share the proton’s momentum increases with  $Q^2$ . There is an increased probability of finding a quark at small  $x$  and a decreased chance of finding one at high  $x$ , because high-momentum quarks lose momentum by radiating gluons.

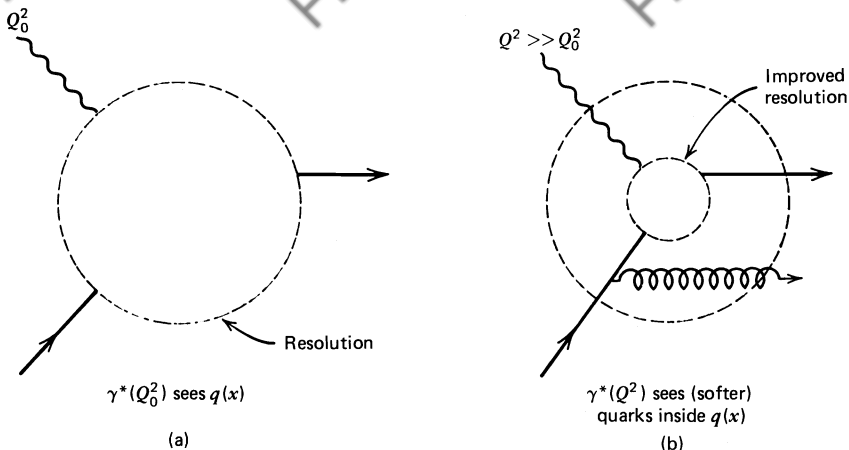


**Fig. 10.9** The quark structure of the proton as seen by a virtual photon as  $Q^2$  increases.

The  $Q^2$  evolution of the quark densities is determined by QCD through (10.36). By considering the change in the quark density,  $\Delta q(x, Q^2)$ , when one probes a further interval of  $\Delta \log Q^2$ , (10.36) can be rewritten as an integro-differential equation for  $q(x, Q^2)$ :

$$\frac{d}{d \log Q^2} q(x, Q^2) = \frac{\alpha_s}{2\pi} \int_x^1 \frac{dy}{y} q(y, Q^2) P_{qq} \left( \frac{x}{y} \right). \quad (10.37)$$

This is an “Altarelli–Parisi evolution equation.” The equation mathematically expresses the fact that a quark with momentum fraction  $x$  [ $q(x, Q^2)$  on the left-hand side] could have come from a parent quark with a larger momentum fraction  $y$  [ $q(y, Q^2)$  on the right-hand side] which has radiated a gluon. The probability that this happens is proportional to  $\alpha_s P_{qq}(x/y)$ . The integral in (10.37) is the sum over all possible momentum fractions  $y (> x)$  of the parent.

To summarize: QCD predicts the breakdown of scaling and allows us to compute explicitly the dependence of the structure function on  $Q^2$ . Given the quark structure function at some reference point  $q(x, Q_0^2)$ , we can compute it for any value of  $Q^2$  using the Altarelli–Parisi equation (10.37). The experimental results for  $q(x, Q^2)$ , or, to be precise,  $F_2(x, Q^2)$ , are displayed in Fig. 10.10. Moment analysis is often used to show that the  $Q^2$  variation of the structure function is described by the differential equation (10.37). This procedure is purely technical and of no interest to us (see, however, Exercise 10.16). The systematics of the  $Q^2$  dependence should be noted, however. Around  $x = 0.25$  ( $\omega = 4$ ), the structure function is found to scale, and Fig. 9.2 displays the absence of  $Q^2$  dependence at this particular  $x$  value. But for  $x \lesssim 0.25$ , the structure function increases with  $Q^2$ , while for  $x \gtrsim 0.25$ , it decreases. Another way to state this result is that we resolve increasing numbers of “soft” quarks with increasing  $Q^2$ .

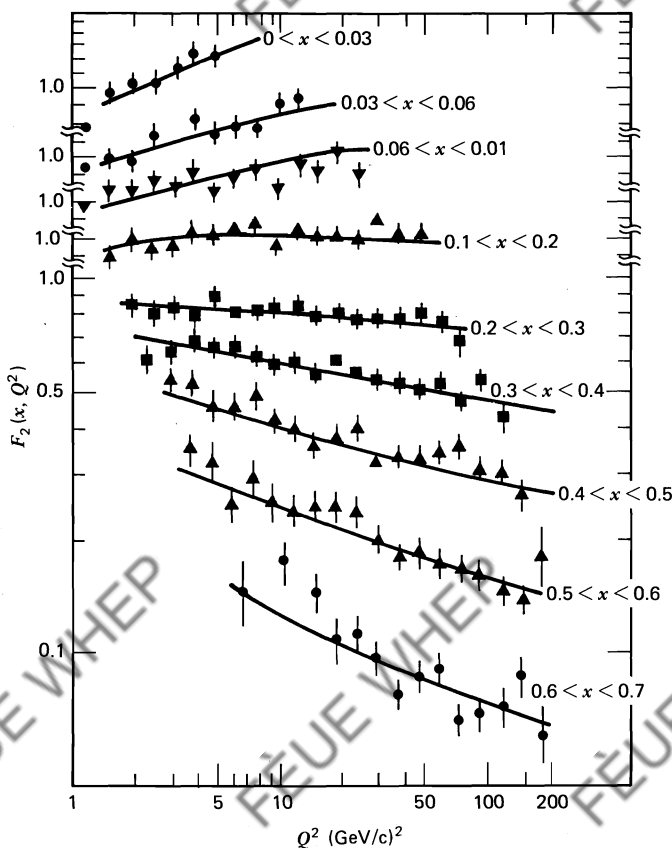


**Fig. 10.10** Deviations from scaling. With increasing  $Q^2$ , the structure function  $F_2(x, Q^2)$  increases at small  $x$  and decreases at large  $x$ . The data are from the CDHS counter experiment at CERN.

The large-momentum quark component ( $x \approx 1$ ) is depleted and shifted toward low momentum ( $x \approx 0$ ). This agrees with our earlier discussion that large- $Q^2$ , high-resolution photons have more chance of seeing “softer” quarks whose momentum has been degraded by gluon emission.

**EXERCISE 10.7** The origin of the scaling violation of  $q(x, Q^2)$  given by (10.37) can be traced back to (10.32). There, we assumed that  $\alpha_s$  is a constant. Show that (10.37) is also obtained for a running coupling constant. Assume that  $\alpha_s$  in (10.32) is  $\alpha_s(p_T^2)$  as given by (7.65).

**Comment** The reason for choosing  $p_T^2$  as the argument of  $\alpha_s$  cannot be exhibited without a discussion of the higher-order diagrams. However, note that we are working in a kinematic regime with two large quantities,  $p_T^2$  and

$Q^2$ , and the dominant region is  $p_T^2 \ll Q^2$ . In this limit, a discussion of higher orders introduces  $p_T^2$  as the argument of  $\alpha_s$  [see, for example, Reya (1981) or Dokshitzer et al. (1980)].

## 10.6 Including Gluon Pair Production

So far, we have only incorporated contributions to deep inelastic scattering,  $e p \rightarrow e X$ , from the quark-initiated processes  $\gamma^* q \rightarrow q$  and  $\gamma^* q \rightarrow q\bar{q}$ . To order  $\alpha_s$ , we should also include contributions where a gluon in the initial proton produces a quark-antiquark pair to which the virtual photon then couples, that is, the process  $\gamma^* g \rightarrow q\bar{q}$  of Fig. 10.3. This is similar to the Compton diagrams of Section 10.4.

**EXERCISE 10.8** Show that the color factor for  $\gamma^* g \rightarrow q\bar{q}$  is  $\frac{1}{2}$ .

**EXERCISE 10.9** Verify that for  $\gamma^* g \rightarrow q\bar{q}$ ,

$$|\mathcal{M}|^2 = 32\pi^2 (e_q^2 \alpha \alpha_s) \frac{1}{2} \left( \frac{\hat{u}}{\hat{t}} + \frac{\hat{t}}{\hat{u}} - \frac{2\hat{s}Q^2}{\hat{t}\hat{u}} \right), \quad (10.38)$$

using  $\sum e_\mu^* e_\nu = -g_{\mu\nu}$  for the  $\gamma^*$ -polarization sum. Hence, show that (10.34) for the proton structure function contains the additional contribution

$$\frac{F_2(x, Q^2)}{x} \Big|_{\gamma^* g \rightarrow q\bar{q}} = \left| \begin{array}{c} \text{Diagram 1: } \text{Wavy line enters from left, splits into two lines meeting at a vertex, which then splits into two lines meeting at a vertex, which finally splits into two lines exiting to the right.} \\ + \\ \text{Diagram 2: } \text{Wavy line enters from left, splits into two lines meeting at a vertex, which then splits into two lines meeting at a vertex, which finally splits into two lines exiting to the right.} \end{array} \right|^2 \quad (10.39)$$

$$= \sum_q e_q^2 \int_x^1 \frac{dy}{y} g(y) \frac{\alpha_s}{2\pi} P_{qg} \left( \frac{x}{y} \right) \log \frac{Q^2}{\mu^2}, \quad (10.40)$$

where  $g(y)$  is the gluon density in the proton and where

$$P_{qg}(z) = \frac{1}{2} (z^2 + (1-z)^2) \quad (10.41)$$

represents the probability that a gluon annihilates into a  $q\bar{q}$  pair such that the quark has a fraction  $z$  of its momentum. Detailed measurements of the scaling violations of  $F_2(x, Q^2)$  probe the gluon distribution inside the proton through (10.40).

### 10.7 Complete Evolution Equations for the Parton Densities

If we include the pair production contribution to the evolution of the quark density, (10.37) becomes

$$\frac{dq_i(x, Q^2)}{d \log Q^2} = \frac{\alpha_s}{2\pi} \int_x^1 \frac{dy}{y} \left( q_i(y, Q^2) P_{qg} \left( \frac{x}{y} \right) + g(y, Q^2) P_{gg} \left( \frac{x}{y} \right) \right) \quad (10.42)$$

for each quark flavor  $i$ . The second term, previously omitted, considers the possibility that a quark with momentum fraction  $x$  is the result of  $q\bar{q}$  pair creation by a parent gluon with momentum fraction  $y (> x)$ . The probability is  $\alpha_s P_{qg}(x/y)$ . The framework is obviously still incomplete since we require an equation for the evolution of the gluon density in the proton. Repeating our previous arguments, we can give a symbolic representation of the gluon evolution equation

$$\frac{d}{d \log Q^2} (g(x, Q^2)) = \sum_i \frac{q_i(y, Q^2)}{P_{gq}(\frac{x}{y})} + \frac{g(y, Q^2)}{P_{gg}(\frac{x}{y})} \quad (10.43)$$

which tells us that

$$\frac{dg(x, Q^2)}{d \log Q^2} = \frac{\alpha_s}{2\pi} \int_x^1 \frac{dy}{y} \left( \sum_i q_i(y, Q^2) P_{gq} \left( \frac{x}{y} \right) + g(y, Q^2) P_{gg} \left( \frac{x}{y} \right) \right), \quad (10.44)$$

where the sum  $i = 1, \dots, 2n_f$  runs over quarks and antiquarks of all flavors.  $P_{gq}$  does not depend on the index  $i$  if the quark masses can be neglected.

**EXERCISE 10.10** How would you set about verifying that

$$P_{gq}(z) = \frac{4}{3} \frac{1 + (1 - z)^2}{z}, \quad (10.45)$$

$$P_{gg}(z) = 6 \left( \frac{1 - z}{z} + \frac{z}{1 - z} + z(1 - z) \right)? \quad (10.46)$$

**EXERCISE 10.11** Express (10.42) in symbolic form.

**EXERCISE 10.12** Obtain the evolution equations for the combinations

$$q_{NS} \equiv q_i - q_j \quad (10.47)$$

$$q_S \equiv \sum_i q_i \quad (10.48)$$

The subscripts are conventional and, in fact, are used to indicate that the combinations refer to nonsinglet and singlet combinations of the quark flavor group.

### 10.8 Physical Interpretation of the $P$ Functions

Let us take stock of where QCD has taken us. At large  $Q^2$ , the structure functions for  $ep \rightarrow eX$  are given by a “parton model-like” formula with parton densities which do not scale but evolve with  $Q^2$  in a way which is calculable from QCD. Although we have arrived at these  $Q^2$ -dependent parton densities by studying deep inelastic scattering, these densities should simply characterize the target proton and should not depend on the nature of the probe. In other words, the parton densities are universal in the sense that they can relate the structure functions found in different processes.

The evolution is governed by the  $P_{qq}$ ,  $P_{gq}$ ,  $P_{qg}$ , and  $P_{gg}$  functions. The physical meaning of the  $P$  functions becomes transparent if we go back to (10.35) and rewrite it in the form of (10.7):

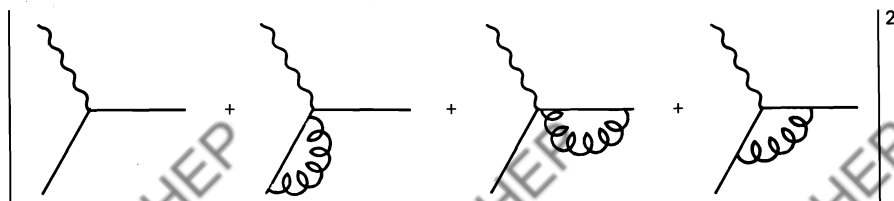
$$q(x, Q^2) + \Delta q(x, Q^2) = \int_0^1 dy \int_0^1 dz q(y, Q^2) \mathcal{P}_{qq}(z, Q^2) \delta(x - zy) \quad (10.49)$$

where

$$\mathcal{P}_{qq}(z, Q^2) \equiv \delta(1 - z) + \frac{\alpha_s}{2\pi} P_{qq}(z) \log \frac{Q^2}{\mu^2}. \quad (10.50)$$

It is natural to interpret  $\mathcal{P}_{qq}(z)$  as the *probability density* of finding a quark inside a quark with fraction  $z$  of the parent quark momentum to first order in  $\alpha_s$ . The  $\delta(1 - z)$  term corresponds to there being no change in  $q(x, Q^2)$ . Clearly, this probability for a quark to remain unchanged will be reduced when the  $O(\alpha_s)$  contributions are included.

At this point, it is crucial to include some virtual gluon diagrams which we have neglected until now. When these diagrams are included, the first term on the right-hand side of (10.34) is enlarged to



There is thus an  $O(\alpha\alpha_s)$  contribution from the interference of the parton diagram with the (three) diagrams containing virtual gluons. These additional interference contributions are also singular at  $z = 1$ . It turns out that their singularity will exactly cancel the  $z = 1$  singularity present in the incomplete  $O(\alpha_s)$  calculation (10.50).

Rather than calculate these contributions explicitly, we can easily see what they must give. The additional contribution is entirely concentrated at  $z = 1$  and is of the form  $\delta(1 - z)$ . It must be such that the total probability  $P_{qq}(z)$  satisfies the constraint

$$\int_0^1 P_{qq}(z) dz = 0. \quad (10.51)$$

This constraint expresses the fact that the total number of quarks minus anti-quarks is conserved; the probability,  $\mathcal{P}_{qq}$ , of finding a quark in a quark integrated over all  $z$  must add up to 1. From (10.50), we see that if the integral of  $\mathcal{P}_{qq}(z)$  is to be unity, we need the condition (10.51).

The virtual diagrams regularize the  $1/(1 - z)$  singularity in  $P_{qq}(z)$  of (10.31) so that (10.51) holds. This modification to  $P_{qq}(z)$  can be conveniently expressed in terms of the so-called “+” prescription” for regularization in which  $1/(1 - z)$  is replaced by  $1/(1 - z)_+$  defined so that

$$\int_0^1 dz \frac{f(z)}{(1 - z)_+} = \int_0^1 dz \frac{f(z) - f(1)}{1 - z} \quad (10.52)$$

where  $(1 - z)_+ = (1 - z)$  for  $z < 1$  but is infinite at  $z = 1$ .

**EXERCISE 10.13** Use (10.51) and (10.52) to show that

$$P_{qq}(z) = \frac{4}{3} \frac{1 + z^2}{(1 - z)_+} + 2\delta(1 - z). \quad (10.53)$$

**EXERCISE 10.14** Use momentum conservation to justify

$$\int_0^1 dz z (q_S(z, Q^2) + g(z, Q^2)) = 1. \quad (10.54)$$

Hence, determine the  $\delta(1 - z)$  term in  $P_{gg}$  and verify

$$P_{gg}(z) = 6 \left( \frac{1 - z}{z} + \frac{z}{(1 - z)_+} + z(1 - z) \right) + \left( \frac{11}{2} - \frac{n_f}{3} \right) \delta(1 - z), \quad (10.55)$$

where  $n_f$  is the number of quark flavors.

**EXERCISE 10.15** Show that momentum conservation at the QCD vertex requires (for  $z < 1$ )

$$P_{qq}(z) = P_{gq}(1 - z),$$

$$P_{qg}(z) = P_{qg}(1 - z), \quad (10.56)$$

$$P_{gg}(z) = P_{gg}(1 - z).$$

Check that the explicit formulas for the “splitting” functions satisfy these relations.

**EXERCISE 10.16** If  $\alpha_s(Q^2) = c/\log Q^2$ , show that (10.37) leads to

$$\frac{\int x^{n-1} q(x, Q^2) dx}{\int x^{n-1} q(x, Q_0^2) dx} = \left( \frac{\log Q^2}{\log Q_0^2} \right)^{A_n},$$

where

$$\begin{aligned} A_n &= \frac{c}{2\pi} \int_0^1 x^{n-1} P_{qq}(x) dx \\ &= \frac{c}{2\pi} \frac{4}{3} \left( -\frac{1}{2} + \frac{1}{n(n+1)} - 2 \sum_{j=2}^n \frac{1}{j} \right). \end{aligned}$$

That is, in QCD, the moments ( $n \geq 1$ ) of the quark structure functions decrease as calculable powers of  $\log Q^2/c$  is given by (7.65).

The observant reader may have noticed what appears to be a contradiction in our interpretation of the  $P$  functions. For example, we regard the  $P_{qq}$  term as the correction factor to the quark density that arises from allowing for gluon emission. However, there are two diagrams: one with the gluon emitted from the initial quark line and the other with the gluon radiated from the final quark line; see Fig. 10.2. Our picture is only valid if the first diagram dominates. Then, the emitted gluon can be considered as part of the proton structure. It is a “parton-like” diagram. It turns out that both diagrams are required to ensure gauge invariance of the amplitude, but that the second only plays the role of canceling the contributions from the unphysical polarization states of the gluon. Adopting a physical gauge, in which we sum only over transverse gluons, only the first diagram remains.

### 10.9 The Altarelli–Parisi Techniques Also Apply to Leptons and Photons: The Weizsäcker–Williams Formula

We conclude this chapter by emphasizing the astonishing simplicity of the Altarelli–Parisi formalism. Let us return to (10.30), which computes the probability for producing a gluon with momentum fraction  $1 - z$  and transverse momentum  $p_T$  in the process  $\gamma^*q \rightarrow qg$ . We should really have written it as a double-differential cross section

$$\frac{d\hat{\sigma}}{dz dp_T^2} = (e_i^2 \hat{\sigma}_0) \gamma_{qq}(z, p_T^2), \quad (10.57)$$

with

$$\gamma_{qq}(z, p_T^2) = \frac{\alpha_s}{2\pi} \frac{1}{p_T^2} P_{qq}(z). \quad (10.58)$$

This cross section for  $\gamma^*q \rightarrow qg$  can be pictured symbolically as

$$\frac{d\hat{\sigma}}{dz dp_T^2} = \text{Diagram} \quad (10.57')$$

(That  $z$  is indeed the fractional momentum of the quark after gluon radiation can be easily seen by adding its momentum  $zp_i$  to that of the photon and noting the mass-shell condition of the resulting outgoing quark,  $(q + zp_i)^2 = 0$ . This shows that  $z$  is given by (10.29), our previous definition.)

In (10.57') we see that the  $O(\alpha\alpha_s)$  cross section factors into the  $O(\alpha)$  parton model cross section ( $e_i^2 \hat{\sigma}_0$ ) and the probability  $\gamma_{qq}$  that the quark radiates a gluon with fraction  $1 - z$  of its momentum and with transverse momentum  $p_T$ . How is this possible? Cross sections are calculated from probability *amplitudes*, where the different amplitudes for the process are added and then the square modulus of the sum is taken. What we have found is that, in the limit that the gluons have a  $p_T$  that is not too large, the calculation of (10.57') can be viewed as two sequential events, that is, provided we retain only the singular part,  $1/p_T^2$ , of the full  $p_T$  distribution as we did in deriving (10.30). The probabilities for the interaction  $e_i^2 \hat{\sigma}_0$  and the gluon emission  $\gamma_{qq}$  can then be calculated separately and multiplied. That is, the probabilistic parton picture thus applies to gluon emission.

This technique is not special to quarks and gluons (QCD). In fact, it was known, since the work of Weizsäcker and Williams in 1934, that it applies equally well to leptons and photons (QED). Consider, for example, the process  $e p \rightarrow e X$ . The cross section may be written

$$\frac{d\sigma}{dz dp_T^2} = \gamma_{ee}(z, p_T^2) [\sigma(\gamma p \rightarrow X)]_{E_\gamma=(1-z)E} \quad (10.59)$$

with

$$\gamma_{ee}(z, p_T^2) = \frac{\alpha}{\pi} \frac{1}{p_T^2} P_{ee}(z), \quad (10.60)$$

where  $z$  and  $p_T$  are, respectively, the momentum fraction and transverse momentum of the outgoing electron, and

$$P_{ee}(z) = \frac{1+z^2}{1-z}; \quad (10.61)$$

see, for example, Chen and Zerwas (1975) *Phys. Rev.* D12, 187. Equation (10.60) follows from (10.58) after taking account of the factor 2 mismatch in the definitions of  $\alpha$  and  $\alpha_s$ , namely,  $\alpha_s \rightarrow 2\alpha$ , see (10.19).  $P_{ee}(z)$  is just  $P_{qq}(z)$  as given by (10.31) but without the color factor. Equation (10.60) is known in QED as the equivalent photon distribution. Similarly, one can define the QED equivalent of  $P_{qg}$  given by (10.41):

$$P_{e\gamma}(z) = z^2 + (1-z)^2. \quad (10.62)$$

In the next chapter, we further illustrate the power of this technique by calculating the cross section for the process  $e^+ e^- \rightarrow q\bar{q}g$ , which we view as  $e^+ e^- \rightarrow q\bar{q}$  followed by the emission of a gluon from the quark (or antiquark).  $\gamma_{qg}(z, p_T^2)$  has been computed once and for all and can just be substituted into other diagrams.

# 11

## $e^+e^-$ Annihilation and QCD

In the previous chapter, we studied QCD in the framework of a truly historic type of experiment, namely, the deep inelastic scattering of leptons by hadrons. The large- $Q^2$ , short-wavelength, virtual photon, prepared by the inelastic scattering of the lepton (see Fig. 11.1a), probes the proton, revealing its constituents (Chapter 9) and their color interactions (Chapter 10). The resulting picture is easy to interpret, because the short-distance (small  $\alpha_s$ ) nature of the quark-gluon interactions allows us to confront the experimental results with quantitative perturbative calculations.

High-resolution photons can also be prepared by colliding high-energy electron and positron beams head-on (see Fig. 11.1b). The exceptional power of this experimental technique is illustrated by the gallery of diagrams in Fig. 11.2:  $e^+e^-$  colliders can be used to study QED, weak interactions, quarks, and gluons and also to study or search for heavy quarks and leptons. Moreover,  $e^+e^-$  annihilation is a “clean” process in the sense that leptons (rather than hadrons, which are complex structures made of partons) appear in the initial state. For these reasons, we choose  $e^+e^-$  processes as our main working example to illustrate how the ideas and techniques of Chapters 9 and 10 carry over to other experimental situations.

### 11.1 $e^-e^+$ Annihilation into Hadrons: $e^-e^+\rightarrow q\bar{q}$

The bulk of hadrons produced in  $e^-e^+$  annihilations are fragments of a quark and antiquark produced by the process  $e^-e^+\rightarrow q\bar{q}$ . (We shall justify this statement by computing the higher-order process  $e^-e^+\rightarrow q\bar{q}g$  in the next section.) The cross section for the (QED) process  $e^-e^+\rightarrow q\bar{q}$  of Fig. 11.2c is readily obtained from that for the process of Fig. 11.2a,

$$\sigma(e^-e^+\rightarrow \mu^-\mu^+) = \frac{4\pi\alpha^2}{3Q^2}, \quad (11.1)$$

a result we obtained in (6.33). Here, the center-of-mass energy squared is

$$s = Q^2 = 4E_b^2, \quad (11.2)$$

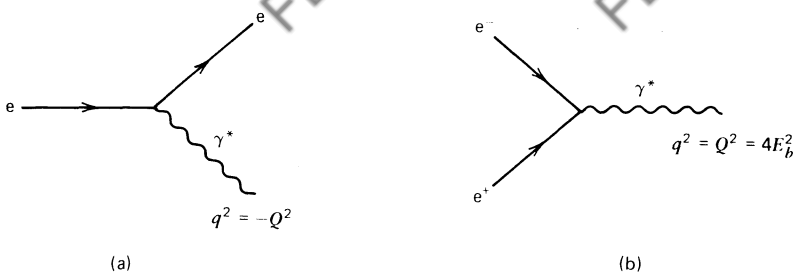


**Fig. 11.1** Virtual photon probes prepared in (a) deep inelastic scattering, and (b) the head-on collision of electron and positron beams each of energy  $E_b$ .

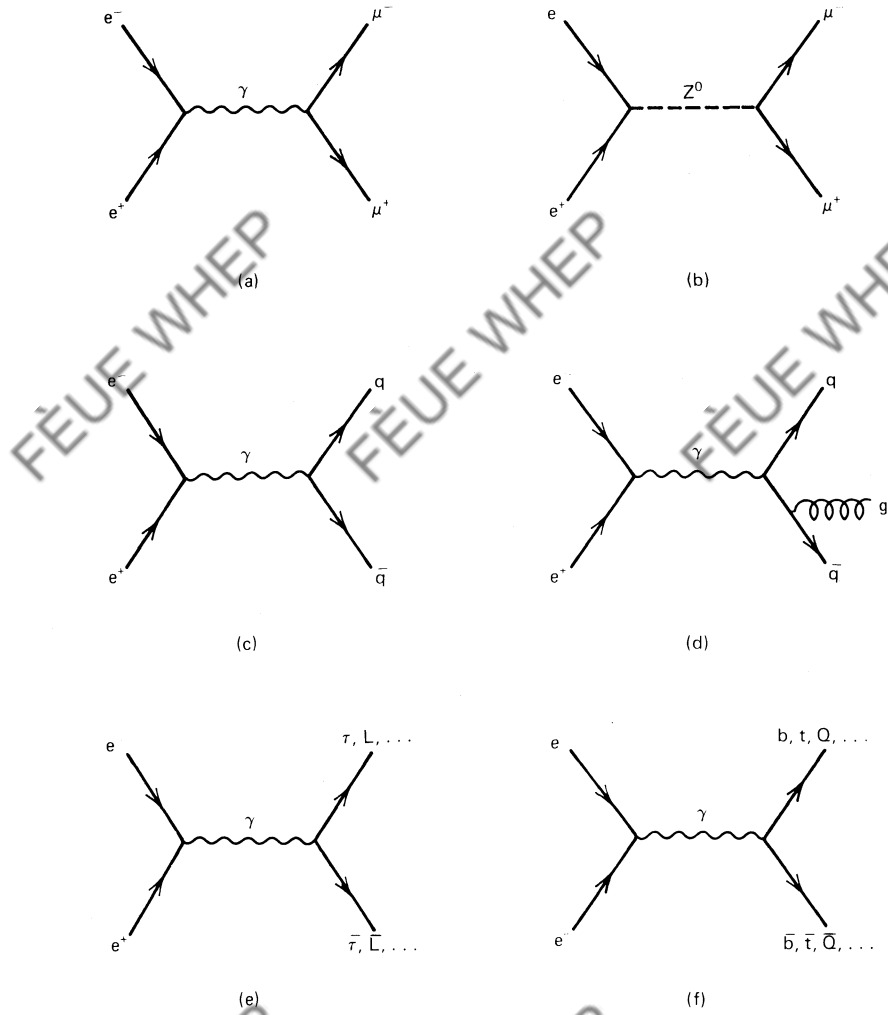


**Fig. 11.2** Some experimental possibilities resulting from  $e^+ e^-$  annihilation.

see Fig. 11.1b. The required cross section is

$$\sigma(e^-e^+\rightarrow q\bar{q}) = 3e_q^2\sigma(e^-e^+\rightarrow \mu^-\mu^+), \quad (11.3)$$

where we have taken account of the fractional charge of the quark,  $e_q$ . The extra factor of 3 arises because we have a diagram for each quark color and the cross sections have to be added. To obtain the cross section for producing all types of hadrons, we must sum over all quark flavors  $q = u, d, s, \dots$ , and therefore

$$\sigma(e^-e^+\rightarrow \text{hadrons}) = \sum_q \sigma(e^-e^+\rightarrow q\bar{q}) \quad (11.4)$$

$$= 3 \sum_q e_q^2 \sigma(e^-e^+\rightarrow \mu^-\mu^+). \quad (11.5)$$

This simple calculation thus leads to the dramatic prediction

$$R \equiv \frac{\sigma(e^-e^+\rightarrow \text{hadrons})}{\sigma(e^-e^+\rightarrow \mu^-\mu^+)} = 3 \sum_q e_q^2. \quad (11.6)$$

As  $\sigma(e^-e^+\rightarrow \mu^-\mu^+)$  is well known (see Fig. 6.6), a measurement of the total  $e^-e^+$  annihilation cross section into hadrons therefore directly counts the number of quarks, their flavors, as well as their colors. We have

$$\begin{aligned} R &= 3 \left[ \left(\frac{2}{3}\right)^2 + \left(\frac{1}{3}\right)^2 + \left(\frac{1}{3}\right)^2 \right] = 2 && \text{for } u, d, s, \\ &= 2 + 3 \left(\frac{2}{3}\right)^2 = \frac{10}{3} && \text{for } u, d, s, c, \\ &= \frac{10}{3} + 3 \left(\frac{1}{3}\right)^2 = \frac{11}{3} && \text{for } u, d, s, c, b. \end{aligned} \quad (11.7)$$

In Fig. 11.3, these predictions are compared to the measurements of  $R$ . The value  $R \approx 2$  is apparent below the threshold for producing charmed particles at  $Q = 2(m_c + m_u) \approx 3.7$  GeV. Above the threshold for all five quark flavors ( $Q > 2m_b \approx 10$  GeV),  $R \approx \frac{11}{3}$  as predicted. These measurements confirm that there are three colors of quark, since  $R = \frac{11}{3}$  would be reduced by a factor 3 if there was only one color, see (11.3).

These results for  $R$  will be modified when interpreted in the context of QCD. Equation (11.4) is based on the (leading order) process  $e^-e^+\rightarrow q\bar{q}$ . However, we should also include contributions from diagrams where the quark and/or anti-quark radiate gluons. To  $O(\alpha_s)$ , the result (11.6) is then modified to

$$R = 3 \sum_q e_q^2 \left( 1 + \frac{\alpha_s(Q^2)}{\pi} \right).$$

That is, the scaling result, (11.6), that  $R$  is independent of  $Q^2$  is violated logarithmically through the  $\log Q^2$  behavior of  $\alpha_s$ , see (7.65). At present, experiments are unable to detect this additional contribution to  $R$ , and our previous comparison with the data remains a good approximation. We postpone the

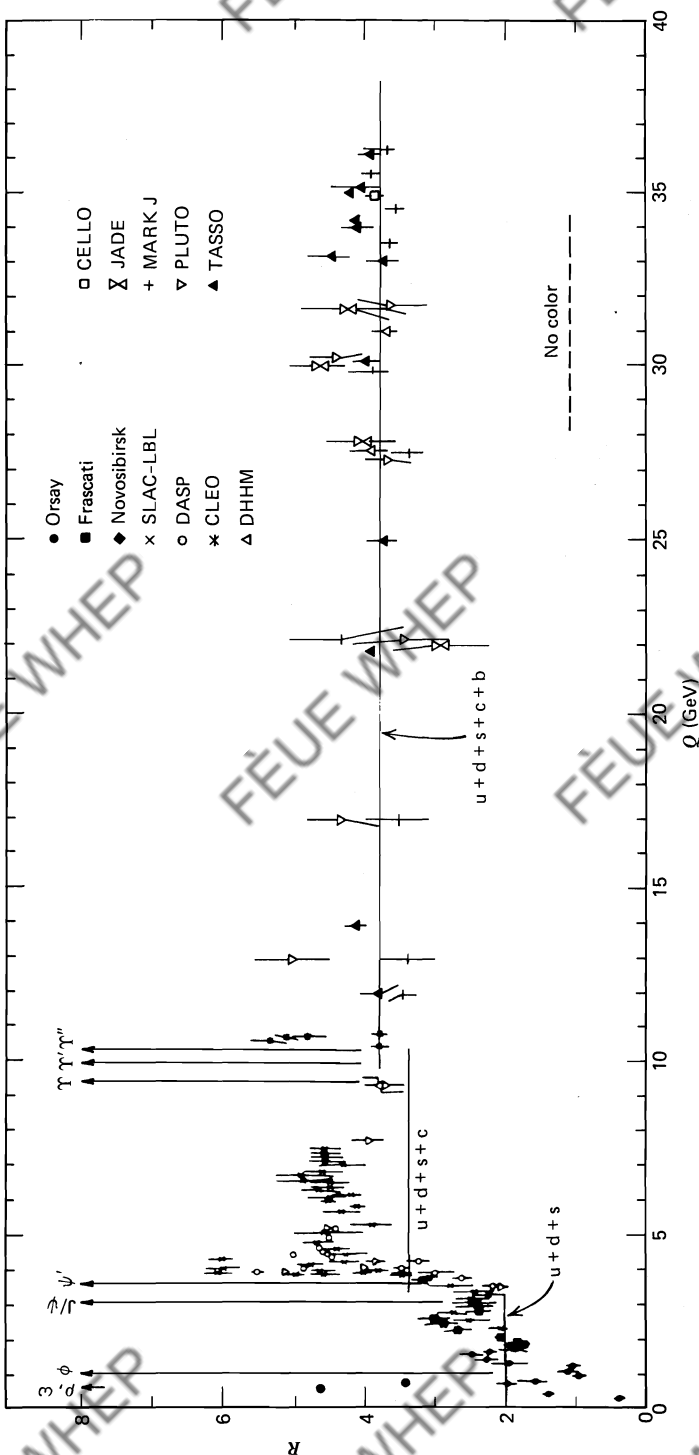


Fig. 11.3 Ratio  $R$  of (11.6) as a function of the total  $e^-e^+$  center-of-mass energy. (The sharp peaks correspond to the production of narrow  $1^-$  resonances just below or near the flavor thresholds.)

derivation of the  $\alpha_s/\pi$  correction until Section 11.7, where it will emerge as a by-product of the study of the three-jet events  $e^-e^+\rightarrow q\bar{q}g$ .

## 11.2 Fragmentation Functions and Their Scaling Properties

So far, we have not faced the problem of how the quarks turn into the hadrons that hit the detector. It was sufficient to state that the quarks must fragment into hadrons with unit probability. This gives (11.4). For more detailed calculations, this problem cannot be sidestepped.

In the center-of-mass frame, the produced quark and antiquark separate with equal and opposite momentum and materialize into two back-to-back jets of hadrons which have momenta roughly collinear with the original  $q$  and  $\bar{q}$  directions. The hadrons may be misaligned by a momentum transverse to the  $q$  or  $\bar{q}$  direction by an amount not exceeding about 300 MeV.

In Chapter 1, we visualized jet formation as hadron bremsstrahlung once the  $q$  and  $\bar{q}$  separate by a distance of around 1 fm. Then,  $\alpha_s$  becomes large, and strong color forces pull on the separating  $q$  and  $\bar{q}$ . The potential energy becomes so large that one or more  $q\bar{q}$  pairs are created (see Fig. 1.14). Eventually, all the energy is degraded into two jets of hadrons moving more or less in the direction of the  $q$  and  $\bar{q}$ .

To describe the fragmentation of quarks into hadrons, we use an analogous formalism to that introduced in Chapter 9 to describe the quarks inside hadrons. Figure 11.4 shows the observation of a hadron  $h$ , whose energy is measured to be  $E_h$ . The corresponding differential cross section can be written as

$$\frac{d\sigma}{dz}(e^-e^+\rightarrow hX) = \sum_q \sigma(e^-e^+\rightarrow q\bar{q}) [D_q^h(z) + D_{\bar{q}}^h(z)]. \quad (11.8)$$

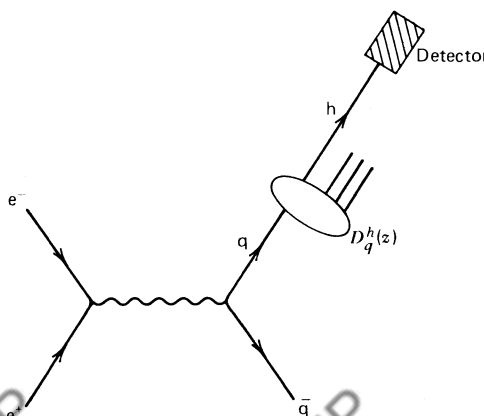


**Fig. 11.4** A hadron  $h$  observed with a fraction  $z$  of the quark's energy;  $z = 2E_h/Q$ .

It describes Fig. 11.4 as two sequential events: the production of a  $q\bar{q}$  pair, followed by the fragmentation of either the  $q$  or the  $\bar{q}$  producing the detected hadron  $h$ . The  $D$  functions therefore represent the probability that the hadron  $h$  is found in the debris of a quark (or antiquark) carrying a fraction  $z$  of its energy. That is,

$$z \equiv \frac{E_h}{E_q} = \frac{E_h}{E_b} = \frac{2E_h}{Q}. \quad (11.9)$$

The summation in (11.8) is over all quark flavors and recognizes the fact that the detector is unaware of the quantum numbers of the parent of the observed hadron.

The fragmentation function,  $D(z)$ , describes the transition (parton  $\rightarrow$  hadron) in the same way that the structure function,  $f(x)$ , of Chapter 9 describes the embedding (hadron  $\rightarrow$  parton). Like the  $f$  functions, the  $D$  functions are subject to constraints imposed by momentum and probability conservation:

$$\sum_h \int_0^1 z D_q^h(z) dz = 1 \quad (11.10)$$

$$\sum_q \int_{z_{\min}}^1 [D_q^h(z) + D_{\bar{q}}^h(z)] dz = n_h, \quad (11.11)$$

where  $z_{\min}$  is the threshold energy  $2m_h/Q$  for producing a hadron of mass  $m_h$ , and  $n_h$  is the average multiplicity of hadrons of type  $h$ . Equation (11.10) simply states that the sum of the energies of all hadrons is the energy of the parent quark. Clearly, the same relation holds for  $D_{\bar{q}}^h(z)$ . Equation (11.11) says that the number  $n_h$  of hadrons of type  $h$  is given by the sum of probabilities of obtaining  $h$  from all possible parents, namely, from  $q$  or  $\bar{q}$  of any flavor.

**EXERCISE 11.1** Fragmentation functions are often parametrized by the form

$$D_q^h(z) = N \frac{(1-z)^n}{z}$$

where  $n$  and  $N$  are constants. Show that

$$N = (n+1)\langle z \rangle,$$

where  $\langle z \rangle$  is the average fraction of the quark energy carried by hadrons of type  $h$  after fragmentation. Further, show that

$$n_h \sim \log \left( \frac{Q}{2m_h} \right)$$

for the two-jet process of Fig. 11.4. That is, the multiplicity of hadrons  $h$  grows logarithmically with the annihilation energy.

Taking the ratio of (11.8) and (11.4), and using (11.3), we find

$$\frac{1}{\sigma} \frac{d\sigma}{dz} (e^-e^+ \rightarrow hX) = \frac{\sum_q e_q^2 [D_q^h(z) + D_{\bar{q}}^h(z)]}{\sum_q e_q^2} \quad (11.12)$$

$$= \mathcal{F}(z) \quad (11.13)$$

That is, the inclusive cross section  $d\sigma/dz$  divided by the total annihilation cross section into hadrons,  $\sigma$ , is predicted to scale. The cross sections  $\sigma$  and  $d\sigma/dz$  depend on the annihilation energy  $Q$ , but (11.12) predicts that the ratio is

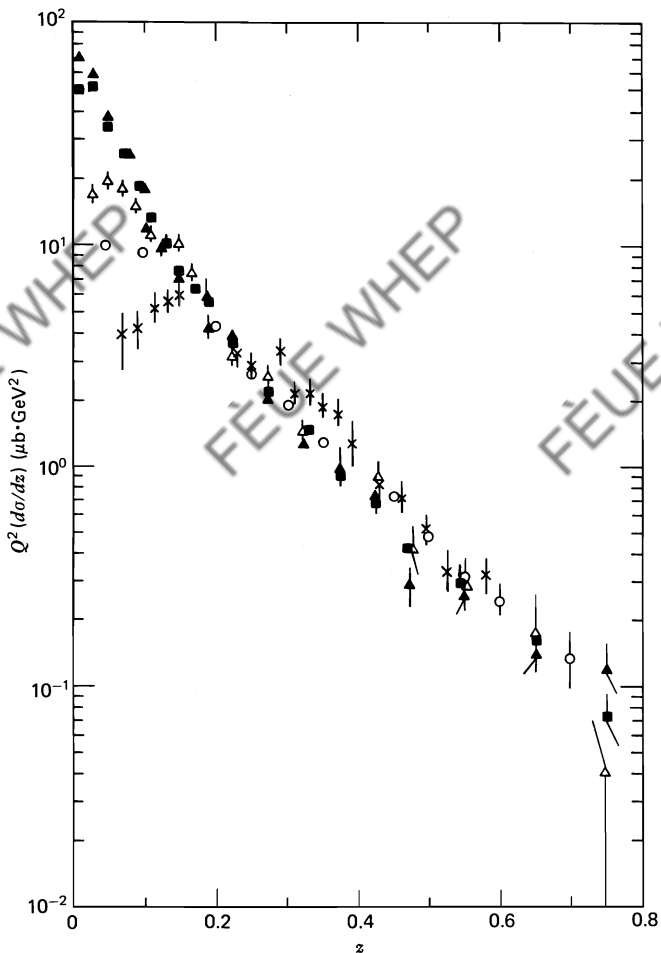


**Fig. 11.5**  $Q^2(d\sigma/dz) \sim 1/\sigma(d\sigma/dz)$  for  $e^-e^+ \rightarrow hX$  as measured as a function  $z$  at different center-of-mass energies  $Q$ : ( $\times$ ) 5 GeV; ( $\circ$ ) 7.4 GeV; ( $\Delta$ ) 12 GeV; ( $\blacksquare$ ) 27.4–31.6 GeV; ( $\blacktriangle$ ) 35.0–36.6 GeV. Data are from the Stanford Linear Accelerator and PETRA.

independent of  $Q$ . Such a scaling result is not a complete surprise, because we have relied on the scaling parton model to derive (11.12), see Fig. 11.4.

Figure 11.5 shows  $(1/\sigma)(d\sigma/dz)$  as a function of  $z$  for different values of  $Q^2$ . The scaling is not perfect. Gluon emission from the  $q$  or  $\bar{q}$  will introduce  $\log Q^2$  scaling violations in (11.13). Their qualitative trend is the same as in electroproduction, that is,  $\mathcal{F}(z, Q^2)$  will increase at small  $z$  with increasing values of  $Q^2$  but decrease for  $z$  near 1. The large violations of scaling for  $z \leq 0.2$ , seen in Fig. 11.5, are not exclusively due to gluon emission, however, and are the subject of the next section.

**EXERCISE 11.2** The fragmentation functions  $D(z)$  describe properties of partons and are therefore the same, no matter how the partons are produced. Consider the inclusive leptoproduction cross section  $\sigma(ep \rightarrow hX)$  and show that

$$\frac{1}{\sigma} \frac{d\sigma}{dz} (ep \rightarrow hX) = \frac{\sum_q e_q^2 f_q(x) D_q^h(z)}{\sum_q e_q^2 f_q(x)},$$

where  $f_q(x)$  are the proton structure functions of Chapter 9, see Fig. 11.6. The sum runs over the quarks and antiquarks that can be a parent of  $h$ .

**EXERCISE 11.3** Using charge conjugation and isospin invariance, show that

$$D_u^{\pi^+} = D_{\bar{u}}^{\pi^-} = D_d^{\pi^-} = D_{\bar{d}}^{\pi^+},$$

$$D_u^{\pi^-} = D_{\bar{u}}^{\pi^+} = D_d^{\pi^+} = D_{\bar{d}}^{\pi^-},$$

$$D_s^{\pi^+} = D_{\bar{s}}^{\pi^-}.$$

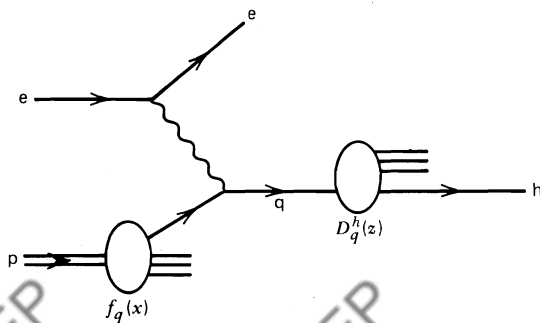


**Fig. 11.6** Deep inelastic leptoproduction of hadron  $h$ ;  $ep \rightarrow hX$ .

**EXERCISE 11.4** Using the notation

$$N_p^\pi(z) \equiv \frac{1}{\sigma} \frac{d\sigma}{dz} (ep \rightarrow \pi X),$$

show that, in the valence quark approximation for p, n,

$$\frac{\int dz [N_n^{\pi^+} - N_n^{\pi^-}]}{\int dz [N_p^{\pi^+} - N_p^{\pi^-}]} = \frac{2}{7}.$$

### 11.3 A Comment on Heavy Quark Production

Although the similarities between  $e^-e^+$  annihilation and lepto-production are becoming more and more evident, we must not forget one major difference. In lepto-production, u, d, and s quarks play a dominant role because they are plentiful inside the nucleon target. Charm quarks occur in roughly one in ten events, and were indeed ignored in the phenomenological discussion of Chapter 9. In  $e^-e^+$  annihilation, the situation is quite different. Beyond threshold ( $Q^2 > 4m_c^2$ ), the cross section rises steeply and readily attains a sizable fraction of its asymptotic value, see Fig. 11.3. It is clear from (11.3) that c and u quarks are produced with the same cross section, since both have  $e_q = +\frac{2}{3}$ . However, close to threshold, the final-state hadron structure of these relatively frequent charm-quark events is very different from the two-jet structure of a typical event involving light quarks. Then, the c and  $\bar{c}$  are produced almost at rest, and subsequently decay weakly into a rather large number of soft hadrons with low z. Therefore, an increase of low-z events is associated with the crossing of the charm threshold. This leads to a violation of scaling which will confuse, indeed simulate, the violations resulting from gluon emission.

The drastic violations of scaling, seen for  $z \lesssim 0.2$  in Fig. 11.5, are associated with the production of c and b quarks, resulting in events with a large multiplicity and low z values when the c and b thresholds are crossed. This mechanism has a positive aspect. The characteristic features of heavy quark events can serve as an experimental signature in the search for yet heavier quarks, such as the t quark in Table 1.5, as the energy of  $e^-e^+$  colliders is increased. A “step” in R also signals a new quark, for example, charm in Fig. 11.3. But for  $e_q = -\frac{1}{3}$ , this step is four times smaller and not easy to observe experimentally. Looking for deviations from the two-jet structure, characteristic of light quarks, is often a more sensitive test.

### 11.4 Three-Jet Events: $e^-e^+ \rightarrow q\bar{q}g$

From the viewpoint of perturbative QCD, we have only considered the leading  $O(\alpha^2)$  contribution to  $\sigma(e^-e^+ \rightarrow \text{hadrons})$ . In order  $\alpha^2\alpha_s$ , the q or  $\bar{q}$  can emit a

gluon, see Fig. 11.2d; and these  $e^- e^+ \rightarrow q\bar{q}g$  events have three fragmenting jets in the final state. The additional jet has a gluon as its parent parton. For larger values of the annihilation energy  $Q$ , such that  $\alpha_s(Q^2) \approx 0.1-0.2$ , we expect that three-jet events will account for roughly 10% of the final states. Our first task is to introduce kinematical variables to describe such events.

The momentum vectors of the  $q$ ,  $\bar{q}$ , and  $g$ , which are produced by a virtual photon ( $\gamma^*$ ) at rest, are displayed in Fig. 11.7. As in (11.9), we work with the energies, and with the longitudinal and transverse momenta of the partons, scaled to the  $e^-$  (and  $e^+$ ) beam energy. That is, we introduce

$$x_q \equiv \frac{2E_q}{O}, \quad x_{\bar{q}} \equiv \frac{2E_{\bar{q}}}{O}, \quad x_g \equiv \frac{2E_g}{O} \quad (11.14)$$

and

$$x_T \equiv \frac{2p_T}{Q}. \quad (11.15)$$

Like  $z$  in (11.9), all these ratios are bounded by 0 and 1. The four-momentum fractions in Fig. 11.7 are

$$\begin{aligned} (x_q; 0, 0, -x_q) &\quad \text{for q,} \\ (x_{\bar{q}}; x_T, 0, x_L) &\quad \text{for } \bar{q}, \\ (x_g; -x_T, 0, x_g - x_L) &\quad \text{for g.} \end{aligned} \tag{11.16}$$

The variables are defined relative to the most energetic jet, for example, the  $q$  jet in Fig. 11.7. Its direction is referred to as the “thrust axis.” The  $q$ ,  $\bar{q}$ , and  $g$  are coplanar in the plane  $y = 0$ . Longitudinal and transverse momentum conservation are embodied in (11.16), but energy conservation introduces the additional requirement that

$$x_g + x_{\bar{a}} + x_g = 2. \quad (11.17)$$

The zero mass of the  $\bar{q}$  and  $g$  leads to the further constraints [see (11.16)]

$$\begin{aligned} x_{\bar{q}}^2 - x_T^2 - x_L^2 &= 0, \\ x_g^2 - x_T^2 - (x_L - x_q)^2 &= 0. \end{aligned} \quad (11.18)$$

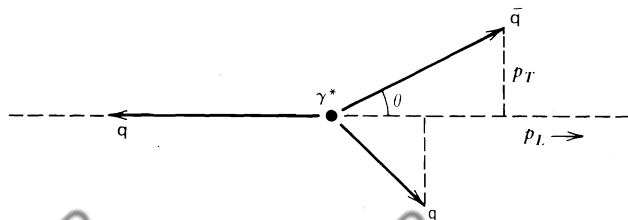


**Fig. 11.7** The process  $e^-e^+ \rightarrow \gamma^* \rightarrow q\bar{q}g$  in the center-of-mass frame.

From (11.18) and (11.17), it follows that

$$x_T^2 = \frac{4}{x_q^2} (1 - x_q)(1 - x_{\bar{q}})(1 - x_g). \quad (11.19)$$

**EXERCISE 11.5** Derive (11.19). Also show that the angle  $\theta$  between the  $q$  and  $\bar{q}$  directions in Fig. 11.7 is determined by the relation

$$x_{\bar{q}} = \frac{2(1 - x_q)}{2 - x_q - x_q \cos \theta}. \quad (11.20)$$

Let us now compute the cross section corresponding to Fig. 11.7. For this particular graph, the  $\bar{q}$  emits a softer gluon, so that

$$x_q \geq x_{\bar{q}} \geq x_g. \quad (11.21)$$

The most obvious experimental signature of gluon emission is that the  $q$  and  $\bar{q}$  are no longer produced back to back. The  $\bar{q}$  is produced with a transverse momentum fraction  $x_T$  relative to the direction of the quark. The relevant observable quantity is therefore  $d\sigma/dx_T^2$ . This cross section can readily be obtained using the Altarelli–Parisi–Weizsäcker–Williams technique of Section 10.9. Referring to Fig. 11.8, we obtain

$$\frac{d\sigma}{dx_{\bar{q}} dp_T^2} = \sigma(e^- e^+ \rightarrow q\bar{q}) \gamma_{\bar{q}\bar{q}}(x_{\bar{q}}, p_T^2), \quad (11.22)$$

see (10.57), where  $\sigma$  gives the probability for producing a  $q\bar{q}$  pair and  $\gamma_{\bar{q}\bar{q}}$  is the probability that the  $\bar{q}$  subsequently emits a gluon with a fraction  $(1 - x_{\bar{q}})$  of its momentum and a transverse momentum  $|p_T|$ . From (11.3) and (10.58), we have

$$\begin{aligned} \sigma(e^- e^+ \rightarrow q\bar{q}) &= \frac{4\pi\alpha^2}{Q^2} e_q^2, \\ \gamma_{\bar{q}\bar{q}}(x_{\bar{q}}, p_T^2) &= \gamma_{qq}(x_{\bar{q}}, p_T^2) = \frac{\alpha_s}{2\pi} \frac{1}{p_T^2} P_{qq}(x_{\bar{q}}). \end{aligned} \quad (11.23)$$

On substitution of (11.23) into (11.22), we find

$$\frac{1}{\sigma} \frac{d\sigma}{dx_{\bar{q}} dx_T^2} = \frac{\alpha_s}{2\pi} \frac{1}{x_T^2} P_{qq}(x_{\bar{q}}). \quad (11.24)$$

To calculate  $d\sigma/dx_T^2$ , it remains to integrate over all possible  $\bar{q}$  energy fractions  $x_{\bar{q}}$ . Using (10.31) for  $P_{qq}$ , we obtain

$$\frac{1}{\sigma} \frac{d\sigma}{dx_T^2} = 2 \frac{\alpha_s}{2\pi} \frac{1}{x_T^2} \int_{(x_{\bar{q}})_{\min}}^{(x_{\bar{q}})_{\max}} dx \frac{4}{3} \left( \frac{1 + x^2}{1 - x} \right). \quad (11.25)$$

An extra factor of 2 is included to allow for the equally probable diagram with  $q \leftrightarrow \bar{q}$ .

The integrand in (11.25) diverges when  $x_{\bar{q}} \rightarrow 1$ . The kinematic situation where  $x_{\bar{q}}$  reaches its maximum value is therefore of special interest. From (11.21), we see

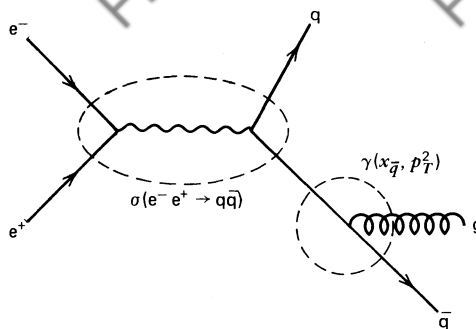


Fig. 11.8 The calculation of  $e^- e^+ \rightarrow q\bar{q}g$  using the probabilistic techniques of §10.9.

that the largest value allowed for  $x_{\bar{q}}$  is

$$x_{\bar{q}} = x_q. \quad (11.26)$$

This value can be approached if we make the emitted gluon as soft as possible, which, remembering that  $x_T$  is fixed, occurs when

$$x_g = x_T. \quad (11.27)$$

This kinematic configuration is shown in Fig. 11.9. Thus, from (11.17), we have

$$(x_q)_{\min} = (x_{\bar{q}})_{\max} = 1 - \frac{x_T}{2}. \quad (11.28)$$

Momentum is conserved for  $\theta$  or  $x_T$  not too large, but  $x_g$  is only exactly equal to  $x_T$  when  $\theta \rightarrow 0$ . Such approximations are implicit in the Altarelli–Parisi calculation of (11.25), see Chapter 10. Using (11.28), (11.25) becomes

$$\frac{1}{\sigma} \frac{d\sigma}{dx_T^2} \simeq \frac{8\alpha_s}{3\pi} \frac{1}{x_T^2} \int_{(x_{\bar{q}})_{\min}}^{1 - \frac{1}{2}x_T} \frac{dx}{1-x}, \quad (11.29)$$

where we have approximated  $1+x^2$  by 2. Finally, omitting all but the leading logarithmic term, we obtain

$$\frac{1}{\sigma} \frac{d\sigma}{dx_T^2} \simeq \frac{4\alpha_s}{3\pi} \frac{1}{x_T^2} \log\left(\frac{1}{x_T^2}\right).$$

(11.30)

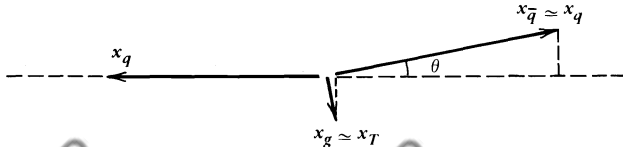


Fig. 11.9 The kinematic configuration giving the maximum value of  $x_{\bar{q}}$  for a given  $x_T$ .

### 11.5 An Alternative Derivation of the $e^-e^+\rightarrow q\bar{q}g$ Cross Section

The cross section (11.30) for  $e^-e^+\rightarrow \gamma^*\rightarrow q\bar{q}g$  can also be obtained using the Feynman rules of Chapter 6. We have calculated similar processes before. For instance, we found that  $\gamma^*q\rightarrow qg$  is given by (10.17) and that  $\gamma^*g\rightarrow q\bar{q}$  is given by (10.38). Proceeding in the same way, we find that the square of the amplitude for the sum of the  $\gamma^*\rightarrow q\bar{q}g$  diagrams of Fig. 11.10 is

$$|\mathcal{M}|^2 = N \left( \frac{t}{s} + \frac{s}{t} + \frac{2uQ^2}{st} \right) \quad (11.31)$$

where  $N$  represents the normalization factors and coupling constants and where

$$\begin{aligned} s &= (p_\gamma - p_q)^2, \\ t &= (p_\gamma - p_{\bar{q}})^2, \\ u &= (p_\gamma - p_g)^2, \end{aligned} \quad (11.32)$$

where  $Q^2 \equiv p_\gamma^2$ . Strictly speaking, for a parton process we should have denoted the Mandelstam variables by  $\hat{s}, \hat{t}, \hat{u}$ .

In order to rewrite (11.31) in terms of the energy fraction variables  $x_i$  of (11.14), we use

$$\begin{aligned} s &= Q^2(1-x_q), \\ t &= Q^2(1-x_{\bar{q}}), \\ u &= Q^2(1-x_g). \end{aligned} \quad (11.33)$$

These relations follow from four-momentum conservation, which gives

$$p_\gamma^2 = (p_q + p_{\bar{q}} + p_g)^2 = 2p_q \cdot p_{\bar{q}} + 2p_q \cdot p_g + 2p_{\bar{q}} \cdot p_g. \quad (11.34)$$

For instance,

$$\begin{aligned} s &= (p_{\bar{q}} + p_g)^2 = 2p_{\bar{q}} \cdot p_g = p_\gamma^2 - 2p_q \cdot (p_{\bar{q}} + p_g) \\ &= p_\gamma^2 - 2p_q \cdot p_\gamma = Q^2 \left( 1 - \frac{2E_q}{Q} \right) = Q^2(1-x_q). \end{aligned}$$

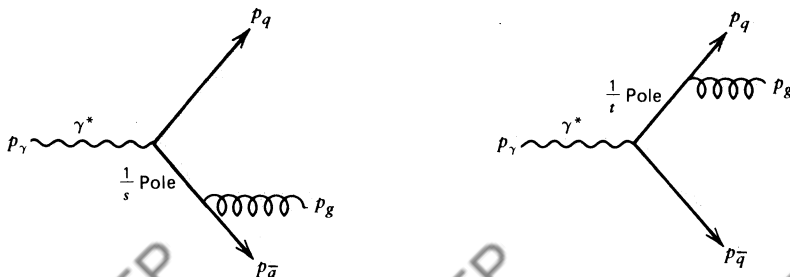


Fig. 11.10 The diagrams for  $\gamma^*\rightarrow q\bar{q}g$  showing the particle four-momenta.

Substituting (11.33) into (11.31), we obtain for  $\gamma^* \rightarrow q\bar{q}g$

$$|\mathcal{M}|^2 = N \frac{x_q^2 + x_{\bar{q}}^2}{(1 - x_q)(1 - x_{\bar{q}})}, \quad (11.35)$$

where we have used (11.17) to eliminate  $x_g$ . If we “attach” the  $e^- e^+$  pair, then, up to a factor (which changes  $N \rightarrow N'$ ), (11.35) gives the cross section for  $e^- e^+ \rightarrow q\bar{q}g$

$$\frac{d\sigma}{dx_q dx_{\bar{q}}} = N' \frac{x_q^2 + x_{\bar{q}}^2}{(1 - x_q)(1 - x_{\bar{q}})}. \quad (11.36)$$

To verify that (11.36) is equivalent to our previous result (11.24), we must change the variable  $x_q$  to  $x_T^2$ . We have

$$\frac{d\sigma}{dx_{\bar{q}} dx_T^2} = \frac{d\sigma}{dx_{\bar{q}} dx_q} \frac{dx_q}{dx_T^2}. \quad (11.37)$$

It is sufficient to use the small  $p_T$  approximation inherent in the Altarelli–Parisi result (11.24). Using (11.19), we find

$$\left| \frac{dx_T^2}{dx_q} \right| \simeq 4x_{\bar{q}}(1 - x_{\bar{q}}) \quad \text{for } x_q \simeq 1. \quad (11.38)$$

Thus, (11.36) may be written

$$\frac{d\sigma}{dx_{\bar{q}} dx_T^2} \simeq N' \left( \frac{1 + x_{\bar{q}}^2}{1 - x_{\bar{q}}} \right) \left[ \frac{1}{4(1 - x_q)(1 - x_{\bar{q}})x_{\bar{q}}} \right], \quad (11.39)$$

where here again we have assumed  $x_q \simeq 1$ . In this limit,  $x_{\bar{q}} \simeq (1 - x_g)$ , and so the factor in square brackets is just  $x_T^{-2}$ , as can be seen from (11.19). Thus, (11.39) becomes

$$\frac{d\sigma}{dx_{\bar{q}} dx_T^2} \simeq N' \frac{3}{4} P_{qq}(x_{\bar{q}}) \frac{1}{x_T^2}, \quad (11.40)$$

where  $P_{qq}$  is given by (10.31). This is the same as the Altarelli–Parisi result of (11.24), and, indeed, we can identify the normalization coefficient to be

$$N' = \frac{2\alpha_s}{3\pi} \sigma.$$

The exact  $O(\alpha_s)$  result is therefore

$$\frac{1}{\sigma} \frac{d\sigma}{dx_q dx_{\bar{q}}} = \frac{2\alpha_s}{3\pi} \frac{x_q^2 + x_{\bar{q}}^2}{(1 - x_q)(1 - x_{\bar{q}})}, \quad (11.41)$$

whereas (11.24) is the leading logarithmic approximation.

### 11.6 A Discussion of Three-Jet Events

The  $e^- e^+ \rightarrow q\bar{q}g$  events led to three hadronic jets in the final state. The distribution (11.30) can be written as

$$\frac{1}{\sigma} \frac{d\sigma}{dp_T^2} \sim \alpha_s \frac{1}{p_T^2} \log \left( \frac{Q^2}{4p_T^2} \right), \quad (11.42)$$

where  $p_T$  is the transverse momentum between the  $q$  and  $\bar{q}$  as a result of the emission of the gluon, recall Fig. 11.7. Only when the  $\bar{q}$  (or  $q$ ) recoils against  $g$  can its  $p_T$  relative to the  $q$  (or  $\bar{q}$ ) be nonzero. For two-jet events,  $e^- e^+ \rightarrow q\bar{q}$ , we have  $p_T = 0$ . Now (11.42) shows that, for a fixed  $p_T$ , the cross section ratio increases with increasing  $Q^2$ . That is, the number of  $\bar{q}$  jets with a transverse momentum  $p_T$  relative to the  $q$  jet increases with  $Q^2$ . This is a result of the increased probability of emitting a gluon with a given  $p_T$  value when the annihilation energy increases. The physics is identical to that in electroproduction. There, also, the cross section

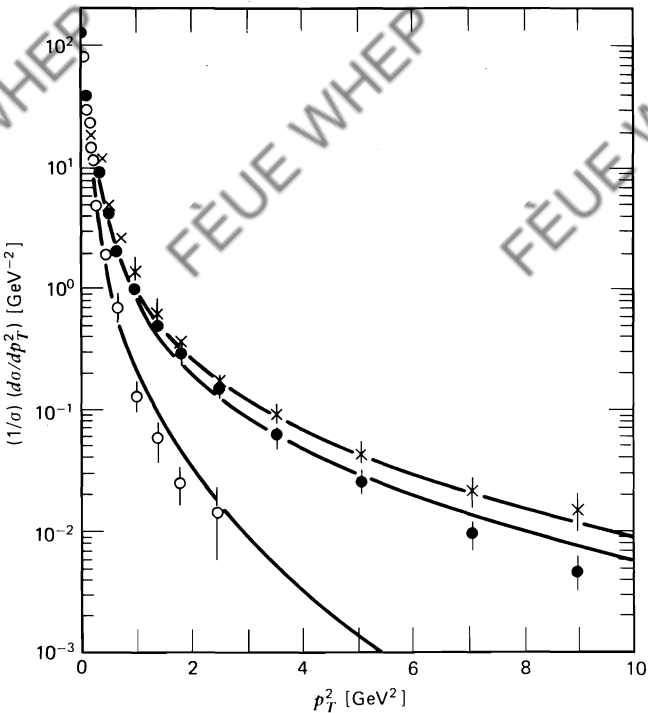


**Fig. 11.11** The transverse momentum distribution  $d\sigma/dp_T^2$  of hadrons relative to the thrust axis for different  $e^- e^+$  center-of-mass energies  $Q$ : (○)  $Q = 12$  GeV; (●)  $27.4 \leq Q \leq 31.6$  GeV; (×)  $35.0 \leq Q \leq 36.6$  GeV. The curves are a QCD calculation. Data are from PETRA.

for producing jets with transverse momentum  $p_T$  relative to the  $\gamma^*$ -direction increased as  $\log Q^2/p_T^2$  [compare (10.30) and (11.24)].

The hadron fragments of the  $\bar{q}$  jet will also have large  $p_T$  relative to the quark direction since the  $p_T$  distribution of these hadrons should follow the trend of the  $p_T$  distribution of jets. The two distributions can be explicitly related using the  $D$  functions introduced in Section 11.2. The resulting  $p_T$  and  $Q^2$  dependence of hadrons relative to the thrust axis (whichever parton it refers to) is shown in Fig. 11.11. In some events, all three jets will be well separated despite the  $k_T \approx 300$  MeV of the daughter hadrons relative to their parent jet. One such event is shown in Fig. 11.12.

The assumption that  $\alpha_s$  is constant in (11.42) requires explanation. If we had taken  $\alpha_s(Q^2) \sim 1/\log Q^2$ , then the above discussion would be meaningless. The

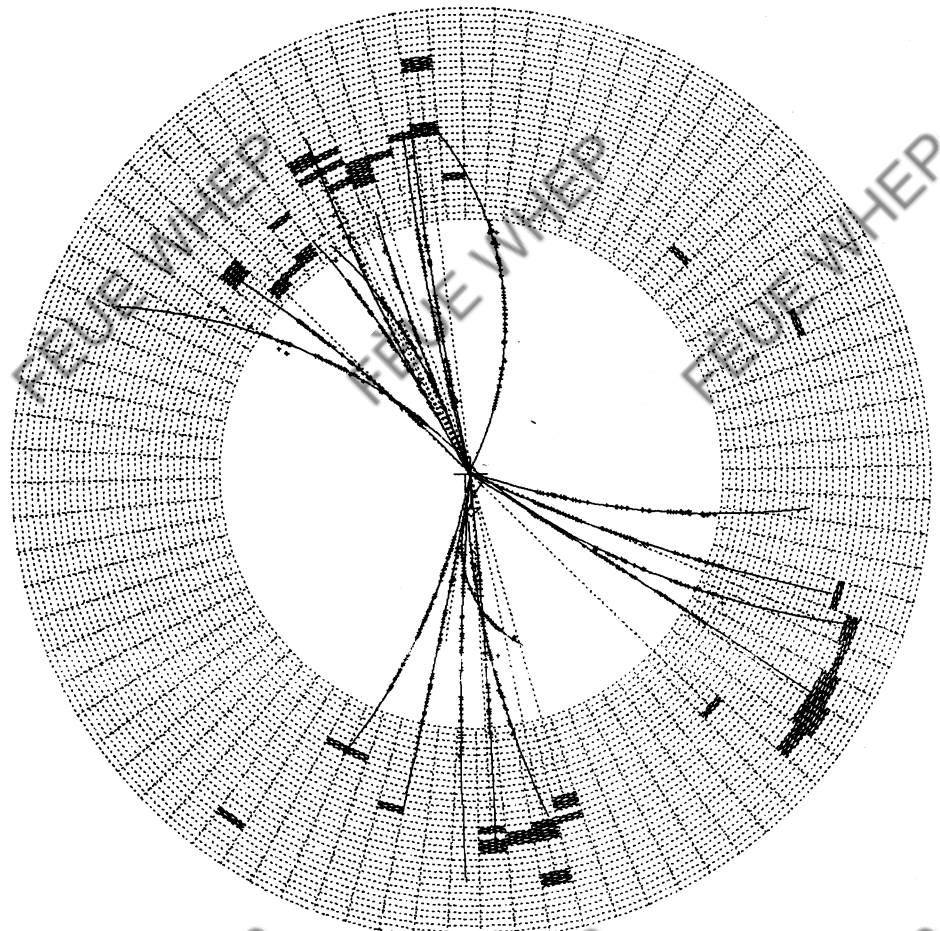


Fig. 11.12 A three-jet event observed by the JADE detector at PETRA.

crucial point is that we are discussing a process with two momentum scales,  $p_T^2$  and  $Q^2$  with  $p_T^2 \ll Q^2$ , a situation already encountered in Exercise 10.7. We argued there that  $\alpha_s$  is in fact  $\alpha_s(p_T^2)$ , but noted that keeping  $\alpha_s$  constant gave the correct result to leading order.

**EXERCISE 11.6** The  $x_T$  distribution (11.30) can be translated into an “acollinearity” distribution  $d\sigma/d\theta$ , where  $\theta$  is the angle between the  $q$  and  $\bar{q}$  jet directions defined in (11.20) and Fig. 11.7. Show that for  $\theta$  not too large,

$$\frac{1}{\sigma} \frac{d\sigma}{d\theta} \simeq \frac{8\alpha_s}{3\pi} \frac{1}{\theta} \log\left(\frac{1}{\theta^2}\right).$$

An exact result can be obtained using (11.41) instead of (11.30).

We have repeatedly drawn attention to the fact that hadrons fragmenting from a quark, or any other parton, form a cone around the direction  $\mathbf{p}_q$ . It is an experimental fact that the  $\langle k_T \rangle$  for the hadron fragments is about 300 MeV, where  $T$  refers to the direction transverse to  $\mathbf{p}_q$ . We might anticipate that at higher energies the fragmentation cone would narrow,

$$\langle \theta \rangle \simeq \frac{\langle k_T \rangle}{p_q} \simeq \frac{0.3 \text{ GeV}}{Q/2}, \quad (11.43)$$

and the jets become narrow bundles of energetic particles when  $Q$  increases. This is not the case. Gluon radiation results in an increase of the  $\langle k_T \rangle$  of the hadrons which we associate with the original quark or antiquark jet. It is increasingly probable that in a very high-energy two-jet event, one of the observed jets is actually the fragmentation product of a  $qg$  or  $\bar{q}g$  state as a result of gluon emission by the  $q$  or  $\bar{q}$ . The experimentalist will recognize such a jet as being “fatter” or having increased  $\langle k_T \rangle$ . This dynamical broadening of  $\langle \theta \rangle$  almost compensates for the kinematic narrowing given by (11.43). As a consequence, it turns out that the narrowing of jets with increasing  $Q^2$  is a logarithmic and not a linear effect, with

$$\langle \theta \rangle \sim \frac{1}{\log Q^2}. \quad (11.44)$$

This result has to be derived with care. We shall only briefly sketch how it comes about. By definition,

$$\langle k_T \rangle \sim \int_0^Q k_T \frac{d\sigma}{dk_T}. \quad (11.45)$$

Let us assume that the  $k_T$  of the hadrons in the broadened jet just reflects the relative  $k_T$  of the  $q$  or  $\bar{q}$  and the emitted gluon. Then,  $d\sigma/dk_T$  in (11.45) is nothing but the familiar transverse momentum distribution of gluon emission

$$\frac{d\sigma}{dk_T} \sim \frac{\alpha_s}{k_T}.$$

We here neglect all logarithms and therefore also take  $\alpha_s$  to be constant. In this approximation,  $d\sigma/dk_T$  is the same as (11.42). Substituting into (11.45) gives

$$\langle k_T \rangle \sim \alpha_s \int_0^Q dk_T \sim \alpha_s Q,$$

and from (11.43) we see that  $\langle \theta \rangle \sim \alpha_s$ . The logarithmic narrowing of the jets (11.44) comes about when we incorporate the running of  $\alpha_s \sim 1/\log Q^2$ . A proper justification of this result is complicated (e.g., Dokshitzer et al., 1980). However, the phenomenological message is clear: jet identification which at low energies is only possible through clever statistical analysis of  $e^+ e^- \rightarrow$  hadron events, should be simpler for high-energy experiments due to the increased collimation predicted by (11.44).

## 11.7 QCD Corrections to $e^- e^+ \rightarrow$ Hadrons

The parton model result (11.6),

$$R \equiv \frac{\sigma(e^- e^+ \rightarrow \text{hadrons})}{\sigma(e^- e^+ \rightarrow \mu^- \mu^+)} = 3 \sum_q e_q^2, \quad (11.46)$$

which we derived from  $\sigma(e^- e^+ \rightarrow q\bar{q})$ , will be modified by the possibility of gluon emission from the  $q$  or  $\bar{q}$ . The order  $\alpha_s$  diagrams are shown in Fig. 11.10, and the cross section  $d\sigma/dx_q dx_{\bar{q}}$  is given in (11.41). To calculate the order  $\alpha_s$  correction to  $R$ , we must integrate over both  $x_q$  and  $x_{\bar{q}}$  from 0 to 1. In doing this, we encounter a problem which is common in perturbative QCD calculations. The integrand, (11.41), diverges as  $x_q$  or  $x_{\bar{q}}$  goes to 1. To trace the origin of the problem, consider, for instance, the factor  $1 - x_q$  in the denominator. Using (11.33),

$$\begin{aligned} 1 - x_q &= \frac{s}{Q^2} = \frac{2 p_{\bar{q}} \cdot p_g}{Q^2} \\ &= \frac{2}{Q^2} E_{\bar{q}} E_g (1 - \cos \theta_{\bar{q}g}) \end{aligned} \quad (11.47)$$

and so  $1 - x_q$  vanishes when the gluon becomes soft ( $E_g \rightarrow 0$ ) or when  $\bar{q}$  and  $g$  become collinear ( $\cos \theta_{\bar{q}g} \rightarrow 1$ ). The first type of divergence is called an *infrared divergence* (see Chapter 7), and the second is called a *collinear divergence* (or mass singularity since, if the quark *or* the gluon had nonzero mass,  $\cos \theta_{\bar{q}g} = 1$  would be kinematically impossible). In QED, where leptons do have a mass, such mass singularities do not occur.

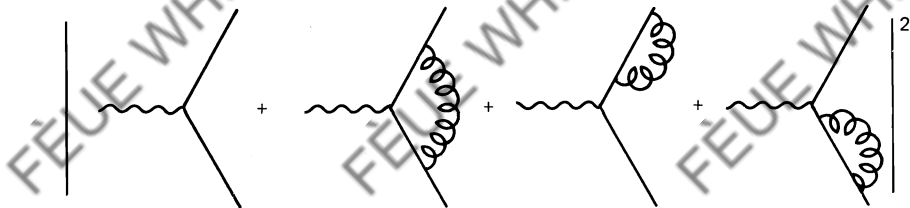
To proceed, we must regularize these infrared and mass singularities. One way to accomplish this is to give the gluon a fictitious mass  $m_g$  and to repeat the calculation of the Feynman diagrams of Fig. 11.10 which led to (11.41). A

straightforward but lengthy calculation yields

$$\begin{aligned}
 \sigma_{\text{real}} &= \left| \text{Diagram 1} + \text{Diagram 2} \right|^2 \\
 &= \int dx_q dx_{\bar{q}} \frac{d\sigma}{dx_q dx_{\bar{q}}} \\
 &= \sigma_q \frac{\alpha_s}{2\pi} \frac{4}{3} \left\{ \log^2 \left( \frac{m_g}{Q} \right) + 3 \log \left( \frac{m_g}{Q} \right) - \frac{\pi^2}{3} + 5 \right\}, \quad (11.48)
 \end{aligned}$$

where  $\sigma_q$  denotes  $\sigma(e^- e^+ \rightarrow q\bar{q})$ . As expected, (11.48) is divergent when  $m_g \rightarrow 0$ .

Obviously, (11.48) cannot be the final answer since it depends on the fictitious mass  $m_g$ , whereas the correct result should not. However, there is another  $O(\alpha_s)$  contribution. This additional  $O(\alpha_s)$  term occurs in



and corresponds to the interference of the  $\gamma^* \rightarrow q\bar{q}$  diagram, with the sum of the three diagrams containing virtual gluon loops (see Section 10.8). This interference term gives a contribution

$$\sigma_{\text{virtual}} = \sigma_q \frac{\alpha_s}{2\pi} \frac{4}{3} \left\{ -\log^2 \left( \frac{m_g}{Q} \right) - 3 \log \left( \frac{m_g}{Q} \right) + \frac{\pi^2}{3} - \frac{7}{2} \right\}. \quad (11.49)$$

The total order  $\alpha_s$  contribution is

$$\sigma = \sigma_{\text{real}} + \sigma_{\text{virtual}} = \sigma_q \frac{\alpha_s}{\pi}, \quad (11.50)$$

which is finite and independent of  $m_g$ , as indeed it must be.

The cancellation of the singularities between the contributions with the emission of real and virtual gluons is not just a property of this particular process. It occurs over and over again. For example, in Section 10.8, we already discussed the analogous cancellation in deep inelastic scattering. These particular cancellations are examples of a general theorem due to Kinoshita, Lee, and Nauenberg. The reason that we did not meet this mechanism earlier in the chapter is because we choose to compute the cross section for the production of gluons with a fixed,

nonzero  $p_T$ . Then,  $x_q$  and  $x_{\bar{q}}$  are unable to reach 1, and the denominator in (11.41) cannot vanish. This choice also excludes the diagrams with the virtual gluon loops for which  $p_T = 0$ .

Including the order  $\alpha_s$  correction to  $R$  of (11.46), we obtain

$$R = 3 \sum_q e_q^2 \left[ 1 + \frac{\alpha_s(Q^2)}{\pi} \right]. \quad (11.51)$$

For a typical  $Q^2$  where  $\alpha_s \sim 0.2$ , the correction is small and cannot easily be distinguished within the errors of the present measurements. Note, however, that  $R$  is no longer exactly constant since  $\alpha_s$  is a function of  $Q^2$ , see (7.65). This is another example of a scaling parton model result being modified by  $\log Q^2$  corrections arising from the emission of gluons.

## 11.8 Perturbative QCD

We have seen that hadrons with unexpectedly large transverse momenta in both deep inelastic scattering ( $ep \rightarrow hX$ ) and  $e^-e^+$  annihilation ( $e^-e^+ \rightarrow h$ ) have a common origin. This is an example of parton diagrams for one process being used, after crossing, in another process. In this way, the same underlying QCD process can be tested in totally different experimental situations. Some examples are shown in Fig. 11.13. The ingredients are  $q$ ,  $\bar{q}$ ,  $g$ ,  $\gamma$ , and  $\gamma^*$ ; a lepton pair (i.e.,  $e^-e^+$ ,  $\mu^-\mu^+$ ); the structure functions  $f(x)$ , giving the probability of finding partons in the parent hadron; and, finally, the fragmentation functions  $D(z)$ , denoting the probability of final-state hadrons emerging from the partons. Figure 11.13 shows just some of the possible ways of combining these ingredients.

To be a useful test of QCD, it is important that the process is a short-distance interaction, so that  $\alpha_s(Q^2)$  is small enough for perturbation theory to be valid. The processes of Fig. 11.13 satisfy this requirement. We must also recall from Chapter 9 the criteria for the validity of the parton model (which is the lowest-order approximation to QCD). A large energy and a large momentum transfer are required to justify the impulse approximation used in the parton model calculation. Through the uncertainty principle, the large energy requirement guarantees that the time scale of the parton interaction is short, so that we can ignore the interactions with “spectator” partons (that is, with constituents which are not directly involved in the QCD subprocess). A large momentum (e.g.,  $Q^2$ ,  $p_T^2$ , a heavy quark mass) guarantees that the process occurs at a short range so that  $\alpha_s$  is small.

As an example, consider processes (d) and (e) of Fig. 11.13. Even when the initial protons collide with very high energy, the momentum transferred in the process also has to be large for perturbative QCD to be valid. This can be ensured by requiring that the photon be produced with a large transverse momentum,

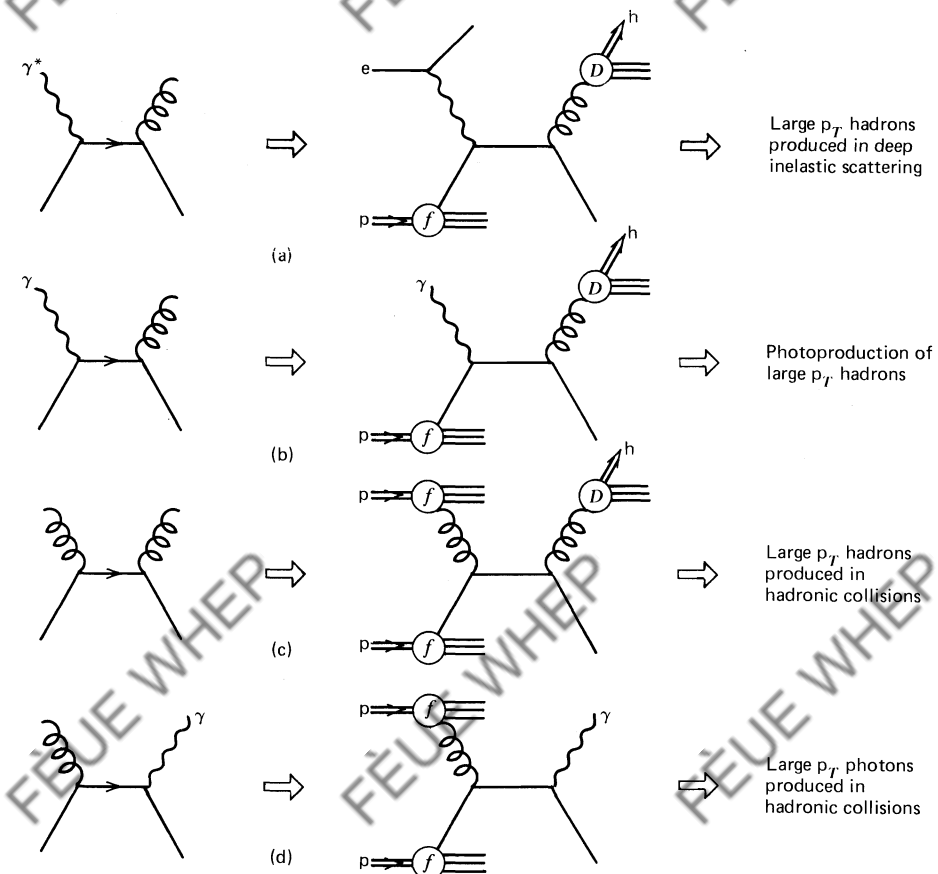


**Fig. 11.13** Various observable processes which contain  $\gamma$  (or gluon)-quark Compton scattering, or the crossed reaction, as a parton subprocess;  $f$  and  $D$  denote structure and fragmentation functions, respectively.

process (d), or by giving it a large  $Q^2$  by detecting a lepton pair in the final state with a large invariant mass, process (e).

Figure 11.13 shows only one parton diagram for each process. To the same order of  $\alpha_s$ , other diagrams have to be computed to obtain a result which can be compared with experiment. For instance, in process (c), another possibility is quark-quark scattering via gluon exchange, whereby quarks in the beam scatter at large angles off target quarks producing two quark jets in the final state with large transverse momentum (see also Exercise 11.7).

There are many applications of perturbative QCD. Reviews are given, for example, by Field (1979), Ellis and Sachrajda (1979), Reya (1981), Altarelli (1982), Collins and Martin (1982), and Pennington (1983). The phenomenological evidence is that the theory can successfully confront experiment in all such

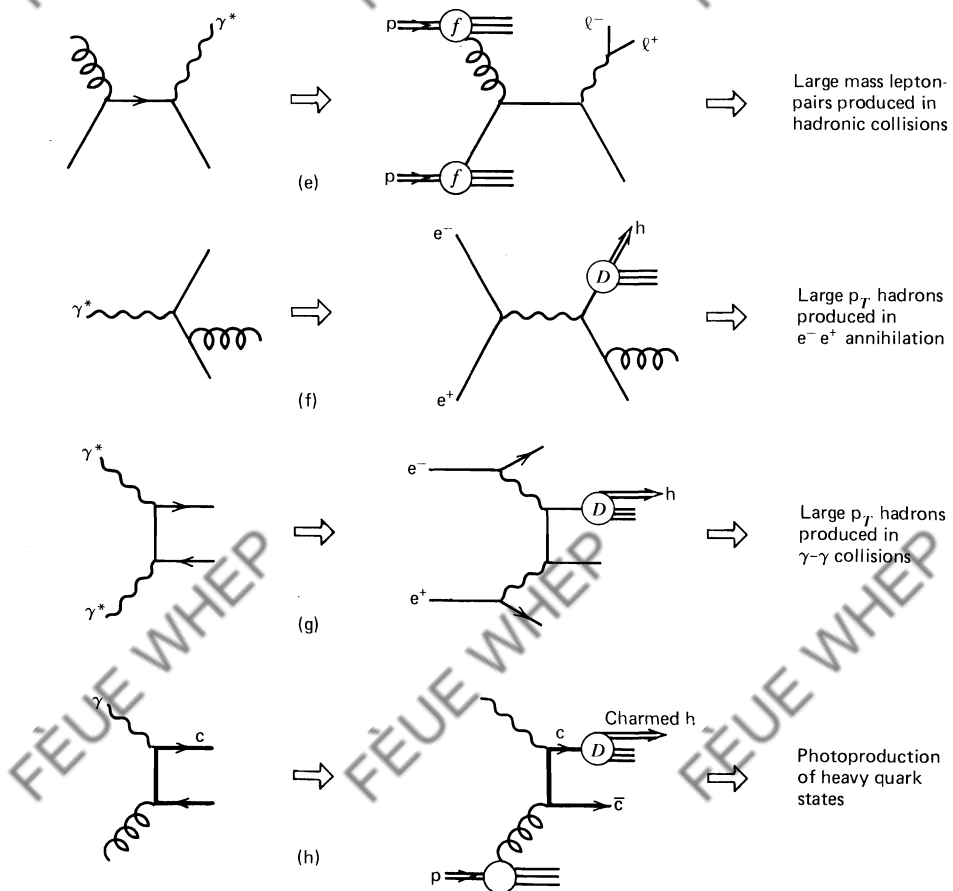


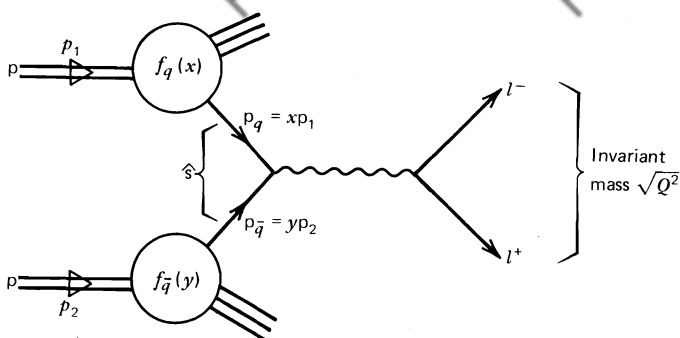
Fig. 11.13 (Continued)

situations. Unfortunately, however, due primarily to color confinement, no QCD tests exist (or can even be envisaged) that are comparable to the accuracy of the lepton magnetic moment calculation in QED.

**EXERCISE 11.7** List all parton processes, in addition to those shown in Fig. 11.13, that can contribute to reaction (c) to the same order of  $\alpha_s$ . Comment on the relative strengths of the subprocesses, comparing, in particular, pp- and p $\bar{p}$ -initiated reactions.

## 11.9 A Final Example: The Drell-Yan Process

Diagram (e) of Fig. 11.13 gives an  $O(\alpha_s^2 \alpha_s)$  contribution to the cross section for the hadronic production of lepton pairs. However, this is a correction to the

Fig. 11.14 The Drell-Yan process,  $pp \rightarrow l^- l^+ X$ .

lower-order process  $q\bar{q} \rightarrow \gamma^* \rightarrow l^- l^+$  shown in Fig. 11.14, which is known as the Drell-Yan process. Together with  $e^- e^+$  annihilation and deep inelastic lepton production, it has played an important role in determining the structure functions and in testing the parton model and its QCD corrections.

To calculate the cross section corresponding to Fig. 11.14, we begin with that for the parton subprocess,

$$\hat{\sigma}(q\bar{q} \rightarrow l^- l^+) = \frac{4\pi\alpha^2}{3Q^2} e_q^2, \quad (11.52)$$

see (11.3). In order to embed (11.52) in the hadronic process, we first rewrite it as a differential cross section,  $d\hat{\sigma}/dQ^2$ , for the production of lepton pairs having invariant mass  $\sqrt{Q^2}$ , where

$$Q^2 = \hat{s} = (p_q + p_{\bar{q}})^2. \quad (11.53)$$

That is,

$$\frac{d\hat{\sigma}}{dQ^2} = \frac{4\pi\alpha^2}{3Q^2} e_q^2 \delta(Q^2 - \hat{s}). \quad (11.54)$$

The hadronic cross section can now be obtained using the structure functions  $f_i(x)$ , familiar from deep inelastic scattering (Chapter 9). We obtain

$$\frac{d\sigma}{dQ^2} (pp \rightarrow l\bar{l}X) = \left(\frac{1}{3}\right)\left(\frac{1}{3}\right) 3 \sum_q \int dx \int dy f_q(x) f_{\bar{q}}(y) \frac{d\hat{\sigma}}{dQ^2}, \quad (11.55)$$

where the sum is over quark flavors. The factors of  $\frac{1}{3}$  average over the initial  $q$  and  $\bar{q}$  colors and the factor 3 sums over the  $q\bar{q}$  color combinations which can annihilate to form a colorless virtual photon. The  $q$  and  $\bar{q}$  carry fractions  $x$  and  $y$  of the momenta of the protons, respectively, and so (11.53) becomes

$$\hat{s} = (xp_1 + yp_2)^2 \approx xys, \quad (11.56)$$

where  $s \approx 2 p_1 \cdot p_2$  is the center-of-mass energy squared of the colliding protons. From (11.54)–(11.56), we obtain

$$\frac{d\sigma}{dQ^2} (\text{pp} \rightarrow l\bar{l} X) = \frac{4\pi\alpha^2}{9Q^4} \sum_q e_q^2 \int dx \int dy f_q(x) f_{\bar{q}}(y) \delta\left(1 - xy \frac{s}{Q^2}\right).$$

(11.57)

In lowest order, with no gluon emission, we expect a scaling result. This is hidden in (11.57). Although the cross section is a function of both the collision energy  $\sqrt{s}$  and the lepton pair mass  $\sqrt{Q^2}$ , the quantity

$$Q^4 \frac{d\sigma}{dQ^2} = \mathcal{F}\left(\frac{s}{Q^2}\right) \quad (11.58)$$

is a function only of the ratio  $s/Q^2$ . Figure 11.15 shows that the data satisfy this scaling law rather well.

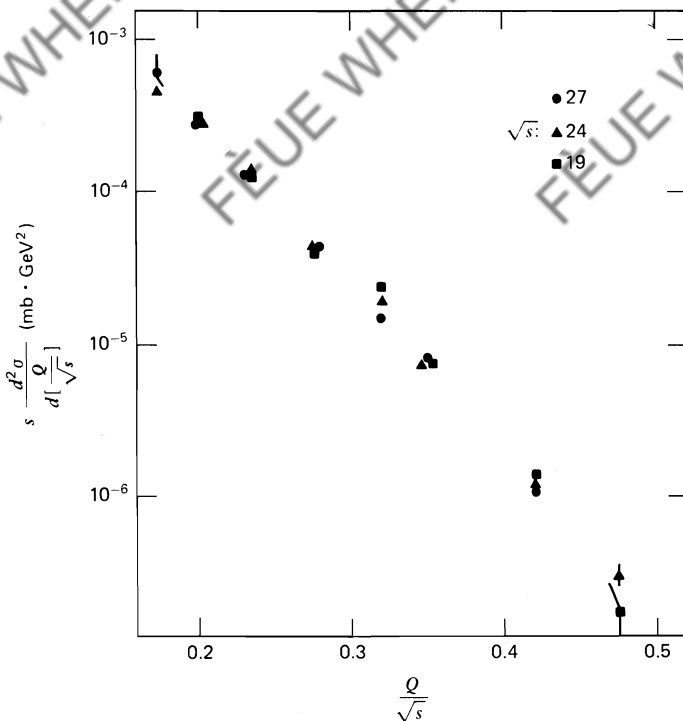


**Fig. 11.15** Scaling in the Drell-Yan process. The scaling test shown is equivalent to (11.58);  $\sqrt{s}$  in GeV. Data are from the Fermi laboratory.

**EXERCISE 11.8** Express the sum in (11.57) in terms of the valence and sea quark structure functions introduced in Chapter 9. Do the same for lepton pair production in  $\bar{p}p$  and  $\pi^\pm p$  interactions.

**EXERCISE 11.9** The data for an (isoscalar) carbon target indicate that the ratio

$$\frac{\sigma(\pi^+ C \rightarrow \mu^-\mu^+ X)}{\sigma(\pi^- C \rightarrow \mu^-\mu^+ X)}$$

is approximately unity for small values of  $Q^2/s$  but decreases toward  $\frac{1}{4}$  as  $Q^2/s$  approaches 1. Explain why this is in agreement with the Drell-Yan prediction. Note that  $xy = Q^2/s$ .

**EXERCISE 11.10** Including diagrams with gluons introduces logarithmic scaling violations in (11.58). Draw the diagrams which give an  $O(\alpha^2\alpha_s)$  contribution to the lepton pair cross section. Compute the cross section for the diagram shown in Fig. 11.13e.

# 12

## Weak Interactions

The observed lifetimes of the pion and muon are considerably longer than those of particles which decay either through color (i.e., strong) or electromagnetic interactions. It is found that

$$\begin{aligned}\pi^- &\rightarrow \mu^- \bar{\nu}_\mu & \text{with } \tau = 2.6 \times 10^{-8} \text{ sec,} \\ \mu^- &\rightarrow e^- \bar{\nu}_e \nu_\mu & \text{with } \tau = 2.2 \times 10^{-6} \text{ sec,}\end{aligned}\tag{12.1}$$

whereas particles decay by color interactions in about  $10^{-23}$  sec and through electromagnetic interactions in about  $10^{-16}$  sec (for example,  $\pi^0 \rightarrow \gamma\gamma$ ). The lifetimes are inversely related to the coupling strength of these interactions, with the longer lifetime of the  $\pi^0$  reflecting the fact that  $\alpha \ll \alpha_s$ . The pion and muon decays are evidence for another type of interaction with an even weaker coupling than electromagnetism.

Though all hadrons and leptons experience this weak interaction, and hence can undergo weak decays, they are often hidden by the much more rapid color or electromagnetic decays. However, the  $\pi^\pm$  and  $\mu$  are special. They cannot decay via the latter two interactions. The  $\pi$  is the lightest hadron. Whereas the neutral  $\pi$  can decay into photons, the charged pions cannot. As a result, the weak decay given in (12.1) is the dominant one. The reason why (12.1) is the dominant decay of the  $\mu$  is interesting. In principle, the  $\mu$  could decay electromagnetically via  $\mu \rightarrow e\gamma$ . The fact that the decay mode  $\mu \rightarrow e\gamma$  is not seen and that the particular decay modes (12.1) occur are evidence for additive conserved lepton numbers: the electron number ( $L_e$ ) and the muon number ( $L_\mu$ ). For example, the electron number assignments are

$$\begin{aligned}L_e &= +1: & e^- \text{ and } \nu_e, \\ L_e &= -1: & e^+ \text{ and } \bar{\nu}_e, \\ L_e &= 0: & \text{all other particles.}\end{aligned}\tag{12.2}$$

Similar assignments are made for  $L_\mu$  and  $L_\tau$ . Clearly,  $L_\mu = 1$  and  $L_e = 0$  for both the initial and final states of  $\mu^- \rightarrow e^- \bar{\nu}_e \nu_\mu$ , so this decay is consistent with the conservation of these quantum numbers; but  $\mu^- \rightarrow e^- \gamma$  is not. In fact, known reactions conserve these three lepton numbers separately (see Section 12.12 for a further discussion).

**EXERCISE 12.1** Give the  $\pi^+$  and  $\mu^+$  decay processes. List the possible decay modes of the  $\tau^-$  lepton (the  $\tau$  is the third lepton in the sequence e,  $\mu$ ,  $\tau$  with a mass  $m_\tau = 1.8$  GeV).

The two examples of weak decays given in (12.1) involve neutrinos. Neutrinos are unique in that they can only interact by weak interactions. They are colorless and electrically neutral and, within experimental limits, also massless. Neutrinos are frequently found among the products of a weak decay, but not always. For example, a  $K^+$  meson has the following weak decay modes:

$$\left. \begin{array}{l} K^+ \rightarrow \mu^+ \nu_\mu, e^+ \nu_e \\ K^+ \rightarrow \pi^0 \mu^+ \nu_\mu, \pi^0 e^+ \nu_e \end{array} \right\} \text{semileptonic decays,} \quad (12.3)$$

$$K^+ \rightarrow \pi^+ \pi^0, \pi^+ \pi^+ \pi^-, \pi^+ \pi^0 \pi^0 \quad \text{nonleptonic decays.}$$

The customary terminology is given on the right.

The weak interaction is also responsible for the  $\beta$ -decay of atomic nuclei, which involves the transformation of a proton to a neutron (or vice versa). Examples involving the emission of an  $e^+ \nu_e$  lepton pair are

$$\begin{aligned} {}^{10}\text{C} &\rightarrow {}^{10}\text{B}^* + e^+ + \nu_e, \\ {}^{14}\text{O} &\rightarrow {}^{14}\text{N}^* + e^+ + \nu_e. \end{aligned} \quad (12.4)$$

Here, one of the protons in the nucleus transforms into a neutron via

$$p \rightarrow n e^+ \nu_e. \quad (12.5)$$

For free protons, this is energetically impossible (check the particle masses), but the crossed reaction, the  $\beta$ -decay process

$$n \rightarrow p e^- \bar{\nu}_e, \quad (12.6)$$

is allowed and is the reason for the neutron's instability (mean life 920 sec). Without the weak interaction, the neutron would be as stable as the proton, which has a lifetime in excess of  $10^{30}$  years.

## 12.1 Parity Violation and the $V-A$ Form of the Weak Current

Fermi's explanation of  $\beta$ -decay (1932) was inspired by the structure of the electromagnetic interaction. Recall that the invariant amplitude for electromagnetic electron–proton scattering (Fig. 12.1) is

$$\mathcal{M} = (e \bar{u}_p \gamma^\mu u_p) \left( \frac{-1}{q^2} \right) (-e \bar{u}_e \gamma_\mu u_e), \quad (12.7)$$

see (6.8), where we have treated the proton as a structureless Dirac particle.  $\mathcal{M}$  is the product of the electron and proton electromagnetic currents, together with the propagator of the exchanged photon, see Section 6.2. To facilitate the comparison

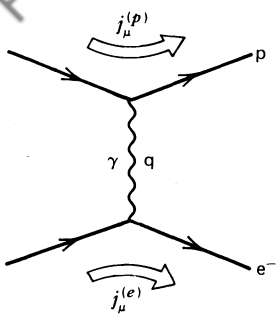


Fig. 12.1 Electron–proton (electromagnetic) scattering.

with weak interactions, we define, for example, an electron electromagnetic current of the form

$$e j_\mu^{em} \equiv j_\mu^{fi}(0) = -e \bar{u}_f \gamma_\mu u_i,$$

where  $j_\mu^{fi}(x)$  is given by (6.6). Thus, the invariant amplitude, (12.7), becomes

$$\mathcal{M} = -\frac{e^2}{q^2} (j_\mu^{em})_p (j_{\mu e}^{emp})_e.$$

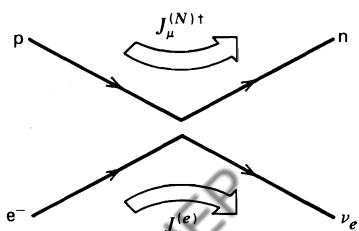
The  $\beta$ -decay process (12.5), or its crossed form

$$pe^- \rightarrow n\nu_e,$$

is shown in Fig. 12.2. By analogy with the current-current form of (12.7), Fermi proposed that the invariant amplitude for  $\beta$ -decay be given by

$$\mathcal{M} = G (\bar{u}_n \gamma^\mu u_p) (\bar{u}_{\nu_e} \gamma_\mu u_e), \quad (12.8)$$

where  $G$  is the weak coupling constant which remains to be determined by experiment;  $G$  is called the Fermi constant. Note the charge-raising or charge-lowering structure of the weak current. We speak of these as the “charged weak currents.” (The existence of a weak current that is electrically neutral, like the electromagnetic current, was not revealed until much later in 1973, see Section 12.9). Also note the absence of a propagator in (12.8). We return to this point in Section 12.2.

Fig. 12.2 The diagram for  $\beta$ -decay,  $p \rightarrow ne^+\nu_e$ , showing the weak currents.

Fermi's inspired guess of a vector–vector form of the weak amplitude  $\mathcal{M}$  is a very specific choice from among the various Lorentz invariant amplitudes that can in general be constructed using the bilinear covariants of (5.52). There is *a priori* no reason to use only vectors. The amplitude (12.8) explained the properties of some features of  $\beta$ -decay, but not others. Over the following 25 years or so, attempts to unravel the true form of the weak interaction led to a whole series of ingenious  $\beta$ -decay experiments, reaching a climax with the discovery of parity violation in 1956. Amazingly, the only essential change required in Fermi's original proposal was the replacement of  $\gamma^\mu$  by  $\gamma^\mu(1 - \gamma^5)$ . Fermi had not foreseen parity violation and had no reason to include a  $\gamma^5\gamma^\mu$  contribution; a mixture of  $\gamma^\mu$  and  $\gamma^5\gamma^\mu$  terms automatically violates parity conservation, see (5.67).

In 1956, Lee and Yang made a critical survey of all the weak interaction data. A particular concern at the time was the observed nonleptonic decay modes of the kaon,  $K^+ \rightarrow 2\pi$  and  $3\pi$ , in which the two final states have opposite parities. (People, in fact, believed that two different particles were needed to explain the two final states.) Lee and Yang argued persuasively that parity was not conserved in weak interactions. Experiments to check their assertion followed immediately. The first of these historic experiments serves as a good illustration of the effects of parity violation. The experiment studied  $\beta$ -transitions of polarized cobalt nuclei:



The nuclear spins in a sample of  $^{60}\text{Co}$  were aligned by an external magnetic field, and an asymmetry in the direction of the emitted electrons was observed. The asymmetry was found to change sign upon reversal of the magnetic field such that electrons prefer to be emitted in a direction opposite to that of the nuclear spin. The essence of the argument is sketched in Fig. 12.3. The observed correlation between the nuclear spin and the electron momentum is explained if the required  $J_z = 1$  is formed by a right-handed antineutrino,  $\bar{\nu}_R$ , and a left-handed electron,  $e_L$ .

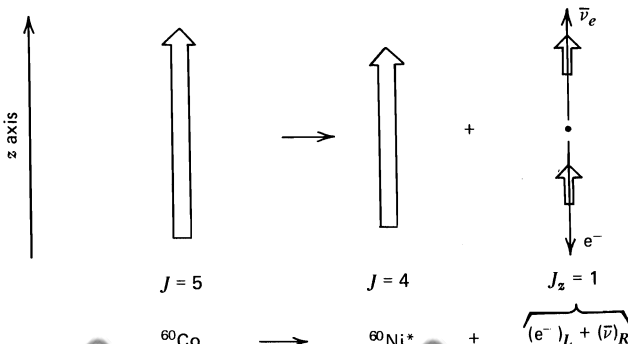


Fig. 12.3 The  $^{60}\text{Co}$  experiment: the electron is emitted preferentially opposite the direction of the spin of the  $^{60}\text{Co}$  nucleus.

The cumulative evidence of many experiments is that indeed only  $\bar{\nu}_R$  (and  $\nu_L$ ) are involved in weak interactions. The absence of the “mirror image” states,  $\bar{\nu}_L$  and  $\nu_R$ , is a clear violation of parity invariance (see Section 5.7). Also, charge conjugation,  $C$ , invariance is violated, since  $C$  transforms a  $\nu_L$  state into a  $\bar{\nu}_L$  state. However, the  $\gamma^\mu(1 - \gamma^5)$  form leaves the weak interaction invariant under the combined CP operation. For instance,

$$\Gamma(\pi^+ \rightarrow \mu^+ \nu_L) \neq \Gamma(\pi^+ \rightarrow \mu^+ \nu_R) = 0 \quad \text{P violation,}$$

$$\Gamma(\pi^+ \rightarrow \mu^+ \nu_L) \neq \Gamma(\pi^- \rightarrow \mu^- \bar{\nu}_L) = 0 \quad \text{C violation,}$$

but

$$\Gamma(\pi^+ \rightarrow \mu^+ \nu_L) = \Gamma(\pi^- \rightarrow \mu^- \bar{\nu}_R) \quad \text{CP invariance.}$$

In this example,  $\nu$  denotes a muon neutrino. We discuss CP invariance in Section 12.13.

**EXERCISE 12.2** Show that a (charge-lowering) weak current of the form

$$\bar{u}_e \gamma^{\mu \frac{1}{2}} (1 - \gamma^5) u_\nu \quad (12.9)$$

involves only left-handed electrons (or right-handed positrons). In the relativistic limit ( $v \approx c$ ), show that the electrons have negative helicity.

The  $\frac{1}{2}(1 - \gamma^5)$  in (12.9) automatically selects a left-handed neutrino (or a right-handed antineutrino). This  $V-A$  (vector–axial vector) structure of the weak current can be directly exposed by scattering  $\nu_e$ ’s off electrons (see Section 12.7), just as the  $\gamma^\mu$  structure of electromagnetism was verified by measurements of the angular distribution of  $e^+ e^-$  scattering.

It is natural to hope that all weak interaction phenomena are described by a  $V-A$  current–current interaction with a universal coupling  $G$ . For example,  $\beta$ -decay of Fig. 12.2 and  $\mu$ -decay of Fig. 12.4 can be described by the amplitudes

$$\mathcal{M}(p \rightarrow ne^+ \nu_e) = \frac{G}{\sqrt{2}} [\bar{u}_n \gamma^\mu (1 - \gamma^5) u_p] [\bar{u}_{\nu_e} \gamma_\mu (1 - \gamma^5) u_e] \quad (12.10)$$

and

$$\mathcal{M}(\mu^- \rightarrow e^- \bar{\nu}_e \nu_\mu) = \frac{G}{\sqrt{2}} [\bar{u}_{\nu_\mu} \gamma^\sigma (1 - \gamma^5) u_\mu] [\bar{u}_{\nu_e} \gamma_\sigma (1 - \gamma^5) u_{\nu_e}], \quad (12.11)$$

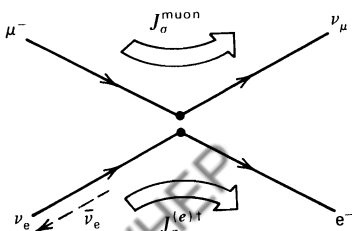


Fig. 12.4 The diagram for  $\mu^-$  decay:  $\mu^- \rightarrow e^- \bar{\nu}_e \nu_\mu$ .

respectively. The  $1/\sqrt{2}$  is pure convention (to keep the original definition of  $G$  which did not include  $\gamma^5$ ). We then proceed in analogy with the Feynman rules for QED. The calculations only involve particles, and the diagrams show only particle lines. Antiparticles do not appear. Thus, the outgoing  $\bar{\nu}_e$  (of momentum  $k$ ) in  $\mu$ -decay is shown in Fig. 12.4 as an ingoing  $\nu_e$  (of momentum  $-k$ ). As before, the spinor  $u_{\nu_e}(-k)$  of (12.11) will be denoted  $u_{\nu_e}(k)$ , see (5.33). The same remarks apply to the outgoing  $e^+$  of (12.10).

**EXERCISE 12.3** Show that the *charge-raising* weak current

$$J^\mu = \bar{u}_\nu \gamma^{\mu \frac{1}{2}} (1 - \gamma^5) u_e \quad (12.12)$$

couples an ingoing negative helicity electron to an outgoing negative helicity neutrino. Neglect the mass of the electron. Besides the configuration  $(e_L^-, \nu_L)$ , show that  $J^\mu$  also couples the following (ingoing, outgoing) lepton pair configurations:  $(\bar{\nu}_R, e_R^+)$ ,  $(0, \nu_L e_R^+)$ , and  $(e_L^- \bar{\nu}_R, 0)$ .

Further, show that the *charge-lowering* weak current, (12.9), is the hermitian conjugate of (12.12):

$$J_\mu^\dagger = \bar{u}_e \gamma_{\mu \frac{1}{2}} (1 - \gamma^5) u_\nu.$$

List the lepton pair configurations coupled by  $J_\mu^\dagger$ .

Weak interaction amplitudes are of the form

$$\mathcal{M} = \frac{4G}{\sqrt{2}} J^\mu J_\mu^\dagger. \quad (12.13)$$

Charge conservation requires that  $\mathcal{M}$  is the product of a charge-raising and a charge-lowering current; see, for example, (12.10) and (12.11). The factor 4 arises because the currents, (12.13), are defined with the normalized projection operator  $\frac{1}{2}(1 - \gamma^5)$  rather than the old-fashioned  $(1 - \gamma^5)$ .

## 12.2 Interpretation of the Coupling $G$

We can use the observed rates for nuclear  $\beta$ -decay and for  $\mu$ -decay to obtain a numerical value for  $G$ . It is also crucial to check the universality of the strength of the weak coupling constant  $G$  of (12.10) and (12.11). We do not want to introduce a new interaction for every weak process! However, because we do this, let us cast  $G$  in a form that can be directly compared to the couplings of the color and electromagnetic interactions.

Examination of the electromagnetic and the weak amplitudes of (12.7) and (12.10) shows that in Fermi's model the analogy between the two interactions has not been fully developed. We see that  $G$  essentially replaces  $e^2/q^2$ . Thus,  $G$ , in

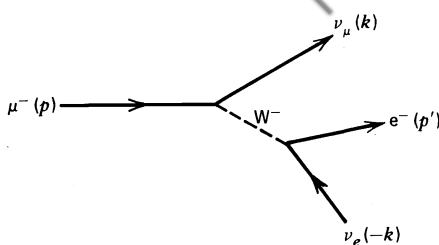


Fig. 12.5 Muon decay.

contrast to the dimensionless coupling  $e$ , has dimensions  $\text{GeV}^{-2}$ . It is tempting to try and extend the analogy by postulating that the weak interactions are generated by the emission and absorption of charged vector bosons, which we call weak bosons,  $W^\pm$ . The weak bosons are the analogues of the photon for the electromagnetic force and the gluons for the color force. For example,  $\mu^-$  decay is mediated by a  $W^-$  boson (see Fig. 12.5) and the amplitude is of the form [see (12.7)]

$$\mathcal{N} = \left( \frac{g}{\sqrt{2}} \bar{u}_\mu \gamma^{\sigma \frac{1}{2}} (1 - \gamma^5) u_\mu \right) \frac{1}{M_W^2 - q^2} \left( \frac{g}{\sqrt{2}} \bar{u}_e \gamma^{\sigma \frac{1}{2}} (1 - \gamma^5) u_{\nu_e} \right), \quad (12.14)$$

where  $g/\sqrt{2}$  is a dimensionless weak coupling and  $q$  is the momentum carried by the weak boson (the factors  $1/\sqrt{2}$  and  $\frac{1}{2}$  are inserted so that we have the conventional definition of  $g$ ). In contrast to the photon, the weak boson must be massive, otherwise it would have been directly produced in weak decays. Indeed, it turns out that  $M_W \sim 80 \text{ GeV}$  (see Chapter 15).

In (12.14), we have been cavalier about the spin sum in the boson propagator, see (6.87). However, at the moment, we are interested in situations where  $q^2 \ll M_W^2$  (e.g.,  $\beta$ -decay and  $\mu$ -decay). Then, (12.14) reverts to (12.11) with

$$\frac{G}{\sqrt{2}} = \frac{g^2}{8M_W^2} \quad (12.15)$$

and the weak currents interact essentially at a point. That is, in the limit (12.15), the propagator between the currents disappears. Equation (12.15) prompts the idea that weak interactions are weak not because  $g \ll e$ , but because  $M_W^2$  is large. If indeed  $g \approx e$ , then at energies  $O(M_W)$  and above, the weak interaction would become of comparable strength to the electromagnetic interaction.

We may think of  $g \approx e$  as a unification of weak and electromagnetic interactions in much the same way as the unification of the electric and magnetic forces in Maxwell's theory of electromagnetism, where

$$\mathbf{F} = e\mathbf{E} + e_M \mathbf{v} \times \mathbf{B}$$

with  $e_M = e$ . At low velocities, the magnetic forces are very weak, whereas for high-velocity particles, the electric and magnetic forces play a comparable role.

The velocity of light  $c$  is the scale which governs the relative strength. The analogue for the electroweak force is  $M_W$  on the energy scale. The unification of the electromagnetic and weak forces is the subject of Chapters 13 and 15.

### 12.3 Nuclear $\beta$ -Decay

Let us use the observed transition rate of the process



to estimate  $G$ . By analogy with the QED calculations of Section 6.2, we write the transition amplitude for this process (Fig. 12.2) in the form

$$T_{fi} = -i \frac{4G}{\sqrt{2}} \int J_\mu^{(N)\dagger}(x) J^{(e)\mu}(x) d^4x \quad (12.16)$$

$$= -i \frac{4G}{\sqrt{2}} \int [\bar{\psi}_n(x) \gamma_{\mu\frac{1}{2}}(1 - \gamma^5) \psi_p(x)] [\bar{\psi}_e(x) \gamma^{\mu\frac{1}{2}}(1 - \gamma^5) \psi_e(x)] d^4x, \quad (12.17)$$

see (12.10). For this problem, it is easier not to perform the  $x$  integration at this stage. Remember that usually we carry out the  $x$  integration and obtain  $(2\pi)^4$  times the “energy-momentum conserving” delta function (see Section 6.2). We then define

$$T_{fi} = -i(2\pi)^4 \delta^{(4)}(p_p - p_n - p_e - p_\nu) \mathcal{M}.$$

Thus, (12.16) reduces to the form (12.13).

In writing down (12.16), we have assumed that the other nucleons in  $^{14}\text{O}$  are simply spectators to the decaying proton. However, *a priori*, we cannot ignore the fact the nucleons participating in  $\beta$ -decay are bound inside nuclei. We also have no reason to believe the idealized form of weak nucleon current,  $J^{(N)}$ , shown in (12.17), since the nucleons themselves are composite objects and not structureless Dirac particles. Despite these problems, it turns out to be quite easy to get an accurate estimate of  $G$ . There are several reasons for this. First, the low-energy weak interaction is essentially a point interaction, and we can ignore the longer-range strong interaction effects we just mentioned. Actually, there is a beautiful and more precise justification for this vague argument. The weak current  $(\bar{\psi}_p \gamma^\mu \psi_n)$  and its conjugate  $(\bar{\psi}_n \gamma^\mu \psi_p)$ , together with the electromagnetic current  $(\bar{\psi}_p \gamma^\mu \psi_p)$ , are believed to form an isospin triplet of conserved vector currents. This is referred to as the *conserved vector current hypothesis*. The intimate connection with the electromagnetic current “protects” the vector part of the weak current from any strong interaction corrections, just as the electromagnetic charge is protected. The axial vector part,  $\bar{\psi}_n \gamma^\mu \gamma^5 \gamma_p$ , will not contribute to the process as we are considering a transition between two  $J^P = 0^+$  nuclear states,

which precludes a change of parity. Moreover, since the process occurs between two  $J = 0$  nuclei, we can safely assume that the nuclear wavefunction is essentially unchanged by the transition.

Another simplifying feature is that the energy released in the decay (about 2 MeV) is small compared to the rest energy of the nuclei. We can therefore use nonrelativistic spinors for the nucleons [see (6.11)], and then only  $\gamma^\mu$  with  $\mu = 0$  contributes [see (6.13)]. Thus,

$$T_{fi} = -i \frac{G}{\sqrt{2}} [\bar{u}(p_\nu) \gamma^0 (1 - \gamma^5) v(p_e)] \int \psi_n^\dagger(x) \psi_p(x) e^{-i(p_\nu + p_e) \cdot x} d^4x, \quad (12.18)$$

where, as remarked after (12.11), the  $v$  spinor  $v(p_e)$  describes an outgoing positron of momentum  $p_e$ . The  $e^+$  and  $\nu$  are emitted with an energy of the order of 1 MeV, and so their de Broglie wavelengths are about  $10^{-11}$  cm, which is much larger than the nuclear diameter. We can therefore set

$$e^{i(p_\nu + p_e) \cdot x} \approx 1$$

and perform the spatial integration of (12.18). Noting the relation between  $T_{fi}$  and the invariant amplitude  $\mathfrak{M}$  (see Section 6.2), we obtain

$$\mathfrak{M} = \frac{G}{\sqrt{2}} (\bar{u}(p_\nu) \gamma^0 (1 - \gamma^5) v(p_e)) (2m_N) \left( \frac{1}{2\sqrt{2}} \right), \quad (12.19)$$

where  $2m_N$  arises from the normalization of the nucleon spinors [see (6.13)] and  $2/\sqrt{2}$  is the hadronic isospin factor for the  $^{14}\text{O} \rightarrow ^{14}\text{N}^*$  transition (see Exercise 12.4).

**EXERCISE 12.4** Verify the isospin factor  $\sqrt{2}$  in (12.19). Note that  $^{14}\text{C}$ ,  $^{14}\text{N}^*$ ,  $^{14}\text{O}$  form an isospin triplet, which can be viewed as nn, np, pp, together with an isospin zero  $^{12}\text{C}$  core (see Fig. 2.2). Keep in mind that for indistinguishable proton decays, we must add amplitudes, not probabilities.

The rate  $d\Gamma$  for the “p”  $\rightarrow$  “n”  $e^+ \nu$  transition is related to  $|\mathfrak{M}|^2$  by (4.36). We obtain

$$d\Gamma = G^2 \sum_{\text{spins}} |\bar{u}(p_\nu) \gamma^0 (1 - \gamma^5) v(p_e)|^2 \frac{d^3 p_e}{(2\pi)^3 2E_e} \times \frac{d^3 p_\nu}{(2\pi)^3 2E_\nu} 2\pi \delta(E_0 - E_e - E_\nu), \quad (12.20)$$

where  $E_0$  is the energy released to the lepton pair. The normalization factor  $(2m_N)^2$  cancels with the equivalent  $2E_e 2E_\nu$  factor in (4.36), as indeed it must. The summation over spins can be performed using the techniques we introduced

in Chapter 6. Neglecting the mass of the electron, we have

$$\begin{aligned}
 \sum_{\text{spins}} |\bar{u} \gamma^0 (1 - \gamma^5) v|^2 &= \sum (\bar{u} \gamma^0 (1 - \gamma^5) v)(\bar{v} (1 + \gamma^5) \gamma^0 u) \\
 &= \text{Tr}(\not{p}_\nu \gamma^0 (1 - \gamma^5) \not{p}_e (1 + \gamma^5) \gamma^0) \\
 &= 2 \text{Tr}(\not{p}_\nu \gamma^0 \not{p}_e (1 + \gamma^5) \gamma^0) \\
 &= 8(E_e E_\nu + \mathbf{p}_e \cdot \mathbf{p}_\nu) \\
 &= 8E_e E_\nu (1 + v_e \cos \theta),
 \end{aligned} \tag{12.21}$$

where  $\theta$  is the opening angle between the two leptons and where the electron velocity  $v_e \approx 1$  in our approximation. Here, we have used the trace theorems of Section 6.4; see also (12.25) and (12.26). Substituting (12.21) into (12.20), the transition rate becomes

$$d\Gamma = \frac{2G^2}{(2\pi)^5} (1 + \cos \theta) [(2\pi d \cos \theta p_e^2 dp_e)(4\pi E_\nu^2 dE_\nu)] \delta(E_0 - E_e - E_\nu), \tag{12.22}$$

where  $d^3 p_e d^3 p_\nu$  has been replaced by the expression in the square brackets.

Many experiments focus attention on the energy spectrum of the emitted positron. From (12.22), we obtain

$$\begin{aligned}
 \frac{d\Gamma}{dp_e} &= \frac{4G^2}{(2\pi)^3} p_e^2 (E_0 - E_e)^2 \int d\cos \theta (1 + \cos \theta) \\
 &= \frac{G^2}{\pi^3} p_e^2 (E_0 - E_e)^2.
 \end{aligned} \tag{12.23}$$

Thus, if from the observed positron spectrum we plot  $p_e^{-1} (d\Gamma/dp_e)^{1/2}$  as a function of  $E_e$ , we should obtain a linear plot with end point  $E_0$ . This is called the Kurie plot. It can be used to check whether the neutrino mass is indeed zero. A nonvanishing neutrino mass destroys the linear behavior, particularly for  $E_e$  near  $E_0$ . (In practice, of course, we must examine the approximations we have made, correct  $E_e$  for the energy gained from the nuclear Coulomb field, and allow for the experimental energy resolution.)

Our immediate interest here is of a different nature. We wish to determine  $G$  from the observed value  $E_0$  and the measured lifetime  $\tau$  of the nuclear state to  $\beta$ -decay. We therefore carry out the  $dp_e$  integration of (12.23) over the interval  $0, E_0$ . Making the relativistic approximation  $p_e \approx E_e$ , we find

$$\boxed{\Gamma = \frac{1}{\tau} = \frac{G^2 E_0^5}{30\pi^3}.}$$

Now, for  $^{14}\text{O} \rightarrow ^{14}\text{N}^* e^+ \nu$ , the nuclear energy difference  $E_0$  is 1.81 MeV, and

the measured half-life is  $\tau \log 2 = 71$  sec. Using this information, we find

$$G \approx 10^{-5}/m_N^2. \quad (12.24)$$

Recall that  $G$  has dimension (mass) $^{-2}$ . We have chosen to quote the value with respect to the nucleon mass.

**EXERCISE 12.5** Calculate  $G$  from the data for the  $\beta$ -transition  ${}^{10}\text{C} \rightarrow {}^{10}\text{B}^*\text{e}^+\nu$ . The measured half-life is  $\tau \log 2 = 20$  sec, and  $E_0 = 2$  MeV. ( ${}^{10}\text{C}$  and  ${}^{10}\text{B}^*$  are both isospin 1,  $J^P = 0^+$  states.)

**EXERCISE 12.6** Accepting the vector boson exchange picture of weak interactions with coupling,  $g = e$ , estimate the mass  $M_W$  of the weak boson. (In the standard model of weak interactions, introduced in Chapter 13,  $g \sin \theta_W = e$ , with  $\sin^2 \theta_W \approx \frac{1}{4}$ .)

## 12.4 Further Trace Theorems

We collect together some results that are useful for the computation of weak interaction processes and that follow directly from the trace theorems of Section 6.4:

$$\text{Tr}(\gamma^\mu p_1^\mu \gamma^\nu p_2) = 4[p_1^\mu p_2^\nu + p_1^\nu p_2^\mu - (p_1 \cdot p_2)g^{\mu\nu}], \quad (12.25)$$

$$\text{Tr}[\gamma^\mu(1 - \gamma^5)p_1 \gamma^\nu(1 - \gamma^5)p_2] = 2\text{Tr}(\gamma^\mu p_1 \gamma^\nu p_2) + 8ie^{\mu\alpha\nu\beta}p_{1\alpha}p_{2\beta}, \quad (12.26)$$

$$\begin{aligned} & \text{Tr}(\gamma^\mu p_1 \gamma^\nu p_2) \text{Tr}(\gamma_\mu p_3 \gamma_\nu p_4) \\ &= 32[(p_1 \cdot p_3)(p_2 \cdot p_4) + (p_1 \cdot p_4)(p_2 \cdot p_3)], \end{aligned} \quad (12.27)$$

$$\begin{aligned} & \text{Tr}(\gamma^\mu p_1 \gamma^\nu \gamma^5 p_2) \text{Tr}(\gamma_\mu p_3 \gamma_\nu \gamma^5 p_4) \\ &= 32[(p_1 \cdot p_3)(p_2 \cdot p_4) - (p_1 \cdot p_4)(p_2 \cdot p_3)], \end{aligned} \quad (12.28)$$

$$\begin{aligned} & \text{Tr}[\gamma^\mu(1 - \gamma^5)p_1 \gamma^\nu(1 - \gamma^5)p_2] \text{Tr}[\gamma_\mu(1 - \gamma^5)p_3 \gamma_\nu(1 - \gamma^5)p_4] \\ &= 256(p_1 \cdot p_3)(p_2 \cdot p_4). \end{aligned} \quad (12.29)$$

**EXERCISE 12.7** Verify these results.

## 12.5 Muon Decay

Muon decay,

$$\mu^-(p) \rightarrow e^-(p') + \bar{\nu}_e(k') + \nu_\mu(k), \quad (12.30)$$

is the model reaction for weak decays. The particle four-momenta are defined in (12.30), and the Feynman diagram is shown in Fig. 12.5. According to the Feynman rules, it must be drawn using only particle lines; and so the outgoing  $\bar{\nu}_e$  is shown as an incoming  $\nu_e$ . The invariant amplitude for muon decay is

$$\mathcal{M} = \frac{G}{\sqrt{2}} [\bar{u}(k)\gamma^\mu(1 - \gamma^5)u(p)][\bar{u}(p')\gamma_\mu(1 - \gamma^5)v(k')], \quad (12.31)$$

see (12.11), where the spinors are labeled by the particle momenta. Recall that the outgoing  $\bar{\nu}_e$  is described by  $v(k')$ . The muon decay rate can now be obtained using (4.36),

$$d\Gamma = \frac{1}{2E} |\mathcal{M}|^2 dQ \quad (12.32)$$

where the invariant phase space is

$$\begin{aligned} dQ &= \frac{d^3 p'}{(2\pi)^3 2E'} \frac{d^3 k}{(2\pi)^3 2\omega} \frac{d^3 k'}{(2\pi)^3 2\omega'} (2\pi)^4 \delta^{(4)}(p - p' - k - k') \\ &= \frac{1}{(2\pi)^5} \frac{d^3 p'}{2E'} \frac{d^3 k'}{2\omega'} \theta(E - E' - \omega') \delta((p - p' - k')^2), \end{aligned} \quad (12.33)$$

with  $p^0 \equiv E$ ,  $k^0 \equiv \omega$ , and so on, and where in reaching the last line we have performed the  $d^3 k$  integration using

$$\int \frac{d^3 k}{2\omega} = \int d^4 k \theta(\omega) \delta(k^2). \quad (12.34)$$

**EXERCISE 12.8** Derive (12.34) by performing the  $d\omega$  integration on the right-hand side (see Exercise 6.7).

Using (12.31) and (12.29), we find the spin-averaged probability is

$$|\mathcal{M}|^2 \equiv \frac{1}{2} \sum_{\text{spins}} |\mathcal{M}|^2 = 64G^2(k \cdot p')(k' \cdot p), \quad (12.35)$$

where  $p = p' + k + k'$  on account of the  $d^4 k$  integration performed in (12.33). Since  $m_\mu > 200m_e$ , we can safely neglect the mass of the electron.

**EXERCISE 12.9** Verify (12.35). Neglect the mass of the electron, but not that of the muon.

**EXERCISE 12.10** Show that

$$2(k \cdot p')(k' \cdot p) = (p - k')^2(k' \cdot p) = (m^2 - 2m\omega')m\omega' \quad (12.36)$$

in the muon rest frame, where  $p = (m, 0, 0, 0)$ .

Gathering these results together, the decay rate in the muon rest frame is

$$\begin{aligned} d\Gamma &= \frac{G^2}{2m\pi^5} \frac{d^3 p'}{2E'} \frac{d^3 k'}{2\omega'} m\omega'(m^2 - 2m\omega') \\ &\times \delta(m^2 - 2mE' - 2m\omega' + 2E'\omega'(1 - \cos\theta)), \end{aligned} \quad (12.37)$$

and, as for  $\beta$ -decay, we can replace  $d^3 p' d^3 k'$  by

$$4\pi E'^2 dE' 2\pi\omega'^2 d\omega' d\cos\theta.$$

We now use the fact that

$$\delta(\dots + 2E'\omega' \cos\theta) = \frac{1}{2E'\omega'} \delta(\dots - \cos\theta)$$

to perform the integration over the opening angle  $\theta$  between the emitted  $e^-$  and  $\bar{\nu}_e$  and obtain

$$d\Gamma = \frac{G^2}{2\pi^3} dE' d\omega' m\omega' (m - 2\omega'). \quad (12.38)$$

The  $\delta$ -function integration introduces the following restrictions on the energies  $E'$ ,  $\omega'$ , stemming from the fact that  $-1 \leq \cos\theta \leq 1$ :

$$\frac{1}{2}m - E' \leq \omega' \leq \frac{1}{2}m, \quad (12.39)$$

$$0 \leq E' \leq \frac{1}{2}m. \quad (12.40)$$

These limits are easily understood in terms of the various limits in which the three-body decay  $\mu \rightarrow e\bar{\nu}_e\nu_\mu$  becomes effectively a two-body decay. For example, when the electron energy  $E'$  vanishes, (12.39) yields  $\omega' = m/2$ , which is expected because then the two neutrinos share equally the muon's rest energy.

To obtain the energy spectrum of the emitted electron, we perform the  $\omega'$  integration of (12.38):

$$\begin{aligned} \frac{d\Gamma}{dE'} &= \frac{mG^2}{2\pi^3} \int_{\frac{1}{2}m-E'}^{\frac{1}{2}m} d\omega' \omega' (m - 2\omega') \\ &= \frac{G^2}{12\pi^3} m^2 E'^2 \left( 3 - \frac{4E'}{m} \right). \end{aligned} \quad (12.41)$$

This prediction is in excellent agreement with the observed electron spectrum. Finally, we calculate the muon decay rate

$$\Gamma \equiv \frac{1}{\tau} = \int_0^{m/2} dE' \frac{d\Gamma}{dE'} = \frac{G^2 m^5}{192\pi^3}. \quad (12.42)$$

Inserting the measured muon lifetime  $\tau = 2.2 \times 10^{-6}$  sec, we can calculate the Fermi coupling  $G$ . We find

$$G \sim 10^{-5}/m_N^2. \quad (12.43)$$

Comparison of the values of  $G$  obtained in (12.24) and (12.43) supports the assertion that the weak coupling constant is the same for leptons and nucleons, and hence universal. It means that nuclear  $\beta$ -decay and the decay of the muon have the same physical origin. Indeed, when all corrections are taken into

account,  $G_\beta$  and  $G_\mu$  are found to be equal to within a few percent:

$$G_\mu = (1.16632 \pm 0.00002) \times 10^{-5} \text{ GeV}^{-2},$$

$$G_\beta = (1.136 \pm 0.003) \times 10^{-5} \text{ GeV}^{-2}. \quad (12.44)$$

The reason for the small difference is important and is discussed in Section 12.11 [see (12.107)].

**EXERCISE 12.11** Draw a diagram showing the particle helicities in the  $\mu^-$  rest frame in the case where the emitted electron has its maximum permissible energy. In this limit, explain why the electron angular distribution has the form  $1 - P \cos \alpha$ , where  $P$  is the polarization of the muon and  $\alpha$  is the angle between the polarization direction and the direction of the emitted electron:

$$P \equiv \frac{N_+ - N_-}{N_+ + N_-},$$

where  $N_\pm$  are the numbers of spin-up, spin-down muons.

**EXERCISE 12.12** “Predict” the rate for the decay  $\tau^- \rightarrow e^- \bar{\nu}_e \nu_\tau$ , where the  $\tau$ -lepton has mass 1.8 GeV. The observed branching ratio of this decay mode is approximately 20%. Calculate the lifetime of the  $\tau$ -lepton. Can you explain this branching ratio?

## 12.6 Pion Decay

Can we now also understand the lifetime of the  $\pi^\pm$ -mesons? To be specific, we take the decay

$$\pi^-(q) \rightarrow \mu^-(p) + \bar{\nu}_\mu(k), \quad (12.45)$$

which is shown in Fig. 12.6. The amplitude is of the form

$$\mathcal{M} = \frac{G}{\sqrt{2}} (\dots)^\mu \bar{u}(p) \gamma_\mu (1 - \gamma^5) v(k) \quad (12.46)$$

where  $(\dots)$  represents the weak quark current of Fig. 12.6. It is tempting to write it as  $\bar{u}_d \gamma^\mu (1 - \gamma^5) v_{\bar{u}}$ , but this is incorrect since the  $\bar{u}$ ,  $d$  quarks in Fig. 12.6 are not free quark states but are quarks bound into a  $\pi^-$ -meson. We know, however, that

- $\mathcal{M}$  is Lorentz invariant, so that  $(\dots)^\mu$  must be a vector or axial-vector, as indicated.
- The  $\pi^-$  is spinless, so that  $q$  is the only four-vector available to construct  $(\dots)^\mu$ .

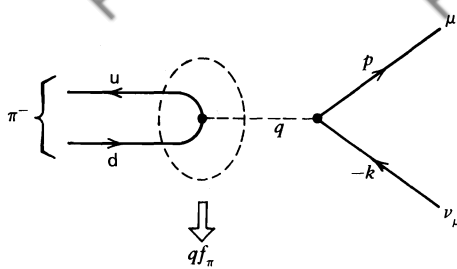


**Fig. 12.6** Feynman diagram for the decay  $\pi^-(\bar{u}d) \rightarrow \mu^-\bar{\nu}_\mu$  with four-momentum  $q = p + k$ .

We therefore have

$$(\dots)^\mu = q^\mu f(q^2) \equiv q^\mu f_\pi, \quad (12.47)$$

where  $f$  is a function of  $q^2$  since it is the only Lorentz scalar that can be formed from  $q$ , but  $q^2 = m_\pi^2$  and  $f(m_\pi^2) \equiv f_\pi$  is a constant. Inserting (12.47) into (12.46), the  $\pi^- \rightarrow \mu^- \bar{\nu}$  decay amplitude is

$$\begin{aligned} \mathcal{M} &= \frac{G}{\sqrt{2}} (p^\mu + k^\mu) f_\pi [\bar{u}(p) \gamma_\mu (1 - \gamma^5) v(k)] \\ &= \frac{G}{\sqrt{2}} f_\pi m_\mu \bar{u}(p) (1 - \gamma^5) v(k). \end{aligned} \quad (12.48)$$

Here, we have used  $\not{k}v(k) = 0$  and  $\bar{u}(p)(\not{p} - m_\mu) = 0$ , the Dirac equations for the neutrino and muon, respectively. In its rest frame, the  $\pi$ -decay rate is

$$d\Gamma = \frac{1}{2m_\pi} \overline{|\mathcal{M}|^2} \frac{d^3 p}{(2\pi)^3 2E} \frac{d^3 k}{(2\pi)^3 2\omega} (2\pi)^4 \delta(q - p - k), \quad (12.49)$$

where the sum over the spins of the outgoing lepton pair can be performed by familiar traceology [see (6.22) and (6.23)]:

$$\begin{aligned} \overline{|\mathcal{M}|^2} &= \frac{G^2}{2} f_\pi^2 m_\mu^2 \text{Tr}((\not{p} + m_\mu)(1 - \gamma^5)\not{k}(1 + \gamma^5)) \\ &= 4G^2 f_\pi^2 m_\mu^2 (p \cdot k). \end{aligned} \quad (12.50)$$

In the  $\pi$  rest frame ( $\mathbf{k} = -\mathbf{p}$ ),

$$p \cdot k = E\omega - \mathbf{k} \cdot \mathbf{p} = E\omega + \mathbf{k}^2 = \omega(E + \omega). \quad (12.51)$$

Gathering these results together, we have

$$\Gamma = \frac{G^2 f_\pi^2 m_\mu^2}{(2\pi)^2 2m_\pi} \int \frac{d^3 p d^3 k}{E\omega} \delta(m_\pi - E - \omega) \delta^{(3)}(\mathbf{k} + \mathbf{p}) \omega(E + \omega).$$

The  $d^3p$  integration is taken care of by the  $\delta^{(3)}$  function and, since there is no angular dependence, we are left with only the integration over  $d\omega$ :

$$\Gamma = \frac{G^2 f_\pi^2 m_\mu^2}{(2\pi)^2 2m_\pi} 4\pi \int d\omega \omega^2 \left(1 + \frac{\omega}{E}\right) \delta(m_\pi - E - \omega), \quad (12.52)$$

where  $E = (m_\mu^2 + \omega^2)^{1/2}$ . The result of the integration is  $\omega_0^2$ , where

$$\omega_0 \equiv \frac{m_\pi^2 - m_\mu^2}{2m_\pi}. \quad (12.53)$$

This can be seen by rewriting the  $\delta$ -function in (12.52) as

$$\delta[f(\omega)] = \delta(\omega - \omega_0) / \left| \frac{\partial f}{\partial \omega} \right|_{\omega=\omega_0} = \delta(\omega - \omega_0) / \left(1 + \frac{\omega_0}{E}\right).$$

Therefore, finally we obtain

$$\boxed{\Gamma = \frac{1}{\tau} = \frac{G^2}{8\pi} f_\pi^2 m_\pi m_\mu^2 \left(1 - \frac{m_\mu^2}{m_\pi^2}\right)^2.} \quad (12.54)$$

Taking the universal value of  $G = 10^{-5} m_N^{-2}$  obtained from  $\beta$ - or  $\mu$ -decay and assuming that  $f_\pi = m_\pi$  (a guess which at least guarantees the correct dimension), we indeed obtain the  $\pi^-$  lifetime announced at the beginning of the chapter. Although the theory can clearly accommodate the long lifetime of the charged  $\pi$ , the decay does not provide a quantitative test, as  $f_\pi = m_\pi$  is a pure guess.

A quantitative test, however, is possible. If we repeat the calculation for the decay mode  $\pi^- \rightarrow e^- \bar{\nu}_e$ , we obtain (12.54) with  $m_\mu$  replaced by  $m_e$ . Therefore,

$$\frac{\Gamma(\pi^- \rightarrow e^- \bar{\nu}_e)}{\Gamma(\pi^- \rightarrow \mu^- \bar{\nu}_\mu)} = \left(\frac{m_e}{m_\mu}\right)^2 \left(\frac{m_\pi^2 - m_e^2}{m_\pi^2 - m_\mu^2}\right)^2 = 1.2 \times 10^{-4}, \quad (12.55)$$

where the numerical value comes from inserting the particle masses. The charged  $\pi$  prefers (by a factor of  $10^4$ ) to decay into a muon, which has a similar mass, rather than into the much lighter electron. This is quite contrary to what one would expect from phase-space considerations, so some dynamical mechanism must be at work.

The pion is spinless, and so, by the conservation of angular momentum, the outgoing lepton pair ( $e^- \bar{\nu}_e$ ) must have  $J = 0$ . As the  $\bar{\nu}_e$  has positive helicity, the  $e^-$  is also forced into a positive helicity state, see Fig. 12.7. But recall that this is



Fig. 12.7 The decay  $\pi^- \rightarrow e^- \bar{\nu}_e$  showing the right-handed helicity of the outgoing leptons.

the “wrong” helicity state for the electron. In the limit  $m_e = 0$ , the weak current only couples negative helicity electrons, and hence the positive helicity coupling is highly suppressed. Thus, in the  $\pi^-$ -decay, the  $e^-$  (or  $\mu^-$ ) is forced by angular momentum conservation into its “wrong” helicity state. This is much more likely to happen for the  $\mu^-$  than for the relatively light  $e^-$ , in fact,  $10^4$  times more likely. Experiment confirms this result, which is a direct consequence of the  $1 - \gamma^5$  or left-handed structure of the weak current, (12.12). It is however interesting to note that prior to the discovery of parity violation, an argument for (12.55) based on helicity conservation was proposed by Ruderman and Finkelstein (1949) (*Phys. Rev.* **76**, 1458).

**EXERCISE 12.13** Predict the ratio of the  $K^- \rightarrow e^- \bar{\nu}_e$  and  $K^- \rightarrow \mu^- \bar{\nu}_\mu$  decay rates. Given that the lifetime of the  $K^-$  is  $\tau = 1.2 \times 10^{-8}$  sec and the  $K^- \rightarrow \mu\nu$  branching ratio is 64%, estimate the decay constant  $f_K$ . Comment on your assumptions and on your result.

## 12.7 Charged Current Neutrino–Electron Scattering

Although the experiments exposing the violation of parity in weak interactions (polarized  ${}^{60}\text{Co}$  decay,  $K^-$  decay,  $\pi^-$ -decay, etc.) are some of the highlights in the development of particle physics, parity violation and its  $V-A$  structure can now be demonstrated experimentally much more directly. In fact, these days neutrinos, particularly muon neutrinos, can be prepared in intense beams which are scattered off hadronic, or even leptonic, targets to probe the structure of the weak interaction. A common method is to allow a high-energy monoenergetic beam of pions (or kaons) to decay (e.g.,  $\pi^+ \rightarrow \mu^+ \bar{\nu}_\mu$ ) in a long decay tunnel and then to absorb the muons by passing the, approximately collinear, decay products through a thick shield which absorbs the charged particles, letting only the neutrinos through. This technological achievement opens up the possibility of exhibiting the  $\gamma^\mu(1 - \gamma^5)$  structure of the weak coupling by measuring the angular distribution of  $\nu_e e$  or  $\bar{\nu}_e e$  scattering. This is the analogue of the confirmation of the  $\gamma^\mu$  structure of the electromagnetic vertex by studying  $ee$  or  $e\mu$  scattering, which we discussed in Chapter 6.

The relevant diagrams are shown in Fig. 12.8, where the particle four-momenta are defined. The invariant amplitude for  $\nu_e e^- \rightarrow \nu_e e^-$  is computed from diagram (a):

$$\mathcal{M} = \frac{G}{\sqrt{2}} (\bar{u}(k') \gamma^\mu (1 - \gamma^5) u(p)) (\bar{u}(p') \gamma_\mu (1 - \gamma^5) u(k)). \quad (12.56)$$

The calculation now proceeds along the lines of that for  $e^- \mu^-$  scattering in Section 6.3, except for the replacement of  $\gamma^\mu$  by  $\gamma^\mu(1 - \gamma^5)$ . Squaring (12.56), summing over the final-state spins, and averaging over the two spin states of the

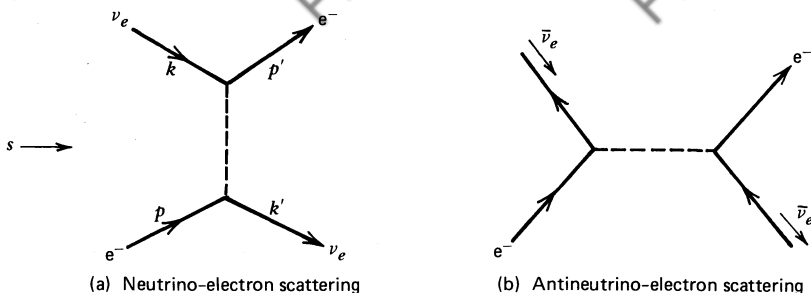


**Fig. 12.8** Charged current contributions to elastic  $\nu_e e^-$  and  $\bar{\nu}_e e^-$  scattering.

initial  $e^-$  gives

$$\begin{aligned} \frac{1}{2} \sum_{\text{spins}} |\mathcal{M}|^2 &= \frac{G^2}{4} \text{Tr}(\gamma^\mu(1 - \gamma^5)\not{p}\gamma^\nu(1 - \gamma^5)\not{k'}) \text{Tr}(\gamma_\mu(1 - \gamma^5)\not{k}\gamma_\nu(1 - \gamma^5)\not{p'}) \\ &= 64G^2(k \cdot p)(k' \cdot p') \\ &= 16G^2s^2 \end{aligned} \quad (12.57)$$

where we have used (12.29). Also we are working in the relativistic limit  $m_e = 0$  and have made use of

$$s = (k + p)^2 = 2k \cdot p = 2k' \cdot p'. \quad (12.58)$$

The angular distribution in the center of mass follows from (4.35) (with  $p_f = p_i$  in the limit  $m_e = 0$ ):

$$\frac{d\sigma(\nu_e e^-)}{d\Omega} = \frac{1}{64\pi^2 s} |\mathcal{M}|^2 = \frac{G^2 s}{4\pi^2}. \quad (12.59)$$

Integration over this isotropic angular distribution gives

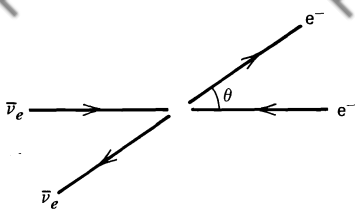
$$\sigma(\nu_e e^-) = \frac{G^2 s}{\pi}. \quad (12.60)$$

**EXERCISE 12.14** On purely dimensional grounds, show that the cross section (for a point interaction) must behave as  $\sigma(\nu_e e^-) \sim G^2 s$  at high energies. Comment on the significance of this result.

**EXERCISE 12.15** Show that

$$\sigma(\nu_e e^-) \approx (E_\nu \text{ in GeV}) \times 10^{-41} \text{ cm}^2,$$

where  $E_\nu$  is the laboratory energy of the neutrino.

Fig. 12.9 Definition of  $\theta$  for  $\bar{\nu}_e e^-$  scattering.

The Feynman diagram for  $\bar{\nu}_e e^- \rightarrow e^- \bar{\nu}_e$  is shown in Fig. 12.8b. We see that it can be obtained by crossing the neutrinos in  $\nu_e e^- \rightarrow e^- \nu_e$  of diagram (a); see Sections 4.6 and 4.7. We therefore simply replace  $s$  by  $t$  in (12.57):

$$\begin{aligned} \frac{1}{2} \sum_{\text{spins}} |\mathcal{M}|^2 &= 16G^2 t^2 \\ &= 4G^2 s^2 (1 - \cos \theta)^2, \end{aligned} \quad (12.61)$$

where  $\theta$  is the angle between the incoming  $\bar{\nu}_e$  and the outgoing  $e^-$  (see Fig. 12.9), and

$$t \approx -\frac{s}{2}(1 - \cos \theta),$$

see (4.45). From (12.61), we obtain

$$\frac{d\sigma(\bar{\nu}_e e^-)}{d\Omega} = \frac{G^2 s}{16\pi^2} (1 - \cos \theta)^2, \quad (12.62)$$

and integrating over angles yields

$$\sigma(\bar{\nu}_e e^-) = \frac{G^2 s}{3\pi}. \quad (12.63)$$

Comparing with (12.60) gives

$$\sigma(\bar{\nu}_e e^-) = \frac{1}{3}\sigma(\nu_e e^-). \quad (12.64)$$

Results (12.59), (12.62), and (12.64) expose the  $\gamma^\mu(1 - \gamma^5)$  structure of the weak current in a way that can be experimentally checked. We can convince ourselves of this important statement by comparing the results with those obtained for the  $\gamma^\mu$  vertex in the electromagnetic process  $e\mu \rightarrow e\mu$  or by performing the following exercise.

**EXERCISE 12.16** If the weak current had had a  $V + A$  structure,  $\gamma^\mu(1 + \gamma^5)$ , show that

$$\frac{d\sigma}{d\Omega} = \frac{G^2 s}{4\pi^2} (1 + \cos \theta)^2$$

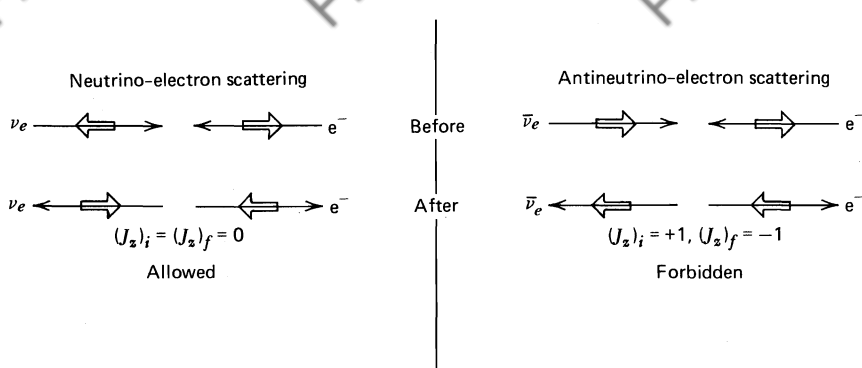


**Fig. 12.10** Backward scattering in the center-of-mass frame. The long arrows represent the particle momenta and the short arrows represent their helicities in the limit in which the masses are negligible. The  $z$  axis is along the incident neutrino direction.

for both  $\nu_e e$  and  $\bar{\nu}_e e$  elastic scattering. If this were the case, then, in contrast to (12.64), we would have

$$\sigma(\bar{\nu}_e e) = \sigma(\nu_e e).$$

The most striking difference between the two angular distributions, (12.59) and (12.62), is that  $\bar{\nu}_e e$  scattering vanishes for  $\cos \theta = 1$ , whereas  $\nu_e e$  scattering does not. With our definition of  $\theta$ , see Fig. 12.9, this corresponds to backward scattering of the beam particle. We could have anticipated these results from the helicity arguments we used to interpret previous calculations. The by now familiar pictures are shown in Fig. 12.10. Backward  $\bar{\nu}_e e$  scattering is forbidden by angular momentum conservation. In fact, the process  $\bar{\nu}_e e \rightarrow \bar{\nu}_e e$  proceeds entirely in a  $J = 1$  state with net helicity +1; that is, only one of the three helicity states is allowed. This is the origin of the factor  $\frac{1}{3}$  in (12.64). With our definition of  $\theta$ , the allowed amplitude is proportional to  $d_{-11}^1(\theta) = \frac{1}{2}(1 - \cos \theta)$ , see (6.39), in agreement with result (12.61).

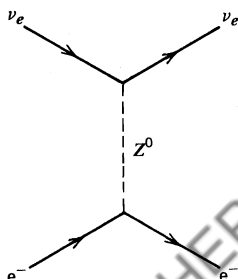


**Fig. 12.11** Neutral current contributions to neutrino-electron elastic scattering.

Elastic  $\nu_e e^-$  and  $\bar{\nu}_e e^-$  scattering can also proceed via a weak neutral current interaction (see Fig. 12.11) which interferes with the charged current interaction (Fig. 12.8a). This is discussed in Section 13.5. However, high-energy neutrino beams are predominantly  $\nu_\mu$  (or  $\bar{\nu}_\mu$ ), and so the most accessible (charged current) purely leptonic scattering process is

$$\nu_\mu + e^- \rightarrow \mu^- + \nu_e \quad (12.65)$$

(i.e., inverse muon decay). Here, there is no neutral current contribution, and so the cross section is given just by (12.59).

## 12.8 Neutrino–Quark Scattering

A study of the scattering of  $\nu_\mu$ 's (or  $\bar{\nu}_\mu$ 's) from quarks is experimentally feasible by impinging high-energy neutrino beams on proton or nuclear targets. This is analogous to the study of the electromagnetic lepton–quark interaction by scattering high-energy electron or muon beams off hadronic targets, which we described in Chapters 8 and 9.

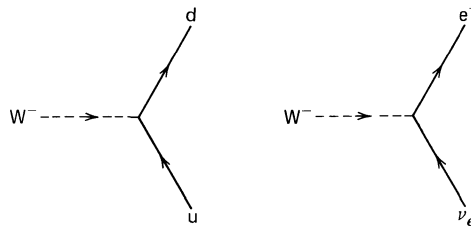
To predict the neutrino–quark cross sections, we clearly need to know the form of the quark weak currents. Quarks interact electromagnetically just like leptons, apart from their fractional charge. Our inclination therefore is to construct the quark weak current just as we did for leptons. For instance, we model the charge-raising quark current

$$J_q^\mu = \bar{u}_u \gamma^{\mu \frac{1}{2}} (1 - \gamma^5) u_d \quad \Rightarrow \quad W^+ \dashrightarrow \begin{array}{c} u \\ \diagdown \\ d \end{array} \quad (12.66)$$

on the electron weak current (12.12)

$$J_e^\mu = \bar{u}_e \gamma^{\mu \frac{1}{2}} (1 - \gamma^5) u_e \quad \Rightarrow \quad W^+ \dashrightarrow \begin{array}{c} \nu_e \\ \diagdown \\ e^- \end{array} \quad (12.67)$$

The hermitian conjugates of (12.66) and (12.67) give the charge-lowering weak currents



The  $V-A$  structure means that the weak current couples only left-handed u and d quarks (or right-handed  $\bar{u}$  and  $\bar{d}$  quarks), see Exercise 12.3. At high energies, this means only negative helicity u and d quarks are coupled, or positive helicity  $\bar{u}$  and  $\bar{d}$  quarks.

Using the above currents, we can evaluate diagrams such as Fig. 12.12. That is, we can calculate the amplitude for

$$d \rightarrow u e^- \bar{\nu}_e$$

which is responsible for a constituent description of neutron  $\beta$ -decay. The “spectator” u and d quarks, shown in Fig. 12.12, can be treated just like the spectator nucleons in the nuclear  $\beta$ -transitions of Section 12.3. The same  $d \rightarrow u$  transition is responsible for the  $\pi^- \rightarrow \pi^0 e^- \bar{\nu}_e$  decay mode, the spectator quark now being a  $\bar{u}$ ; alternatively, we may have a  $\bar{u} \rightarrow \bar{d}$  transition with a spectator d quark.

**EXERCISE 12.17** Using the above approach, show that

$$\Gamma(\pi^- \rightarrow \pi^0 e^- \bar{\nu}_e) = \frac{G^2}{30\pi^3} (\Delta m)^5, \quad (12.68)$$

where  $\Delta m = m(\pi^-) - m(\pi^0) = 4.6$  MeV. Evaluate the decay rate and compare with  $\Gamma(\pi^- \rightarrow \mu^- \bar{\nu}_\mu)$ .

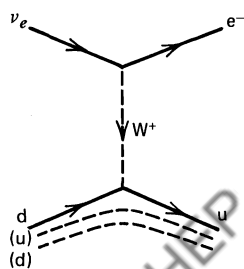


**Fig. 12.12** The quark diagram responsible for neutron  $\beta$ -decay,  $n \rightarrow p e^- \bar{\nu}_e$ . The two spectator quarks which do not take part in the weak interaction are shown by dashed lines.

We are now ready to tackle neutrino–quark scattering. As the quarks and lepton weak currents have identical forms, we can carry over the results for  $\nu e$  scattering that we obtained in Section 12.7. From (12.59) and (12.62), we obtain in the center-of-mass frame

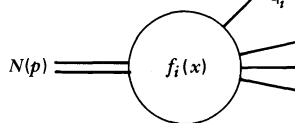
$$\frac{d\sigma(\nu_\mu d \rightarrow \mu^- u)}{d\Omega} = \frac{G^2 s}{4\pi^2} \quad (12.69)$$

$$\frac{d\sigma(\bar{\nu}_\mu u \rightarrow \mu^+ d)}{d\Omega} = \frac{G^2 s}{16\pi^2} (1 + \cos \theta)^2, \quad (12.70)$$

where  $\theta$  is defined as in Fig. 12.13. From the figure, it is immediately apparent that the backward  $\bar{\nu}_\mu u \rightarrow \mu^+ d$  scattering ( $\theta = \pi$ ) is forbidden by helicity considerations. The cross sections for scattering from antiquarks,  $\bar{\nu}_\mu \bar{d} \rightarrow \mu^+ \bar{u}$  and  $\nu_\mu \bar{u} \rightarrow \mu^- \bar{d}$ , are given by (12.69) and (12.70), respectively. We see that, for instance,  $\nu_\mu$  does not interact with either  $u$  or  $\bar{d}$  quarks.

To compare these results with experiment, we have to embed the constituent cross sections, (12.69) and (12.70), in the overall  $\nu N$  inclusive cross section. The procedure is familiar from Chapter 9. We obtain

$$\frac{d\sigma(\nu N \rightarrow \mu X)}{dx dy} = \sum_i f_i(x) \left( \frac{d\sigma_i}{dy} \right)_{\hat{s}=xs} \quad (12.71)$$



$$= \sum_i f_i(x) \left( \frac{d\sigma_i}{dy} \right)_{\hat{s}=xs}. \quad (12.72)$$

First, note that the angular distributions of the constituent process have been expressed in terms of the dimensionless variable  $y$ . It is related to  $\cos \theta$  by

$$1 - y \equiv \frac{p \cdot k'}{p \cdot k} \simeq \frac{1}{2}(1 + \cos \theta),$$

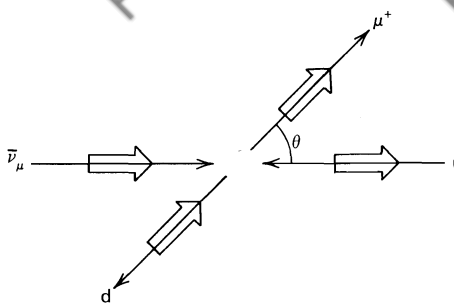


**Fig. 12.13** The helicity configuration for high-energy  $\bar{\nu}_\mu u \rightarrow \mu^+ d$  scattering.

see (9.25). The four-momenta are given in (12.71). The constituent cross sections, (12.69) and (12.70), are therefore

$$\frac{d\sigma}{dy}(\nu_\mu d \rightarrow \mu^- u) = \frac{G^2 xs}{\pi}, \quad (12.73)$$

$$\frac{d\sigma}{dy}(\bar{\nu}_\mu u \rightarrow \mu^+ d) = \frac{G^2 xs}{\pi}(1-y)^2. \quad (12.74)$$

The appropriate  $\nu q \rightarrow \mu q'$  center-of-mass energy is  $xs$ , where now  $s$  refers to  $\nu N \rightarrow \mu X$  (see Exercise 9.3). Using these results, together with the nucleon structure functions  $f_i(x)$  introduced in Chapter 9, we can calculate the deep inelastic  $\nu_\mu N \rightarrow \mu X$  cross section.

To confront these parton model predictions with experiment, it is simplest to take an isoscalar target, in which the nuclei contain equal numbers of protons and neutrons. The neutrinos interact only with  $d$  or  $\bar{u}$  quarks. They therefore measure

$$\begin{aligned} d^p(x) + d^n(x) &= d(x) + u(x) \equiv Q(x) \\ \bar{u}^p(x) + \bar{u}^n(x) &= \bar{u}(x) + \bar{d}(x) \equiv \bar{Q}(x), \end{aligned} \quad (12.75)$$

see (9.29), where we have denoted the distribution functions,  $f_i(x)$ , of up- and down-quarks in a proton by  $u(x)$  and  $d(x)$ . Inserting (12.73) and the cross section for  $\nu_\mu \bar{u} \rightarrow \mu^- \bar{d}$  into (12.72), we find the  $\nu_\mu N \rightarrow \mu^- X$  cross section per nucleon to be

$$\frac{d\sigma}{dx dy}(\nu_\mu N \rightarrow \mu^- X) = \frac{G^2 xs}{2\pi} (Q(x) + (1-y)^2 \bar{Q}(x)). \quad (12.76)$$

On the other hand, antineutrinos interact with  $\bar{d}$  and  $u$  constituents; and going through the same steps, we obtain

$$\frac{d\sigma}{dx dy}(\bar{\nu}_\mu N \rightarrow \mu^+ X) = \frac{G^2 xs}{2\pi} [\bar{Q}(x) + (1-y)^2 Q(x)]. \quad (12.77)$$

**EXERCISE 12.18** Show that deep inelastic electron electromagnetic scattering on an isoscalar target gives

$$\frac{d\sigma(eN \rightarrow eX)}{dx dy} = \frac{2\pi\alpha^2}{Q^4} xs [1 + (1 - y)^2] \frac{5}{18} [Q(x) + \bar{Q}(x)] \quad (12.78)$$

per nucleon, see Exercise 9.5. Note that, in contrast to  $\nu N \rightarrow \mu^- X$ , (12.78) embodies parity conservation so  $Q$  and  $\bar{Q}$  appear symmetrically.

If there were just three valence quarks in a nucleon,  $\bar{Q} = 0$ , the  $\nu N \rightarrow \mu^- X$  and  $\bar{\nu} N \rightarrow \mu^+ X$  data would exhibit the dramatic  $V-A$  properties of the weak interaction exactly. That is,

$$\frac{d\sigma(\nu)}{dy} = c, \quad \frac{d\sigma(\bar{\nu})}{dy} = c(1 - y)^2, \quad (12.79)$$

where  $c$  can be found from (12.76); and for the integrated cross sections,

$$\frac{\sigma(\bar{\nu})}{\sigma(\nu)} = \frac{1}{3}.$$

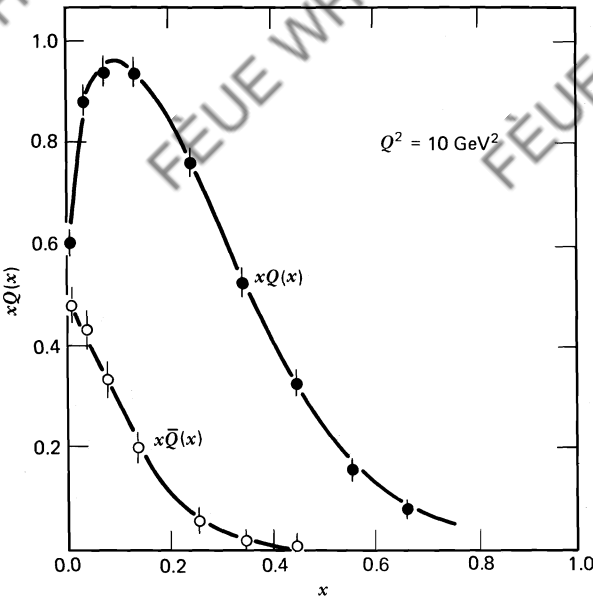


**Fig. 12.14** Quark and antiquark momentum distributions in a nucleon as measured at CERN and the Fermi laboratory. The experiments reveal that only about half the proton's momentum is carried by quarks. We have associated the remainder with the gluon constituents (see Section 9.4).

The data approximately reproduce these expectations. In fact, (12.76) and (12.77) allow a determination of  $Q(x)$  and  $\bar{Q}(x)$ . An example is shown in Fig. 12.14. There is about a 5%  $\bar{Q}$  component in a proton.

**EXERCISE 12.19** If  $\sigma(\bar{\nu})/\sigma(\nu) = R$ , show that

$$\frac{\int x \bar{Q}(x) dx}{\int x Q(x) dx} = \frac{3R - 1}{3 - R}.$$

Detailed analyses show that the functions  $u(x)$ ,  $d(x)$ , ..., are indeed the same whether one extracts them from electroproduction or neutrino experiments. This is a definitive success of the parton model: the  $u(x)$ ,  $d(x)$ , describe the intrinsic structure of the hadronic target and are the same whatever experimental probe is used to determine them.

## 12.9 First Observation of Weak Neutral Currents

The detection in 1973 of neutrino events of the type

$$\bar{\nu}_\mu e^- \rightarrow \bar{\nu}_\mu e^-, \quad (12.80)$$

$$\left. \begin{array}{l} \nu_\mu N \rightarrow \nu_\mu X \\ \bar{\nu}_\mu N \rightarrow \bar{\nu}_\mu X \end{array} \right\} \quad (12.81)$$

heralded a new chapter in particle physics. These events are evidence of a weak neutral current. Until then, no weak neutral current effects had been observed, and indeed very stringent limits had been set on the (strangeness changing) neutral current by the absence of decay modes such as

$$\begin{aligned} K^0 &\rightarrow \mu^+ \mu^-, \\ K^+ &\rightarrow \pi^+ e^+ e^-, \\ K^+ &\rightarrow \pi^+ \nu \bar{\nu}. \end{aligned}$$

Induced weak neutral current effects are expected to occur by the combined action of the (neutral) electromagnetic and the (charged) weak current (for example,  $K^+ \rightarrow \pi^+ e^+ e^-$  can proceed via a virtual photon:  $K^+ \rightarrow \pi^+ \gamma$  with  $\gamma \rightarrow e^+ e^-$ ), but these effects are very small. The rate, compared to the corresponding allowed weak decay, is of the order

$$\frac{\Gamma(K^+ \rightarrow \pi^+ e^+ e^-)}{\Gamma(K^+ \rightarrow \pi^0 e^+ \nu_e)} \sim \left( \frac{\alpha G}{G} \right)^2 \sim 10^{-5}, \quad (12.82)$$

in agreement with the data. (Here, the  $1/q^2$  behavior of the propagator of the virtual photon is canceled by the helicity suppression of the  $0^- \rightarrow 0^- \gamma$  coupling.)

However, reactions (12.80) and (12.81) were found to occur at rates very similar to those of other weak scattering processes.

### 12.10 Neutral Current Neutrino–Quark Scattering

A quantitative comparison of the strength of neutral current (NC) to charged current (CC) weak processes has been obtained, for example, by scattering neutrinos off an iron target. The present experimental values are

$$\begin{aligned} R_\nu &\equiv \frac{\sigma^{NC}(\nu)}{\sigma^{CC}(\nu)} \equiv \frac{\sigma(\nu_\mu N \rightarrow \nu_\mu X)}{\sigma(\nu_\mu N \rightarrow \mu^- X)} = 0.31 \pm 0.01, \\ R_{\bar{\nu}} &\equiv \frac{\sigma^{NC}(\bar{\nu})}{\sigma^{CC}(\bar{\nu})} \equiv \frac{\sigma(\bar{\nu}_\mu N \rightarrow \bar{\nu}_\mu X)}{\sigma(\bar{\nu}_\mu N \rightarrow \mu^+ X)} = 0.38 \pm 0.02. \end{aligned} \quad (12.83)$$

The  $\nu N \rightarrow \nu X$  data can be explained in terms of neutral current–current  $\nu q \rightarrow \nu q$  interactions, see Fig. 12.15, with amplitudes

$$\mathcal{M} = \frac{G_N}{\sqrt{2}} [\bar{u}_\nu \gamma^\mu (1 - \gamma^5) u_\nu] [\bar{u}_q \gamma_\mu (c_V^q - c_A^q \gamma^5) u_q] \quad (12.84)$$

where  $q = u, d, \dots$  are the quarks in the target. *A priori*, there is no reason why the neutral weak interaction should have the four-vector current–current form of (12.84). It is decided by experiment, for instance, by the observed  $y$  distribution (see Exercise 12.20).

It is appropriate at this stage to introduce the conventional normalization of the weak neutral currents,  $J_\mu^{NC}$ . The invariant amplitude for an arbitrary neutral current process is written

$$\boxed{\mathcal{M} = \frac{4G}{\sqrt{2}} 2\rho J_\mu^{NC} J^{\mu NC},} \quad (12.85)$$

compare (12.13) for a charged current process. The  $\nu q \rightarrow \nu q$  amplitude of (12.84)

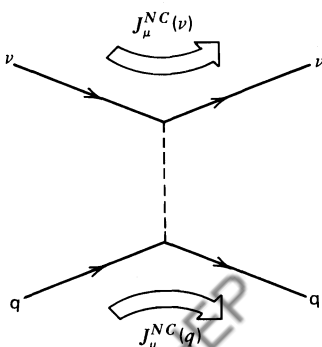


Fig. 12.15 Neutral current  $\nu q \rightarrow \nu q$  scattering.

is of this form; the customary definition of the neutral currents is

$$J_\mu^{NC}(\nu) = \frac{1}{2} (\bar{u}_\nu \gamma_{\mu\frac{1}{2}}^1 (1 - \gamma^5) u_\nu), \quad (12.86)$$

$$J_\mu^{NC}(q) = (\bar{u}_q \gamma_{\mu\frac{1}{2}}^1 (c_V^q - c_A^q \gamma^5) u_q). \quad (12.87)$$

In general, the  $J_\mu^{NC}$ , unlike the charged current  $J_\mu$ , are not pure  $V-A$  currents ( $c_V \neq c_A$ ); they have right-handed components. However, the neutrino is left-handed; and so,  $c_V^\nu = c_A^\nu \equiv \frac{1}{2}$  in (12.86). The parameter  $\rho$  in (12.85) determines the relative strength of the neutral and charged current processes. In the standard theoretical model all the  $c_V^i$ ,  $c_A^i$  (with  $i = \nu, e, u, \dots$ ) are given in terms of one parameter, and  $\rho = 1$  (see Chapters 13 and 15). In other words, if the model is successful, all neutral current phenomena will be described by a common parameter. In fact, the present experiments give  $\rho = 1$  to within small errors. However, for the moment let us leave  $c_V^i$ ,  $c_A^i$  and  $\rho$  as free parameters to be determined by experiment. Upon inserting the currents (12.86) and (12.87) into (12.85), we obtain the  $\nu q \rightarrow \nu q$  amplitude of (12.84) with

$$G_N = \rho G (\simeq G). \quad (12.88)$$

We now return to our interpretation of the  $\nu N \rightarrow \nu X$  data. The calculation of the  $\nu q \rightarrow \nu q$  cross sections proceeds exactly as that for the charged current processes  $\nu q \rightarrow \mu q'$ . For example, using the results (12.73) and (12.74),

$$\begin{aligned} \frac{d\sigma(\nu_L d_L \rightarrow \mu u)}{dy} &= \frac{G^2 x_S}{\pi}, \\ \frac{d\sigma(\nu_L \bar{u}_R \rightarrow \mu \bar{d})}{dy} &= \frac{G^2 x_S}{\pi} (1-y)^2, \end{aligned} \quad (12.89)$$

we obtain directly

$$\frac{d\sigma(\nu q \rightarrow \nu q)}{dy} = \frac{G_N^2 x_S}{\pi} ((g_L^q)^2 + (g_R^q)^2 (1-y)^2), \quad (12.90)$$

where we have introduced

$$g_L^q \equiv \frac{1}{2} (c_V^q + c_A^q), \quad g_R^q \equiv \frac{1}{2} (c_V^q - c_A^q). \quad (12.91)$$

As compared to (12.89), the new feature of (12.90) is the possibility of a right-handed component  $g_R^q$  of  $J_\mu^{NC}(q)$ .

**EXERCISE 12.20** Show that  $|\mathcal{M}(\nu q \rightarrow \nu q)|^2$  behaves like  $s^2$ ,  $s^2(1-y)^2$ ,  $s^2y^2$  for pure  $V-A$ , pure  $V+A$ , and  $S, P$  neutral couplings of the quark, respectively. Pure  $V \pm A$  denote  $\gamma^\mu(1 \pm \gamma^5)$  couplings, and  $S, P$  stands for the scalar, pseudoscalar interaction amplitude

$$\mathcal{M} = \frac{G_N}{\sqrt{2}} (\bar{u}_\nu (1 - \gamma^5) u_\nu) (\bar{u}_q (g_S - g_P \gamma^5) u_q).$$

The parton model predictions for the neutral current (NC) processes  $\nu N \rightarrow \nu X$  and  $\bar{\nu} N \rightarrow \bar{\nu} X$  are obtained by following the calculation of the CC processes  $\nu N \rightarrow \mu^- X$  and  $\bar{\nu} N \rightarrow \mu^+ X$  of Section 12.8. For an isoscalar target, we find that the cross section per nucleon is

$$\frac{d\sigma(\nu N \rightarrow \nu X)}{dx dy} = \frac{G_N^2 s}{2\pi} \left[ g_L^2 (Q(x) + (1-y)^2 \bar{Q}(x)) + g_R^2 (\bar{Q}(x) + (1-y)^2 Q(x)) \right], \quad (12.92)$$

where, if we assume only u, d,  $\bar{u}$ ,  $\bar{d}$  quarks within the nucleon,

$$g_L^2 \equiv (g_L^u)^2 + (g_L^d)^2, \quad (12.93)$$

and similarly for  $g_R^2$ . We may integrate over  $x$  and define

$$Q \equiv \int x Q(x) dx = \int x [u(x) + d(x)] dx, \quad (12.94)$$

see (12.75). Cross section (12.92) and that for  $\bar{\nu} N \rightarrow \bar{\nu} X$  become

$$\begin{aligned} \frac{d\sigma^{NC}(\nu)}{dy} &= \frac{G_N^2 s}{2\pi} \left\{ g_L^2 (Q + (1-y)^2 \bar{Q}) + g_R^2 (\bar{Q} + (1-y^2) Q) \right\}, \\ \frac{d\sigma^{NC}(\bar{\nu})}{dy} &= \frac{G_N^2 s}{2\pi} \left\{ g_L^2 (\bar{Q} + (1-y)^2 Q) + g_R^2 (Q + (1-y^2) \bar{Q}) \right\}, \end{aligned} \quad (12.95)$$

which are to be contrasted with the charged current expressions (12.76) and (12.77)

$$\begin{aligned} \frac{d\sigma^{CC}(\nu)}{dy} &= \frac{G^2 s}{2\pi} (Q + (1-y)^2 \bar{Q}), \\ \frac{d\sigma^{CC}(\bar{\nu})}{dy} &= \frac{G^2 s}{2\pi} (\bar{Q} + (1-y)^2 Q). \end{aligned} \quad (12.96)$$

Correcting (12.95) and (12.96) for the neutron excess in an iron target and for an s quark contribution, the present data give

$$g_L^2 = 0.300 \pm 0.015, \quad g_R^2 = 0.024 \pm 0.008. \quad (12.97)$$

The experimental verdict is that the weak neutral current is predominantly  $V-A$  (i.e., left-handed) but, since  $g_R \neq 0$ , not pure  $V-A$ . The NC and the CC have a tantalizingly similar structure, but the CC is believed to have a pure  $V-A$  form. Chapter 13 takes up this point, but first we must look more carefully at the quark sector.

## 12.11 The Cabibbo Angle

So far, we have seen that leptons and quarks participate in weak interactions through charged  $V-A$  currents constructed from the following pairs of (left-

handed) fermion states:

$$\begin{pmatrix} \nu_e \\ e^- \end{pmatrix}, \quad \begin{pmatrix} \nu_\mu \\ \mu^- \end{pmatrix}, \quad \text{and} \quad \begin{pmatrix} u \\ d \end{pmatrix}. \quad (12.98)$$

All these charged currents couple with a universal coupling constant  $G$ . It is natural to attempt to extend this universality to embrace the doublet

$$\begin{pmatrix} c \\ s \end{pmatrix} \quad (12.99)$$

formed from the heavier quark states. However, we already know that this cannot be quite correct. For instance, the decay  $K^+ \rightarrow \mu^+ \nu_\mu$  occurs. The  $K^+$  is made of  $u$  and  $\bar{s}$  quarks. There must thus be a weak current which couples a  $u$  to an  $\bar{s}$  quark (see Fig. 12.16). This contradicts the above scheme, which only allows weak transitions between  $u \leftrightarrow d$  and  $c \leftrightarrow s$ .

Instead of introducing new couplings to accommodate observations like  $K^+ \rightarrow \mu^+ \nu_\mu$ , let us try to keep universality but modify the quark doublets. We assume that the charged current couples “rotated” quark states

$$\begin{pmatrix} u \\ d' \end{pmatrix}, \quad \begin{pmatrix} c \\ s' \end{pmatrix}, \dots \quad (12.100)$$

where

$$\begin{aligned} d' &= d \cos \theta_c + s \sin \theta_c \\ s' &= -d \sin \theta_c + s \cos \theta_c. \end{aligned} \quad (12.101)$$

This introduces an arbitrary parameter  $\theta_c$ , the quark mixing angle, known as the Cabibbo angle. In 1963, Cabibbo first introduced the doublet  $u, d'$  to account for the weak decays of strange particles. Indeed, the mixing of the  $d$  and  $s$  quark can be determined by comparing  $\Delta S = 1$  and  $\Delta S = 0$  decays. For example,

$$\begin{aligned} \frac{\Gamma(K^+ \rightarrow \mu^+ \nu_\mu)}{\Gamma(\pi^+ \rightarrow \mu^+ \nu_\mu)} &\sim \sin^2 \theta_c, \\ \frac{\Gamma(K^+ \rightarrow \pi^0 e^+ \nu_e)}{\Gamma(\pi^+ \rightarrow \pi^0 e^+ \nu_e)} &\sim \sin^2 \theta_c. \end{aligned}$$

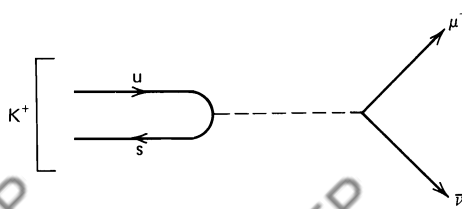
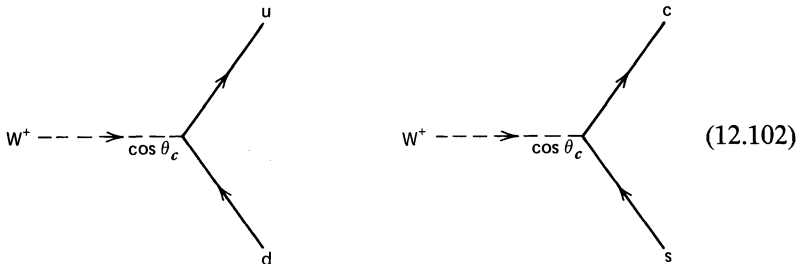


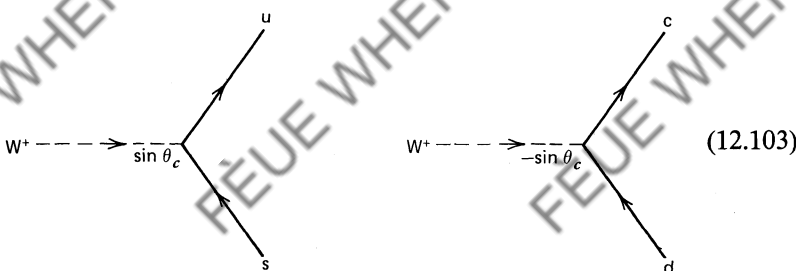
Fig. 12.16 The decay  $K^+ \rightarrow \mu^+ \bar{\nu}_\mu$ .

After allowing for the kinematic factors arising from the different particle masses, the data show that the  $\Delta S = 1$  transitions are suppressed by a factor of about 20 as compared to the  $\Delta S = 0$  transitions. This corresponds to a Cabibbo angle  $\theta_c \approx 13^\circ$ .

What we have done is to change our mind about the charged current (12.66). We now have “Cabibbo favored” transitions (proportional to  $\cos \theta_c$ )



and “Cabibbo suppressed” transitions



[see (12.101)], and similar diagrams for the charge-lowering transitions. We can summarize this by writing down the explicit form of the matrix element describing the charged current weak interactions of the quarks. From (12.13),

$$\mathcal{M} = \frac{4G}{\sqrt{2}} J^\mu J_\mu^\dagger \quad (12.104)$$

with

$$J^\mu = (\bar{u} \quad \bar{c}) \frac{\gamma^\mu (1 - \gamma^5)}{2} U \begin{pmatrix} d \\ s \end{pmatrix}. \quad (12.105)$$

The unitary matrix  $U$  performs the rotation (12.101) of the d and s quark states:

$$U = \begin{pmatrix} \cos \theta_c & \sin \theta_c \\ -\sin \theta_c & \cos \theta_c \end{pmatrix}. \quad (12.106)$$

Of course, there will also be amplitudes describing semileptonic decays constructed from the product of a quark with a lepton current,  $J^\mu(\text{quark}) J_\mu^\dagger(\text{lepton})$ .

All this has implications for our previous calculations. For instance, we must replace  $G$  in the formula for the nuclear  $\beta$ -decay rate by

$$G_\beta = G \cos \theta_c, \quad (12.107)$$

whereas the purely leptonic  $\mu$ -decay rate, which involves no mixing, is unchanged:  $G_\mu = G$ . The detailed comparison of these rates, (12.44), supports Cabibbo's hypothesis.

The weak interactions discussed so far involve only the u and d' quark states. However, in (12.100), we have coupled s' to the charmed quark c, so that we have weak transitions  $c \leftrightarrow s'$  as well as  $d' \leftrightarrow u$ . In fact, following this line of argument, Glashow, Iliopoulos, and Maiani (GIM) proposed the existence of the c quark some years before its discovery. A reason for doing this can be seen by studying the decay  $K^0 \rightarrow \mu^+ \mu^-$ . With only  $u \leftrightarrow d'$  transitions, the diagram of Fig. 12.17a predicts that the  $K_L^0 \rightarrow \mu^+ \mu^-$  decay would occur at a rate far in excess of what is observed:

$$\frac{\Gamma(K_L^0 \rightarrow \mu^+ \mu^-)}{\Gamma(K_L^0 \rightarrow \text{all modes})} = (9.1 \pm 1.9) \times 10^{-9}.$$

However, with the introduction of the c quark, a second diagram, Fig. 12.17b, occurs which would exactly cancel with diagram 12.17a if it were not for the mass difference of the u and c quarks. We take up this discussion in the next section.

The c, s' weak current is responsible for the weak decays of charmed particles. A delightful example is the decay of a  $D^+$  meson. The  $D^+$  meson consists of a c and  $\bar{d}$  quark. Since  $\cos^2 \theta_c \gg \sin^2 \theta_c$ , it follows from (12.100) and (12.101) that the favored quark decay pattern is that shown in Fig. 12.18, with amplitude

$$\mathcal{M}(c \rightarrow \bar{s}ud) \sim \cos^2 \theta_c. \quad (12.108)$$

That is, a  $\bar{K}$  meson should preferentially feature among the decay products of a  $D^+$ . On the other hand, the decay  $D^+ \rightarrow K \dots$  is highly (Cabibbo) suppressed since

$$\mathcal{M}(c \rightarrow \bar{s}ud) \sim \sin^2 \theta_c. \quad (12.109)$$

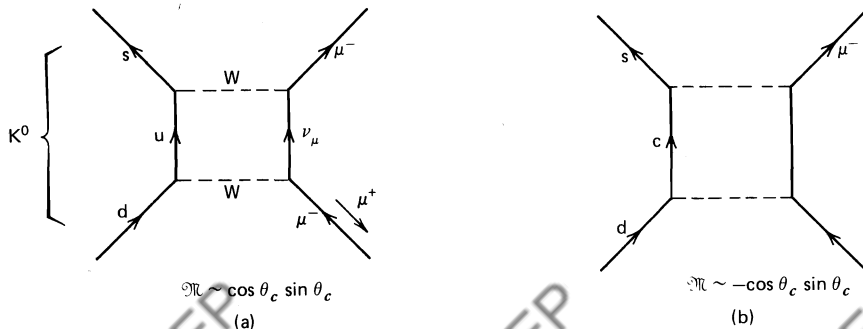
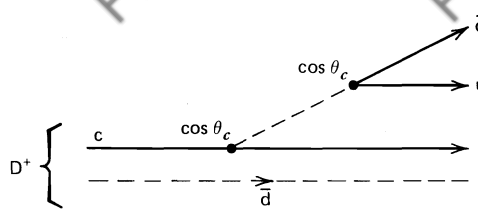


Fig. 12.17 Two contributions to  $K^0 \rightarrow \mu^+ \mu^-$ . Diagram (b) is simply (a) with  $u \rightarrow c$ .



**Fig. 12.18** A quark description of  $D^+$  decay: the Cabibbo-favored process is  $c \rightarrow su\bar{d}$  with a spectator  $\bar{d}$  quark.

We thus have a very characteristic signature for  $D^+$  decay, that for instance the decay mode  $K^-\pi^+\pi^+$  is highly favored as compared to the  $K^+\pi^+\pi^-$  mode.

**EXERCISE 12.21** Estimate the relative rates for the following three decay modes of the  $D^0(\bar{c}\bar{u})$  meson:  $D^0 \rightarrow K^-\pi^+, \pi^-\pi^+, K^+\pi^-$ .

**EXERCISE 12.22** Given that the partial rate

$$\Gamma(K^+ \rightarrow \pi^0 e^+ \nu) = 4 \times 10^6 \text{ sec}^{-1},$$

calculate the rate for  $D^0 \rightarrow K^- e^+ \nu$ . Hence, estimate the lifetime of the  $D^0$  meson.

**EXERCISE 12.23** Show, in the “spectator” quark model approach, that the charmed meson lifetimes satisfy

$$\tau(D^0) = \tau(D^+) = \tau(F^+),$$

where  $F^+$  is made of  $c$  and  $\bar{s}$  quarks, see Chapter 2.

## 12.12 Weak Mixing Angles

We can summarize the above Cabibbo-GIM scheme as follows. The charged (or flavor-changing) current couples  $u \leftrightarrow d'$  or  $c \leftrightarrow s'$  (left-handed) quark states, where  $d'$  and  $s'$  are orthogonal combinations of the physical (i.e., mass) eigenstates of quarks of definite flavor  $d, s$ :

$$\begin{pmatrix} d' \\ s' \end{pmatrix} = \begin{pmatrix} \cos \theta_c & \sin \theta_c \\ -\sin \theta_c & \cos \theta_c \end{pmatrix} \begin{pmatrix} d \\ s \end{pmatrix}. \quad (12.110)$$

The quark mixing is described by a single parameter, the Cabibbo angle  $\theta_c$ .

The original motivation for the GIM proposal was to ensure that there are no  $s \leftrightarrow d$  transitions, which change flavor but not charge. The experimental evidence for the absence of strangeness-changing neutral currents is compelling. For

instance, decays such as  $K^0 \rightarrow \mu^+ \mu^-$ ,  $K^+ \rightarrow \pi^+ e^+ e^-$ ,  $K^+ \rightarrow \pi^+ \nu \bar{\nu}$ , which would be otherwise allowed, are either absent or highly suppressed.

How does the GIM mechanism work? To see this, it is convenient to rewrite (12.110) in the form

$$d'_i = \sum_j U_{ij} d_j, \quad (12.111)$$

with  $d_1 \equiv d_L$  and  $d_2 \equiv s_L$  where  $L$  denotes a left-handed quark state. Now the matrix  $U$ , introduced in (12.105), is unitary (provided we adopt the universal weak coupling hypothesis), and therefore we have

$$\begin{aligned} \sum_i \bar{d}'_i d'_i &= \sum_{i,j,k} \bar{d}_j U_{ji}^\dagger U_{ik} d_k \\ &= \sum_j \bar{d}_j d_j. \end{aligned} \quad (12.112)$$

That is, only transitions  $d \rightarrow d$  and  $s \rightarrow s$  are allowed; flavor-changing transitions,  $s \leftrightarrow d$ , are forbidden.

Before we extend the GIM mechanism to incorporate additional quark flavors, we must answer two questions that may have come to mind. First, why is the mixing taken in the  $d, s$  sector? In fact, the mixing could equally well have been formulated in the  $u, c$  sector; no observable difference would result since the absolute phases of the quark wavefunctions are not observable. Indeed, a more involved mixing in both the  $u, c$  and  $d, s$  sectors can be used, but it can always be simplified (by appropriately choosing the phases of the quark states) to the one-parameter form given in (12.110). This will become clearer in a moment.

A second question is, “Why is there no Cabibbo-like angle in the leptonic sector?”

$$\begin{pmatrix} \nu_e \\ e^- \end{pmatrix}, \quad \begin{pmatrix} \nu_\mu \\ \mu^- \end{pmatrix}. \quad (12.113)$$

The reason is that if  $\nu_e$  and  $\nu_\mu$  are massless, then lepton mixing is unobservable. Any Cabibbo-like rotation still leaves us with neutrino mass eigenstates. By definition, we take  $\nu_e$  to be the partner of the electron. This guarantees conserved lepton numbers  $L_e$  and  $L_\mu$ . By contrast, the weak interaction eigenstates  $d', s'$  are not the same as the mass eigenstates but are related by (12.110).

Now consider the generalization of the Cabibbo-GIM ideas to more than four quark flavors. Imagine for a moment that weak interactions operate on  $N$  doublets of left-handed quarks,

$$\begin{pmatrix} u_i \\ d'_i \end{pmatrix} \quad \text{with } i = 1, 2, \dots, N \quad (12.114)$$

where  $d'_i$  are mixtures of the mass eigenstates  $d_j$ :

$$d'_i = \sum_{j=1}^N U_{ij} d_j, \quad (12.115)$$

$U$  is a unitary  $N \times N$  matrix to be determined by the flavor-changing weak processes. How many observable parameters does  $U$  contain? We can change the phase of each of the  $2N$  quark states independently without altering the physics. Therefore,  $U$  contains

$$N^2 - (2N - 1)$$

real parameters. One phase is omitted as an overall phase change still leaves  $U$  invariant. On the other hand, an orthogonal  $N \times N$  matrix has only  $\frac{1}{2}N(N - 1)$  real parameters [e.g., (12.110)]. Therefore, by redefining the quark phases, it is not possible, in general, to make  $U$  real.  $U$  must contain

$$N^2 - (2N - 1) - \frac{1}{2}N(N - 1) = \frac{1}{2}(N - 1)(N - 2) \quad (12.116)$$

residual phase factors. Thus, for two doublets ( $N = 2$ ), there is one real parameter ( $\theta_c$ ), whereas for three doublets, there are three real parameters and one phase factor,  $e^{i\delta}$ .

We have in fact conclusive evidence for a fifth flavor of quark, the bottom quark  $b$  with charge  $Q = -\frac{1}{3}$  (see Chapter 2), and it is widely believed that its partner, the top quark  $t$  with  $Q = +\frac{2}{3}$ , exists. Weak interactions would then operate on three doublets of left-handed quarks,

$$\begin{pmatrix} u \\ d' \end{pmatrix}, \quad \begin{pmatrix} c \\ s' \end{pmatrix}, \quad \begin{pmatrix} t \\ b' \end{pmatrix}. \quad (12.117)$$

Why should we expect quarks to come in pairs? There are two reasons for this. First, it provides a natural way to suppress the flavor-changing neutral current; the argument leading to (12.112) applies just as well for three as for two doublets. The second reason is concerned with the desire to obtain a renormalizable gauge theory of weak interactions (see Chapters 14 and 15). This requires a delicate cancellation between different diagrams, relations which can easily be upset by “anomalies” due to fermion loops such as Fig. 12.19. These anomalies must be canceled for a renormalizable theory. Each triangle is proportional to  $c_A^f Q_f^2$ , where  $Q_f$  is the charge and  $c_A^f$  is the axial coupling of the weak neutral current. Thus, for an equal number  $N$  of lepton and quark doublets, the total anomaly is proportional to

$$\sum_{i=1}^N \left( \frac{1}{2}(0)^2 - \frac{1}{2}(-1)^2 + \frac{1}{2}N_c(+\frac{2}{3})^2 - \frac{1}{2}N_c(-\frac{1}{3})^2 \right) = 0. \quad (12.118)$$

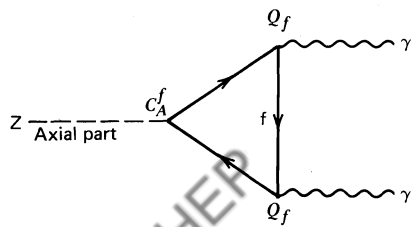


Fig. 12.19 A fermion (quark or lepton) triangle diagram which potentially could cause an anomaly.

The values used for  $c_A^f$  are determined in the next chapter (see Table 13.2). Thus, taking account of the three colors of each quark ( $N_c = 3$ ), the anomalies are canceled. Since we have three lepton doublets (electron, muon, and tau), it is therefore natural to anticipate the three quark doublets of (12.117).

It is straightforward to extend the weak current, (12.105), to embrace the new doublet of quarks:

$$J^\mu = (\bar{u} \bar{c} \bar{t}) \frac{\gamma_\mu (1 - \gamma^5)}{2} U \begin{pmatrix} d \\ s \\ b \end{pmatrix}. \quad (12.119)$$

The  $3 \times 3$  mixing matrix  $U$  contains three real parameters (Cabibbo-like mixing angles) and a phase factor  $e^{i\delta}$  [see (12.116)]. The original parametrization was due to Kobayashi and Maskawa. Due to the phase  $\delta$ , the matrix  $U$  is complex, unlike the  $2 \times 2$  matrix of (12.110). That is, with the discovery of the b quark, complex elements  $U_{ij}$  enter the weak current. This has fundamental implications concerning  $CP$  invariance, which we discuss in the next section.

We illustrated how each element of the  $2 \times 2$  Cabibbo matrix can be determined from experimental information on the corresponding quark flavor transition. The elements of the  $3 \times 3$  matrix can also be studied in the same way. The present status of the experimental situation may be summarized as follows:

$$U = \begin{bmatrix} |U_{ud}| = 0.973 & |U_{us}| = 0.23 & |U_{ub}| \approx 0 \\ |U_{cd}| \approx 0.24 & |U_{cs}| \approx 0.97 & |U_{cb}| \approx 0.06 \\ |U_{td}| \approx 0 & |U_{ts}| \approx 0 & |U_{tb}| \approx 1 \end{bmatrix}. \quad (12.120)$$

where  $|U| \approx 0$  means that the element is very small, but not yet determined. It is not surprising that some elements are not known, since there is no experimental information on the t quark. An incomplete sketch of how the results of (12.120) are obtained is shown in Table 12.1. The most striking feature of (12.120) is that the diagonal elements  $U_{ud}$ ,  $U_{cs}$ ,  $U_{tb}$  are clearly dominant. The large value of  $|U_{cs}|$  simply reflects the experimental fact that charm particles preferentially decay into strange particles. The experimental observation that B mesons prefer to decay into charm particles implies  $|U_{cb}| > |U_{ub}|$ . Moreover (12.120) indicates that T mesons (when found) should preferentially decay into B mesons. All this has interesting consequences for the study of heavy quark states or for their detection in the case of T mesons. Spectacular experimental signatures result from the favored “cascade” decays, which may be characterized by the presence of multiple leptons (or strange particles) in the final state, for example:

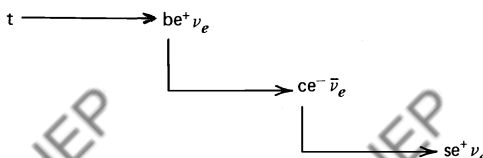


**TABLE 12.1**

A Summary of the Determination of the Elements  $U_{qq'}$  of the Kobayashi–Maskawa Matrix

Element	Experimental Information
$U_{ud}$	$\beta$ -Decay, generalize (12.107)
$U_{us}$	$K \rightarrow \pi e \nu$ and semileptonic hyperon decays, generalize discussion following (12.101)
$U_{ub}$	$b \rightarrow u e^- \bar{\nu}_e$ , look for B meson decays with no K's in final state: gives $ U_{ub} ^2 < 0.02  U_{cb} ^2$ .
$U_{cd}$	$\nu_\mu d \rightarrow \mu^- c$ , charmed particle production by neutrinos
$U_{cs}$	$\nu_\mu s \rightarrow \mu^- c$ and $D^+ \rightarrow \bar{K}^0 e^+ \nu_e$ , see (12.108); also constrained by the unitarity of $U$ , which implies $ U_{cd} ^2 +  U_{cs} ^2 +  U_{cb} ^2 = 1$ , together with the information on $ U_{cd} $ and $ U_{cb} $ .
$U_{cb}$	The (long) lifetime of the B meson, $\tau_B \sim 10^{-12}$ secs, and $ U_{ub} $ .
$U_{tq}$	From unitarity bounds

### 12.13 CP Invariance?

To investigate  $CP$  invariance, we first compare the amplitude for a weak process, say, the quark scattering process  $ab \rightarrow cd$ , with that for the antiparticle reaction  $\bar{a}\bar{b} \rightarrow \bar{c}\bar{d}$ . We take  $ab \rightarrow cd$  to be the charged current interaction of Fig. 12.20a. The amplitude

$$\begin{aligned} \mathcal{M} &\sim J_{ca}^\mu J_{\mu bd}^\dagger \\ &\sim (\bar{u}_c \gamma^\mu (1 - \gamma^5) U_{ca} u_a) (\bar{u}_b \gamma_\mu (1 - \gamma^5) U_{bd} u_d)^\dagger \\ &\sim U_{ca}^* U_{db} (\bar{u}_c \gamma^\mu (1 - \gamma^5) u_a) (\bar{u}_d \gamma_\mu (1 - \gamma^5) u_d), \end{aligned} \quad (12.121)$$

since  $U_{bd}^\dagger = U_{db}^*$ .  $\mathcal{M}$  describes either  $ab \rightarrow cd$  or  $\bar{c}\bar{d} \rightarrow \bar{a}\bar{b}$  (remembering the antiparticle description of Chapter 3).

On the other hand, the amplitude  $\mathcal{M}'$  for the antiparticle process  $\bar{a}\bar{b} \rightarrow \bar{c}\bar{d}$  (or  $cd \rightarrow ab$ ) is

$$\begin{aligned} \mathcal{M}' &\sim (J_{ca}^\mu)^\dagger J_{\mu bd} \\ &\sim U_{ca}^* U_{db} (\bar{u}_a \gamma^\mu (1 - \gamma^5) u_c) (\bar{u}_b \gamma_\mu (1 - \gamma^5) u_d); \end{aligned} \quad (12.122)$$

that is,

$$\mathcal{M}' = \mathcal{M}^\dagger.$$

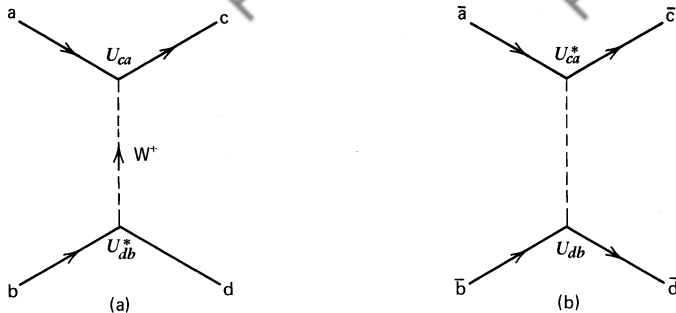


**Fig. 12.20** The processes described by (a) the weak amplitude  $\mathcal{M}(ab \rightarrow cd)$  and (b) its hermitian conjugate.

This should not be surprising. It is demanded by the hermicity of the Hamiltonian. By glancing back at (4.6) and (4.17), we see that  $\mathcal{M}$  is essentially the interaction Hamiltonian  $V$  for the process. The total interaction Hamiltonian must contain  $\mathcal{M} + \mathcal{M}^\dagger$ , where  $\mathcal{M}$  describes the  $i \rightarrow f$  transition and  $\mathcal{M}^\dagger$  describes the  $f \rightarrow i$  transition in the notation of Chapter 4.

In Section 12.1, we have seen that weak interactions violate both  $P$  invariance and  $C$  invariance, but have indicated that invariance under the combined  $CP$  operation may hold. How do we verify that the theory is  $CP$  invariant? We calculate from  $\mathcal{M}(ab \rightarrow cd)$  of (12.121) the amplitude  $\mathcal{M}_{CP}$ , describing the  $CP$ -transformed process, and see whether or not the Hamiltonian remains hermitian. If it does, that is, if

$$\mathfrak{M}_{CP} = \mathfrak{M}^\dagger,$$

then the theory is  $CP$  invariant. If it does not, then  $CP$  is violated.

$\mathcal{M}_{CP}$  is obtained by substituting the  $CP$ -transformed Dirac spinors in (12.121):

$$u_i \rightarrow P(u_i)_C, \quad i = a, \dots, d \quad (12.123)$$

where  $u_C$  are the charge-conjugate spinors of Section 5.4,

$$u_C = C\bar{u}^T. \quad (12.124)$$

Clearly, to form  $\mathfrak{M}_{CP}$ , we need  $\bar{u}_C$  and, also, to know how  $\gamma^\mu(1 - \gamma^5)$  transforms under  $C$ . In the standard representation of the  $\gamma$ -matrices, we have [see (5.39)]

$$\begin{aligned}\bar{u}_C &= -u^T C^{-1}, \\ C^{-1} \gamma^\mu C &= -(\gamma^\mu)^T, \\ C^{-1} \gamma^\mu \gamma^5 C &= +(\gamma^\mu \gamma^5)^T.\end{aligned}\tag{12.125}$$

**EXERCISE 12.24** Verify (12.125) using (5.39).

With the replacements (12.123), the first charged current of (12.121) becomes

$$\begin{aligned}
 (J_{ca}^\mu)_C &= U_{ca}(\bar{u}_c)_C \gamma^\mu(1 - \gamma^5)(u_a)_C \\
 &= -U_{ca}u_c^T C^{-1} \gamma^\mu(1 - \gamma^5) C \bar{u}_a^T \\
 &= U_{ca}u_c^T [\gamma^\mu(1 + \gamma^5)]^T \bar{u}_a^T \\
 &= (-)U_{ca}\bar{u}_a \gamma^\mu(1 + \gamma^5) u_c.
 \end{aligned} \tag{12.126}$$

The above procedure is exactly analogous to that used to obtain the charge-conjugate electromagnetic current, (5.40).

The parity operation  $P = \gamma^0$ , see (5.62), and so

$$P^{-1} \gamma^\mu(1 + \gamma^5) P = \gamma^{\mu\dagger}(1 - \gamma^5),$$

see (5.9)–(5.11). Thus,

$$(J_{ca}^\mu)_{CP} = (-)U_{ca}\bar{u}_a \gamma^{\mu\dagger}(1 - \gamma^5) u_c,$$

and hence

$$\mathcal{M}_{CP} \sim U_{ca}U_{db}^* [\bar{u}_a \gamma^\mu(1 - \gamma^5) u_c] [\bar{u}_b \gamma_\mu(1 - \gamma^5) u_d]. \tag{12.127}$$

We can now compare  $\mathcal{M}_{CP}$  with  $\mathcal{M}^\dagger$  of (12.122). Provided the elements of the matrix  $U$  are real, we find

$$\mathcal{M}_{CP} = \mathcal{M}^\dagger,$$

and the theory is  $CP$  invariant. At the four-quark ( $u, d, c, s$ ) level, this is the case, as the  $2 \times 2$  matrix  $U$ , (12.106), is indeed real. However, with the advent of the  $b$  (and  $t$ ) quarks, the matrix  $U$  becomes the  $3 \times 3$  Kobayashi–Maskawa (KM) matrix. It now contains a complex phase factor  $e^{i\delta}$ . Then, in general, we have

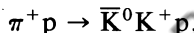
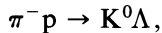
$$\mathcal{M}_{CP} \neq \mathcal{M}^\dagger,$$

and the theory necessarily violates  $CP$  invariance.

In fact, a tiny  $CP$  violation had been established many years before the introduction of the KM matrix. The violation was discovered by observing the decays of neutral kaons. These particles offer a unique “window” through which to look for small  $CP$  violating effects. We discuss this next.

## 12.14 CP Violation: The Neutral Kaon System

The observations of neutral kaons have led to several fundamental discoveries in particle physics.  $K^0$  and  $\bar{K}^0$ , with definite  $I_3$  and  $Y$ , are the states produced by strong interactions (see Chapter 2). For example,



However, experimentally it is found that  $K^0$  decay occurs with two different

lifetimes:

$$\begin{aligned}\tau(K_S^0 \rightarrow 2\pi) &= 0.9 \times 10^{-10} \text{ sec} \\ \tau(K_L^0 \rightarrow 3\pi) &= 0.5 \times 10^{-7} \text{ sec.}\end{aligned}\quad (12.128)$$

In other words, the  $K^0$  produced by the strong interactions seems to be two different particles ( $K_S^0$  and  $K_L^0$ ) when we study its weak decays. The same dilemma appears for the  $\bar{K}^0$ , and it was therefore proposed that the  $K^0$  and  $\bar{K}^0$  are nothing but two different admixtures of the  $K_S^0$  and  $K_L^0$ , the particles associated with the short- and long-lived  $2\pi$  and  $3\pi$  decay modes.

In the absence of orbital angular momentum, the  $2\pi$  and  $3\pi$  final states differ in parity, with  $P = +1$  and  $-1$ , respectively. We mentioned that these observations were in fact instrumental in the discovery of parity violation in weak interactions in 1957. For some time, it was thought that weak interactions were at least invariant under the combined  $CP$  operation. We make the conventional choice of phase of  $|K^0\rangle$  and  $|\bar{K}^0\rangle$  such that

$$CP|K^0\rangle = |\bar{K}^0\rangle.$$

Since the final  $2\pi$  and  $3\pi$  states are eigenstates of  $CP$  with eigenvalues  $+1$  and  $-1$ , respectively (see Exercise 12.26), it is tempting to identify the neutral kaon  $CP$  eigenstates with  $K_S^0$  and  $K_L^0$ :

$$\begin{aligned}|K_S^0\rangle &= \sqrt{\frac{1}{2}}(|K^0\rangle + |\bar{K}^0\rangle) \quad [CP = +1] \\ |K_L^0\rangle &= \sqrt{\frac{1}{2}}(|K^0\rangle - |\bar{K}^0\rangle) \quad [CP = -1].\end{aligned}\quad (12.129)$$

To a very good approximation, this is true. However, in 1964 it was demonstrated that  $K_L^0 \rightarrow \pi^+ \pi^-$  with a branching ratio of order  $10^{-3}$ . Therefore, a small  $CP$  violating effect is indeed present. An excellent summary of the experiments and other  $K^0$  phenomena is given, for example, by Perkins (1982).

**EXERCISE 12.25** Show that  $C = -1$  for a photon and hence that  $C = +1$  for a  $\pi^0$ .

**Hint** Under  $e \rightarrow -e$ , the amplitude corresponding to Fig. 1.9a will change sign.

**EXERCISE 12.26** Show that in the absence of angular momentum, a  $\pi^+ \pi^-$  or  $\pi^0 \pi^0$  state is an eigenstate of  $CP$  with eigenvalue  $+1$ . Further, show that by adding an S wave  $\pi^0$ , we obtain  $CP$  eigenstates  $\pi^+ \pi^- \pi^0$  or  $3\pi^0$  with eigenvalue  $-1$ .

**Hint** A  $\pi^+ \pi^-$  state is totally symmetric under the interchange of the  $\pi$ -mesons, by Bose statistics. Interchange of the particles corresponds to the operation  $C$  followed by  $P$ .

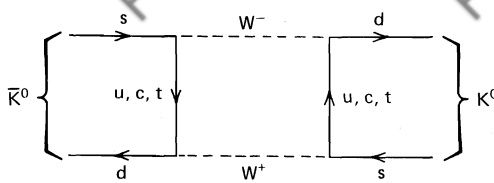


**Fig. 12.21** Diagram responsible for  $K^0 \leftrightarrow \bar{K}^0$  mixing.

The appearance of complex elements  $U_{ij}$  in the KM matrix may be related to the  $\Delta S = 2$  transition mixing the  $S = \pm 1$   $K^0$  and  $\bar{K}^0$  states. The connection is not simple; the diagram of Fig. 12.21 is responsible for  $K^0-\bar{K}^0$  mixing. With only u and c quarks exchanged (in the four-quark theory), the mixing would conserve  $CP$  and the resulting mass matrix would have eigenstates, (12.129), that differ by a small mass. In a six-quark theory, the values are slightly perturbed and  $|K_S^0\rangle$  and  $|K_L^0\rangle$  are no longer exactly  $CP$  eigenstates. Finally, it is widely believed that  $CP$  nonconservation in the early universe is the source of the apparent imbalance between matter and antimatter which we observe around us.

# 13

## Electroweak Interactions

The picture of weak interactions we have discussed so far is only satisfactory at a superficial level. We have only calculated lowest-order graphs where the momentum exchanged between the weak currents satisfies  $|q^2| \ll (100 \text{ GeV})^2$ . The results do not depend on whether or not massive intermediate vector bosons  $W^\pm$  exist. The existence of  $W^\pm$  simply leads to a reinterpretation of the Fermi coupling  $G$ , see (12.15). However, calculations of anything other than lowest-order, low-energy amplitudes lead to very serious problems. For many years, the current-current interaction was regarded merely as a phenomenological prescription rather than a proper theory. With hindsight, we can see that to assume that massive weak bosons exist is indeed a step toward converting weak interaction phenomenology into a respectable (that is, renormalizable) theory. This seemed impossible until the discovery of “spontaneously broken non-Abelian gauge symmetries,” an idea we introduce in the next chapter. Suffice it to say here that a necessary ingredient is that the weak currents form a symmetry group. We therefore continue our discussion of weak interactions with this objective in mind.

### 13.1 Weak Isospin and Hypercharge

Can the weak neutral current ( $J_\mu^{NC}$  of Section 12.10), taken together with the charged currents ( $J_\mu$  and  $J_\mu^\dagger$ ), form a symmetry group of weak interactions? First, we recall the form of the charge currents,

$$\left. \begin{aligned} J_\mu &\equiv J_\mu^+ = \bar{u}_\nu \gamma_{\mu \frac{1}{2}} (1 - \gamma^5) u_e \\ &\equiv \bar{v}_\mu \gamma_{\frac{1}{2}} (1 - \gamma^5) e = \bar{v}_L \gamma_\mu e_L \end{aligned} \right\} \Rightarrow W^+ \rightarrow \begin{array}{c} v_e \\ \nearrow \\ \downarrow \\ e^- \end{array} \quad (13.1)$$

$$\left. \begin{aligned} J_\mu^\dagger &\equiv J_\mu^- = \bar{u}_e \gamma_{\mu \frac{1}{2}} (1 - \gamma^5) u_\nu \\ &= \bar{e}_L \gamma_\mu v_L \end{aligned} \right\} \Rightarrow W^- \rightarrow \begin{array}{c} e \\ \nearrow \\ \downarrow \\ v_e \end{array}$$

where the + and - superscripts are to indicate the charge-raising and charge-lowering character of the currents, respectively. The subscript  $L$  is used to denote left-handed spinors and records the  $V-A$  nature of the charged currents. Here, we have used the particle names to denote the Dirac spinors ( $\bar{u}_\nu \equiv \bar{\nu}$ ,  $u_e \equiv e$ , etc.).

We can rewrite these two charged currents in a suggestive two-dimensional form. We introduce the doublet

$$\chi_L = \begin{pmatrix} \nu \\ e^- \end{pmatrix}_L \quad (13.2)$$

and the “step-up” and “step-down” operators  $\tau_\pm = \frac{1}{2}(\tau_1 \pm i\tau_2)$ :

$$\tau_+ = \begin{pmatrix} 0 & 1 \\ 0 & 0 \end{pmatrix}, \quad \tau_- = \begin{pmatrix} 0 & 0 \\ 1 & 0 \end{pmatrix}, \quad (13.3)$$

where the  $\tau$ 's are the usual Pauli spin matrices. The charged currents (13.1) then become (with  $x$  dependence as in (6.6))

$$\begin{aligned} J_\mu^+(x) &= \bar{\chi}_L \gamma_\mu \tau_+ \chi_L, \\ J_\mu^-(x) &= \bar{\chi}_L \gamma_\mu \tau_- \chi_L. \end{aligned} \quad (13.4)$$

Anticipating a possible  $SU(2)$  structure for the weak currents, we are led to introduce a neutral current of the form

$$\left. \begin{aligned} J_\mu^3(x) &= \bar{\chi}_L \gamma_\mu \frac{1}{2} \tau_3 \chi_L \\ &= \frac{1}{2} \bar{\nu}_L \gamma_\mu \nu_L - \frac{1}{2} \bar{e}_L \gamma_\mu e_L \end{aligned} \right\} \Rightarrow W^0 \text{---} \begin{array}{l} \nearrow \nu_e(e^-) \\ \searrow \bar{\nu}_e(e^-) \end{array} \quad (13.5)$$

$$(13.6)$$

We have thus constructed an “isospin” triplet of weak currents,

$$J_\mu^i(x) = \bar{\chi}_L \gamma_\mu \frac{1}{2} \tau_i \chi_L, \quad \text{with } i = 1, 2, 3, \quad (13.7)$$

whose corresponding charges

$$T^i = \int J_0^i(x) d^3x \quad (13.8)$$

generate an  $SU(2)_L$  algebra

$$[T^i, T^j] = i\epsilon_{ijk} T^k. \quad (13.9)$$

The subscript  $L$  on  $SU(2)$  is to remind us that the weak isospin current couples only left-handed fermions.

Can the current  $J_\mu^3(x)$  which we have just introduced be identified directly with the weak neutral current of Section 12.10? Unfortunately, we see immediately that this attractive idea does not work; the observed weak neutral current  $J_\mu^{NC}$  has

a right-handed component, see (12.97). However, the electromagnetic current is a neutral current with right- as well as left-handed components. For example, for the electron we have from (6.35)

$$j_\mu^{em}(x) = -\bar{e}\gamma_\mu e = -\bar{e}_R\gamma_\mu e_R - \bar{e}_L\gamma_\mu e_L. \quad (13.10)$$

Note, in passing, that we have omitted the coupling  $e$  in our definition of  $j_\mu^{em}$ . This will simplify our discussion of electroweak interactions. Thus, the electromagnetic current  $j_\mu$  of (6.5) is written

$$j_\mu \equiv ej_\mu^{em} = e\bar{\psi}\gamma_\mu Q\psi, \quad (13.11)$$

where  $Q$  is the charge operator, with eigenvalue  $Q = -1$  for the electron. Technically speaking, we say that  $Q$  is the generator of a  $U(1)_{em}$  symmetry group of electromagnetic interactions (see Section 14.2).

We include  $j_\mu^{em}$  in an attempt to save the  $SU(2)_L$  symmetry. Note that neither of the neutral currents  $J_\mu^{NC}$  or  $j_\mu^{em}$  respects the  $SU(2)_L$  symmetry. However, the idea is to form two orthogonal combinations which do have definite transformation properties under  $SU(2)_L$ ; one combination,  $J_\mu^3$ , is to complete the weak isospin triplet  $J_\mu^i$ , while the second,  $j_\mu^Y$ , is unchanged by  $SU(2)_L$  transformations (i.e., is a weak isospin singlet).  $j_\mu^Y$  is called the weak hypercharge current and is given by

$$j_\mu^Y = \bar{\psi}\gamma_\mu Y\psi, \quad (13.12)$$

where the weak hypercharge  $Y$  is defined by

$$Q = T^3 + \frac{Y}{2}. \quad (13.13)$$

That is,

$$j_\mu^{em} = J_\mu^3 + \frac{1}{2}j_\mu^Y.$$

(13.14)

Just as  $Q$  generates the group  $U(1)_{em}$ , so the hypercharge operator  $Y$  generates a symmetry group  $U(1)_Y$ . Thus, we have incorporated the electromagnetic interaction, and as a result the symmetry group has been enlarged to  $SU(2)_L \times U(1)_Y$ . In a sense we have unified the electromagnetic with the weak interaction. However, rather than a single unified symmetry group, we have two groups each with an independent coupling strength. So, in addition to  $e$ , we will need another coupling to fully specify the electroweak interaction. Thus, from an aesthetic viewpoint the unification is perhaps not completely satisfying (see Section 15.7).

The proposed weak isospin and weak hypercharge scheme is mathematically an exact copy of the original Gell-Mann–Nishijima scheme for arranging strange particles in  $SU(2)$  hadronic isospin multiplets (see Section 2.9). The names “weak isospin” and “weak hypercharge” are taken from this analogy.

The  $SU(2)_L \times U(1)_Y$  proposal was first made by Glashow in 1961, long before the discovery of the weak neutral current, and, as we describe in Chapter 15, was

**TABLE 13.1**

Weak Isospin and Hypercharge Quantum Numbers of Leptons and Quarks

Lepton	$T$	$T^3$	$Q$	$Y$	Quark	$T$	$T^3$	$Q$	$Y$
$\nu_e$	$\frac{1}{2}$	$\frac{1}{2}$	0	-1	$u_L$	$\frac{1}{2}$	$\frac{1}{2}$	$\frac{2}{3}$	$\frac{1}{3}$
$e_L^-$	$\frac{1}{2}$	$-\frac{1}{2}$	-1	-1	$d_L$	$\frac{1}{2}$	$-\frac{1}{2}$	$-\frac{1}{3}$	$\frac{1}{3}$
$e_R^-$	0	0	-1	-2	$u_R$	0	0	$\frac{2}{3}$	$\frac{4}{3}$
					$d_R$	0	0	$-\frac{1}{3}$	$-\frac{2}{3}$

extended to accommodate massive vector bosons ( $W^\pm, Z^0$ ) by Weinberg (1967) and Salam (1968). It is frequently referred to as the “standard model” for electroweak interactions.

Since we have a product of symmetry groups, the generator  $Y$  must commute with the generators  $T^i$ . As a consequence, all the members of an isospin multiplet must have the same value of the hypercharge. For example, for the electron multiplets, (13.14) becomes

$$\begin{aligned} j_\mu^Y &= 2j_\mu^{em} - 2J_\mu^3 \\ &= -2(\bar{e}_R \gamma_\mu e_R + \bar{e}_L \gamma_\mu e_L) - (\bar{\nu}_L \gamma_\mu \nu_L - \bar{e}_L \gamma_\mu e_L) \\ &= -2(\bar{e}_R \gamma_\mu e_R) - 1(\bar{\chi}_L \gamma_\mu \chi_L), \end{aligned} \quad (13.15)$$

where we have used (13.6) and (13.10). Thus, the isospin doublet  $(\nu, e)_L$  has  $Y = -1$ , and the isospin singlet  $e_R$  has  $Y = -2$ . These quantum numbers are summarized in Table 13.1.

We can readily incorporate quarks into the scheme. The weak isospin current  $J_\mu^i$  couples only to doublets of left-handed quarks  $(u, d)_L$ ; we assign  $T = \frac{1}{2}$  to  $q_L$  and  $T = 0$  to  $q_R$  states.

**EXERCISE 13.1** Verify the quark quantum numbers given in Table 13.1.

### 13.2 The Basic Electroweak Interaction

To complete the unification of the electromagnetic and weak interactions, we must modify the current-current form of the weak interactions given in (12.13) and (12.85). We assume that the current-current structure is an effective interaction which results from the exchange of massive vector bosons with only a small momentum transfer.

In Section 6.1, we developed QED from the basic interaction

$$-ie(j^{em})^\mu A_\mu. \quad (13.16)$$

Just as the electromagnetic current is coupled to the photon, we assume that the

electroweak currents of Section 13.1 are coupled to vector bosons. The “standard” model consists of an isotriplet of vector fields  $W_\mu^i$  coupled with strength  $g$  to the weak isospin current  $J_\mu^i$ , together with a single vector field  $B_\mu$  coupled to the weak hypercharge current  $j_\mu^Y$  with strength conventionally taken to be  $g'/2$ . The basic electroweak interaction is therefore

$$\boxed{-i g (J^i)^\mu W_\mu^i - i \frac{g'}{2} (j^Y)^\mu B_\mu.} \quad (13.17)$$

The fields

$$W_\mu^\pm = \sqrt{\frac{1}{2}} (W_\mu^1 \mp i W_\mu^2) \quad (13.18)$$

describe massive charged bosons  $W^\pm$ , whereas  $W_\mu^3$  and  $B_\mu$  are neutral fields. The basic interactions are pictured in Fig. 13.1.

The electromagnetic interaction (13.16) is embedded in (13.17). Indeed, when we generate the masses of the bosons by symmetry breaking (see Chapter 15), the two neutral fields  $W_\mu^3$  and  $B_\mu$  must mix in such a way that the physical states (i.e., the mass eigenstates) are

$$A_\mu = B_\mu \cos \theta_W + W_\mu^3 \sin \theta_W \quad (\text{massless}), \quad (13.19)$$

$$Z_\mu = -B_\mu \sin \theta_W + W_\mu^3 \cos \theta_W \quad (\text{massive}), \quad (13.20)$$

where  $\theta_W$  is called the Weinberg or weak mixing angle (although Glashow was the first to introduce the idea). We may therefore write the electroweak neutral current interaction

$$\begin{aligned} & -ig J_\mu^3 (W^3)^\mu - i \frac{g'}{2} j_\mu^Y B^\mu \\ &= -i \left( g \sin \theta_W J_\mu^3 + g' \cos \theta_W \frac{j_\mu^Y}{2} \right) A^\mu \\ & \quad - i \left( g \cos \theta_W J_\mu^3 - g' \sin \theta_W \frac{j_\mu^Y}{2} \right) Z^\mu. \end{aligned} \quad (13.21)$$

The first term is the electromagnetic interaction, (13.16), and so the expression in

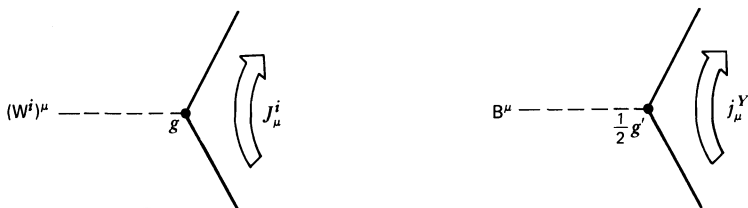


Fig. 13.1 The vector boson couplings to the weak isospin and hypercharge currents.

brackets must be

$$ej_{\mu}^{em} \equiv e(J_{\mu}^3 + \frac{1}{2}j_{\mu}^Y), \quad (13.22)$$

see (13.14). Therefore, we have

$$g \sin \theta_W = g' \cos \theta_W = e. \quad (13.23)$$

That is, the mixing angle in (13.19) and (13.20) is given by the ratio of the two independent group coupling constants,  $\tan \theta_W = g'/g$ .

Using (13.22) and (13.23), we may express the weak neutral current interaction of (13.21) in the form

$$-i \frac{g}{\cos \theta_W} (J_{\mu}^3 - \sin^2 \theta_W j_{\mu}^{em}) Z^{\mu} \equiv -i \frac{g}{\cos \theta_W} J_{\mu}^{NC} Z^{\mu}. \quad (13.24)$$

It is this definition,

$$J_{\mu}^{NC} \equiv J_{\mu}^3 - \sin^2 \theta_W j_{\mu}^{em}, \quad (13.25)$$

which relates the neutral current  $J^{NC}$  to the weak isospin current  $\mathbf{J}$ .

Very early in our discussion of the weak interaction, we speculated that perhaps it was not a new fundamental interaction but that it was a manifestation of the electromagnetic interaction. We suggested that this electroweak unification might be achieved by setting the coupling  $g = e$ . We now see that this simple unification is not true. The standard model relation,

$$g \sin \theta_W = g' \cos \theta_W = e,$$

is more complicated. The electromagnetic interaction (a  $U(1)$  gauge symmetry with coupling  $e$ ) “sits across” weak isospin (an  $SU(2)_L$  symmetry with coupling  $g$ ) and weak hypercharge (a  $U(1)$  symmetry with coupling  $g'$ ). We discuss these gauge symmetries in Chapters 14 and 15. Using (13.23), we see that the two couplings  $g$  and  $g'$  can be replaced by  $e$  and  $\theta_W$ , where the parameter  $\theta_W$  is to be determined by experiment.

To summarize, we have achieved our objective of expressing the observed neutral currents

$$\begin{aligned} j_{\mu}^{em} &= J_{\mu}^3 + \frac{1}{2}j_{\mu}^Y, \\ J_{\mu}^{NC} &= J_{\mu}^3 - \sin^2 \theta_W j_{\mu}^{em} \end{aligned} \quad (13.26)$$

in terms of currents  $J_{\mu}^3$  and  $j_{\mu}^Y$  belonging to symmetry groups  $SU(2)_L$  and  $U(1)_Y$ , respectively. The right-handed component of  $J_{\mu}^{NC}$  (the original problem) has been arranged to cancel with that in  $\sin^2 \theta_W j_{\mu}^{em}$  to leave a pure left-handed  $J_{\mu}^3$  of  $SU(2)_L$ , where  $\sin^2 \theta_W$  is to be determined by experiment. Of course, for the model to be successful, the same  $\sin^2 \theta_W$  must be found in all electroweak phenomena.

### 13.3 The Effective Current–Current Interaction

Before we continue, we should relate our basic interactions to the current–current structure of weak interactions that we used throughout Chapter 12. There, we saw that *charged current* phenomena could be explained by invariant amplitudes of the form

$$\mathcal{M}^{CC} = \frac{4G}{\sqrt{2}} J^\mu J_\mu^\dagger, \quad (13.27)$$

see (12.13), where in the new isospin notation [see (13.7)]

$$J_\mu \equiv J_\mu^+ = \bar{\chi}_L \gamma_\mu \tau_+ \chi_L = \frac{1}{2} (J_\mu^1 + i J_\mu^2). \quad (13.28)$$

For an interaction proceeding via the exchange of a massive charged boson, we can follow the QED procedure of Section 6.2 to calculate  $\mathcal{M}$ . The analogue of Fig. 6.2 is Fig. 13.2. First, we rewrite the basic charged current interaction of (13.17) in the form

$$-i \frac{g}{\sqrt{2}} (J^\mu W_\mu^+ + J^{\mu\dagger} W_\mu^-), \quad (13.29)$$

where we have used the identity

$$\frac{1}{2} (\tau_1 W^1 + \tau_2 W^2) = \sqrt{\frac{1}{2}} (\tau_+ W^+ + \tau_- W^-) \quad (13.30)$$

with  $W^\pm$  given by (13.18). Then, we copy the QED procedure leading to (6.8) and obtain

$$\mathcal{M}^{CC} = \left( \frac{g}{\sqrt{2}} J_\mu \right) \left( \frac{1}{M_W^2} \right) \left( \frac{g}{\sqrt{2}} J^{\mu\dagger} \right), \quad (13.31)$$

where  $1/M_W^2$  is the approximation to the  $W$  propagator at low  $q^2$  (see Section 6.17). Comparison of (13.31) with (13.27) gives

$$\frac{G}{\sqrt{2}} = \frac{g^2}{8M_W^2}. \quad (13.32)$$

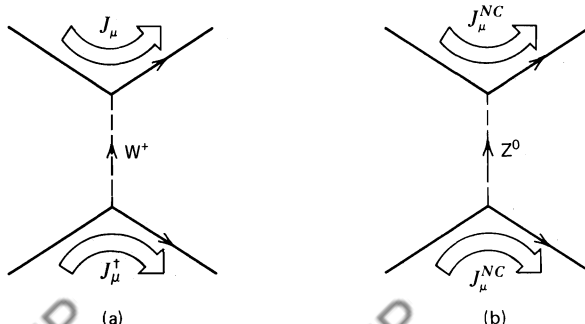


Fig. 13.2 Charged and neutral current weak interactions.

In an analogous way, we may express the amplitude for a *neutral current* process in terms of  $Z$  exchange, see Fig. 13.2b. Using (13.24), we have, for  $|q^2| \ll M_Z^2$ ,

$$\mathcal{M}^{NC} = \left( \frac{g}{\cos \theta_W} J_\mu^{NC} \right) \left( \frac{1}{M_W^2} \right) \left( \frac{g}{\cos \theta_W} J^{NC\mu} \right). \quad (13.33)$$

If we now compare (13.33) with the current-current form we used for the invariant amplitude, (12.85),

$$\mathcal{M}^{NC} = \frac{4G}{\sqrt{2}} 2\rho J_\mu^{NC} J^{NC\mu}, \quad (13.34)$$

we can identify

$$\rho \frac{G}{\sqrt{2}} = \frac{g^2}{8M_Z^2 \cos^2 \theta_W}. \quad (13.35)$$

From (13.32) and (13.35), we find that the parameter  $\rho$ , which specifies the relative strength of the neutral and charged current weak interactions, is given by

$$\rho = \frac{M_W^2}{M_Z^2 \cos^2 \theta_W}. \quad (13.36)$$

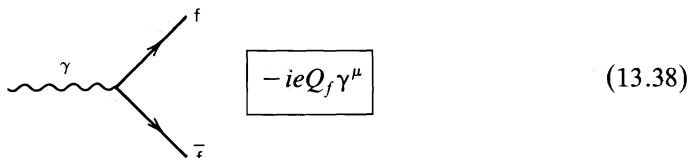
We shall see that, experimentally,  $\rho = 1$  to within a small error. This value is also predicted by the minimal model proposed by Weinberg and Salam (see Chapter 15).

### 13.4 Feynman Rules for Electroweak Interactions

To obtain the Feynman rules (for  $-i\mathcal{M}$ ) for electroweak interactions, we follow the procedure that we used for QED. In Section 6.1, we showed how the *electromagnetic interaction*

$$-i e (j^{em})^\mu A_\mu = -i e (\bar{\psi} \gamma^\mu Q \psi) A_\mu \quad (13.37)$$

led to the vertex factor



where  $Q_f$  is the charge of fermion  $f$ ;  $Q_f = -1$  for the electron. The outgoing  $f$  should be drawn as an ingoing  $f$ , and spinors attached to the fermion lines as in Section 6.17.

We copy this procedure for the *charged current interaction*, (13.29),

$$\begin{aligned}
 & -i \frac{g}{\sqrt{2}} (\bar{\chi}_L \gamma^\mu \tau_+ \chi_L) W_\mu^+ \\
 & = -i \frac{g}{\sqrt{2}} (\bar{\nu}_L \gamma^\mu e_L) W_\mu^+ \quad \left. \right\} W^+ \rightarrow \begin{array}{c} e^+ \\ \nu \end{array} \\
 & \boxed{-i \frac{g}{\sqrt{2}} \gamma^{\mu \frac{1}{2}} (1 - \gamma^5)} \quad (13.39) \\
 & -i \frac{g}{\sqrt{2}} (\bar{\chi}_L \gamma^\mu \tau_- \chi_L) W_\mu^- \\
 & = -i \frac{g}{\sqrt{2}} (\bar{e}_L \gamma^\mu \nu_L) W_\mu^- \quad \left. \right\} W^- \rightarrow \begin{array}{c} e^- \\ \bar{\nu} \end{array}
 \end{aligned}$$

For  $\chi_L = (\nu_e, e^-)$ , these interactions lead to the vertex factor shown; spinors are associated with the external fermion lines just as in QED. Clearly, the vertex factor will be the same for the  $W^\pm$  couplings to the other fermion doublets ( $\nu_\mu, \mu^-$ ), ( $u, d'$ ), and so on.

The *neutral current interaction* is given by (13.24),

$$\begin{aligned}
 & -i \frac{g}{\cos \theta_W} (J_\mu^3 - \sin^2 \theta_W j_\mu^{em}) Z^\mu = \\
 & \quad -i \frac{g}{\cos \theta_W} \bar{\psi}_f \gamma^\mu [\frac{1}{2}(1 - \gamma^5) T^3 - \sin^2 \theta_W Q] \psi_f Z_\mu
 \end{aligned} \quad (13.40)$$

for the coupling  $Z \rightarrow f\bar{f}$ . It is customary to express the vertex factor in the general form

$$\Rightarrow z^0 \rightarrow \begin{array}{c} f \\ \bar{f} \end{array} \quad \boxed{-i \frac{g}{\cos \theta_W} \gamma^{\mu \frac{1}{2}} (c_V^f - c_A^f \gamma^5)}. \quad (13.41)$$

If we compare (13.40) with (13.41), we see that the vector and axial-vector couplings,  $c_V$  and  $c_A$ , are determined in the standard model (given the value of

**TABLE 13.2**

The  $Z \rightarrow f\bar{f}$  Vertex Factors, (13.41), in the Standard Model (with  $\sin^2 \theta_W = 0.234$ )

$f$	$Q_f$	$c_A^f$	$c_V^f$
$\nu_e, \nu_\mu, \dots$	0	$\frac{1}{2}$	$\frac{1}{2}$
$e^-, \mu^-, \dots$	-1	$-\frac{1}{2}$	$-\frac{1}{2} + 2 \sin^2 \theta_W \approx -0.03$
$u, c, \dots$	$\frac{2}{3}$	$\frac{1}{2}$	$\frac{1}{2} - \frac{4}{3} \sin^2 \theta_W \approx 0.19$
$d, s, \dots$	$-\frac{1}{3}$	$-\frac{1}{2}$	$-\frac{1}{2} + \frac{2}{3} \sin^2 \theta_W \approx -0.34$

$\sin^2 \theta_W$ ). Their values are

$$\begin{aligned} c_V^f &= T_f^3 - 2 \sin^2 \theta_W Q_f, \\ c_A^f &= T_f^3, \end{aligned} \quad (13.42)$$

where  $T_f^3$  and  $Q_f$  are, respectively, the third component of the weak isospin and the charge of fermion  $f$ . The values of  $c_V$  and  $c_A$  are listed in Table 13.2.

The Feynman rules allow us to predict the decay properties of the  $W^\pm$  and  $Z^0$  bosons in the standard model, see Exercises 13.2–13.6 below.

**EXERCISE 13.2** If the vertex factor for the decay of a vector boson  $X$  into two spin- $\frac{1}{2}$  fermions  $f_1$  and  $\bar{f}_2$  is

$$-ig_X \gamma^\mu \frac{1}{2}(c_V - c_A \gamma^5),$$

then show that

$$\Gamma(X \rightarrow f_1 \bar{f}_2) = \frac{g_X^2}{48\pi} (c_V^2 + c_A^2) M_X, \quad (13.43)$$

where  $M_X$  is the mass of the boson and where we have neglected the masses of the fermions.

**Hint** Use (6.93) to show that after summing over the fermion and averaging over the boson spins,

$$|\mathcal{M}|^2 = \frac{1}{12} g_X^2 (c_V^2 + c_A^2) (-g_{\mu\nu}) \text{Tr}(\gamma^\mu k \gamma^\nu k') \quad (13.44)$$

where  $k, k'$  are the four-momenta of the fermions. Work in the boson rest frame. Use (4.37).

**EXERCISE 13.3** Assuming the standard model coupling, show that

$$\Gamma(Z \rightarrow \nu_e \bar{\nu}_e) = \frac{g^2}{96\pi \cos^2 \theta_W} M_Z, \quad (13.45)$$

see Exercise 13.2. Given that  $\sin^2 \theta_W = 0.25$  and  $M_Z = 90$  GeV, predict the numerical value of the partial width.

**EXERCISE 13.4** Calculate the partial widths of the three decay modes  $Z \rightarrow e^+ e^-$ ,  $\bar{u}u$ ,  $\bar{d}d$ . Hence, predict the total width of the  $Z$  in the standard model, assuming  $\sin^2 \theta_W = \frac{1}{4}$  and  $M_Z = 90$  GeV. Do not forget color.

**EXERCISE 13.5** Repeat Exercise 13.3 for the  $W^+ \rightarrow e^+ \nu_e$  decay mode; take  $M_W = 80$  GeV.

**EXERCISE 13.6** Calculate the partial widths of the two decay modes  $W^+ \rightarrow \bar{d}u$ ,  $\bar{s}u$ ; use (12.102) and (12.103). Predict the total width of the  $W^+$  in the standard model.

### 13.5 Neutrino–Electron Scattering

The  $\nu_\mu e^-$  and  $\bar{\nu}_\mu e^-$  elastic scattering processes can only proceed via a neutral current interaction, see Fig. 13.3. The current–current form of the invariant amplitude for the process  $\nu_\mu e^- \rightarrow \nu_\mu e^-$  is analogous to (12.84) for  $\nu q \rightarrow \nu q$  scattering:

$$\mathcal{M}^{NC}(\nu e \rightarrow \nu e) = \frac{G_N}{\sqrt{2}} (\bar{\nu} \gamma^\mu (1 - \gamma^5) \nu) (\bar{e} \gamma_\mu (c_V^e (c_A^e \gamma^5) e)), \quad (13.46)$$

where  $G_N = \rho G \approx G$  [see (12.88)]. In fact, assuming electron–muon universality, we shall find that the four elastic scattering processes,  $\nu_\mu e^-$ ,  $\bar{\nu}_\mu e^-$ ,  $\nu_e e^-$ , and  $\bar{\nu}_e e^-$ , can all be explained in terms of the two parameters  $c_V \equiv c_V^e$  and  $c_A \equiv c_A^e$ .

**EXERCISE 13.7** If  $\nu e \rightarrow \nu e$  scattering proceeds by  $Z$  exchange, show that (13.46) is obtained from the Feynman rules using (13.41) as the vertex factor. In particular, use the expression for the boson propagator (see Section 6.17) to verify that (13.46) is valid provided the four-momentum transfer  $q$  is such that  $|q^2| \ll M_Z^2$ .

Given that (13.46) is of identical form to that for  $\nu q \rightarrow \nu q$  scattering, we may use the results of Section 12.10 to obtain the  $\nu_\mu e^- \rightarrow \nu_\mu e^-$  cross section. We

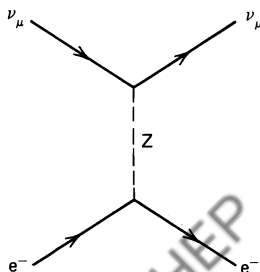


Fig. 13.3 The neutral current  $\nu_\mu e^- \rightarrow \nu_\mu e^-$  interaction.

therefore have [see (12.90) and (12.91)]

$$\frac{d\sigma(\nu_\mu e)}{dy} = \frac{G_N^2 s}{4\pi} [(c_V + c_A)^2 + (c_V - c_A)^2(1 - y)^2]. \quad (13.47)$$

Carrying out the  $y$  integration from 0 to 1 gives

$$\sigma(\nu_\mu e \rightarrow \nu_\mu e) = \frac{G_N^2 s}{3\pi} (c_V^2 + c_V c_A + c_A^2). \quad (13.48)$$

For  $\bar{\nu}_\mu e^-$  elastic scattering,  $c_A \rightarrow -c_A$  in (13.47), and so

$$\sigma(\bar{\nu}_\mu e \rightarrow \bar{\nu}_\mu e) = \frac{G_N^2 s}{3\pi} (c_V^2 - c_V c_A + c_A^2). \quad (13.49)$$

**EXERCISE 13.8** Equation (13.47) is valid if  $m^2/s \ll 1$ . If the electron mass  $m$  is not ignored, show that the extra contribution to (13.47) is

$$-G^2 m^2 y (c_V^2 - c_A^2)/2\pi.$$

The process  $\nu_e e^- \rightarrow \nu_e e^-$  offers the intriguing possibility of studying charged current and neutral current interference, see Fig. 13.4. The amplitude for diagram (a) is  $\mathcal{M}^{NC}$  of (13.46) with  $\nu = \nu_e$ . For diagram (b), we have

$$\mathcal{M}^{CC} = -\frac{G}{\sqrt{2}} [\bar{e}\gamma^\mu(1 - \gamma^5)\nu_e] [\bar{\nu}_e\gamma_\mu(1 - \gamma^5)e], \quad (13.50)$$

where the minus sign relative to (13.46) arises from interchange of the outgoing leptons [see (6.9)]. We may use the Fierz reordering theorem, see, for example, Bailin (1982), to rewrite (13.50) as

$$\mathcal{M}^{CC} = \frac{G}{\sqrt{2}} (\bar{\nu}_e\gamma^\mu(1 - \gamma^5)\nu_e)(\bar{e}\gamma_\mu(1 - \gamma^5)e). \quad (13.51)$$

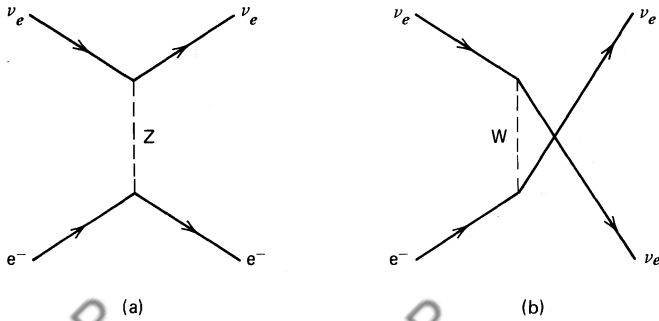


Fig. 13.4 The neutral and charged current  $\nu_e e^- \rightarrow \nu_e e^-$  interaction.

**EXERCISE 13.9** Show that (13.51) follows from (13.50). The invariance under reordering of the spinors is an important property of the  $V-A$  interaction. The effect of reordering in the scalar product of bilinear covariants is, in general, much more involved. The answer is the Fierz theorem.

To obtain the amplitude  $\mathcal{M}(\nu_e e^- \rightarrow \nu_e e^-)$ , we add the amplitudes ( $\mathcal{M}^{NC}$  and  $\mathcal{M}^{CC}$ ) for the two diagrams of Fig. 13.4. If we take  $\rho = 1$ , then  $G_N = G$  [see (12.88)], and we find  $\mathcal{M} = \mathcal{M}^{NC} + \mathcal{M}^{CC}$  is given by (13.46) with

$$c_V \rightarrow c_V + 1, \quad c_A \rightarrow c_A + 1. \quad (13.52)$$

Thus, the  $\nu_e e^-$  and  $\bar{\nu}_e e^-$  elastic scattering cross sections are in turn given by (13.48) and (13.49) with these replacements.

It is customary to present the results of a given neutrino-electron cross section measurement as an ellipse of possible values of  $c_V$  and  $c_A$  in the  $c_V, c_A$  plane. Recent results are shown in Fig. 13.5. The three “experimental” ellipses mutually intersect to give two possible solutions. The  $c_A$  dominant solution is

$$\begin{aligned} c_A^e &= -0.52 \pm 0.06, \\ c_V^e &= 0.06 \pm 0.08, \end{aligned} \quad (13.53)$$

in excellent agreement with the standard model and  $\sin^2 \theta_W \approx \frac{1}{4}$  (see Table 13.2).

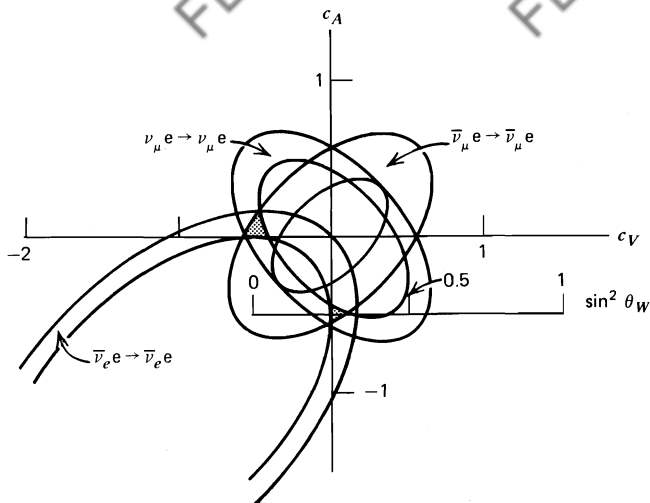


**Fig. 13.5** Determination of the parameters  $c_V$  and  $c_A$  of (13.46) by neutrino-electron data. Figure is taken from Hung and Sakurai (1981). The absence of  $\nu_e$  data is because reactor beams only have  $\bar{\nu}_e$ .

However, the best determinations of  $\sin^2 \theta_W$  come from the analyses of data for inclusive and exclusive neutrino–nucleon processes. A recent simultaneous analysis (Kim et al., 1981) of all available data gives

$$\begin{aligned}\sin^2 \theta_W &= 0.234 \pm 0.013, \\ \rho &= 1.002 \pm 0.015.\end{aligned}\quad (13.54)$$

### 13.6 Electroweak Interference in $e^+e^-$ Annihilation

Shortly after Bludman in 1958 first speculated about the existence of a weak neutral current, Zel'dovich gave a very simple argument to estimate the size of the asymmetry arising from the interference of the electromagnetic amplitude  $\mathcal{M}^{EM}$   $\sim e^2/k^2$  with a small weak contribution. He predicted

$$\frac{|\mathcal{M}^{EM}\mathcal{M}^{NC}|}{|\mathcal{M}^{EM}|^2} \approx \frac{G}{e^2/k^2} \approx \frac{10^{-4}k^2}{m_N^2}, \quad (13.55)$$

using  $G \approx 10^{-5}/m_N^2$  and  $e^2/4\pi = 1/137$ .

The high-energy  $e^+e^-$  colliding beam machines are an ideal testing ground for such interference effects. The  $e^+e^-$  annihilations can occur through electromagnetic ( $\gamma$ ) or weak neutral current ( $Z$ ) interactions, see, for example, Fig. 13.6. With  $e^\pm$  beam energies of 15 GeV we have  $k^2 \approx s = (30 \text{ GeV})^2$ , and so (13.55) predicts about a 10% effect, which is readily observable.

To make a detailed prediction for the process  $e^+e^- \rightarrow \mu^+\mu^-$ , we assume that the neutral current interaction is mediated by a  $Z$  boson with couplings given by (13.41). Using the Feynman rules (Section 6.17), the amplitudes  $\mathcal{M}_\gamma$  and  $\mathcal{M}_Z$  corresponding to the diagrams of Fig. 13.6 are

$$\mathcal{M}_\gamma = -\frac{e^2}{k^2} (\bar{\mu} \gamma^\nu \mu)(\bar{e} \gamma_\nu e), \quad (13.56)$$

$$\mathcal{M}_Z = -\frac{g^2}{4 \cos^2 \theta_W} [\bar{\mu} \gamma^\nu (c_V^\mu - c_A^\mu \gamma^5) \mu] \left( \frac{g_{\nu\sigma} - k_\nu k_\sigma/M_Z^2}{k^2 - M_Z^2} \right) [\bar{e} \gamma^\sigma (c_V^e - c_A^e \gamma^5) e], \quad (13.57)$$

where  $k$  is the four-momentum of the virtual  $\gamma$  (or  $Z$ ),  $s \approx k^2$ . With electron–muon universality, the superscripts on  $c_{V,A}$  are superfluous here, but we keep them so as to be able to translate the results directly to  $e^+e^- \rightarrow q\bar{q}$  (where  $c^q \neq c^\mu$ ). We

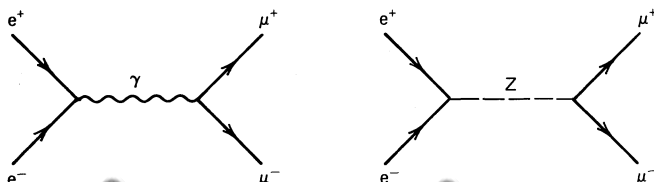


Fig. 13.6 Electromagnetic and weak contributions to  $e^+e^- \rightarrow \mu^+\mu^-$

ignore the lepton masses, so the Dirac equation for the incident positron reads  $(\frac{1}{2}k_\sigma)\bar{e}\gamma^\sigma = 0$  and the numerator of the propagator simplifies to  $g_{\nu\sigma}$ . Thus, (13.57) becomes

$$\mathcal{M}_Z = \frac{-\sqrt{2}GM_Z^2}{s - M_Z^2} [c_R^\mu(\bar{\mu}_R\gamma^\nu\mu_R) + c_L^\mu(\bar{\mu}_L\gamma^\nu\mu_L)] [c_R^e(\bar{e}_R\gamma_\nu e_R) + c_L^e(\bar{e}_L\gamma_\nu e_L)], \quad (13.58)$$

using (13.32) and (13.36) with  $\rho = 1$ , and where

$$c_R \equiv c_V - c_A, \quad c_L \equiv c_V + c_A. \quad (13.59)$$

That is, we have chosen to write

$$c_V - c_A\gamma^5 = (c_V - c_A)\frac{1}{2}(1 + \gamma^5) + (c_V + c_A)\frac{1}{2}(1 - \gamma^5).$$

The  $\frac{1}{2}(1 \pm \gamma^5)$  are projection operators, see (5.78), which enable  $\mathcal{M}_Z$  to be expressed explicitly in terms of right- and left-handed spinors. It is easier to calculate  $|\mathcal{M}_\gamma + \mathcal{M}_Z|^2$  in this form. With definite electron and muon helicities, we can directly apply the results of the QED calculation of  $e^-e^+ \rightarrow \mu^-\mu^+$  given in Sections 6.5 and 6.6. For instance,

$$\begin{aligned} \frac{d\sigma(e_L^-e_R^+ \rightarrow \mu_L^-\mu_R^+)}{d\Omega} &= \frac{\alpha^2}{4s}(1 + \cos\theta)^2[1 + rc_L^\mu c_L^e]^2, \\ \frac{d\sigma(e_L^-e_R^+ \rightarrow \mu_R^-\mu_L^+)}{d\Omega} &= \frac{\alpha^2}{4s}(1 - \cos\theta)^2[1 + rc_R^\mu c_L^e]^2 \end{aligned} \quad (13.60)$$

[see (6.39) and (6.32)], where  $r$  is the ratio of the coefficients in front of the brackets in (13.58) and (13.56), that is,

$$r = \frac{\sqrt{2}GM_Z^2}{s - M_Z^2 + iM_Z\Gamma_Z} \left( \frac{s}{e^2} \right), \quad (13.61)$$

where we have included the finite resonance width  $\Gamma_Z$ , which is important for  $s \sim M_Z^2$  [see  $\chi(E)$  of (2.56) multiplied by  $1/(E + M)$ ].

Expressions similar to (13.60) hold for the other two nonvanishing helicity configurations. To calculate the unpolarized  $e^+e^- \rightarrow \mu^+\mu^-$  cross section, we average over the four allowed  $L, R$  helicity combinations. We find

$$\frac{d\sigma}{d\Omega} = \frac{\alpha^2}{4s}[A_0(1 + \cos^2\theta) + A_1\cos\theta], \quad (13.62)$$

where (assuming electron-muon universality  $c_i^e = c_i^\mu \equiv c_i$ )

$$\begin{aligned} A_0 &\equiv 1 + \frac{1}{2}\text{Re}(r)(c_L + c_R)^2 + \frac{1}{4}|r|^2(c_L^2 + c_R^2)^2 \\ &= 1 + 2\text{Re}(r)c_V^2 + |r|^2(c_V^2 + c_A^2)^2 \end{aligned} \quad (13.63)$$

$$\begin{aligned} A_1 &\equiv \text{Re}(r)(c_L - c_R)^2 + \frac{1}{2}|r|^2(c_L^2 - c_R^2)^2 \\ &= 4\text{Re}(r)c_A^2 + 8|r|^2c_V^2c_A^2. \end{aligned} \quad (13.64)$$

The lowest-order QED result ( $A_0 = 1$ ,  $A_1 = 0$ ) gives a symmetric angular distribution. We now see that the weak interaction introduces a forward–backward asymmetry ( $A_1 \neq 0$ ). Let us calculate the size of the integrated asymmetry defined by

$$A_{FB} \equiv \frac{F - B}{F + B} \quad \text{with } F = \int_0^1 \frac{d\sigma}{d\Omega} d\Omega, \quad B = \int_{-1}^0 \frac{d\sigma}{d\Omega} d\Omega. \quad (13.65)$$

Integrating (13.62), we obtain for  $s \ll M_Z^2$  (i.e.,  $|r| \ll 1$ )

$$A_{FB} = \frac{A_1}{(8A_0/3)} \simeq \frac{3}{2} \operatorname{Re}(r) c_A^2 \simeq -\frac{3c_A^2}{\sqrt{2}} \left( \frac{Gs}{e^2} \right). \quad (13.66)$$

This is in agreement with the expectations of the order of magnitude estimate,  $Gs/e^2$ , of (13.55); an asymmetry which grows quadratically with the energy of the colliding  $e^+$  and  $e^-$  beams (for  $s \ll M_Z^2$ ).

We may use the standard model couplings ( $c_A = -\frac{1}{2}$ ,  $c_V = -\frac{1}{2} + \sin^2 \theta_W \simeq 0$ ) to compare (13.62) with the experimental measurements of the high-energy  $e^+ e^- \rightarrow \mu^+ \mu^-$  angular distribution, see Fig. 13.7. The agreement is good. Since  $c_V = 0$ , these data do not, however, offer an accurate determination of  $\sin^2 \theta_W$ .

Integrating (13.62) over  $d\Omega$ , we find

$$\sigma(e^+ e^- \rightarrow \mu^+ \mu^-) = \frac{\alpha^2}{4s} \left( 2\pi \frac{8}{3} A_0 \right) = \left( \frac{4\pi\alpha^2}{3s} \right) A_0 \equiv \sigma_0 A_0, \quad (13.67)$$

where  $\sigma_0$  is the QED cross section of (6.32). That is,

$$\frac{\sigma(e^+ e^- \rightarrow \mu^+ \mu^-)}{\sigma_0} \equiv R_\mu = 1 + 2 \operatorname{Re}(r) c_V^2 + |r|^2 (c_V^2 + c_A^2)^2. \quad (13.68)$$

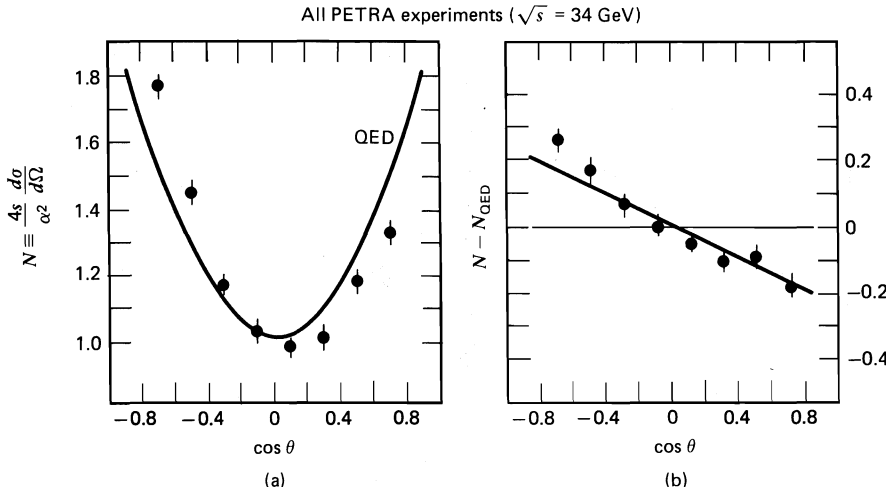


**Fig. 13.7** (a) The  $\cos \theta$  distribution for the process  $e^+ e^- \rightarrow \mu^+ \mu^-$  does not follow the  $1 + \cos^2 \theta$  QED prediction. (b) The discrepancy is explained by the interference of the virtual  $Z$  and  $\gamma$  contributions. (Compilation by R. Marshall.)

**EXERCISE 13.10** Using the couplings in the standard model, calculate  $R_\mu$  at  $s = M_Z^2$ . Use  $\sin^2 \theta_W = \frac{1}{4}$ ,  $M_Z = 90$  GeV, and  $\Gamma_Z = 2.5$  GeV.

It is relevant to ask what electroweak effects occur in  $e^+ e^- \rightarrow \bar{q}q$ . They are not the same as in  $e^+ e^- \rightarrow \mu^+ \mu^-$ , since  $c_{V,A}^q \neq c_{V,A}^\mu$ . However, the calculation proceeds exactly as above. For instance, the counterpart to (13.60) is

$$\frac{d\sigma(e_L^- e_R^+ \rightarrow q_L^- q_R^+)}{d\Omega} = 3 \frac{\alpha^2}{4s} (1 + \cos \theta)^2 |Q_q + r c_L^q c_L^e|^2, \quad (13.69)$$

where  $Q_q$  is the charge of the quark and the factor 3 is for color. Following through the calculation, the analogous result to (13.68) is

$$\frac{\sigma(e^+ e^- \rightarrow \bar{q}q)}{\sigma_0} \equiv R_q = 3 [Q_q^2 + 2Q_q \operatorname{Re}(r) c_V^q c_V^e + |r|^2 (c_V^{q2} + c_A^{q2})(c_V^{e2} + c_A^{e2})]. \quad (13.70)$$

**EXERCISE 13.11** Follow Exercise 13.10 and calculate  $R_u$  and  $R_d$  at  $s = M_Z^2$ . Hence, calculate  $\sigma(e^+ e^- \rightarrow \text{hadrons})$  at the Z resonance.

The numerical results of Exercises 13.10 and 13.11 give  $R$ 's in the region 100–1000. This has crucial implications. Very large enhancements over  $\sigma_0$  are therefore expected at beam energies  $E \sim M_Z/2$ , provided the neutral current interaction is mediated by a Z boson. This is a major motivation for the new 50 + 50 GeV  $e^+ e^-$  collider being constructed at CERN, Geneva. Since  $M_Z \approx 90$  GeV, the Z boson should be copiously produced at the new collider and its properties, and those of its decay products, studied in a clean environment, without the confusing background debris which accompanies a hadronic collision.

### 13.7 Other Observable Electroweak Interference Effects

Several other ingenious experiments have been performed to exhibit parity-violating effects arising from the interference between the electromagnetic and weak neutral current interactions.

One type of experiment involves the delicate measurement of *parity-violating effects in atomic transitions*. The idea is that  $Z^0$  exchange between an electron and the nucleus leads to a modification of the Coulomb potential. At first sight, detection of the effect appears to be a hopeless task. Our rule of thumb, (13.55), predicts an effect of size

$$\frac{Gk^2}{e^2} \simeq \frac{10^{-4}k^2}{m_p^2} \simeq \frac{10^{-4}}{m_p^2 R^2} \simeq 10^{-15}, \quad (13.71)$$

where  $R$  is a typical atomic radius ( $\sim 1$  Å). However, a large enhancement can be achieved by studying highly forbidden electromagnetic transitions and by using

atoms of high  $Z$  (in fact, the effect goes as  $Z^3$ ). The general method is to look for optical rotation of transmitted LASER light induced by the parity-violating interference terms  $c_V^e c_A^q$  and  $c_A^e c_V^q$ .

Another type of experiment measures the minute *parity-violating asymmetry in the inelastic scattering of longitudinally polarized electrons* (or muons) off nuclear targets. The asymmetry is defined by

$$A = \frac{\sigma_R - \sigma_L}{\sigma_R + \sigma_L} \quad (13.72)$$

where, for instance,  $\sigma_R$  is the cross section  $d\Omega/dy$  for  $e_R N \rightarrow e_R X$ ;  $e_R$  denotes a right-handed electron ( $\lambda = +\frac{1}{2}$ ). In the laboratory frame, recall that  $y$  is the fractional energy loss of the electron,  $y = (E - E')/E$ . A nonzero asymmetry indicates the presence of a parity-violating effect. From (13.55), we anticipate an asymmetry from the interference between  $\gamma$  and  $Z^0$  exchange of magnitude

$$A \sim \frac{Gk^2}{e^2} \sim \frac{10^{-4}}{m_p^2} k^2,$$

where  $k$  is the four-momentum carried by the exchanged boson.

For the deep inelastic scattering process  $eN \rightarrow eX$ , we can use the parton model to predict the asymmetry. Taking  $N$  to be an isoscalar target, we find (see Exercise 13.12)

$$A = \frac{6}{5} \left( \frac{\sqrt{2} Gk^2}{e^2} \right) \left( a_1 + a_2 \frac{1 - (1 - y)^2}{1 + (1 - y)^2} \right), \quad (13.73)$$

with

$$\begin{aligned} a_1 &= c_A^e (2c_V^u - c_V^d) \\ a_2 &= c_V^e (2c_A^u - c_A^d), \end{aligned} \quad (13.74)$$

where the  $c$ 's are the neutral-current couplings of (13.41) and Table 13.2. By measuring the asymmetry as a function of  $k^2$  and  $y$ , the coefficients  $a_1$  and  $a_2$  can be determined. Experiments have been performed by scattering polarized electrons off deuterons and polarized  $\mu^\pm$  off carbon. The results are in agreement with the standard model and with the values of  $\sin^2 \theta_W$  obtained by other data.

**EXERCISE 13.12** Verify (13.73). Assume that  $k^2 \ll M_Z^2$  and that the target contains equal numbers of u and d quarks (i.e., it is an isoscalar target), and neglect antiquarks. Show that, in the standard model,

$$\begin{aligned} a_1 &= -\frac{3}{4} \left( 1 - \frac{20}{9} \sin^2 \theta_W \right), \\ a_2 &= -\frac{3}{4} \left( 1 - 4 \sin^2 \theta_W \right). \end{aligned} \quad (13.75)$$

**Hint** As for  $e^+ e^- \rightarrow \mu^+ \mu^-$ , it is easiest to use definite helicity states. For example, in the electron–quark center-of-mass frame,

$$\frac{d\sigma(e_R u_L \rightarrow e_R u_L)}{d\Omega} = \frac{\alpha^2}{4s} (1 + \cos \theta)^2 |Q_u + r c_R^e c_L^u|^2, \quad (13.76)$$

where  $r = -\sqrt{2} Gk^2/e^2$ , see (13.60) and (13.61). Rewrite (13.76) in terms of the parton model (invariant) variable  $y$ , using  $1 - y = \frac{1}{2}(1 + \cos \theta)$ , see (9.25).

# 14

## Gauge Symmetries

### 14.1 The Lagrangian and Single-Particle Wave Equations

One of the most profound insights in theoretical physics is that interactions are dictated by symmetry principles. Einstein made great use of the predictive power of this idea. By considering invariance under general coordinate transformations (together with the equivalence principle), he was led to the general theory of relativity. The present belief is that all particle interactions may be dictated by so-called local gauge symmetries. We shall see that this is intimately connected with the idea that the conserved physical quantities (such as electric charge, color, etc.) are conserved in local regions of space, and not just globally.

The connection between symmetries and conservation laws is best discussed in the framework of Lagrangian field theory, which we have not introduced.\* However, you are probably familiar with the fact that in classical mechanics the particle equations of motion can be obtained from Lagrange's equations [see, for example, Goldstein (1951)]

$$\frac{d}{dt} \left( \frac{\partial L}{\partial \dot{q}_i} \right) - \frac{\partial L}{\partial q_i} = 0, \quad (14.1)$$

where  $q_i$  are the generalized coordinates of the particles,  $t$  is the time variable, and  $\dot{q}_i = dq_i/dt$ . The Lagrangian is

$$L \equiv T - V, \quad (14.2)$$

where  $T$  and  $V$  are the kinetic and potential energies of the system, respectively. It is straightforward to extend the formalism from a discrete system, with coordinates  $q_i(t)$ , to a continuous system, that is, a system with continuously varying coordinates  $\phi(\mathbf{x}, t)$ . The Lagrangian

$$L(q_i, \dot{q}_i, t) \rightarrow \mathcal{L}\left(\phi, \frac{\partial \phi}{\partial x_\mu}, x_\mu\right), \quad (14.3)$$

\*The formalism introduced in this book for computing particle interactions has been based entirely on the single-particle wave equations. Chapters 3 through 7 explain in detail how this can be done, despite the fact that we are routinely dealing with many-particle systems.

where the field  $\phi$  itself is a function of the continuous parameters  $x_\mu$ , and (14.1) becomes

$$\frac{\partial}{\partial x_\mu} \left( \frac{\partial \mathcal{L}}{\partial (\partial \phi / \partial x_\mu)} \right) - \frac{\partial \mathcal{L}}{\partial \phi} = 0, \quad (14.4)$$

the Euler–Lagrange equation.  $\mathcal{L}$  is the Lagrangian density,

$$L = \int \mathcal{L} d^3x. \quad (14.5)$$

We shall follow common practice and call  $\mathcal{L}$  itself the Lagrangian.

**EXERCISE 14.1** If you are unfamiliar with this formalism, consult, for example, Goldstein (1977) or work through the example given in Sakurai (1967), page 3.

Instead of writing down a relativistic wave equation, we simply choose a Lagrangian  $\mathcal{L}$ . Provided our choice is a Lorentz scalar, the equation of motion resulting from (14.4) will be covariant. For example, substituting the Lagrangian

$$\mathcal{L} = \frac{1}{2} (\partial_\mu \phi)(\partial^\mu \phi) - \frac{1}{2} m^2 \phi^2 \quad (14.6)$$

into (14.4) gives the Klein–Gordon equation

$$\partial_\mu \partial^\mu \phi + m^2 \phi \equiv (\square^2 + m^2) \phi = 0. \quad (14.7)$$

There is no mystery here. The choice of  $\mathcal{L}$  was specifically designed to reproduce (14.7).

**EXERCISE 14.2** Verify that the Dirac equation follows from

$$\mathcal{L} = i \bar{\psi} \gamma_\mu \partial^\mu \psi - m \bar{\psi} \psi, \quad (14.8)$$

where each of the four components of  $\psi$  and  $\bar{\psi}$  is regarded as an independent field variable.

**EXERCISE 14.3** Show that the substitution of the Lagrangian

$$\mathcal{L} = -\frac{1}{4} F_{\mu\nu} F^{\mu\nu} - j^\mu A_\mu \quad (14.9)$$

into the Euler–Lagrange equation for  $A_\mu$  gives the Maxwell equations, (6.57),

$$\partial_\mu F^{\mu\nu} = j^\nu, \quad (14.10)$$

where  $F^{\mu\nu} \equiv \partial^\mu A^\nu - \partial^\nu A^\mu$ . Hence, show that the current is conserved, that is,  $\partial_\nu j^\nu = 0$ .

**EXERCISE 14.4** With the addition of a term  $\frac{1}{2}m^2 A_\mu A^\mu$ , show that the Lagrangian of (14.9) leads to an equation of motion

$$(\square^2 + m^2) A^\mu = j^\mu.$$

The new term is therefore a photon mass contribution. We shall see in Section 14.3 that it is forbidden by gauge invariance. The photon is massless.

What is the relation between the Lagrangian approach and the perturbative method based on Feynman rules obtained from single-particle wave equations? To each Lagrangian, there corresponds a set of Feynman rules; and so, once we identify these rules, the connection is made. We can then calculate physical quantities by just following the methods presented in Chapters 4 and 6.

The identification of the Feynman rules proceeds as follows:

- 1 We associate with the various terms in the Lagrangian a set of propagators and vertex factors.
- 2 The propagators are determined by the terms quadratic in the fields, that is, the terms in the Lagrangian containing  $\phi^2$ ,  $\bar{\psi}\psi$ , and so on, such as  $\frac{1}{2}(\partial_\mu\phi)^2 - \frac{1}{2}m^2\phi^2$  and  $\bar{\psi}(i\gamma_\mu\partial^\mu - m)\psi$ . The propagators can then be identified from the Euler–Lagrange equations using the methods of Section 6.10.
- 3 The other terms in the Lagrangian are associated with interaction vertices. The Feynman vertex factor is just given by the coefficient of the corresponding term in  $i\mathcal{L}$  containing the interacting fields. QED provides us with a simple illustration of this. As we shall see in Section 14.3, the second term in (14.9) describes the electron–photon interaction. The electron current is given by  $j^\mu = -e\bar{\psi}\gamma^\mu\psi$ , see (5.17); and so the interaction term in  $i\mathcal{L}$  is

$$i\mathcal{L} = \dots + ie\bar{\psi}\gamma^\mu\psi A_\mu$$

We recognize the coefficient ( $ie\gamma^\mu$ ) of the interacting fields  $\bar{\psi}\psi A_\mu$  as the familiar vertex factor of QED, see Chapter 6.

In the orthodox approach to quantum field theory, we would now proceed to formally derive these assertions. In order to do this, the classical Lagrangian is quantized. Fields such as  $\psi$  and  $A_\mu$  become operators describing the creation and annihilation of particles. Interactions are computed by evaluating a perturbation series in  $i\mathcal{L}_{\text{int}}$ , the interaction term(s) in  $i\mathcal{L}$ . The end result of this lengthy and formal approach can always be translated into a set of Feynman rules which are exactly those we just described. So, we might as well take these rules and proceed to investigate the physical implications of a given Lagrangian using the methods with which we are already familiar. The canonical formalism was formerly regarded as more rigorous and can be found in many books [for introductory

discussions see, e.g., Mandl (1966), Muirhead (1965), and Sakurai (1967)]. We do not present it, as we will never use it. We hereby subscribe to the growing belief that “the diagrams contain more truth than the underlying formalism” [t’ Hooft and Veltman (1973)].

## 14.2 Noether’s Theorem: Symmetries and Conservation Laws

Invariance under translations, time displacements, rotations, and Lorentz transformations leads to the conservation of momentum, energy, and angular momentum. Rather than studying these conservation laws, we are interested here in “internal” symmetry transformations that do not mix fields with different space-time properties (that is, transformations that commute with the space-time components of the wavefunction).

For example, an electron is described by a complex field, and inspection of the Lagrangian (14.8) shows that it is invariant under the phase transformation

$$\psi(x) \rightarrow e^{i\alpha} \psi(x), \quad (14.11)$$

where  $\alpha$  is a real constant. This can be easily checked by noting

$$\partial_\mu \psi \rightarrow e^{i\alpha} \partial_\mu \psi, \quad (14.12)$$

$$\bar{\psi} \rightarrow e^{-i\alpha} \bar{\psi}. \quad (14.13)$$

The family of phase transformations  $U(\alpha) \equiv e^{i\alpha}$ , where a single parameter  $\alpha$  may run continuously over real numbers, forms a unitary Abelian group known as the  $U(1)$  group. Abelian just records the property that the group multiplication is commutative:

$$U(\alpha_1)U(\alpha_2) = U(\alpha_2)U(\alpha_1). \quad (14.14)$$

You may think that the observation of  $U(1)$  invariance of  $\mathcal{L}$  is rather trivial and unimportant. This is not so. Through Noether’s theorem, it implies the existence of a conserved current. To see this, it is sufficient to study the invariance of  $\mathcal{L}$  under an infinitesimal  $U(1)$  transformation,

$$\psi \rightarrow (1 + i\alpha)\psi. \quad (14.15)$$

Invariance requires the Lagrangian to be unchanged, that is,

$$\begin{aligned} 0 = \delta \mathcal{L} &= \frac{\partial \mathcal{L}}{\partial \psi} \delta \psi + \frac{\partial \mathcal{L}}{\partial (\partial_\mu \psi)} \delta (\partial_\mu \psi) + \delta \bar{\psi} \frac{\partial \mathcal{L}}{\partial \bar{\psi}} + \delta (\partial_\mu \bar{\psi}) \frac{\partial \mathcal{L}}{\partial (\partial_\mu \bar{\psi})} \\ &= \frac{\partial \mathcal{L}}{\partial \psi} (i\alpha \psi) + \frac{\partial \mathcal{L}}{\partial (\partial_\mu \psi)} (i\alpha \partial_\mu \psi) + \dots \\ &= i\alpha \left[ \frac{\partial \mathcal{L}}{\partial \psi} - \partial_\mu \left( \frac{\partial \mathcal{L}}{\partial (\partial_\mu \psi)} \right) \right] \psi + i\alpha \partial_\mu \left( \frac{\partial \mathcal{L}}{\partial (\partial_\mu \psi)} \psi \right) + \dots \end{aligned} \quad (14.16)$$

The term in square brackets vanishes by virtue of the Euler–Lagrange equation, (14.4), for  $\psi$  (and similarly for  $\bar{\psi}$ ), and so (14.16) reduces to the form of an equation for a conserved current:

$$\partial_\mu j^\mu = 0, \quad (14.17)$$

where

$$j^\mu = \frac{ie}{2} \left( \frac{\partial \mathcal{L}}{\partial(\partial_\mu \psi)} \psi - \bar{\psi} \frac{\partial \mathcal{L}}{\partial(\partial_\mu \bar{\psi})} \right) = -e \bar{\psi} \gamma^\mu \psi, \quad (14.18)$$

using (14.8). The proportionality factor is chosen so that  $j^\mu$  matches up with the electromagnetic charge current density of an electron of charge  $-e$ , see (5.17). It follows from (14.17) that the charge

$$Q = \int d^3x j^0$$

must be a conserved quantity because of the  $U(1)$  phase invariance.

**EXERCISE 14.5** Show that  $dQ/dt = 0$ .

**EXERCISE 14.6** Show that  $U(1)$  phase invariance of the Lagrangian

$$\mathcal{L} = (\partial_\mu \phi)^* (\partial^\mu \phi) - m^2 \phi^* \phi \quad (14.19)$$

of a complex scalar field implies the existence of a conserved current

$$j^\mu = -ie(\phi^* \partial^\mu \phi - \phi \partial^\mu \phi^*), \quad (14.20)$$

and compare with (3.25). Note that the Lagrangian, (14.19), for a complex field  $\phi = (\phi_1 + i\phi_2)/\sqrt{2}$  is normalized to ensure that

$$\mathcal{L}(\phi) = \mathcal{L}(\phi_1) + \mathcal{L}(\phi_2),$$

where  $\mathcal{L}(\phi_i)$ , the Lagrangian for a real field  $\phi_i$ , is given by (14.6).

From a physicist's point of view, the existence of a symmetry implies that some quantity is unmeasurable. For example, translation invariance means that we cannot determine an absolute position in space. Similarly, (14.11) implies that the phase  $\alpha$  is unmeasurable, it has no physical meaning and can be chosen arbitrarily.  $\alpha$  is a constant; therefore, once we fix it, the value is specified for all space and time. We speak of *global* “gauge” (a historical misnomer for “phase”) invariance. This is surely not the most general invariance, for it would be more satisfactory if  $\alpha$  could differ from space-time point to point, that is,  $\alpha = \alpha(x)$ .

### 14.3 $U(1)$ Local Gauge Invariance and QED

The message of the last paragraph is that we should generalize (14.11) to the transformation

$$\psi(x) \rightarrow e^{i\alpha(x)}\psi(x), \quad (14.21)$$

where  $\alpha(x)$  now depends on space and time in a completely arbitrary way. This is known as local gauge invariance. However, this does not work. The Lagrangian, (14.8),

$$\mathcal{L} = i\bar{\psi}\gamma^\mu\partial_\mu\psi - m\bar{\psi}\psi,$$

is not invariant under such local phase transformations. From (14.21),

$$\bar{\psi} \rightarrow e^{-i\alpha(x)}\bar{\psi},$$

so the last term of  $\mathcal{L}$  is invariant; however, the derivative of  $\psi$  does not follow (14.21). Rather,

$$\partial_\mu\psi \rightarrow e^{i\alpha(x)}\partial_\mu\psi + ie^{i\alpha(x)}\psi\partial_\mu\alpha \quad (14.22)$$

and the  $\partial_\mu\alpha$  term breaks the invariance of  $\mathcal{L}$ .

If, on aesthetic grounds, we insist on imposing invariance of the Lagrangian under local gauge transformations, we must seek a modified derivative,  $D_\mu$ , that transforms covariantly under phase transformations, that is, like  $\psi$  itself:

$$D_\mu\psi \rightarrow e^{i\alpha(x)}D_\mu\psi. \quad (14.23)$$

To form the “covariant derivative”  $D_\mu$ , we must introduce a vector field  $A_\mu$  with transformation properties such that the unwanted term in (14.22) is canceled. This can be accomplished by the construction

$$D_\mu \equiv \partial_\mu - ieA_\mu,$$

(14.24)

where  $A_\mu$  transforms as

$$A_\mu \rightarrow A_\mu + \frac{1}{e}\partial_\mu\alpha. \quad (14.25)$$

It is easy to check that  $D_\mu$  satisfies (14.23). Invariance of the Lagrangian (14.8) is then achieved by replacing  $\partial_\mu$  by  $D_\mu$ :

$$\begin{aligned} \mathcal{L} &= i\bar{\psi}\gamma^\mu D_\mu\psi - m\bar{\psi}\psi \\ &= \bar{\psi}(i\gamma^\mu\partial_\mu - m)\psi + e\bar{\psi}\gamma^\mu\psi A_\mu. \end{aligned} \quad (14.26)$$

Hence, by demanding local phase invariance, we are forced to introduce a vector field  $A_\mu$ , called the *gauge field*, which couples to the Dirac particle (charge  $-e$ ) in exactly the same way as the photon field; compare (14.24) with (6.1). Indeed, the new interaction term in (14.26) may be written  $-j^\mu A_\mu$ , where  $j^\mu$  is the current density of (5.17).

If we are to regard this new field as the physical photon field, we must add to the Lagrangian a term corresponding to its kinetic energy, analogous to  $\frac{1}{2}(\partial_\mu\phi)^2$  in (14.6). Since the kinetic term must be invariant under (14.25), it can only involve the gauge invariant field strength tensor

$$F_{\mu\nu} = \partial_\mu A_\nu - \partial_\nu A_\mu. \quad (14.27)$$

We are thus led to the Lagrangian of QED:

$$\mathcal{L} = \bar{\psi}(i\gamma^\mu\partial_\mu - m)\psi + e\bar{\psi}\gamma^\mu A_\mu\psi - \frac{1}{4}F_{\mu\nu}F^{\mu\nu}. \quad (14.28)$$

Note that the addition of a mass term  $\frac{1}{2}m^2A_\mu A^\mu$  (see Exercise 14.4) is prohibited by gauge invariance. The gauge particle, the photon, must be *massless*.

It was clear from the outset that a new field would have to be introduced, since changing the phase locally will create phase differences which would be observable if not compensated in some way. The surprising result is that local gauge invariance can be restored, and restored by the photon field  $A_\mu$ . We expect the gauge field to have infinite range (that is, the photon will be massless) since there is no limit to the distance over which the phases of the electron field might have to be reconciled.

In summary, we see that by imposing the “natural” requirement of local phase invariance on the free fermion Lagrangian, we are led to the interacting field theory of QED. Gauge invariance, which in your study of classical electrodynamics you may have conceived to be some formal curiosity of Maxwell theory, has become one of the most basic and essential ingredients.

**EXERCISE 14.7** Read about the Bohm–Aharonov effect. Suggested references are the *Feynman Lectures on Physics*, Volume 2, or Wu, T. T. and Yang, C. N. (1975) *Phys. Rev. D* **12**, 3845.

#### 14.4 Non-Abelian Gauge Invariance and QCD

In an analogous way, we can hope to infer the structure of quantum chromodynamics from local gauge invariance. QCD is based on the extension of the above idea, but with the  $U(1)$  gauge group replaced by the  $SU(3)$  group of phase transformations on the quark color fields. The free Lagrangian is

$$\mathcal{L}_0 = \bar{q}_j(i\gamma^\mu\partial_\mu - m)q_j, \quad (14.29)$$

where  $q_1, q_2, q_3$  denote the three color fields. For simplicity, we show just one quark flavor.

We can explore the consequences of requiring  $\mathcal{L}_0$  to be invariant under local phase transformations of the form

$$q(x) \rightarrow Uq(x) \equiv e^{i\alpha_a(x)T_a}q(x), \quad (14.30)$$

where  $U$  is an arbitrary  $3 \times 3$  unitary matrix which we show parametrized by its

general form. A summation over the repeated suffix  $a$  is implied.  $T_a$  with  $a = 1, \dots, 8$  are a set of linearly independent traceless  $3 \times 3$  matrices, and  $\alpha_a$  are the group parameters. The matrices  $\lambda_a/2$  of Section 2.8 are the conventional choice of the  $T_a$  matrices.

**EXERCISE 14.8** Show that  $\det U = e^{i\phi}$ , where  $\phi$  is real. We separate off such an overall phase by restricting the group transformations to those with  $\det U = +1$ , see Section 2.3. We called this the group of special unitary  $3 \times 3$  matrices  $SU(3)$ . Show that the requirement  $\det U = +1$  implies  $\text{Tr}(T_a) = 0$ . Verify that  $U^\dagger = U^{-1}$  requires

$$\alpha_a T_a = \alpha_a^* T_a^\dagger, \quad (14.31)$$

so that choosing  $T_a$  to be hermitian means the group parameters  $\alpha_a$  are real.

The group is non-Abelian since not all the generators  $T_a$  commute with each other. It is easy to show that the commutator of any two is a linear combination of all the  $T$ 's:

$$[T_a, T_b] = if_{abc} T_c \quad (14.32)$$

where  $f_{abc}$  are real constants, called the structure constants of the group.

**EXERCISE 14.9** Show that the structure constants  $f_{abc}$  are antisymmetric under interchange of any pair of indices.

To impose  $SU(3)$  local gauge invariance on the Lagrangian (14.29), we follow the steps of Section 14.3. It is sufficient to consider infinitesimal phase transformations,

$$\begin{aligned} q(x) &\rightarrow [1 + i\alpha_a(x)T_a]q(x), \\ \partial_\mu q &\rightarrow (1 + i\alpha_a T_a)\partial_\mu q + iT_a q \partial_\mu \alpha_a. \end{aligned} \quad (14.33)$$

The last term spoils the invariance of  $\mathcal{L}$ . At first sight, it looks as if we can proceed exactly as for QED. That is, we introduce (eight) gauge fields  $G_\mu^a$ , each transforming as [see (14.25)]

$$G_\mu^a \rightarrow G_\mu^a - \frac{1}{g}\partial_\mu \alpha_a, \quad (14.34)$$

and form a covariant derivative [see (14.24)]

$$D_\mu = \partial_\mu + igT_a G_\mu^a. \quad (14.35)$$

We then make the replacement  $\partial_\mu \rightarrow D_\mu$  in Lagrangian (14.29) and obtain

$$\mathcal{L} = \bar{q}(i\gamma^\mu \partial_\mu - m)q - g(\bar{q}\gamma^\mu T_a q)G_\mu^a. \quad (14.36)$$

This is the QCD analogue of (14.26). However, for a non-Abelian gauge transfor-

mation, this is not enough to produce a gauge-invariant Lagrangian. The problem is that

$$(\bar{q}\gamma^\mu T_a q) \rightarrow (\bar{q}\gamma^\mu T_a q) + i\alpha_b \bar{q}\gamma^\mu (T_a T_b - T_b T_a) q \rightarrow (\bar{q}\gamma^\mu T_a q) - f_{abc} \alpha_b (\bar{q}\gamma^\mu T_c q), \quad (14.37)$$

using (14.32). Taking note of this result, we see that we can achieve gauge invariance of  $\mathcal{L}$  provided we rewrite (14.34) as

$$G_\mu^a \rightarrow G_\mu^a - \frac{1}{g} \partial_\mu \alpha_a - f_{abc} \alpha_b G_\mu^c. \quad (14.38)$$

Finally, we may add to  $\mathcal{L}$  a gauge invariant kinetic energy term for each of the  $G_\mu^a$  fields. The final gauge invariant QCD Lagrangian is then

$$\boxed{\mathcal{L} = \bar{q}(i\gamma^\mu \partial_\mu - m)q - g(\bar{q}\gamma^\mu T_a q)G_\mu^a - \frac{1}{4}G_{\mu\nu}^a G_a^{\mu\nu}.} \quad (14.39)$$

**EXERCISE 14.10** Due to the additional term in (14.38),  $G_{\mu\nu}^a$  has a more complicated form than its counterpart in QED, (14.27). In order that the kinetic energy be invariant under (14.38), show that

$$G_{\mu\nu}^a = \partial_\mu G_\nu^a - \partial_\nu G_\mu^a - g f_{abc} G_\mu^b G_\nu^c. \quad (14.40)$$

Equation (14.39) is the Lagrangian for interacting colored quarks  $q$  and vector gluons  $G_\mu^a$ , with coupling specified by  $g$ , which follows simply from demanding that the Lagrangian be invariant under local color phase transformations to the quark fields. Since we can arbitrarily vary the phase of the three quark color fields, it is not surprising that eight vector gluon fields ( $G_\mu^a$  with  $a = 1, \dots, 8$ ) are needed to compensate all possible phase changes. Just as for the photon, local gauge invariance requires the gluons to be *massless*.

The field strength tensor  $G_{\mu\nu}^a$  has a remarkable new property on account of the extra term in (14.40). Imposing the gauge symmetry has required that the kinetic energy term in  $\mathcal{L}$  is not purely kinetic but includes an induced self-interaction between the gauge bosons. This becomes clear if we rewrite Lagrangian (14.39) in the symbolic form

$$\mathcal{L} = \text{"}\bar{q}q\text{"} + \text{"}G^2\text{"} + g\text{"}\bar{q}qG\text{"} + g\text{"}G^3\text{"} + g^2\text{"}G^4\text{"}.$$



The first three terms have QED analogues. They describe the free propagation of quarks and gluons and the quark-gluon interaction. The remaining two terms show the presence of three and four gluon vertices in QCD and reflect the fact

that gluons themselves carry color charge. They have no analogue in QED and arise on account of the non-Abelian character of the gauge group. We emphasize that gauge invariance uniquely determines the structure of these gluon self-coupling terms. There is only one coupling  $g$ .

**EXERCISE 14.11** Using the prescription for obtaining the Feynman rules from the Lagrangian that we mentioned in Section 14.1, show that the vertex factors for the quark-gluon and triple gluon vertices of Fig. 14.1 are, respectively,

$$-ig\gamma_\mu(T_a)_{ij},$$

$$-gf_{abc}[g_{\mu\nu}(p_1 - p_2)_\lambda + g_{\nu\lambda}(p_2 - p_3)_\mu + g_{\lambda\mu}(p_3 - p_1)_\nu].$$

Theories with non-Abelian gauge invariance are frequently referred to as Yang-Mills theories, as these authors were the first to study the implications of a non-Abelian gauge group.

#### 14.5 Massive Gauge Bosons?

We have seen that both photons and gluons are required to be massless, since the presence of mass terms for gauge fields destroys the gauge invariance of the Lagrangian. This raises a serious problem if we want to apply these ideas also to the weak interaction. How can we apply gauge symmetry to interactions which are mediated by gauge bosons ( $W^\pm, Z$ ) with masses of the order of 100 GeV? You could argue that we demanded local gauge invariance on the basis of pure aesthetics; so why not introduce mass terms of the form  $M^2 W_\mu W^\mu$  into the Lagrangian and just ignore their symmetry-breaking effect? If we go ahead and do this, we encounter (unrenormalizable) divergences which make the theory meaningless.

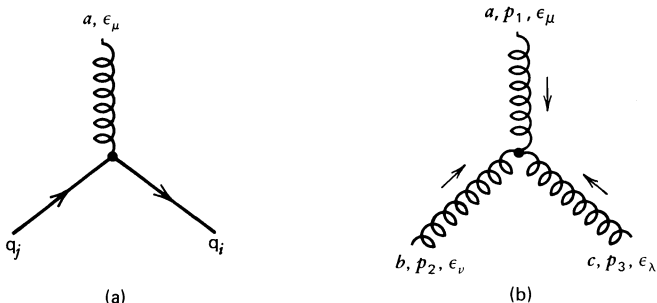


**Fig. 14.1** (a) The quark-gluon vertex and (b) the triple-gluon vertex, showing the color, the four-momenta, and the polarization vectors of the gluons.

For example, let us calculate the diagram shown in Fig. 14.2. The momentum  $q$  circling around the loop may take any value. It must therefore be integrated over so that the amplitude is of the form

$$\int d^4q (\text{propagators}) \dots, \quad (14.41)$$

see Chapter 7. In QED, one can calculate the exchange of two photons between electrons (topologically the same as Fig. 14.2) and perform the integration (14.41). The answer is finite. The momentum in the loop can of course be arbitrarily large, but the  $1/q^2$  behavior of the photon propagators makes the integral (14.41) well behaved. For massive gauge bosons, the result is different. The propagators (6.87) are of the form

$$i \frac{-g_{\mu\nu} + q_\mu q_\nu / M^2}{q^2 - M^2} \underset{q^2 \rightarrow \infty}{\sim} i \frac{q_\mu q_\nu}{q^2 M^2}, \quad (14.42)$$

and they no longer prevent (14.41) from diverging for large loop momenta. Our only hope is to introduce a cutoff in  $q^2$ . It represents a new parameter in the theory which might perhaps be determined by experiment. But this hope is shattered by inspecting diagrams containing more loops. New, ever more severe divergences appear in each order, and ultimately an infinite number of unknown parameters have to be introduced. Unlike the divergences discussed in Chapter 7, it is not possible to interpret these divergences as merely “renormalizing” the couplings in the Lagrangian. Such a theory is meaningless: no predictions are possible. It is said to be “unrenormalizable.” Giving up local gauge invariance to introduce  $W^\pm, Z$  masses “by hand” in this way is clearly no good. Is it possible then to introduce mass without breaking gauge invariance? Surprisingly, it can be done. The following sections describe this intriguing development.

## 14.6 Spontaneous Symmetry Breaking. “Hidden” Symmetry

The way to generate the mass of a particle by “spontaneous symmetry breaking,” as opposed to putting it in by hand as we did in (14.6), can be seen in a very simple example. Consider a simple world consisting just of scalar particles described by the Lagrangian

$$\mathcal{L} \equiv T - V = \frac{1}{2}(\partial_\mu \phi)^2 - \left(\frac{1}{2}\mu^2 \phi^2 + \frac{1}{4}\lambda \phi^4\right), \quad (14.43)$$

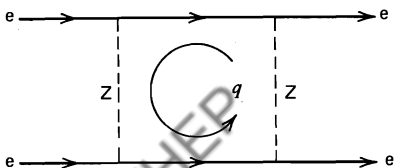


Fig. 14.2 A loop contribution to electron-electron scattering.

with  $\lambda > 0$ . Here, we have required  $\mathcal{L}$  to be invariant under the symmetry operation which replaces  $\phi$  by  $-\phi$ . It suffices to keep the first two allowed terms in the general expansion of  $V$  in powers of  $\phi$ . The two possible forms of the potential are shown in Fig. 14.3. Case (a) for  $\mu^2 > 0$  is already familiar; see (14.6). It simply describes a scalar field with mass  $\mu$ . The  $\phi^4$  term shows that the four-particle vertex exists with coupling  $\lambda$ . We say that  $\phi$  is a self-interacting field. The ground state (the vacuum) corresponds to  $\phi = 0$ . It obeys the reflection symmetry of the Lagrangian.

However, case (b) of Fig. 14.3, where  $\mu^2 < 0$ , is the possibility we really wish to explore. Now, the Lagrangian (14.43) has a mass term of the wrong sign for the field  $\phi$ , since the relative sign of the  $\phi^2$  term and the kinetic energy  $T$  is positive. Unlike case (a), in case (b) the potential has two minima. These minima satisfy

$$\frac{\partial V}{\partial \phi} = \phi(\mu^2 + \lambda\phi^2) = 0$$

and are therefore at

$$\phi = \pm v \quad \text{with} \quad v = \sqrt{-\mu^2/\lambda}. \quad (14.44)$$

The extremum  $\phi = 0$  does not correspond to the energy minimum. Perturbative calculations should involve expansions around the classical minimum  $\phi = v$  or  $\phi = -v$ . We therefore write

$$\phi(x) = v + \eta(x), \quad (14.45)$$

where  $\eta(x)$  represents the quantum fluctuations about this minimum. We have chosen to translate the field to  $\phi = +v$ , but this does not imply any loss of generality since  $\phi = -v$  can always be reached by reflection symmetry. (Nature has also to make such a choice.) Substituting (14.45) into Lagrangian (14.43), we

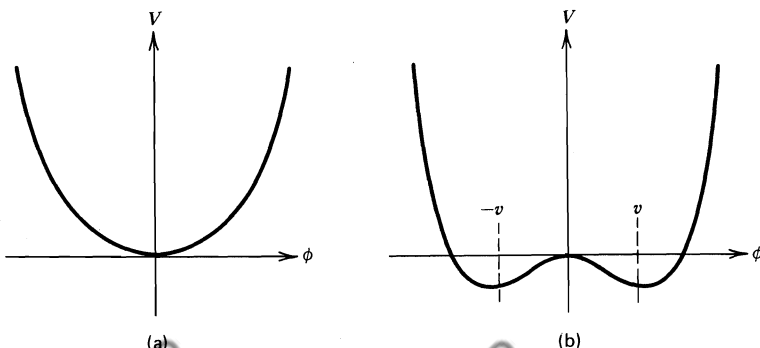


Fig. 14.3 The potential  $V(\phi) = \frac{1}{2}\mu^2\phi^2 + \frac{1}{4}\lambda\phi^4$  for (a)  $\mu^2 > 0$  and (b)  $\mu^2 < 0$ , and  $\lambda > 0$ .

obtain

$$\mathcal{L}' = \frac{1}{2}(\partial_\mu \eta)^2 - \lambda v^2 \eta^2 - \lambda v \eta^3 - \frac{1}{4}\lambda \eta^4 + \text{const.} \quad (14.46)$$

The field  $\eta$  has a mass term of the correct sign! Indeed, the relative sign of the  $\eta^2$  term and the kinetic energy is negative. Identifying the first two terms of  $\mathcal{L}'$  with (14.6) gives

$$m_\eta = \sqrt{2\lambda v^2} = \sqrt{-2\mu^2}. \quad (14.47)$$

The higher-order terms in  $\eta$  represent the interaction of the  $\eta$  field with itself.

There is of course a puzzle here. The Lagrangians,  $\mathcal{L}$  of (14.43) and  $\mathcal{L}'$  of (14.46), are completely equivalent. A transformation of the type (14.45) cannot change the physics. If we could solve the two Lagrangians exactly, they must yield identical physics. But in particle physics, we are not able to perform such a calculation. Instead, we do perturbation theory and calculate the fluctuations around the minimum energy. Using  $\mathcal{L}$ , we would discover that the perturbation series did not converge because we are trying to expand around the unstable point  $\phi = 0$ . The correct way to proceed is to use  $\mathcal{L}'$  and expand in  $\eta$  around the stable vacuum  $\phi = +v$ . In perturbation theory,  $\mathcal{L}'$  gives the correct picture of physics;  $\mathcal{L}$  does not. The scalar particle (described by the in-principle-equivalent Lagrangians  $\mathcal{L}, \mathcal{L}'$ ) therefore does have a mass!

We refer to the way this mass was “generated” (or, better, “revealed”) as “spontaneous symmetry breaking.” In the  $\mathcal{L}'$  version of our scalar theory, the reflection symmetry of the Lagrangian has apparently been broken by our choice of the ground state  $\phi = +v$  (rather than  $\phi = -v$ ) around which to do our perturbation calculations.

Other physical systems are known in which the ground state does not possess the symmetry of the Lagrangian. An infinitely extended ferromagnet is described by a Lagrangian which is invariant under rotations in space. In the ground state, all the elementary spins are aligned in a particular direction, and the rotational symmetry is apparently broken. This direction is arbitrary, however; and by rotational symmetry, we can reach an infinite number of other ground states, each corresponding to a different alignment of the spins. In our scalar field example, only two ground states were possible. Other examples are superconductors, crystal lattices, and the buckling of a compressed needle! If we take a knitting needle and compress it with a force  $F$  along its axis (the  $z$  axis in Fig. 14.4), the obvious solution is that it stays in the configuration  $x = y = 0$ . However, if the force gets too large ( $F > F_{\text{critical}}$ ), the needle will jump into the bent position shown in the figure. It does this because the energy in this state is lower than in the metastable state, where it stays aligned along the  $z$  axis. The cylindrical symmetry of the system around the  $z$  axis is apparently broken by the buckling of the needle. But the needle can buckle in any direction in the  $x$ - $y$  plane, reaching a ground state with the same energy, so it is not possible to predict which way it will go.

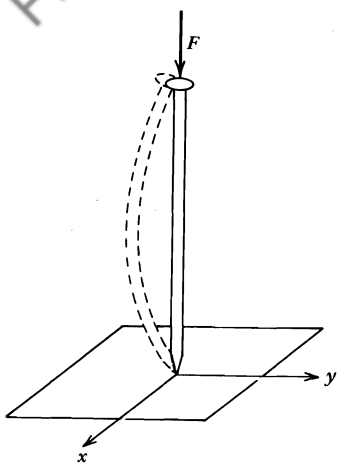


Fig. 14.4 An example of spontaneous symmetry breaking: the buckling of a knitting needle.

#### 14.7 Spontaneous Breaking of a Global Gauge Symmetry

To approach our goal of generating a mass for the gauge bosons, we repeat the above procedure for a complex scalar field  $\phi = (\phi_1 + i\phi_2)/\sqrt{2}$  described by Lagrangian

$$\mathcal{L} = (\partial_\mu \phi)^* (\partial^\mu \phi) - \mu^2 \phi^* \phi - \lambda (\phi^* \phi)^2, \quad (14.48)$$

which is invariant under  $\phi \rightarrow e^{i\alpha} \phi$ . That is,  $\mathcal{L}$  possesses a  $U(1)$  global gauge symmetry. As before, we consider the case when  $\lambda > 0$  and  $\mu^2 < 0$ . We rewrite (14.48) in the form

$$\mathcal{L} = \frac{1}{2} (\partial_\mu \phi_1)^2 + \frac{1}{2} (\partial_\mu \phi_2)^2 - \frac{1}{2} \mu^2 (\phi_1^2 + \phi_2^2) - \frac{1}{4} \lambda (\phi_1^2 + \phi_2^2)^2.$$

There is now a circle of minima of the potential  $V(\phi)$  in the  $\phi_1, \phi_2$  plane of radius  $v$ , such that

$$\phi_1^2 + \phi_2^2 = v^2 \quad \text{with} \quad v^2 = -\frac{\mu^2}{\lambda}, \quad (14.49)$$

as shown in Fig. 14.5. Again, we translate the field  $\phi$  to a minimum energy position, which without loss of generality we may take as the point  $\phi_1 = v$ ,  $\phi_2 = 0$ . We expand  $\mathcal{L}$  about the vacuum in terms of fields  $\eta, \xi$  by substituting

$$\phi(x) = \sqrt{\frac{1}{2}} [v + \eta(x) + i\xi(x)] \quad (14.50)$$

into (14.48) and obtain

$$\mathcal{L}' = \frac{1}{2} (\partial_\mu \xi)^2 + \frac{1}{2} (\partial_\mu \eta)^2 + \mu^2 \eta^2 + \text{const.} + \text{cubic and quartic terms in } \eta, \xi. \quad (14.51)$$

The third term has the form of a mass term  $(-\frac{1}{2} m_\eta^2 \eta^2)$  for the  $\eta$ -field. Thus, the

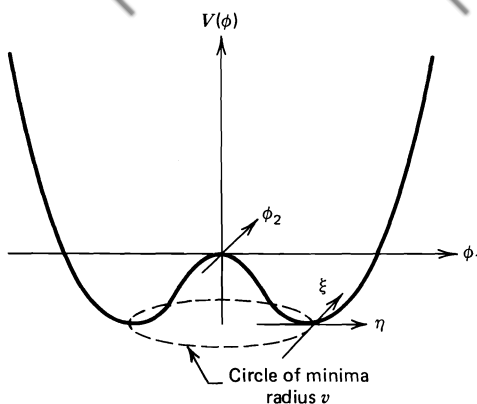


**Fig. 14.5** The potential  $V(\phi)$  for a complex scalar field for the case  $\mu^2 < 0$  and  $\lambda > 0$ .

$\eta$ -mass is  $m_\eta = \sqrt{-2\mu^2}$ , just as before, see (14.47). The first term in  $\mathcal{L}'$  represents the kinetic energy of the  $\xi$ -field, but there is no corresponding mass term for  $\xi$ . That is, the theory also contains a massless scalar, which is known as a Goldstone boson. Thus, we have encountered a problem; in attempting to generate a massive gauge boson, we see that a spontaneously broken gauge theory appears to be plagued with its own massless scalar particle. Intuitively, it is easy to see the reason for its presence. The potential in the tangent ( $\xi$ ) direction is flat, implying a massless mode; there is no resistance to excitations along the  $\xi$ -direction in Fig. 14.5.

Our Lagrangian is a simple example of the Goldstone theorem, which states that massless scalars occur whenever a continuous symmetry of a physical system is “spontaneously broken” (or, more accurately, is “not apparent in the ground state”). In the ferromagnet example, the analogue of our Goldstone boson is the long-range spin waves which are oscillations of the spin alignment.

**EXERCISE 14.12** The Lagrangian for three interacting real fields  $\phi_1, \phi_2, \phi_3$  is

$$\mathcal{L} = \frac{1}{2}(\partial_\mu \phi_i)^2 - \frac{1}{2}\mu^2\phi_i^2 - \frac{1}{4}\lambda(\phi_i^2)^2$$

with  $\mu^2 < 0$  and  $\lambda > 0$ , and where a summation of  $\phi_i^2$  over  $i$  is implied.

Show that it describes a massive field of mass  $\sqrt{-2\mu^2}$  and two massless Goldstone bosons.

Our hope of finding a gauge theory of weak interactions with massive gauge bosons looks forlorn. It appears that we shall also have unwanted (unobserved) massless scalar particles to worry about. Nevertheless, let us proceed from a global to a local gauge theory. A miracle is about to happen.

### 14.8 The Higgs Mechanism

The final step is to study spontaneous breaking of a local gauge symmetry. Here, we take the simplest example: a  $U(1)$  gauge symmetry. In the following section, we extend the discussion to  $SU(2)$ . First, we must make our Lagrangian, (14.48), invariant under a  $U(1)$  local gauge transformation,

$$\phi \rightarrow e^{i\alpha(x)}\phi. \quad (14.52)$$

As in Section 14.3, this requires  $\partial_\mu$  to be replaced by the covariant derivative,

$$D_\mu = \partial_\mu - ieA_\mu,$$

where the gauge field transforms as

$$A_\mu \rightarrow A_\mu + \frac{1}{e}\partial_\mu\alpha. \quad (14.53)$$

The gauge invariant Lagrangian is thus

$$\mathcal{L} = (\partial^\mu + ieA^\mu)\phi^*(\partial_\mu - ieA_\mu)\phi - \mu^2\phi^*\phi - \lambda(\phi^*\phi)^2 - \frac{1}{4}F_{\mu\nu}F^{\mu\nu}. \quad (14.54)$$

If  $\mu^2 > 0$ , this is just the QED Lagrangian for a charged scalar particle of mass  $\mu$  (apart from the  $\phi^4$  self-interaction term). We already obtained the analogous QED Lagrangian for a fermion field in (14.28). However, here we take  $\mu^2 < 0$  since we want to generate masses by spontaneous symmetry breaking.

We repeat the by now familiar procedure of translating the field  $\phi$  to a true ground state. On substituting (14.50), the Lagrangian (14.54) becomes

$$\begin{aligned} \mathcal{L}' = & \frac{1}{2}(\partial_\mu\xi)^2 + \frac{1}{2}(\partial_\mu\eta)^2 - v^2\lambda\eta^2 + \frac{1}{2}e^2v^2A_\mu A^\mu \\ & - evA_\mu\partial^\mu\xi - \frac{1}{4}F_{\mu\nu}F^{\mu\nu} + \text{interaction terms.} \end{aligned} \quad (14.55)$$

The particle spectrum of  $\mathcal{L}'$  appears to be a massless Goldstone boson  $\xi$ , a massive scalar  $\eta$ , and more crucially a massive vector  $A_\mu$  for which we have sought so long. Indeed, from (14.55), we have

$$m_\xi = 0, \quad m_\eta = \sqrt{2\lambda v^2}, \quad m_A = ev$$

[see (14.6) and Exercise 14.4]. We have dynamically generated a mass for the gauge field, but we still have the problem of the occurrence of a massless Goldstone boson. But wait, the presence of a term off-diagonal in the fields,  $A_\mu\partial^\mu\xi$ , means we must take care in interpreting  $\mathcal{L}'$ . Indeed, the particle spectrum we assigned to  $\mathcal{L}'$  cannot be correct. By giving mass to  $A_\mu$ , we have clearly raised the polarization degrees of freedom from 2 to 3, because it can now have longitudinal polarization. But simply translating field variables, as in (14.50), does not create a new degree of freedom. We deduce that the fields in  $\mathcal{L}'$  do not all correspond to distinct physical particles. This need not worry us; indeed, in QED we use a Lagrangian containing unphysical (longitudinal as well as scalar) massless photons. But which field in  $\mathcal{L}'$  is unphysical? Can we find a particular gauge transformation which will eliminate a field from the Lagrangian? A clue is

to note that

$$\begin{aligned}\phi &= \sqrt{\frac{1}{2}}(v + \eta + i\xi) \\ &\simeq \sqrt{\frac{1}{2}}(v + \eta)e^{i\xi/v}\end{aligned}\quad (14.56)$$

to lowest order in  $\xi$ . This suggests that we should substitute a different set of real fields  $h, \theta, A_\mu$ , where

$$\begin{aligned}\phi &\rightarrow \sqrt{\frac{1}{2}}(v + h(x))e^{i\theta(x)/v}, \\ A_\mu &\rightarrow A_\mu + \frac{1}{ev}\partial_\mu\theta\end{aligned}\quad (14.57)$$

into the original Lagrangian (14.54). This is a particular choice of gauge, with  $\theta(x)$  chosen so that  $h$  is real. We therefore anticipate that the theory will be independent of  $\theta$ . Indeed, we obtain

$$\begin{aligned}\mathcal{L}'' = \frac{1}{2}(\partial_\mu h)^2 - \lambda v^2 h^2 + \frac{1}{2}e^2 v^2 A_\mu^2 - \lambda v h^3 - \frac{1}{4}\lambda h^4 \\ + \frac{1}{2}e^2 A_\mu^2 h^2 + v e^2 A_\mu^2 h - \frac{1}{4}F_{\mu\nu}F^{\mu\nu}.\end{aligned}\quad (14.58)$$

The Goldstone boson actually does *not* appear in the theory. That is, the apparent extra degree of freedom is actually spurious, because it corresponds only to the freedom to make a gauge transformation. The Lagrangian describes just two interacting massive particles, a vector gauge boson  $A_\mu$  and a massive scalar  $h$ , which is called a Higgs particle. The unwanted massless Goldstone boson has been turned into the badly needed longitudinal polarization of the massive gauge particle. This is called the “Higgs mechanism.”

## 14.9 Spontaneous Breaking of a Local $SU(2)$ Gauge Symmetry

In the previous section, we studied the spontaneous breaking of a  $U(1)$  gauge symmetry. It is necessary to repeat the procedure for an  $SU(2)$  gauge symmetry. This final example will serve as a useful summary of the chapter. It encapsulates all the ideas we have introduced, as well as providing preparation for the discussion of the gauge symmetries of electroweak interactions to be given in Chapter 15.

We take a Lagrangian

$$\mathcal{L} = (\partial_\mu\phi)^\dagger(\partial^\mu\phi) - \mu^2\phi^\dagger\phi - \lambda(\phi^\dagger\phi)^2,\quad (14.59)$$

where  $\phi$  is an  $SU(2)$  doublet of complex scalar fields:

$$\phi = \begin{pmatrix} \phi_\alpha \\ \phi_\beta \end{pmatrix} = \sqrt{\frac{1}{2}} \begin{pmatrix} \phi_1 + i\phi_2 \\ \phi_3 + i\phi_4 \end{pmatrix}.\quad (14.60)$$

$\mathcal{L}$  is manifestly invariant under global  $SU(2)$  phase transformations

$$\phi \rightarrow \phi' = e^{i\alpha_a \sigma_a/2}\phi\quad (14.61)$$

[see (14.30)]. To achieve local, that is,  $\alpha_a(x)$ ,  $SU(2)$  invariance of  $\mathcal{L}$ , we follow the steps of Section 14.4. We replace  $\partial_\mu$  by the covariant derivative

$$D_\mu = \partial_\mu + ig\frac{\tau_a}{2}W_\mu^a, \quad (14.62)$$

and three gauge fields,  $W_\mu^a(x)$  with  $a = 1, 2, 3$ , thereby join the cast. Under an infinitesimal gauge transformation

$$\phi(x) \rightarrow \phi'(x) = (1 + \alpha(x) \cdot \tau/2)\phi(x), \quad (14.63)$$

the three gauge fields transform as

$$\mathbf{W}_\mu \rightarrow \mathbf{W}_\mu - \frac{1}{g}\partial_\mu\alpha - \alpha \times \mathbf{W}_\mu \quad (14.64)$$

[see (14.38)]. The  $\alpha \times \mathbf{W}_\mu$  term occurs because  $\mathbf{W}_\mu$  is an  $SU(2)$  vector; it is “rotated” even if  $\alpha$  is independent of  $x$ . The gauge invariant Lagrangian is then

$$\mathcal{L} = \left( \partial_\mu\phi + ig\frac{1}{2}\tau \cdot \mathbf{W}_\mu\phi \right)^\dagger \left( \partial^\mu\phi + ig\frac{1}{2}\tau \cdot \mathbf{W}^\mu\phi \right) - V(\phi) - \frac{1}{4}\mathbf{W}_{\mu\nu} \cdot \mathbf{W}^{\mu\nu}, \quad (14.65)$$

with

$$V(\phi) = \mu^2\phi^\dagger\phi + \lambda(\phi^\dagger\phi)^2, \quad (14.66)$$

and where we have added the kinetic energy term of the gauge fields with

$$\mathbf{W}_{\mu\nu} = \partial_\mu\mathbf{W}_\nu - \partial_\nu\mathbf{W}_\mu - g\mathbf{W}_\mu \times \mathbf{W}_\nu. \quad (14.67)$$

The last term in (14.67), and in (14.64), arises from the non-Abelian character of the group; that is, it occurs because the  $\tau$ 's do not commute with each other. If  $\mu^2 > 0$ , the Lagrangian (14.65) describes a system of four scalar particles [ $\phi_i$  of (14.60)], each of mass  $\mu$ , interacting with three massless gauge bosons ( $\mathbf{W}_\mu^a$ ).

We are interested in the case  $\mu^2 < 0$  and  $\lambda > 0$ . The potential  $V(\phi)$  of (14.66) then has its minimum at a finite value of  $|\phi|$  where

$$\phi^\dagger\phi \equiv \frac{1}{2}(\phi_1^2 + \phi_2^2 + \phi_3^2 + \phi_4^2) = -\frac{\mu^2}{2\lambda}. \quad (14.68)$$

This manifold of points at which  $V(\phi)$  is minimized is invariant under the  $SU(2)$  transformations. We must expand  $\phi(x)$  about a particular minimum. We can choose, say,

$$\phi_1 = \phi_2 = \phi_4 = 0, \quad \phi_3^2 = -\frac{\mu^2}{\lambda} \equiv v^2. \quad (14.69)$$

The effect is equivalent to the spontaneous breaking of the  $SU(2)$  symmetry. The symmetry, which, for example, was manifest in (14.68), has become hidden.

We now expand  $\phi(x)$  about this particular vacuum:

$$\phi_0 \equiv \sqrt{\frac{1}{2}} \begin{pmatrix} 0 \\ v \end{pmatrix}. \quad (14.70)$$

The result is that, due to gauge invariance, we can simply substitute the expansion

$$\phi(x) = \sqrt{\frac{1}{2}} \begin{pmatrix} 0 \\ v + h(x) \end{pmatrix} \quad (14.71)$$

into the Lagrangian (14.65). That is, of the four scalar fields, the only one that remains is (the Higgs field)  $h(x)$ . At first sight, this may seem surprising. However, the reason is similar to that found for the spontaneously broken  $U(1)$  gauge symmetry of the previous section. The argument is as follows. Proceeding in analogy to (14.57), we parametrize the fluctuations from the vacuum  $\phi_0$  in terms of four real fields  $\theta_1, \theta_2, \theta_3$ , and  $h$ , using the form

$$\phi(x) = e^{i\tau \cdot \theta(x)/v} \begin{pmatrix} 0 \\ \frac{v + h(x)}{\sqrt{2}} \end{pmatrix}. \quad (14.72)$$

To verify that this is perfectly general, we examine small perturbations. We find

$$\begin{aligned} \phi(x) &= \sqrt{\frac{1}{2}} \begin{pmatrix} 1 + i\theta_3/v & i(\theta_1 - i\theta_2)/v \\ i(\theta_1 + i\theta_2)/v & 1 - i\theta_3/v \end{pmatrix} \begin{pmatrix} 0 \\ v + h(x) \end{pmatrix} \\ &\simeq \sqrt{\frac{1}{2}} \begin{pmatrix} \theta_2 + i\theta_1 \\ v + h - i\theta_3 \end{pmatrix}. \end{aligned} \quad (14.73)$$

We see that the four fields are indeed independent and fully parametrize the deviations from the vacuum  $\phi_0$ . Now, the Lagrangian is locally  $SU(2)$  invariant. Therefore, we can gauge the three (massless Goldstone boson) fields  $\theta(x)$  of (14.72). The Lagrangian will then contain no trace of the  $\theta(x)$ . Hence, we arrive at the result of (14.71).

To determine the masses generated for the gauge bosons  $W_\mu^a$ , it is sufficient to substitute  $\phi_0$  of (14.70) into the Lagrangian. The relevant term of (14.65) is

$$\begin{aligned} \left| ig \frac{1}{2} \tau \cdot \mathbf{W}_\mu \phi \right|^2 &= \frac{g^2}{8} \left| \begin{pmatrix} W_\mu^3 & W_\mu^1 - iW_\mu^2 \\ W_\mu^1 + iW_\mu^2 & W_\mu^3 \end{pmatrix} \begin{pmatrix} 0 \\ v \end{pmatrix} \right|^2 \\ &= \frac{g^2 v^2}{8} \left[ (W_\mu^1)^2 + (W_\mu^2)^2 + (W_\mu^3)^2 \right], \end{aligned} \quad (14.74)$$

where here  $| \cdot |^2$  has been used as shorthand for  $(\cdot)^\dagger (\cdot)$ . We compare these terms with a typical mass term of a boson,  $\frac{1}{2} M^2 B_\mu^2$ , and find  $M = \frac{1}{2} gv$ . That is, the Lagrangian describes three massive gauge fields and one massive scalar  $h$ . In summary, the gauge fields have “eaten up” the Goldstone bosons and become massive. The scalar degrees of freedom become the longitudinal polarizations of the massive vector bosons. This is another example of the Higgs mechanism.

**EXERCISE 14.13** Rather than (14.60), take instead  $\phi$  to be an  $SU(2)$  triplet of real scalar fields. For  $\mu^2 < 0$  and  $\lambda > 0$ , show that in this case two gauge bosons acquire mass but that the third remains massless.

**Hint** Verify, and use,  $(T_k)_{ij} = -ie_{ijk}$  for the triplet representation of  $SU(2)$ .

The Higgs mechanism has enabled us to avoid massless particles. However, we need a second “miracle.” Remember that the basic problem is not just to generate masses but to incorporate the mass of the weak bosons while still preserving the renormalizability of the theory. We noted in Section 14.5 that although *a priori* there is nothing to prevent us from brutally breaking the gauge symmetry by inserting explicit gauge mass terms into the Lagrangian, the resulting (unrenormalizable) theory loses all predictive power. In a spontaneously broken gauge theory, the symmetry is, in a sense, still present; it is merely “hidden” by our choice of ground state, and the theory can be shown to remain renormalizable. In a way, this is not so miraculous. It had already been conjectured to be true by Weinberg and Salam. However, the proof is far from simple. It was finally completed in 1971 by ’t Hooft and goes beyond the scope of this book.

For the above reasons, it is widely believed that gauge principles may generate the structure of all particle interactions. The standard model for weak and electromagnetic interactions is constructed from a gauge theory with four gauge fields, the photon and the massive bosons,  $W^\pm$  and  $Z^0$ . We generate the masses of the gauge fields (as well as the fermions) by spontaneous symmetry breaking, ensuring that one of them (the photon) remains massless. We also require that the theory must reproduce the low-energy (low  $q^2$ ) phenomenology of Chapters 12 and 13. Such a theory will be renormalizable and will contain one (or possibly more) Higgs scalars but no Goldstone bosons. This exercise is the subject of the next chapter.

# 15

## The Weinberg–Salam Model and Beyond

Our objective is to obtain a renormalized theory of electroweak interactions incorporating the massive gauge bosons ( $W^\pm, Z^0$ ). This will be achieved by spontaneously breaking a local gauge symmetry. A pertinent example of this technique was described in Section 14.9. But what is the gauge symmetry of electroweak interactions? The data on weak and electromagnetic processes suggest that the interactions are invariant under weak isospin  $SU(2)_L$  and weak hypercharge  $U(1)_Y$  transformations (see Chapter 13). Our first task is therefore to cast the results of Chapter 13 into an  $SU(2) \times U(1)$  invariant Lagrangian.

### 15.1 Electroweak Interactions Revisited

To begin, we recall QED. In Chapter 6, electromagnetic amplitudes ( $-i\mathcal{M}$ ) were calculated using an interaction

$$-iej_\mu^{em}A^\mu = -ie(\bar{\psi}\gamma_\mu Q\psi)A^\mu \quad U(1)_{em}, \quad (15.1)$$

where  $Q$  is the charge operator (with eigenvalue  $-1$  for the electron). Subsequently, we saw in Section 14.3 that precisely this interaction arose from demanding invariance of the Lagrangian for a free fermion,

$$\mathcal{L} = \bar{\psi}(i\gamma^\mu\partial_\mu - m)\psi,$$

under local gauge (or phase) transformations

$$\psi \rightarrow \psi' = e^{ia(x)Q}\psi. \quad (15.2)$$

Indeed, by insisting on local gauge invariance, we were inevitably led to the Lagrangian of QED, (14.28):

$$\mathcal{L} = \underbrace{\bar{\psi}(i\gamma^\mu\partial_\mu - m)\psi}_{\text{Kinetic energy and mass of } \psi} - \underbrace{e\bar{\psi}\gamma^\mu Q\psi A_\mu}_{\text{Interaction}} - \underbrace{\frac{1}{4}F_{\mu\nu}F^{\mu\nu}}_{\substack{\text{Kinetic energy} \\ \text{of } A_\mu}}. \quad (15.3)$$

In Section 14.3, we considered only the electron field and we omitted the charge operator  $Q$ . However, to incorporate all the quark and lepton fields, charge conservation requires the presence of  $Q$  in (15.2), see (15.11). The electromagnetic coupling is therefore proportional to the charge of the appropriate field;  $Q_e = -1$ ,  $Q_u = +\frac{2}{3}$ , and so on.

To include weak processes in the formalism, we must replace (15.1) by two basic interactions; first, an isotriplet of weak currents  $\mathbf{J}_\mu$  coupled to three vector bosons  $\mathbf{W}^\mu$ ,

$$-ig\mathbf{J}_\mu \cdot \mathbf{W}^\mu = -ig\bar{\chi}_L \gamma_\mu \mathbf{T} \cdot \mathbf{W}^\mu \chi_L \quad SU(2)_L, \quad (15.4)$$

and second, a weak hypercharge current coupled to a fourth vector boson  $B^\mu$ ,

$$-\frac{g'}{2} j_\mu^Y B^\mu = -ig\bar{\psi} \gamma_\mu \frac{Y}{2} \psi B^\mu \quad U(1)_Y, \quad (15.5)$$

see (13.17). The operators  $\mathbf{T}$  and  $Y$  are the generators of the  $SU(2)_L$  and  $U(1)_Y$  groups of gauge transformations, respectively. Taken together, the  $SU(2) \times U(1)$  transformations of the left- and right-hand components of  $\psi$  are

$$\begin{aligned} \chi_L &\rightarrow \chi'_L = e^{i\alpha(x) \cdot \mathbf{T} + i\beta(x) Y} \chi_L, \\ \psi_R &\rightarrow \psi'_R = e^{i\beta(x) Y} \psi_R, \end{aligned} \quad (15.6)$$

where the left-handed fermions form isospin doublets  $\chi_L$  and the right-handed fermions are isosinglets  $\psi_R$ . For example, for the electron and its neutrino, we have [see (13.15)]

$$\begin{aligned} \chi_L &= \begin{pmatrix} \nu_e \\ e^- \end{pmatrix}_L \quad \text{with } T = \frac{1}{2}, Y = -1, \\ \psi_R &= e_R^- \quad \text{with } T = 0, Y = -2. \end{aligned} \quad (15.7)$$

But for quarks,

$$\chi_L = \begin{pmatrix} u \\ d \end{pmatrix}_L, \quad \psi_R = u_R \text{ or } d_R.$$

Here, a right-handed up quark has been included since quarks, unlike neutrinos, have a finite mass and hence have both right- and left-handed components.

The electromagnetic interaction (15.1) is embedded in (15.4) and (15.5). Before we continue, it is appropriate to recall how this was achieved. The generators of the three groups satisfy

$$Q = T^3 + \frac{Y}{2},$$

so that

$$j_\mu^{em} = J_\mu^3 + \frac{1}{2} j_\mu^Y,$$

see (13.26). In other words, the electromagnetic current is a combination of the two neutral currents  $J_\mu^3$  and  $j_\mu^Y$  occurring in (15.4) and (15.5). The two physical neutral gauge fields  $A_\mu$  and  $Z_\mu$  are thus orthogonal combinations of the gauge fields  $W_\mu^3$  and  $B_\mu$ , with mixing angle  $\theta_W$ , and the interaction in the neutral current sector can be rewritten in terms of these physical fields as in (13.21):

$$\begin{aligned} -igJ_\mu^3 W^{3\mu} - i\frac{g'}{2}j_\mu^Y B^\mu &= -i \left[ g \sin \theta_W J_\mu^3 + g' \cos \theta_W \frac{j_\mu^Y}{2} \right] A^\mu \\ &\quad - i \left[ g \cos \theta_W J_\mu^3 - g' \sin \theta_W \frac{j_\mu^Y}{2} \right] Z^\mu \\ &= -ie j_\mu^{em} A^\mu - \frac{ie}{\sin \theta_W \cos \theta_W} \left[ J_\mu^3 - \sin^2 \theta_W j_\mu^{em} \right] Z^\mu. \end{aligned} \tag{15.8}$$

The requirement that the electromagnetic interaction, (15.1), must appear on the right-hand side has specified the weak neutral current interaction and fixed the couplings  $g$  and  $g'$  in terms of  $e$  and  $\theta_W$ , namely,

$$e = g \sin \theta_W = g' \cos \theta_W. \tag{15.9}$$

**EXERCISE 15.1** As revision, derive (15.8) and (15.9) from the statements of the above paragraph.

Just as the QED Lagrangian, (15.3), resulted from imposing  $U(1)_{em}$  local gauge invariance, so we are led to the electroweak Lagrangian by requiring an  $SU(2) \times U(1)_Y$  invariant form. For example, for the electron–neutrino lepton pair, we have

$$\begin{aligned} \mathcal{L}_1 &= \bar{\chi}_L \gamma^\mu \left[ i \partial_\mu - g \frac{1}{2} \boldsymbol{\tau} \cdot \mathbf{W}_\mu - g' \left( -\frac{1}{2} \right) B_\mu \right] \chi_L \\ &\quad + \bar{e}_R \gamma^\mu \left[ i \partial_\mu - g' (-1) B_\mu \right] e_R - \frac{1}{4} \mathbf{W}_{\mu\nu} \cdot \mathbf{W}^{\mu\nu} - \frac{1}{4} B_{\mu\nu} B^{\mu\nu}, \end{aligned} \tag{15.10}$$

where we have inserted the hypercharge values  $Y_L = -1$ ,  $Y_R = -2$  of (15.7).  $\mathcal{L}_1$  embodies the weak isospin and hypercharge interactions of (15.4) and (15.5). The final two terms are the kinetic energy and self-coupling of the  $\mathbf{W}_\mu$  fields, see (14.67), and the kinetic energy of the  $B_\mu$  field,  $B_{\mu\nu} \equiv \partial_\mu B_\nu - \partial_\nu B_\mu$ .

Gauge invariance means that the Lagrangian transforms as a singlet under transformations of each gauge group. Take the  $U(1)_{em}$  gauge group as an example. A term in the Lagrangian which is the product of fields  $\phi_1, \phi_2, \dots, \phi_n$  transforms as

$$(\phi_1 \phi_2 \dots \phi_n) \rightarrow e^{i\alpha(x)(Q_1 + Q_2 + \dots + Q_n)} (\phi_1 \phi_2 \dots \phi_n),$$

see (15.2). Gauge invariance requires the Lagrangian to be neutral, that is, to transform as a  $U(1)_{em}$  singlet; therefore,

$$Q_1 + Q_2 + \cdots + Q_n = 0. \quad (15.11)$$

This is charge conservation.

So far, so good. However, note that  $\mathcal{L}_1$  describes massless gauge bosons and massless fermions. Mass terms such as  $\frac{1}{2}M^2B_\mu B^\mu$  and  $-m\bar{\psi}\psi$  are not gauge invariant and so cannot be added. The requirement of a massless gauge boson is familiar (for example, the photon of Section 14.3). The electron mass term

$$\begin{aligned} -m_e\bar{e}e &= -m_e\bar{e}\left[\frac{1}{2}(1-\gamma^5) + \frac{1}{2}(1+\gamma^5)\right]e \\ &= -m_e(\bar{e}_R e_L + \bar{e}_L e_R). \end{aligned} \quad (15.12)$$

Since  $e_L$  is a member of an isospin doublet and  $e_R$  is a singlet, this term manifestly breaks gauge invariance.

To generate the particle masses in a gauge invariant way, we must use the Higgs mechanism. That is, we spontaneously break the gauge symmetry, which has the paramount virtue that the theory remains renormalizable.

## 15.2 Choice of the Higgs Field

We want to formulate the Higgs mechanism so that the  $W^\pm$  and  $Z^0$  become massive and the photon remains massless. To do this, we introduce four real scalar fields  $\phi_i$ . We have to add to  $\mathcal{L}_1$  an  $SU(2) \times U(1)$  gauge invariant Lagrangian for the scalar fields

$$\mathcal{L}_2 = \left| \left( i\partial_\mu - g\mathbf{T} \cdot \mathbf{W}_\mu - g'\frac{Y}{2}B_\mu \right) \phi \right|^2 - V(\phi) \quad (15.13)$$

where  $| \phi |^2 \equiv (\phi)(\phi)^\dagger$ . The structure of  $\mathcal{L}_2$  is explained in Section 14.9, see (14.65). To keep  $\mathcal{L}_2$  gauge invariant, the  $\phi_i$  must belong to  $SU(2) \times U(1)$  multiplets. The most economical choice is to arrange four fields in an isospin doublet with weak hypercharge  $Y = 1$ :

$$\phi = \begin{pmatrix} \phi^+ \\ \phi^0 \end{pmatrix}$$

with

$\phi^+ \equiv (\phi_1 + i\phi_2)/\sqrt{2},$ 
 $\phi^0 \equiv (\phi_3 + i\phi_4)/\sqrt{2}.$

(15.14)

This is in fact the choice originally made in 1967 by Weinberg. It completes the specification of the standard (or minimal) model of electroweak interactions. It is also called the “Weinberg–Salam model.”

To generate gauge boson masses, we use the familiar Higgs potential  $V(\phi)$  of (14.66) with  $\mu^2 < 0$  and  $\lambda > 0$  and choose a vacuum expectation value,  $\phi_0$ , of  $\phi(x)$ . The appropriate choice is (14.70),

$$\phi_0 \equiv \sqrt{\frac{1}{2}} \begin{pmatrix} 0 \\ v \end{pmatrix}. \quad (15.15)$$

Why is an isospin doublet of complex scalar fields, with  $Y = 1$  and vacuum expectation value of  $\phi_0$  of (15.15), suitable for the problem in hand? Any choice of  $\phi_0$  which breaks a symmetry operation will inevitably generate a mass for the corresponding gauge boson. However, if the vacuum  $\phi_0$  is still left invariant by some subgroup of gauge transformations, then the gauge bosons associated with this subgroup will remain massless. Now, the choice  $\phi_0$  with  $T = \frac{1}{2}$ ,  $T^3 = -\frac{1}{2}$ , and  $Y = 1$  breaks both  $SU(2)$  and  $U(1)_Y$  gauge symmetries. But since  $\phi_0$  is neutral, the  $U(1)_{em}$  symmetry with generator

$$Q = T^3 + \frac{Y}{2}$$

remains unbroken. That is,

$$Q\phi_0 = 0, \quad (15.16)$$

so that

$$\phi_0 \rightarrow \phi'_0 = e^{i\alpha(x)Q}\phi_0 = \phi_0$$

for any value of  $\alpha(x)$ . The vacuum is thus invariant under  $U(1)_{em}$  transformations, and the photon remains massless. Out of the four  $SU(2) \times U(1)_Y$  generators  $T$ ,  $Y$ , only the combination  $Q$  obeys relation (15.16). The other three break the symmetry and generate massive gauge bosons. To put it another way, due to the conservation of electric charge, we can only allow neutral scalars to acquire vacuum expectation values; hence, the choice of vacuum (15.15) for the charge assignments of (15.14).

The same Higgs isospin doublet is essential for the generation of fermion masses (see Section 15.4).

### 15.3 Masses of the Gauge Bosons

Just as in Section 14.9, the gauge boson masses are identified by substituting the vacuum expectation value  $\phi_0$  for  $\phi(x)$  in the Lagrangian  $\mathcal{L}_2$ . The relevant term in (15.13) is

$$\begin{aligned} & \left| \left( -ig \frac{\tau}{2} \cdot \mathbf{W}_\mu - i \frac{g'}{2} B_\mu \right) \phi \right|^2 \\ &= \frac{1}{8} \left| \begin{pmatrix} gW_\mu^3 + g'B_\mu & g(W_\mu^1 - iW_\mu^2) \\ g(W_\mu^1 + iW_\mu^2) & -gW_\mu^3 + g'B_\mu \end{pmatrix} \begin{pmatrix} 0 \\ v \end{pmatrix} \right|^2 \\ &= \frac{1}{8} v^2 g^2 \left[ (W_\mu^1)^2 + (W_\mu^2)^2 \right] + \frac{1}{8} v^2 (g'B_\mu - gW_\mu^3)(g'B^\mu - gW^{3\mu}) \\ &= \left( \frac{1}{2} vg \right)^2 W_\mu^+ W^{-\mu} + \frac{1}{8} v^2 (W_\mu^3, B_\mu) \begin{pmatrix} g^2 & -gg' \\ -gg' & g'^2 \end{pmatrix} \begin{pmatrix} W^{3\mu} \\ B^\mu \end{pmatrix}, \end{aligned} \quad (15.17)$$

since  $W^\pm = (W^1 \mp iW^2)/\sqrt{2}$ . Comparing the first term with the mass term expected for a charged boson,  $M_W^2 W^+ W^-$ , we have

$$M_W = \frac{1}{2}vg. \quad (15.18)$$

The remaining term is off-diagonal in the  $W_\mu^3$  and  $B_\mu$  basis:

$$\begin{aligned} \frac{1}{8}v^2 \left[ g^2 (W_\mu^3)^2 - 2gg'W_\mu^3 B^\mu + g'^2 B_\mu^2 \right] &= \frac{1}{8}v^2 \left[ gW_\mu^3 - g'B_\mu \right]^2 \\ &\quad + 0 \left[ g'W_\mu^3 + gB_\mu \right]^2. \end{aligned} \quad (15.19)$$

One of the eigenvalues of the  $2 \times 2$  matrix in (15.17) is zero, and we have included this term in (15.19) with a combination of fields that is orthogonal to the combination given in the first term. Now, the physical fields  $Z_\mu$  and  $A_\mu$  diagonalize the mass matrix so that (15.19) must be identified with

$$\frac{1}{2}M_Z^2 Z_\mu^2 + \frac{1}{2}M_A^2 A_\mu^2,$$

where the  $\frac{1}{2}$  is appropriate for a mass term of a neutral vector boson (see Exercise 14.4). So, on normalizing the fields, we have

$$A_\mu = \frac{g'W_\mu^3 + gB_\mu}{\sqrt{g^2 + g'^2}} \quad \text{with } M_A = 0, \quad (15.20)$$

$$Z_\mu = \frac{gW_\mu^3 - g'B_\mu}{\sqrt{g^2 + g'^2}} \quad \text{with } M_Z = \frac{1}{2}v\sqrt{g^2 + g'^2}. \quad (15.21)$$

We can reexpress these results in the notation introduced in Chapter 13. From either (13.23) or (15.9),

$$\frac{g'}{g} = \tan \theta_W. \quad (15.22)$$

In terms of  $\theta_W$ , (15.20) and (15.21) therefore become

$$\begin{aligned} A_\mu &= \cos \theta_W B_\mu + \sin \theta_W W_\mu^3, \\ Z_\mu &= -\sin \theta_W B_\mu + \cos \theta_W W_\mu^3; \end{aligned} \quad (15.23)$$

and from (15.18) and (15.21), we have

$$\frac{M_W}{M_Z} = \cos \theta_W. \quad (15.24)$$

The inequality  $M_Z \neq M_W$  is due to the mixing between the  $W_\mu^3$  and  $B_\mu$  fields. The mass eigenstates are then automatically a massless photon ( $A_\mu$ ) and a massive  $Z_\mu$ .

field with  $M_Z > M_W$ . In the limit  $\theta_W = 0$ , we see that  $M_Z = M_W$ . The model was constructed with the requirement that the photon be massless, and so the result  $M_A = 0$  is just a consistency check on our calculation and not a prediction. However, the result (15.24) for  $M_W/M_Z$  is a prediction of the standard model (with its Higgs doublet). More complicated choices in the Higgs sector will lead to different mass relations (see Exercise 15.4).

The Weinberg–Salam model with a Higgs doublet therefore fixes the parameter  $\rho$  of (13.36) to be

$$\rho \equiv \frac{M_W^2}{M_Z^2 \cos^2 \theta_W} = 1.$$

Recall that  $\rho$  is the parameter which specifies the relative strength of the neutral and charged current weak interactions and that the data require  $\rho = 1$  to within a small error, see (13.54).

**EXERCISE 15.2** Show that in the Weinberg–Salam model

$$\frac{1}{2v^2} = \frac{g^2}{8M_W^2} = \frac{G}{\sqrt{2}} \quad (15.25)$$

and hence, using the empirical value of  $G$  of Chapter 12, verify that  $v = 246$  GeV. Derive the mass relations

$$M_W = \frac{37.3}{\sin \theta_W} \text{ GeV}, \quad M_Z = \frac{74.6}{\sin 2\theta_W} \text{ GeV} \quad (15.26)$$

and give the lower bounds for their masses. Predict  $M_W$  and  $M_Z$  using the experimental determination of  $\sin^2 \theta_W$ .

Very recently (1983) the W and Z bosons have been discovered at the CERN  $\bar{p}p$  collider via the processes

$$\begin{aligned} \bar{p}p &\rightarrow W^\pm X \rightarrow (e^\pm \nu)X \\ \bar{p}p &\rightarrow ZX \rightarrow (e^+ e^-)X, \end{aligned}$$

where X denotes all the other particles produced in the high-energy head-on collision. By studying the momentum distribution of the emitted decay electrons and positrons, the masses are measured to be

$$M_W = 81 \pm 2 \text{ GeV}$$

$$M_Z = 93 \pm 2 \text{ GeV},$$

which are in impressive agreement with the predictions of the standard electro-weak model.

**EXERCISE 15.3** Suppose that the Higgs scalar field  $\phi(x)$  has weak isospin  $T = 3$  and hypercharge  $Y = -4$ . If the neutral component  $\phi^0$  (with

$T^3 = 2$ ) develops a vacuum expectation value  $v/\sqrt{2}$ , show that

$$\begin{aligned} M_W^2 &= \frac{g^2}{2} \phi^\dagger (T^+ T^- + T^- T^+) \phi \\ &= 4g^2 v^2. \end{aligned} \quad (15.27)$$

Further show that, as it happens,  $M_W/M_Z = \cos \theta_W$ , just as in the standard model. (However, we would still need a Higgs isodoublet to generate the fermion masses, see Section 15.4.)

**EXERCISE 15.4** Suppose that there exist several representations ( $i = 1, \dots, N$ ) of Higgs scalars whose charge-zero members acquire vacuum expectation values  $v_i$ . Show that

$$\rho \equiv \left( \frac{M_W}{M_Z \cos \theta_W} \right)^2 = \frac{\sum v_i^2 [T_i(T_i + 1) - \frac{1}{4} Y_i^2]}{\sum \frac{1}{2} v_i^2 Y_i^2}, \quad (15.28)$$

where  $T_i$  and  $Y_i$  are, respectively, the weak isospin and hypercharge of representation  $i$ . Show that  $\rho = 1$  if only Higgs doublets with  $Y_i = +1$  exist.

**Hint** Use (15.27) and note that the neutral scalars have  $T^3 = -Y/2$ .

**EXERCISE 15.5** The Lagrangian for the scalar field, (15.13), contains trilinear  $hW^+W^-$  and quadrilinear  $hhW^+W^-$  Higgs boson couplings. Use

$$\phi = \sqrt{\frac{1}{2}} \begin{pmatrix} 0 \\ v + h(x) \end{pmatrix} \quad (15.29)$$

[see (14.71)] to show that in the standard model the vertex factors are

$$igM_W \quad \text{and} \quad \frac{1}{4}ig^2, \quad (15.30)$$

respectively. Determine the  $hZZ$  and  $hhZZ$  vertex factors.

## 15.4 Masses of the Fermions

Recall that in the original Lagrangian, (15.10), a fermion mass term  $-m\bar{\psi}\psi$  was excluded by gauge invariance. An attractive feature of the standard model is that the same Higgs doublet which generates  $W^\pm$  and  $Z$  masses is also sufficient to give masses to the leptons and quarks. For example, to generate the electron mass, we include the following  $SU(2) \times U(1)$  gauge invariant term in the

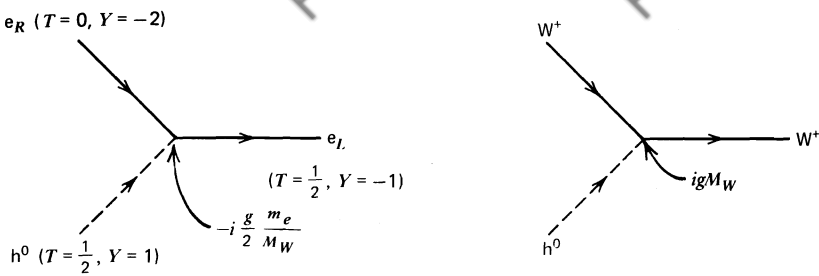


**Fig. 15.1** The Higgs scalar  $h^0$  coupling to the electron and  $W$  boson in the standard model.

Lagrangian:

$$\mathcal{L}_3 = -G_e \left[ (\bar{\nu}_e, \bar{e})_L \begin{pmatrix} \phi^+ \\ \phi^0 \end{pmatrix} e_R + \bar{e}_R (\phi^-, \bar{\phi}^0) \begin{pmatrix} \nu_e \\ e \end{pmatrix}_L \right]. \quad (15.31)$$

The Higgs doublet has exactly the required  $SU(2) \times U(1)$  quantum numbers to couple to  $\bar{e}_L e_R$ , see Fig. 15.1. We spontaneously break the symmetry and substitute

$$\phi = \sqrt{\frac{1}{2}} \begin{pmatrix} 0 \\ v + h(x) \end{pmatrix}$$

into (15.31). The neutral Higgs field  $h(x)$  is the only remnant of the Higgs doublet, (15.14), after the spontaneous symmetry breaking has taken place. The other three fields can be gauged away, see (14.72). On substitution of  $\phi$ , the Lagrangian becomes

$$\mathcal{L}_3 = -\frac{G_e}{\sqrt{2}} v (\bar{e}_L e_R + \bar{e}_R e_L) - \frac{G_e}{\sqrt{2}} (\bar{e}_L e_R + \bar{e}_R e_L) h.$$

We now choose  $G_e$  so that

$$m_e = \frac{G_e v}{\sqrt{2}} \quad (15.32)$$

and hence generate the required electron mass,

$$\mathcal{L}_3 = -m_e \bar{e} e - \frac{m_e}{v} \bar{e} e h, \quad (15.33)$$

using (15.12). Note however that, since  $G_e$  is arbitrary, the actual mass of the electron is not predicted. Besides the mass term, the Lagrangian contains an interaction term coupling the Higgs scalar to the electron. However, since  $v = 246$  GeV, the coupling  $m_e/v$  is very small and so far has not produced a detectable effect in electroweak interactions. The  $he^+e^-$  vertex factor is shown in Fig. 15.1 together with (15.30) for the much stronger  $hW^+W^-$  coupling.

The quark masses are generated in the same way. The only novel feature is that to generate a mass for the upper member of a quark doublet, we must construct a

new Higgs doublet from  $\phi$ :

$$\phi_c = -i\tau_2\phi^* = \begin{pmatrix} -\bar{\phi}^0 \\ \phi^- \end{pmatrix} \xrightarrow{\text{breaking}} \sqrt{\frac{1}{2}} \begin{pmatrix} v + h \\ 0 \end{pmatrix}. \quad (15.34)$$

Due to the special properties of  $SU(2)$ ,  $\phi_c$  transforms identically to  $\phi$ , see (2.41), (but has opposite weak hypercharge to  $\phi$ , namely,  $Y = -1$ ). It can therefore be used to construct a gauge invariant contribution to the Lagrangian,

$$\begin{aligned} \mathcal{L}_4 &= -G_d(\bar{u}, \bar{d})_L \begin{pmatrix} \phi^+ \\ \phi^0 \end{pmatrix} d_R - G_u(\bar{u}, \bar{d})_L \begin{pmatrix} -\bar{\phi}^0 \\ \phi^- \end{pmatrix} u_R + \text{hermitian conjugate} \\ &= -m_d \bar{d}d - m_u \bar{u}u - \frac{m_d}{v} \bar{d}dh - \frac{m_u}{v} \bar{u}uh. \end{aligned} \quad (15.35)$$

Here, we have just considered the  $(u, d)_L$  quark doublet. However, weak interactions operate on  $(u, d')_L, (c, s')_L, \dots$  doublets, where the primed states are linear combinations of the flavor eigenstates, see Sections 12.11 and 12.12. Using the notation of Section 12.12, the quark Lagrangian is therefore of the form

$$\mathcal{L}_4 = -G_d^{ij}(\bar{u}_i, \bar{d}'_i)_L \begin{pmatrix} \phi^+ \\ \phi^0 \end{pmatrix} d_{jR} - G_u^{ij}(\bar{u}_i, \bar{d}'_i)_L \begin{pmatrix} -\bar{\phi}^0 \\ \phi^- \end{pmatrix} u_{jR} + \text{hermitian conjugate}, \quad (15.36)$$

with  $i, j = 1, \dots, N$ , where  $N$  is the number of quark doublets. Proceeding as in Section 12.12, we can rewrite the quark Lagrangian in diagonal form:

$$\mathcal{L}_4 = -m_d^i \bar{d}'_i d_i \left(1 + \frac{h}{v}\right) - m_u^i \bar{u}_i u_i \left(1 + \frac{h}{v}\right). \quad (15.37)$$

Again, the masses depend on the arbitrary couplings  $G_{u,d}$  and cannot be predicted. This has the desirable consequence that the Higgs coupling is flavor conserving and will give no contribution to processes such as  $K_L \rightarrow \mu^+ \mu^-$ .

Notwithstanding the attractive features above, it is fair to say that the Higgs sector is the least satisfactory and least well-determined aspect of electroweak gauge theory. The minimal choice of a single Higgs doublet is sufficient to generate the masses both of the gauge bosons and of the fermions, but the masses of the fermions are just parameters of the theory and are not predicted; their empirical values must be input. However, on the positive side, the Higgs coupling to the fermions is proportional to their masses, a prediction which could be tested when, and if, the Higgs particle is actually observed. A second deficiency is that the mass  $m_h$  of the neutral Higgs meson itself is not predicted either. Using the first two terms of the effective potential,

$$V(\phi) = \mu^2 \phi^\dagger \phi + \lambda (\phi^\dagger \phi)^2 + \dots, \quad (15.38)$$

we find

$$m_h^2 = 2v^2\lambda. \quad (15.39)$$

**EXERCISE 15.6** Derive (15.39), see (14.58).

Since  $v$  is fixed, larger values of  $m_h$  correspond to large  $\lambda$ . For a meaningful perturbation expansion, it turns out that  $m_h$  must be smaller than a few hundred GeV. On the other hand, corrections to (15.38) from loop diagrams will wash out the nontrivial minimum at  $v \neq 0$  if  $m_h$  is too small. Theoretical limits indicate that  $m_h \gtrsim 10$  GeV. Experimental confirmation of the existence of this particle is of course eagerly awaited.

The Higgs is a difficult particle to discover precisely because of its characteristic property of coupling to fermions in proportion to their mass. The most readily experimentally accessible particles are light fermions (electrons and u, d quarks in protons and neutrons), and they couple to the Higgs particle only very weakly. The heavier fermions ( $\tau$ , c, b, t) couple more readily to the Higgs but are difficult to produce themselves.

## 15.5 The Standard Model: The Final Lagrangian

To summarize the standard (Weinberg–Salam) model, we gather together all the ingredients of the Lagrangian. The complete Lagrangian is:

$$\mathcal{L} = -\frac{1}{4}\mathbf{W}_{\mu\nu} \cdot \mathbf{W}^{\mu\nu} - \frac{1}{4}B_{\mu\nu}B^{\mu\nu} + \bar{L}\gamma^\mu \left( i\partial_\mu - g\frac{1}{2}\boldsymbol{\tau} \cdot \mathbf{W}_\mu - g'\frac{Y}{2}B_\mu \right) L + \bar{R}\gamma^\mu \left( i\partial_\mu - g'\frac{Y}{2}B_\mu \right) R + \left| \left( i\partial_\mu - g\frac{1}{2}\boldsymbol{\tau} \cdot \mathbf{W}_\mu - g'\frac{Y}{2}B_\mu \right) \phi \right|^2 - V(\phi) - (G_1 \bar{L}\phi R + G_2 \bar{L}\phi_c R + \text{hermitian conjugate})$$

(15.40)

$\left. \begin{array}{l} \text{W}^\pm, Z, \gamma \text{ kinetic} \\ \text{energies and} \\ \text{self-interactions} \end{array} \right\}$   
 $\left. \begin{array}{l} \text{lepton and quark} \\ \text{kinetic energies} \\ \text{and their} \\ \text{interactions with} \\ \text{W}^\pm, Z, \gamma \end{array} \right\}$   
 $\left. \begin{array}{l} \text{W}^\pm, Z, \gamma, \text{ and Higgs} \\ \text{masses and} \\ \text{couplings} \end{array} \right\}$   
 $\left. \begin{array}{l} \text{lepton and quark} \\ \text{masses and} \\ \text{coupling to Higgs} \end{array} \right\}$

$L$  denotes a left-handed fermion (lepton or quark) doublet, and  $R$  denotes a right-handed fermion singlet.

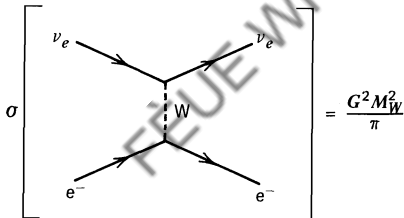
### 15.6 Electroweak Theory is Renormalizable

Future experiments will decide whether the simplest Higgs model is correct. However, remember that the motivation for introducing the Higgs scalar was entirely theoretical, and there is at present no evidence that this particle actually exists. Its importance arises from the fact that it allows us to generate the masses of the weak bosons without spoiling the renormalizability of the electroweak gauge theory, see Section 14.5. The renormalizability of the theory is not trivial. It was eventually demonstrated by 't Hooft some four years after the model was proposed.

The structure of the lowest-order amplitudes for weak processes hints that we may have trouble. Consider the cross section of (12.60),

$$\sigma(\nu_e e \rightarrow \nu_e e) = \frac{G^2 s}{\pi}. \quad (15.41)$$

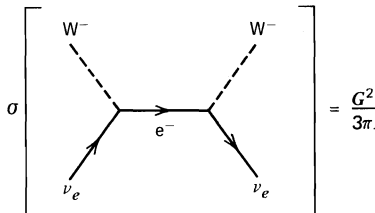
It becomes infinite as  $s \rightarrow \infty$ . A careful discussion, see, for example, Bjorken and Drell (1964) or Pilkuhn (1979), shows that this behavior cannot be reconciled with probability conservation. The introduction of a finite-mass W boson removes the divergence, and for large  $s$  it can be shown that



A Feynman diagram showing the cross section  $\sigma$  for the process  $\nu_e e \rightarrow \nu_e e$ . It consists of two incoming lines: a neutrino  $\nu_e$  from the top-left and an electron  $e^-$  from the bottom-left. They meet at a vertex where a virtual  $W$  boson is exchanged. From this vertex, two outgoing lines emerge: an electron  $e^-$  going up-right and another neutrino  $\nu_e$  going up-left. The entire diagram is enclosed in a large square bracket and equated to the formula  $\frac{G^2 M_W^2}{\pi}$ .

$$\sigma = \frac{G^2 M_W^2}{\pi} \quad (15.42)$$

However, the introduction of the W boson causes its own problems, for now we must consider



A Feynman diagram showing the cross section  $\sigma$  for the process  $\nu_e e \rightarrow \nu_e e$ . It consists of two incoming lines: a neutrino  $\nu_e$  from the bottom-left and an electron  $e^-$  from the bottom-right. They meet at a vertex where a virtual  $W^-$  boson is exchanged. From this vertex, two outgoing lines emerge: an electron  $e^-$  going up-right and another neutrino  $\nu_e$  going up-left. The entire diagram is enclosed in a large square bracket and equated to the formula  $\frac{G^2 s}{3\pi\Lambda}$ .

$$\sigma = \frac{G^2 s}{3\pi\Lambda} \quad (15.43)$$

which similarly diverges at large  $s$ . It is here that we glimpse the beautiful structure of gauge theory.  $\nu_e W^-$  scattering can proceed through a second diagram, Fig. 15.2, and in fact the standard model neutral current couplings are just such that this contribution cancels the divergence of the first diagram. We may be tempted to conclude that we are required to introduce the neutral current! This is

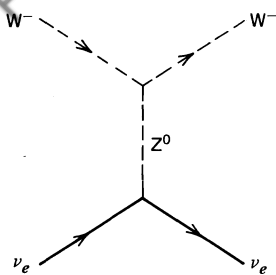
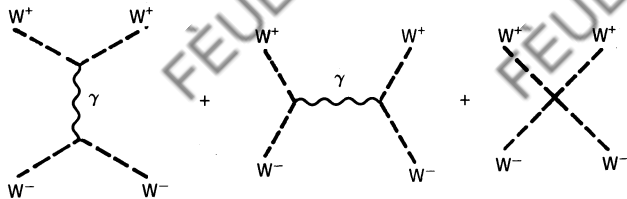


**Fig. 15.2** The neutral current contribution to  $\nu_e W^-$  scattering.

not quite true. We could in principle have introduced a new, heavy electron, thus providing us with a second diagram of the form (15.43) exchanging the new lepton. Then, a cancellation of the divergence between the two diagrams can be arranged. This is reminiscent of the introduction of a second u quark (the c quark) in the GIM mechanism. However, unlike GIM, the heavy-lepton option is not favored by experiment.

The process  $e^- e^+ \rightarrow W^- W^+$  is another example where the self-coupling of gauge bosons ensures a finite answer. The individual diagrams of Fig. 15.3 diverge, but the sum is finite.

As a final example, we consider the scattering of charged W bosons,



Direct computation reveals that the individual diagrams diverge as  $s^2/M_W^4$ , but

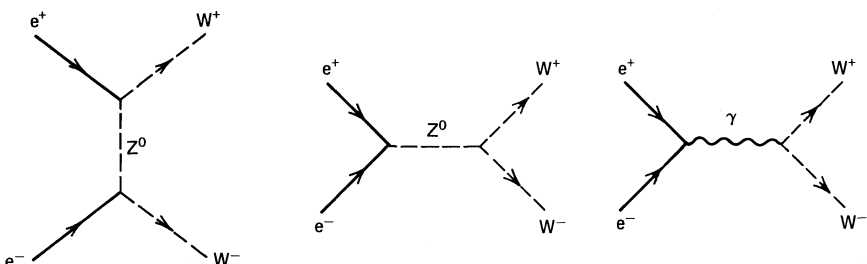
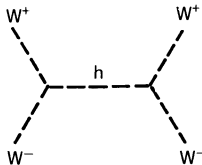


**Fig. 15.3** Three contributions to the process  $e^- e^+ \rightarrow W^- W^+$ .

the divergence of the sum is more gentle:

$$-i\mathcal{M}(W^+ W^- \rightarrow W^+ W^-) \sim \frac{s}{M_W^2} \quad \text{as } s \rightarrow \infty.$$

Even after introducing similar diagrams with  $Z^0$  exchange, the sum of all diagrams still diverges as  $s/M_W^2$ . Heavy leptons cannot help us, so the only solution is to introduce a scalar particle which cancels these residual divergences through diagrams of the type



Here,  $h$  is just the Higgs particle. If we had not previously introduced it to generate the heavy boson masses, we would have been forced to invent it now to guarantee renormalizability. A detailed investigation of this point would reveal that the Higgs couplings are proportional to masses, a result we are also familiar with. Finally, we reiterate that Higgs particles have so far eluded experimental searches. This may be because we have not used the right experimental probes or because they are too heavy to be produced by existing accelerators. Alternatively, one might speculate that they do not exist as elementary fields, and the Higgs “particle” we have introduced actually corresponds to a more complex object, for example, a bound state of other particles which have yet to be incorporated in the theory.

The interested student is encouraged to perform this and previous calculations explicitly; for assistance, see, for example, Llewellyn Smith (1974), Abers and Lee (1973), and Bernstein (1974).

It is clear from the few examples mentioned that the various couplings must be closely related to ensure the “conspiratorial” cancellations of various divergences. Any electroweak theory must therefore meet the dual requirements that (1) it reproduces the phenomenology of Chapters 12 and 13, and (2) it has the correct relation between various couplings to ensure a desirable high-energy behavior. The Weinberg–Salam model (15.40) is the simplest model that achieves these ends.

In fact, 't Hooft has shown that for a theory to be renormalizable, it must be a Yang–Mills theory, that is, a theory with a local gauge invariance. Only if we have such a high degree of symmetry can we obtain the systematic cancellations of divergences order by order.

## 15.7 Grand Unification

The electroweak  $SU(2) \times U(1)$  gauge theory is in impressive agreement with experiment. However, does it really unify the electromagnetic and weak interac-

tions? The  $SU(2) \times U(1)$  gauge group is a product of two disconnected sets of gauge transformations: the  $SU(2)$  group with coupling strength  $g$  and the  $U(1)$  group with strength  $g'$ . Therefore, these two couplings are not related by the theory; and, as we know from Chapter 13, their ratio

$$\frac{g'}{g} = \tan \theta_W \quad (15.44)$$

has to be measured experimentally.

Only if the  $SU(2)$  and  $U(1)$  gauge transformations are embedded into a larger set of transformations  $G$  can  $g$  and  $g'$  be related by the gauge theory. Symbolically, we write

$$G \supset SU(2) \times U(1), \quad (15.45)$$

and some of the new transformations in the group  $G$  will link the previously disconnected  $SU(2)$  and  $U(1)$  subsets of gauge transformations. So,  $g$  and  $g'$  are related by a number (actually a Clebsch–Gordan coefficient of  $G$ ) whose value depends on the choice of “unifying” group  $G$ . In the quest for the “ultimate” theory, it seems natural to attempt to unify strong interactions with the electro-weak  $SU(2) \times U(1)$  interaction. That is, we seek a group  $G$  that also contains the color gauge group  $SU(3)$  which successfully describes the strong interactions. Let us speculate that such a “grand unified group”  $G$  exists. Then (15.45) would be generalized to some grand unified group

$$G \supset SU(3) \times SU(2) \times U(1), \quad (15.46)$$

and gauge transformations in  $G$  also relate the electroweak couplings  $g, g'$  to the color coupling  $\alpha_s$ . All the interactions would then be described by a grand unified gauge theory (GUT) with a single coupling  $g_G$  to which all couplings are related in a specific way once the gauge group  $G$  has been found.

This unification is pictured in Fig. 15.4, where we have denoted the couplings associated with the  $SU(3)$ ,  $SU(2)$ , and  $U(1)$  subgroups by  $g_i(Q)$  with  $i = 3, 2, 1$ , respectively. The figure recalls the fact that the gauge couplings depend on the characteristic momentum  $Q$  (or distance  $1/Q$ ) of the interactions. The couplings  $g_2(Q)$  and  $g_3(Q)$  of the non-Abelian groups are asymptotically free, whereas the Abelian coupling  $g_1(Q)$  increases with increasing momentum  $Q$  similar to the conventional charge screening of electromagnetism. The figure suggests that for some large-momentum (or short-distance) scale  $Q = M_X$ , the three couplings merge into a single grand unified coupling  $g_G$ ; that is, for  $Q \geq M_X$ ,

$$g_i(Q) = g_G(Q), \quad (15.47)$$

and the group  $G$  describes a unified interaction with coupling  $g_G(Q)$ . When  $Q$  is decreased below  $M_X$ , the couplings  $g_i(Q)$  separate and eventually give the phenomenological couplings  $g, g'$ , and  $\alpha_s$ , which describe the interactions observed in the present-day experiments for which  $Q \approx \mu \approx 10$  GeV or thereabouts.

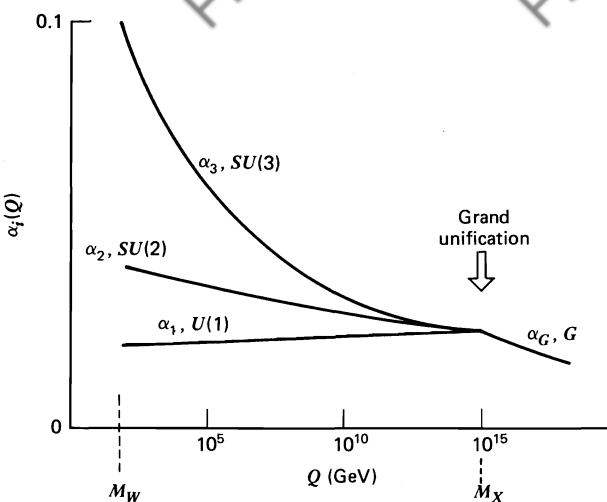


**Fig. 15.4** The variation of  $\alpha_i \equiv g_i^2/4\pi$  with  $Q$ , showing the speculative grand unification of strong [ $SU(3)_{\text{color}}$ ] and electroweak [ $SU(2)_L \times U(1)_Y$ ] interactions at very short distances  $1/Q \approx 1/M_X$ .

With the conventional choice of couplings, we have

$$\begin{aligned} \alpha_s(Q) &= \frac{g_3^2(Q)}{4\pi}, \\ g(Q) &= g_2(Q), \\ g'(Q) &= \frac{1}{C}g_1(Q), \end{aligned} \tag{15.48}$$

where the constant  $C$  is a Clebsch–Gordan coefficient of  $G$ . Equation (15.44) becomes, in terms of  $g_1$  and  $g_2$ ,

$$\frac{1}{C} \frac{g_1(Q)}{g_2(Q)} = \tan \theta_W(Q). \tag{15.49}$$

So, for  $Q \gtrsim M_X$ , where  $g_1 = g_2$ ,  $C$  determines the Weinberg angle  $\theta_W$ .

Assuming that there exists a group  $G$ , we can use the phenomenological values of the couplings at  $Q = \mu$  to estimate the unification mass  $M_X$ . This can be done because the  $Q$  dependence of the couplings  $g_i(Q)$  is prescribed by the gauge theory, see Chapter 7. For instance, the  $Q$  dependence of  $\alpha_s$  is given by (7.63). We use (15.48) to replace  $\alpha_s$  by  $g_3$ , and after simple rearrangement, (7.63) becomes

$$\frac{1}{g_3^2(\mu)} = \frac{1}{g_3^2(Q)} + 2b_3 \log \frac{Q}{\mu}, \tag{15.50}$$

with

$$b_3 = \frac{1}{(4\pi)^2} \left( \frac{2}{3} n_f - 11 \right), \quad (15.51)$$

where  $n_f$  is the number of quark flavors. For  $Q = M_X$ , we have  $g_3 = g_G$ ; and so (15.50) gives

$$\boxed{\frac{1}{g_i^2(\mu)} = \frac{1}{g_G^2} + 2b_i \log \frac{M_X}{\mu}}, \quad (15.52)$$

with  $i = 3$ .

This equation applies equally well to the  $SU(2)$  and  $U(1)$  couplings, see (15.47). The different routes, pictured in Fig. 15.4, by which the three couplings  $g_i(Q)$  reach  $g_G$  are due to the different  $b_i$  coefficients in (15.52). We have

$$b_1 = \frac{1}{(4\pi)^2} \left( \frac{4}{3} n_g \right), \quad (15.53a)$$

$$b_2 = \frac{1}{(4\pi)^2} \left( -\frac{22}{3} \right) + b_1, \quad (15.53b)$$

$$b_3 = \frac{1}{(4\pi)^2} (-11) + b_1, \quad (15.53c)$$

where  $n_g$  is the number of families (or generations) of fermions, that is,  $N$  of (12.118). Here,  $b_3$  is just (15.51). In fact, for  $SU(N)$ ,

$$b_N = \frac{1}{(4\pi)^2} \left[ -\frac{11}{3} N + \frac{4}{3} n_g \right], \quad (15.54)$$

where the two terms correspond to the gauge boson and fermion loops, respectively, see (7.58). For further discussion and references, see Langacker (1981).

Given the  $Q$  dependence of the couplings, it is straightforward to estimate  $M_X$ . We eliminate  $n_g$  and  $g_G$  from the three equations (15.52) with  $i = 1, 2, 3$ . Using (15.53), we form the particular linear combination

$$\frac{C^2}{g_1^2} + \frac{1}{g_2^2} - \frac{(1 + C^2)}{g_3^2} = 2[C^2 b_1 + b_2 - (1 + C^2) b_3] \log \frac{M_X}{\mu}, \quad (15.55)$$

where  $g_i^2 = g_i^2(\mu)$ . The left-hand side has been chosen so that it can be expressed in terms of  $e^2$  and  $g_3^2$ , or equivalently  $\alpha$  and  $\alpha_s$ . Indeed,

$$\frac{C^2}{g_1^2} + \frac{1}{g_2^2} = \frac{1}{g'^2} + \frac{1}{g^2} = \frac{1}{e^2}, \quad (15.56)$$

using (15.48) and (13.23). Inserting the explicit expressions for the  $b_i$  coefficients,

(15.53), into (15.55), we therefore have

$$\begin{aligned}\log \frac{M_X}{\mu} &= \frac{3(4\pi)^2}{22(1+3C^2)} \left[ \frac{1}{e^2} - (1+C^2) \frac{1}{g_3^2} \right] \\ &= \frac{6\pi}{11(1+3C^2)} \left( \frac{1}{\alpha} - \frac{1+C^2}{\alpha_s} \right).\end{aligned}\quad (15.57)$$

For  $\mu \approx 10$  GeV, we know that  $\alpha \approx \frac{1}{137}$  and  $\alpha_s \approx 0.1$ , and we take  $C^2 = \frac{5}{3}$  for reasons that will become apparent in the next section. So,

$$M_X \approx 5 \times 10^{14} \text{ GeV}. \quad (15.58)$$

Strictly speaking, we should use  $\mu \sim M_W$ , but the couplings are slowly varying and the order-of-magnitude estimates are not particularly sensitive to the “ordinary” mass chosen for  $\mu$ , nor to the precise value of the Clebsch–Gordan coefficient  $C$ . The dependence of  $M_X$  on the value of  $\alpha_s$  is shown in Table 15.1.

The unification scale  $M_X$  is very large. Can we still neglect the gravitational interaction? Recall that the gravitational force between two particles ( $Gm_1 m_2 / r^2$ ) can be significant if the separation  $r$  becomes sufficiently small. Here,  $G$  is the gravitational constant. Gravitational effects become of order unity when the masses ( $m_1 \approx m_2 \approx M$ ) are such that the potential is comparable to the rest mass energy

$$\frac{GM^2/r}{Mc^2} \approx 1.$$

For masses separated by a natural unit of length,  $r = \hbar/Mc$  [see (1.3)], this happens when

$$Mc^2 = \left( \frac{\hbar c^5}{G} \right)^{1/2} = 1.22 \times 10^{19} \text{ GeV}.$$

This value of  $M$  is known as the Planck mass, and it is the only dimensional quantity appearing in gravity. Comparing its value with (15.58), we see that it may still be a good approximation to neglect gravity, but it is intriguing that we are now contemplating mass scales so close to the Planck mass. For completeness,

**TABLE 15.1**

Values for  $M_X$ ,  $\sin^2 \theta_W$ , and the Proton Lifetime  $\tau_p$  Evaluated from the “Order-of-Magnitude” Estimates (15.57), (15.60), and (15.66) Following Georgi, Quinn, and Weinberg

$\alpha_s$	$M_X$ (GeV)	$\sin^2 \theta_W$	$\tau_p$ (years)
0.1	$5 \times 10^{14}$	0.21	$\sim 10^{27}$
0.2	$2 \times 10^{16}$	0.19	$\sim 10^{34}$

we have included  $\hbar$  and  $c$  in the above discussion. From now on, we revert back to natural units with  $\hbar = c = 1$ .

The Weinberg angle  $\theta_W$  is determined in a grand unified theory, and so we can compare the value with experiment. Indeed, from (15.49), we have

$$\sin^2 \theta_W = \frac{g_1^2(Q)}{g_1^2(Q) + C^2 g_2^2(Q)}. \quad (15.59)$$

Thus, if we take  $C^2 = \frac{5}{3}$ , we have  $\sin^2 \theta_W = \frac{3}{8}$  at  $Q = M_X$ , where  $g_1 = g_2$ . However, at  $Q \approx \mu$ , the value will be different because of the separation of  $g_1$  and  $g_2$  as  $Q$  decreases from  $M_X$  (see Fig. 15.4).

**EXERCISE 15.7** Show that

$$\sin^2 \theta_W = \frac{1}{1 + 3C^2} \left( 1 + 2C^2 \frac{\alpha}{\alpha_s} \right). \quad (15.60)$$

**Hint** By forming the combination  $C^2(1/g_1^2 - 1/g_2^2)$ , verify that

$$2C^2(b_1 - b_2) \log \frac{M_X}{\mu} = \frac{1}{e^2} (1 - (1 + C^2) \sin^2 \theta_W).$$

Then, use (15.54) and (15.53).

From (15.60), we can calculate  $\sin^2 \theta_W$  at  $Q \approx 10$  GeV, using  $C^2 = \frac{5}{3}$  as before. The results are entered in Table 15.1. We see that  $\sin^2 \theta_W \approx 0.2$ . This is close to the experimental value discussed in Chapter 13.

## 15.8 Can the Proton Decay?

In Section 15.7, we speculated that a grand unified group  $G$  exists such that

$$G \supset SU(3) \times SU(2) \times U(1).$$

Georgi and Glashow have shown that the smallest such group of gauge transformations is the group  $SU(5)$ . Of course, different GUT's with larger groups than  $SU(5)$  can be constructed.

Once a group is chosen for investigation, we have to assign the quarks and leptons to multiplets (i.e., irreducible representations) of the group. In the earlier chapters, we presented empirical evidence for distinct families (or generations) of fermions,  $(u, d; \nu_e, e)$ ,  $(c, s; \nu_\mu, \mu), \dots$ , where in the first family, for instance, we have

$$\begin{aligned} \begin{pmatrix} u \\ d \end{pmatrix}_L, u_R, d_R \Biggr) &\quad \text{each with three colors,} \\ \begin{pmatrix} \nu_e \\ e^- \end{pmatrix}_L, e_R^- , \end{aligned} \quad (15.61)$$

together with their antiparticles. This grouping ensures that we can construct

gauge theories free of anomalies, see Section 12.12. In a family, there are thus 15 left-handed states, for example, those in (15.61) together with  $\bar{u}_L$ ,  $\bar{d}_L$ , and  $e_L^+$ . For the  $SU(5)$  model, these can be accommodated in a fundamental  $\bar{5}$ - and a 10-representation (the 10 is the antisymmetric part of the product of two fundamental 5-representations, compare (2.58)). Explicitly, we have for the left-handed states,

$$\bar{5} = (1, 2) + (\bar{3}, 1) = (v_e, e^-)_L + \bar{d}_L, \quad (15.62)$$

$$10 = (1, 1) + (\bar{3}, 1) + (3, 2) = e_L^+ + \bar{u}_L + (u, d)_L, \quad (15.63)$$

where we have shown the  $(SU(3)_{\text{color}}, SU(2)_L)$  decomposition of the multiplets.

What are the gauge bosons of  $SU(5)$ ? An  $SU(N)$  gauge theory has  $N^2 - 1$  gauge bosons. For the  $SU(5)$  model, these are

$$24 = (8, 1) + \underbrace{(1, 3) + (1, 1)}_{\text{gluons}} + \underbrace{(3, 2) + (\bar{3}, 2)}_{W^\pm, Z, \gamma} + \underbrace{X, Y}_{\text{bosons}} \quad (15.64)$$

So, we have a new pair of superheavy gauge bosons, X and Y. They form a weak doublet and are colored. They mediate interactions which turn quarks into leptons:

$$(u, d)_L \rightarrow e_L^+ + (\bar{Y}, \bar{X}), \quad (15.65)$$

or, in  $SU(5)$  parlance,

$$(3, 2) \rightarrow (1, 1) \otimes (3, 2).$$

Is the appearance of such transitions really surprising? First, recall that at energies above  $M_W$ , the distinction between weak and electromagnetic interactions disappears. Similarly, at the GUT-scale  $M_{X,Y}$ , which we identify with (15.58), the strong color force merges with the electroweak force, and the sharp separation of particles into colored quarks and colorless leptons, which interact only through the electroweak force, disappears. This leads to lepton/baryon number-violating interactions such as (15.65).

**EXERCISE 15.8** What are the charges of the superheavy bosons X and Y?

**EXERCISE 15.9** Comment on the behavior of  $g_G(Q)$  for  $Q > M_X$ , see Fig. 15.4.

Can we ever hope to build accelerators to observe, via (15.65), the production of X particles weighing about  $10^{-10}$  grams [see (15.58)]? This is most unlikely. However, low- $Q$  effects associated with the weak gauge bosons ( $W^\pm, Z$ ) were revealed long before accelerator technology achieved interactions with  $Q \simeq M_W$ . An example is  $\mu$ -decay. The slow decay of the muon is a direct result of the large

**TABLE 15.2**Low- $Q^2$  Phenomena Associated with the Scales  $Q^2 = M_W^2$  and  $Q^2 = M_X^2$ 

Muon Decay ( $\mu^- \rightarrow e^- \bar{\nu}_e \nu_\mu$ ) at $Q^2 \ll M_W^2$	Proton Decay ( $p \rightarrow \pi^0 e^+$ ) at $Q^2 \ll M_X^2$

$$\frac{G}{\sqrt{2}} = \frac{g^2}{8M_W^2} \quad (12.15)$$

$$\begin{aligned} \Gamma(\mu \rightarrow e \bar{\nu}_e \nu_\mu) &= \dots G^2 m_\mu^5 & (12.42) \\ &= \dots \frac{m_\mu^5}{M_W^4} \end{aligned}$$

$$\frac{G_G}{\sqrt{2}} = \frac{g_G^2}{8M_X^2}$$

$$\begin{aligned} \Gamma(p \rightarrow \pi e) &= \dots G_G^2 m_p^5 \\ &= \dots \frac{m_p^5}{M_X^4} \end{aligned}$$

mass of the  $W$ . This argument, presented in detail in Chapter 12, is sketched again in Table 15.2. Using this analogy, we can infer low- $Q$  manifestations of interactions with scale  $M_X$ . Such interactions will result in the (very) slow decay of the proton, see Table 15.2. The decay rate can be estimated in just the same way as the  $\mu$ -decay rate. In the table, we find a proton lifetime of

$$\tau_p \simeq \frac{M_X^4}{m_p^5}, \quad (15.66)$$

and so its numerical value is very sensitive to the precise value of  $M_X$  (see Table 15.1). The estimated lifetime is in the vicinity of the present experimental limits, which are of order  $10^{30}$  years. An accurate prediction of the lifetime requires calculations which are much more sophisticated than the order-of-magnitude estimates for  $M_X$  and  $\tau_p$  presented above; see, for example, Langacker (1981). Such calculations give some hope that the  $SU(5)$  GUT could be tested by experiments that detect the decay of the proton. In the meantime, the value of  $\sin^2 \theta_W \simeq 0.2$  computed from (15.60) with  $C^2 = \frac{5}{3}$  (the  $SU(5)$  value of the

Clebsch–Gordan coefficient relating  $g$  and  $g'$ ) is the main empirical evidence for this “great house of cards.”

The GUT approach, however, offers a framework that permits the scientific pursuit of problems and goals that were until recently only idle dreams. Note for example the implications of  $SU(5)$  for the electric charge of quarks and leptons. Since the photon is one of the gauge bosons of  $SU(5)$ , the charge operator  $Q$  is a generator of the group. But for a simple group, such as  $SU(5)$ , the trace of each generator vanishes for any representation. For example, for the  $\bar{5}$  representation, (51.62), we have

$$\text{Tr } Q = 3Q_{\bar{d}} + Q_{\nu} + Q_{e^-} = 0,$$

which implies that

$$Q_{\bar{d}} = \frac{1}{3}Q_{e^-}.$$

This is an amazing result. Clearly, it implies that charges are quantized. A similar calculation for the  $10$  representation, (15.63), yields

$$Q_u = -2Q_{\bar{d}},$$

and the combined result resolves the mystery (Chapter 7) of why  $Q_p = -Q_e$ . Moreover, classifications like (15.62) and (15.63) also imply that the helicity structures of the weak interactions of quarks and leptons are very similar, an experimental fact that we repeatedly emphasized.

Clearly, proton decay would have profound implications, but one could argue that it would not be all that surprising. The conservation of charge is connected with the existence of a massless photon, but no massless particles are associated with the conservation of baryon number. Indeed, its nonconservation may already be apparent in the universe surrounding us. We discuss this next.

## 15.9 The Early Universe as a High-Energy Physics Experiment

Whereas the highest energies achieved with accelerators do not exceed  $10^5$  GeV, energies of  $10^{19}$  GeV may have been commonplace at the very early times after the Big Bang. If we extrapolate our expanding universe backward in time toward the initial singularity in our past associated with the Big Bang, the matter and radiation get hotter, and eventually the average particle collision energies significantly exceed those which can be achieved in accelerator laboratories.

A speculative chronology of past events is shown in Table 15.3. A famous “tell-tale” event occurred when the universe was  $10^6$  years old. Then, energies had cooled to a fraction of an eV and photons were no longer sufficiently energetic to excite atoms. The photon radiation decoupled from matter and is still with us today in the form of the isotropic background radiation. Since decoupling, it has cooled from  $10^3$  K to 3 K through the expansion of the universe, see Table 15.3. The detection of this 3 K (microwave) background radiation in 1965 by Penzias and Wilson was crucial evidence for the expanding (or Big Bang) model of the universe.

**TABLE 15.3**  
A Summary of Past Events in Standard Big Bang Cosmology

Past Events	Time	Temperature $T$ (degrees Kelvin)	Energy $kT$ (GeV)
Quantum gravity effects are large	$10^{-45}$ sec	$10^{32}$	$10^{19}$
Matter–antimatter asymmetry through X-boson interactions	$10^{-35}$ sec	$10^{27}$	$10^{14}$
Helium abundance established	$10^3$ sec	$10^9$	$10^{-4}$
$\gamma$ 's decouple from matter, origin of photon background	$10^6$ years	$10^3$	$10^{-10}$
NOW!	$10^{10}$ years	3	$10^{-12}$

Making a bold extrapolation back past primordial “nucleosynthesis” at  $10^3$  sec, when such nuclei as helium and deuterium are believed to have been formed, all the way to  $10^{-35}$  sec, we reach a phase of the universe where matter exists in the form of quarks and leptons in thermal equilibrium with the gauge bosons of (15.64). The thermal energies are of order of the GUT-scale  $M_X$ . But when the universe cools below this temperature, the superheavy X and  $\bar{X}$  particles decay; and if C and CP are violated, their partial decay rates may differ,

$$\frac{\Gamma(X \rightarrow q + q)}{\Gamma(X \rightarrow \text{all})} \neq \frac{\Gamma(\bar{X} \rightarrow \bar{q} + \bar{q})}{\Gamma(\bar{X} \rightarrow \text{all})}.$$

Thus, although we have equal densities of X and  $\bar{X}$  before  $10^{-35}$  sec, we could emerge from this equilibrium period with unequal numbers of q and  $\bar{q}$  quarks. It is difficult to make quantitative predictions of the baryon asymmetry as the most important CP-violating processes involve the interaction and decay of the Higgs particles. Nevertheless, a GUT has the necessary ingredients so that we could emerge from the GUT era in Table 15.3 with a small net excess of matter over antimatter. The excess would survive subsequent matter–antimatter annihilation into photons, producing the observed ratio of baryons to photons:

$$\frac{N_B}{N_\gamma} \simeq \frac{N_B - N_{\bar{B}}^-}{N_B + N_{\bar{B}}^-} \simeq 10^{-9}.$$

The fact that our universe is made up of matter may therefore be accounted for by the same physical processes that are responsible for the eventual death of the proton. Though this explanation of the origin of matter in our present universe is still very speculative, it provides us with a good example of the inevitable symbiosis of astrophysics and the particle physics discussed in this book [see, e.g., Ellis in Mulvey (1981) or Ellis (1982)].

### 15.10 “Grander” Unification?

Although crucial tests remain to be done, it is widely believed that all matter is composed of spin- $\frac{1}{2}$  particles (quarks and leptons) whose interactions are a consequence of exact local gauge symmetries. The gauge bosons mediating these color and electroweak interactions have spin 1 (the photon, the gluons, and the weak bosons  $W^\pm, Z$ ). Through spontaneous symmetry breaking, the weak bosons and the fermions acquire a mass, and the theory remains renormalizable. In this book, we have attempted to describe the details of this picture.

On the other hand, the concept of a grand unified theory is much more speculative. Even if you are willing to accept the underlying assumption that there is a “desert” with no new physics between  $Q = M_W$  and  $Q = M_X$ , it brings many unanswered questions to the forefront. Why are the mass scales  $M_W$  and  $M_X$  separated by the enormous factor  $10^{12}$ ? What about gravity? Is there a principle which relates matter fields to gauge fields so they can be unified, too?

These questions take us well beyond the frontiers of our knowledge of the world of quarks and leptons. But we shall conclude with a brief mention of just two speculations regarding the possible structure of a more “ultimate” theory. One approach is to directly link matter and gauge fields. Such a symmetry is necessarily very different from any symmetry previously encountered since it links spin- $\frac{1}{2}$  Dirac matter fields with spin-1 boson gauge fields. A symmetry directly associating fields of integer and half-integer spin has been constructed mathematically and is called “supersymmetry” [see, e.g., Salam in Mulvey (1981)]. Such a symmetry can also encompass the spin-2 fields of Einstein gravity, the gravitons which mediate the interactions of masses.

This approach starts with GUT’s and attempts to “tack on” gravity. A second idea follows the reverse approach. We could start with gravity, a force that is “well understood” classically as a result of the geometrical curvature of four-dimensional space-time, and ask the question, “What is the geometry associated with electromagnetism, color...?” Two answers are possible. One postulates that gravity is connected with the “gross” geometrical structure of space-time but that, at a much smaller scale, more complex topologies exist with which other interactions are associated. The alternative possibility is to introduce more space-time dimensions. This has been vigorously investigated since Kaluza and Klein suggested in the early twenties that electromagnetism may be a geometrical theory with a fifth dimension.

The most important achievement of the last two decades is not just to have established that our world is made of quarks, leptons, and gauge bosons, but to have brought us toward a new frontier where even more exciting questions can be raised. These speculations do inevitably include the possibility that quarks and leptons are themselves composite.

# ANSWERS AND COMMENTS ON THE EXERCISES

## CHAPTER 1

**1.1**  $\hbar c = 0.1973 \text{ GeV}$   $F = 1$  and  $1 \text{ mb} = 0.1 F^2$ .

**1.3** Typical atomic energies and dimensions are, respectively, factors of  $\alpha^2$  and  $1/\alpha$  different from natural units of energy and length, and  $v/c \sim \alpha$  (with  $\alpha \approx \frac{1}{137}$ ). An illuminating discussion is given by Wichmann in *Quantum Physics* (Berkeley Physics Course Vol. 4, 1967).

## CHAPTER 2

**2.1** (i) States (2.1) are defined with respect to a given  $z$  axis. Now take an NN state  $\uparrow\uparrow$  quantized along a different axis, say,  $z'$ . We can write this state as a linear combination of the original  $S = 1$  states

$$|S = 1, M_S = 1\rangle' = \sum_{M_S} \alpha(M_S) |S = 1, M_S\rangle.$$

But the states  $|M_S = 1\rangle'$  and  $|M_S = \pm 1\rangle$  are manifestly symmetric and so  $|S = 1, M_S = 0\rangle'$  must also be symmetric. Orthogonality then demands  $|S = 0, M_S = 0\rangle$  to be antisymmetric.

(ii) Applying the step-down operator to  $|S = 1, M_S = 1\rangle = \uparrow\uparrow$ , we obtain [see  $J_-$  of (2.18)]

$$\sqrt{2} |S = 1, M_S = 0\rangle = \uparrow\downarrow + \downarrow\uparrow.$$

**2.2**  $\psi = \psi_{\text{space}} \psi_{\text{spin}} \psi_{\text{isospin}}$ , where for  $L = 0$ ,  $\psi_{\text{space}}$  is symmetric under interchange of the two nucleons, whereas

$$\psi_{\text{spin}}(1, 2) = (-1)^{S+1} \psi_{\text{spin}}(2, 1)$$

$$\psi_{\text{isospin}}(1, 2) = (-1)^{I+1} \psi_{\text{isospin}}(2, 1),$$

see (2.1) and (2.2), respectively. For the overall  $\psi$  to be antisymmetric,  $S + I$  must therefore be an odd integer.

**2.3**  $\text{pp} = |I = 1, I_3 = 1\rangle$  and  $\text{np} = \sqrt{\frac{1}{2}}(|I = 1, I_3 = 0\rangle - |I = 0, I_3 = 0\rangle)$ . Since the  $\pi d$  states are pure  $I = 1$ , the  $\text{np} \rightarrow \pi^0 d$  reaction can only proceed with probability  $(\sqrt{\frac{1}{2}})^2$  that of  $\text{pp} \rightarrow \pi^+ d$ .

### 356 Answers and Comments on the Exercises

- 2.4** See, for example, Feynman (1961) or Rose (1957).
- 2.6**  $j = \frac{1}{2}$  elements follow from (2.26). See Rose (1957).
- 2.7** Expand and use  $(\sigma_2)^2 = 1$ ,  $(\sigma_2)^3 = \sigma_2$ , and so on.
- 2.8** The  $3 \times 3$  matrices  $\lambda_1, \lambda_2, \lambda_3$  are the  $2 \times 2$  Pauli matrices supplemented by a third row and column constructed from zeros. Similarly,  $\lambda_4, \lambda_5$  have zeros in the second row and column such that when these are removed, the remaining elements are those of  $\sigma_1, \sigma_2$ . The normalization of the  $\lambda_i$  is thus taken to be that of the  $\sigma_i$ ,

$$\text{Tr}(\lambda_i \lambda_j) = 2\delta_{ij}.$$

Examples of  $\lambda_i$  are

$$\lambda_4 = \begin{pmatrix} 0 & 0 & 1 \\ 0 & 0 & 0 \\ 1 & 0 & 0 \end{pmatrix}, \quad \lambda_7 = \begin{pmatrix} 0 & 0 & 0 \\ 0 & 0 & -i \\ 0 & i & 0 \end{pmatrix}.$$

- 2.9** The main decay modes are  $\phi \rightarrow K^+ K^-$  and  $\phi \rightarrow K^0 \bar{K}^0$ , which in the limit of exact symmetry would occur equally. However, the energy release is so small that the equality is broken by the mass difference of the  $K^+$  and  $K^0$ . We have

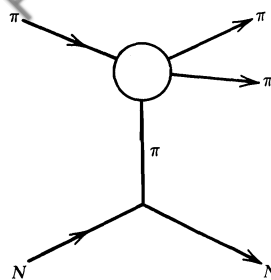
$$\frac{\Gamma(\phi \rightarrow K^+ K^-)}{\Gamma(\phi \rightarrow K^0 \bar{K}^0)} \approx \left( \frac{p_{K^+}}{p_{K^0}} \right)^{2L+1}$$

where  $p_i \equiv |\mathbf{p}_i|$  are the kaon momenta in the rest frame of the  $\phi$ , and  $L$  is the orbital angular momentum of the  $K\bar{K}$  system;  $\phi$  and  $K$  have spin 1 and 0, respectively, and so  $L = 1$ . The observed branching ratios are

$$K^+ K^- : K^0 \bar{K}^0 : \pi^+ \pi^- \pi^0 = 0.49 : 0.35 : 0.15.$$

The smallness of the  $3\pi$  mode, despite being kinematically favored, supports the  $\phi \simeq s\bar{s}$  identification. The  $K^0 \bar{K}^0$  mode is seen as  $K_L^0 K_S^0$ , since  $\phi$  has  $J^P = 1^-$  and  $C = -1$ , see eq. (12.129). The  $\phi \rightarrow K\bar{K}$  decay rate can be estimated from the  $SU(3)$ -related  $\rho \rightarrow \pi\pi$  decay. The kinematic suppression of  $\phi \rightarrow K\bar{K}$  is apparent in the comparison of the observed widths  $\Gamma(\phi) = 4$  MeV,  $\Gamma(\rho) = 150$  MeV.

- 2.10** The production of the  $(\pi\pi)$ -system at small momentum transfer is dominated by  $\pi$ -exchange. The exchange (virtual) pion is almost real (i.e., on its mass shell), and so this experimentally accessible process is an excellent way of studying  $\pi^+\pi^- \rightarrow \pi\pi$  scattering (see Fig. 4.8). Pions obey Bose statistics and a symmetric  $\pi\pi$ -wavefunction requires  $(-1)^J (-1)^I = +1$ .



**2.12** In addition to (2.63), we have

$$\Sigma(M_S) = \sqrt{\frac{1}{12}} ((sd + ds)u + (su + us)d - 2(du + ud)s)$$

$$\Sigma(M_A) = \frac{1}{2} ((sd - ds)u + (su - us)d)$$

$$\Lambda(M_S) = \frac{1}{2} ((sd + ds)u - (su + us)d)$$

$$\Lambda(M_A) = \sqrt{\frac{1}{12}} ((sd - ds)u + (us - su)d - 2(du - ud)s)$$

$$\Sigma(S) = \sqrt{\frac{1}{6}} ((sd + ds)u + (su + us)d + (du + ud)s)$$

where  $\Sigma$  and  $\Lambda$  denote states of  $I = 1$  and  $I = 0$ , respectively.

$$\mathbf{2.14} \quad |\pi^+\rangle = \sqrt{\frac{1}{6}} \sum_{a=R, G, B} (\bar{d}_a \uparrow u_a \downarrow - \bar{d}_a \downarrow u_a \uparrow)$$

**2.15** The members of a  $U$ -spin multiplet have the same charge. The charge operator  $Q$  commutes with the three generators of  $U$  spin.

$\Sigma^\pm$  and  $\Sigma^*(1385)^+$  are members of  $U = \frac{1}{2}$  multiplets, whereas  $\Sigma^*(1385)^-$  is a member of a  $U = \frac{3}{2}$  multiplet. Conservation of  $U$  spin therefore forbids  $\Sigma^* \rightarrow \Sigma^- \gamma$  if  $\gamma$  has  $U = 0$ .

**2.16** The total angular momentum  $J$  and parity  $P$  are conserved in  $\pi N$  interactions and, since states with  $L' = J \pm \frac{1}{2}$  have opposite parity,  $L'$  is also conserved.  $P = \eta_\pi \eta_N (-1)^{L'}$ , where the product of the intrinsic parities  $\eta_\pi \eta_N = -1$ . The quark model predicts that the first excited baryon level contains the following  $\pi N$  states:  $S_{11}$  (twice),  $D_{13}$  (twice),  $D_{15}$ ,  $S_{31}$ , and  $D_{33}$ , where we have used the notation  $L'_{2I,2J}$  where  $I$  is the isospin of the resonance. See also Close (1979).

**2.17**  $\mu_\Lambda = \mu_s$ ,  $\mu_{\Sigma^+} = \frac{1}{3}(4\mu_u - \mu_s)$ ,  $\mu_{\Xi^0} = \frac{1}{3}(4\mu_s - \mu_u)$ , and so on. Using  $\mu_p = 2.79$  nm, we have

$$\mu_d = \mu_s = -\frac{1}{2}\mu_u = -0.93 \text{ nm}.$$

We can obtain a better estimate of  $\mu_s$  if we allow for quark mass differences (see Section 2.14)

$$\mu_s = \frac{m_d}{m_s} \mu_d.$$

**2.20**  $|\omega(M_J = 1)\rangle = \sqrt{\frac{1}{2}}(\bar{u}u + \bar{d}d)\uparrow\uparrow,$

$$|\pi^0\rangle = \sqrt{\frac{1}{2}}(\bar{u}u - \bar{d}d)\sqrt{\frac{1}{2}}(\uparrow\downarrow - \downarrow\uparrow),$$

$$(\mu\sigma_-)_i(q\uparrow)_i = \mu_q(q\downarrow)_i, \quad (\mu\sigma_-)_i(q\downarrow)_i = 0, \quad \text{and } \mu_{\bar{q}} = -\mu_q.$$

**2.22**  $D^0 \rightarrow K^- \pi^+$  due to  $c \rightarrow s(\bar{d}u)$ ,  $D^0 \rightarrow \pi^- \pi^+$  due to  $c \rightarrow d(\bar{d}u)$ , with, in each case,  $\bar{u}$  as a spectator. In Section 12.11, we see that the  $c \rightarrow d$  transmutation is “Cabibbo-suppressed” in comparison to  $c \rightarrow s$ .

**2.23** The hadronic state must have  $I = 0$  and  $C = +1$ . The dominant hadronic decay modes are observed to be  $\psi' \rightarrow \psi\pi^+\pi^-$ ,  $\psi\pi^0\pi^0$ ,  $\psi\eta$  with branching ratios 33, 17, and 3%, respectively.

**2.24** Radiative transitions occur between states of opposite  $C$  parity; the ( $\Delta J = 1$ ) transitions are  $E_1$  or  $M_1$  according to whether the relative parity of the levels is odd or even. The approximate equality of the  $\psi' \rightarrow \chi\gamma$  branching ratios is due to the balancing compensation of the  $2J + 1$  and phase space ( $k^3$ ) factors which occur in the  $E_1$  transition probability formula.

**2.25**  $\Gamma(q\bar{q} \rightarrow e^+e^-)$  is proportional to  $e_q^2$ ;  $|\rho\rangle$  and  $|\omega\rangle$  are  $(u\bar{u} \mp d\bar{d})/\sqrt{2}$ , respectively. Since the  $u\bar{u}$  and  $d\bar{d}$  annihilations are indistinguishable, we must add amplitudes; and so

$$\Gamma_{\rho, \omega} \propto \frac{1}{2}\left(\frac{2}{3} \mp \left(-\frac{1}{3}\right)\right)^2.$$

**2.26** See, for example, Close (1979).

**2.27** See, for example, Close (1979).

**2.28** The strong  $\Sigma_c^{++} \rightarrow \Lambda_c^+\pi^+$  decay, followed by the weak decays  $\Lambda_c^+ \rightarrow \Lambda\pi^+\pi^+\pi^-$  and  $\Lambda \rightarrow p\pi^-$ .

**2.29** The eigenvalues of  $\sigma_1 \cdot \sigma_2$  are  $-3$  and  $+1$  for  $S = 0$  and  $1$ , respectively.

**2.32**  $\sum_{i>j} \frac{\sigma_i \cdot \sigma_j}{m_i m_j} = \frac{4}{m_u^2} \left( \mathbf{S}_1 \cdot \mathbf{S}_2 + \frac{m_u}{m_Q} (\mathbf{S}_1 + \mathbf{S}_2) \cdot \mathbf{S}_3 \right).$

## CHAPTER 3

**3.2**  $\sum_{\mu\nu} g_{\mu\nu} g^{\mu\nu} = \sum_{\mu} (g_{\mu\mu})^2 = 4.$

**3.3**

Center-of-Mass Frame:  $p_1 = (\frac{1}{2}E_{cm}, \mathbf{p}), p_2 = (\frac{1}{2}E_{cm}, -\mathbf{p})$

Laboratory Frame:  $p_1 = (E_{lab}, \mathbf{p}_{lab}), p_2 = (M, \mathbf{0})$

$$\therefore s = (E_{lab} + M)^2 - (E_{lab}^2 - M^2)$$

Advantages of Fixed Target: higher flux because of the density of the target;

choice of reaction  $\pi p$ ,  $Kp$ ,  $\pi d$ , and so on; need detectors over less solid angle about the interaction point and hence a less expensive experiment.

## 3.4

$$\sum_{m \neq n} V_{fn} \frac{1}{E_m - E_n + i\epsilon} V_{nm} \frac{1}{E_i - E_m + i\epsilon} V_{mi}$$

3.5 (a) Let  $E$  and  $E'$  be the energies of the outgoing  $e^-$  and  $e^+$ , respectively; and so the matrix element contains

$$\int (e^{-iEt})^* e^{-i\omega t} e^{-i(-E')t} dt = 2\pi \delta(E + E' - \omega)$$

## CHAPTER 4

4.1 To satisfy the periodic boundary conditions, the allowed values of  $p_x$  are such that  $Lp_x = 2\pi n$ , where  $n$  is an integer. Hence, the number of allowed states in the range  $p_x$  to  $p_x + dp_x$  is  $L dp_x / 2\pi$ .

4.2 From (4.30), we have

$$\begin{aligned} dQ &= \frac{1}{4\pi^2} \frac{d^3 p_C}{2E_C} \frac{d^3 p_D}{2E_D} \delta^{(4)}(p_A + p_B - p_C - p_D) \\ &= \frac{1}{4\pi^2} \frac{d^3 p_C}{2E_C} \frac{1}{2E_D} \delta(W - E_C - E_D). \end{aligned}$$

In the center-of-mass frame ( $\sqrt{s} \equiv W = E_A + E_B$ ),

$$dQ = \frac{1}{4\pi^2} \frac{p_f^2 dp_f d\Omega}{4E_C E_D} \delta(W - E_C - E_D).$$

Using

$$W = E_C + E_D = (m_C^2 + p_f^2)^{1/2} + (m_D^2 + p_f^2)^{1/2},$$

we have

$$\frac{dW}{dp_f} = p_f \left( \frac{1}{E_C} + \frac{1}{E_D} \right).$$

Substituting for  $dW/dp_f$ , we find

$$dQ = \frac{1}{4\pi^2} \frac{p_f}{4} \left( \frac{1}{E_C + E_D} \right) dW d\Omega \delta(W - E_C - E_D)$$

$$dQ = \frac{1}{4\pi^2} \frac{p_f}{4\sqrt{s}} d\Omega.$$

From (4.32),

$$F = 4(p_i E_B + p_i E_A) = 4p_i \sqrt{s}.$$

**4.3** Neglecting masses, we may write in the center-of-mass frame

$$p_A = (p, \mathbf{p}), \quad p_B = (p, -\mathbf{p}),$$

$$p_C = (p, \mathbf{p}'), \quad p_D = (p, -\mathbf{p}'),$$

where  $p = |\mathbf{p}| = |\mathbf{p}'|$ . Substitute these values into (4.18), with  $q = p_D - p_B$ , and use (4.35).

**4.5** Using (4.43) and  $p_i^2 = m_i^2$ ,

$$s + t + u = \sum_i m_i^2 + 2p_A^2 + 2p_A \cdot (p_B - p_C - p_D) = \sum_i m_i^2.$$

**4.6** If  $e^-e^- \rightarrow e^-e^-$  is the  $s$  channel process  $A + B \rightarrow C + D$ , then

$$p_A = (E, \mathbf{k}_i), \quad p_B = (E, -\mathbf{k}_i), \quad p_C = (E, \mathbf{k}_f), \quad p_D = (E, -\mathbf{k}_f)$$

where  $E = (k^2 + m^2)^{1/2}$ . So, for example,

$$t = (p_A - p_C)^2 = -(\mathbf{k}_i - \mathbf{k}_f)^2 = -2k^2(1 - \cos \theta)$$

since  $\mathbf{k}_i \cdot \mathbf{k}_f = k^2 \cos \theta$ . As  $k^2 \geq 0$ , we have  $s \geq 4m^2$ ; and since  $-1 \leq \cos \theta \leq 1$ , we have  $t \leq 0$  and  $u \leq 0$ .

**4.7** If we keep  $p_A, \dots, p_D$  defined as for the  $s$  channel  $AB \rightarrow CD$  process, then for  $A\bar{D} \rightarrow C\bar{B}$  in the center-of-mass frame,

$$p_A = (E, \mathbf{k}_i), -p_D = (E, -\mathbf{k}_i), p_C = (E, \mathbf{k}_f), -p_B = (E, -\mathbf{k}_f),$$

where  $\mathbf{k}_i, -\mathbf{k}_i, \mathbf{k}_f, -\mathbf{k}_f$  are the three-momenta of  $A$ ,  $\bar{D}$ ,  $C$ , and  $\bar{B}$ , respectively. The required results now follow upon using (4.43).

**4.8** See, for example, Martin and Spearman (1970), Chapter 4, Section 3.

$$\begin{aligned} 4.9 \quad -(p_A + p_C) \cdot (p_D + p_B) &= -(2p_A + p_B - p_D) \cdot (p_D + p_B) \\ &= -2p_A \cdot (p_D + p_B) = u - s. \end{aligned}$$

## CHAPTER 5

**5.1** See, for example, Aitchison (1972), Chapter 8, Section 1.

**5.2**

$$\begin{aligned} 0 &= \gamma^\nu \partial_\nu (i\gamma^\mu \partial_\mu - m) \psi = i\frac{1}{2} (\gamma^\nu \gamma^\mu + \gamma^\mu \gamma^\nu) \partial_\nu \partial_\mu \psi - m \gamma^\nu \partial_\nu \psi \\ &= ig^{\mu\nu} \partial_\nu \partial_\mu \psi + im^2 \psi = i(\square^2 + m^2) \psi. \end{aligned}$$

**5.3** The momentum  $\mathbf{p}' = (p \sin \theta, 0, p \cos \theta)$  is obtained from  $\mathbf{p} = (0, 0, p)$  by a rotation through  $\theta$  around the  $y$  axis. The required helicity eigenspinor  $u(\mathbf{p}')$  may therefore be obtained from  $u^{(1)}(\mathbf{p})$  of (5.27) using (2.26):

$$u(\mathbf{p}') = N \begin{pmatrix} \cos \frac{\theta}{2} - i\sigma_2 \sin \frac{\theta}{2} & 0 \\ 0 & \cos \frac{\theta}{2} - i\sigma_2 \sin \frac{\theta}{2} \end{pmatrix} \begin{pmatrix} 1 \\ 0 \\ \frac{p}{E+m} \\ 0 \end{pmatrix}.$$

**5.4** One way to proceed is to evaluate explicit components, for example,  
 $[H, L_1] = [\mathbf{a} \cdot \mathbf{P}, x_2 P_3 - x_3 P_2] = -i(\alpha_2 P_3 - \alpha_3 P_2) = -i(\mathbf{a} \times \mathbf{P})_1$ .

**5.5** Act on the first of eqs. (5.24) with the operator  $(E + eA^0 + m)$ ,

$$(E + eA^0 + m)\boldsymbol{\sigma} \cdot (\mathbf{P} + e\mathbf{A})u_B = (E + eA^0 + m)(E + eA^0 - m)u_A \\ = 2m(E_{NR} + eA^0)u_A.$$

If we were able to commute the two operators then, upon using the second of eqs. (5.24), the left-hand side would reduce to  $(\mathbf{P} + e\mathbf{A})^2$ . The lack of commutation gives rise to the extra term involving  $\mathbf{B} = \nabla \times \mathbf{A}$ .

**5.6**

$$\gamma^\mu = -(C\gamma^0)\gamma^{\mu*}(C\gamma^0)^{-1} = -C\gamma^0\gamma^{\mu*}\gamma^0 C^{-1} = -C\gamma^{\mu T}C^{-1}.$$

Thus,  $\gamma^0 = -C\gamma^0 C^{-1}$ , and so  $(C\gamma^0) = (C\gamma^0)^T$  implies  $C = -C^T$ , and  $(C\gamma^0)^2 = 1$  implies  $C = -C^{-1}$ . Also,

$$\bar{\psi}_C = \psi_C^\dagger \gamma^0 = (C\gamma^0 \psi^*)^\dagger \gamma^0 = \psi^T C \gamma^0 \gamma^0 = -\psi^T C^{-1}.$$

**5.7**

$$\bar{u}\gamma^0(\gamma^\mu p_\mu - m)u = 0$$

$$\bar{u}(\gamma^\mu p_\mu - m)\gamma^0 u = 0$$

Adding:  $2\bar{u}p_0u - 2mu^\dagger u = 0$ , since  $\gamma^0\gamma^k = -\gamma^k\gamma^0$ .

$$\bar{u}^{(r)}u^{(s)} = \frac{m}{E}u^{(r)\dagger}u^{(s)} = 2m\delta_{rs}.$$

**5.9**

$$u^{(s)} = N \begin{pmatrix} \chi^{(s)} \\ \frac{\boldsymbol{\sigma} \cdot \mathbf{p}}{E+m} \chi^{(s)} \end{pmatrix}, \quad \bar{u}^{(s)} = N \left( \chi^{(s)\dagger}, \frac{-\boldsymbol{\sigma} \cdot \mathbf{p}}{E+m} \chi^{(s)\dagger} \right)$$

$$\sum_{s=1,2} u^{(s)} \bar{u}^{(s)} = N^2 \begin{pmatrix} I & \frac{-\boldsymbol{\sigma} \cdot \mathbf{p}}{E+m} \\ \frac{\boldsymbol{\sigma} \cdot \mathbf{p}}{E+m} & -\left(\frac{\boldsymbol{\sigma} \cdot \mathbf{p}}{E+m}\right)^2 \end{pmatrix} = \begin{pmatrix} E+m & -\boldsymbol{\sigma} \cdot \mathbf{p} \\ \boldsymbol{\sigma} \cdot \mathbf{p} & m-E \end{pmatrix} = \not{p} + m,$$

since  $\sum \chi^{(s)\dagger} \chi^{(s)} = I$  and  $N^2 = E + m$ .

## 5.10

$$\not{p} \not{p} = \gamma^\nu \gamma^\mu p_\nu p_\mu = -\gamma^\mu \gamma^\nu p_\nu p_\mu + 2g^{\mu\nu} p_\nu p_\mu = -\not{p} \not{p} + 2p^2.$$

**5.11** The action of  $\Lambda_+$  on an arbitrary spinor is

$$\begin{aligned}\Lambda_+ \left( \sum_{r=1}^4 a_r u^{(r)} \right) &= \sum_{r=1}^4 a_r \left( \sum_{s=1}^2 \frac{u^{(s)} \bar{u}^{(s)}}{2m} \right) u^{(r)} = \sum_{r=1}^2 a_r u^{(r)}. \\ \Lambda_+^2 &= \frac{\not{p} \not{p} + 2m \not{p} + m^2}{4m^2} = \frac{p^2 + 2m \not{p} + m^2}{4m^2} = \frac{\not{p} + m}{2m} = \Lambda_+.\end{aligned}$$

**5.12** Particular examples of (5.59) (rotations and Lorentz boosts) are given by Sakurai (1967), but note the different metric and properties of  $\gamma$ -matrices.

## 5.14

$$[(\alpha \cdot \mathbf{P} + \beta m), \gamma^5] = [\gamma^5, (\alpha \cdot \mathbf{P} - \beta m)],$$

whereas

$$[(\alpha \cdot \mathbf{P} + \beta m), \sigma \cdot \hat{\mathbf{p}}] = [\sigma \cdot \hat{\mathbf{p}}, (\alpha \cdot \mathbf{P} + \beta m)].$$

## 5.15

$$\gamma^5 \left( \frac{\chi^{(s)}}{\sigma \cdot \mathbf{p}} \chi^{(s)} \right) \simeq \left( \sigma \cdot \hat{\mathbf{p}} \chi^{(s)} \right) \simeq \sigma \cdot \hat{\mathbf{p}} \left( \frac{\chi^{(s)}}{\sigma \cdot \mathbf{p}} \chi^{(s)} \right)$$

in the limit  $E \gg m$ .

## CHAPTER 6

**6.1** Start with  $\bar{u}_f i \sigma^{\mu\nu} (p_f - p_i)_\nu u_i$  and rewrite the individual terms with the help of (5.9) so that you can make use of the Dirac equations

$$\gamma^\nu p_{i\nu} u_i = m u_i, \quad \bar{u}_f \gamma^\nu p_{f\nu} = m \bar{u}_f.$$

$$\text{6.3} \quad \text{Tr}(\not{a} \not{b}) = \frac{1}{2} \text{Tr}(\not{a} \not{b} + \not{b} \not{a}) = \frac{1}{2} 2g^{\mu\nu} a_\mu b_\nu \text{Tr}(I) = 4a \cdot b.$$

$$\begin{aligned}\text{Tr}(\not{a}_1 \dots \not{a}_n) &= \text{Tr}(\widehat{\not{a}_1} \dots \widehat{\not{a}_n} \gamma^5 \gamma^5) \\ &= (-1)^n \underbrace{\text{Tr}(\gamma^5 \not{a}_1 \dots \not{a}_n \gamma^5)}_{=} = (-1)^n \text{Tr}(\not{a}_1 \dots \not{a}_n),\end{aligned}$$

and so, if  $n$  is odd, the trace vanishes.

**6.4** Since the  $\bar{\nu}_e$  is right-handed, the  $e^-$  must be left-handed (see Fig. 6.8). The  $e^+$  from  $\mu^+$  decay is right-handed. See Chapter 12 for details.

**6.5** From (2.21),

$$d_{00}^1(\theta) = \cos \theta = \frac{t - u}{s}.$$

**6.7**

$$\int dp'_0 2p'_0 \theta(p'_0) \delta(p'^2 - M^2) = 1$$

where  $p'^2 = p_0'^2 - \mathbf{p}'^2$ . This result follows from the identity

$$\delta(p_0'^2 - a^2) = \frac{1}{2|a|} (\delta(p'_0 - a) + \delta(p'_0 + a)),$$

$$\begin{aligned} \delta((p + q)^2 - M^2) &= \delta(2p \cdot q + q^2) = \frac{1}{2M} \delta\left(v + \frac{q^2}{2M}\right) \\ &= \frac{1}{2M} \delta[E - E' - EE'(1 - \cos \theta)/M]. \end{aligned}$$

**6.9** Substitute (6.55) into (6.53). Show that the equations for  $\nabla \cdot \mathbf{B}$  and  $\nabla \times \mathbf{E}$  are automatically satisfied and that the remaining two equations can be arranged to give (6.54).  $\partial_\mu \partial_\nu F^{\mu\nu} = 0$  follows on considering  $\mu \leftrightarrow \nu$ .

**6.11** Show that under a rotation  $\phi$  about the photon propagation direction (the  $z$  axis)

$$\boldsymbol{\epsilon}_i \rightarrow \boldsymbol{\epsilon}'_i = e^{-i\lambda_i \phi} \boldsymbol{\epsilon}_i$$

where  $\lambda_R = +1$  and  $\lambda_L = -1$ , see (2.12).

**6.13**

$$(Aq^2 g_{\mu\nu} + Bq_\mu q_\nu)(-g^{\nu\lambda} q^2 + q^\nu q^\lambda) = Aq^2 (-\delta_\mu^\lambda q^2 + q_\mu q^\lambda)$$

which cannot be made equal to  $\delta_\mu^\lambda$  for any choice of the arbitrary functions  $A$  and  $B$ .

**6.15** See Exercise 6.11;  $\boldsymbol{\epsilon}^{(\lambda=0)}$  is chosen to satisfy (6.91) and to be suitably normalized.

**6.16** Equation (6.93) can be checked explicitly component by component or, more elegantly, by writing the sum in its most general Lorentz form  $A g_{\mu\nu} + B p_\mu p_\nu$ . Then take the scalar product with  $p^\mu$  to show  $A = -BM^2$ , and with  $g^{\mu\nu}$  to show  $A = -1$ .

**6.17** For verification of (6.101) itself, see, for example, Sakurai (1967), page 8, where it is shown that

$$(|\mathbf{q}|^2 + \mu^2)^{-1} \leftrightarrow e^{-\mu|\mathbf{x}|}/4\pi|\mathbf{x}|$$

are Fourier transforms.

**6.18** To evaluate the  $\mathcal{M}_1$  contribution to  $k_\mu T^{\mu\nu}$ , note that

$$\left( \frac{(\not{p} + \not{k} + m)\not{k}}{(p + k)^2 - m^2} \right) u(p) = \left( \frac{-\not{k}\not{p} + 2k \cdot p + m\not{k}}{2k \cdot p} \right) u(p) = u(p),$$

since  $\not{p}\not{k} + \not{k}\not{p} = 2k \cdot p$  and  $\not{k}\not{k} = 0$  and  $(\not{p} - m)u = 0$ .

**6.19** The variables (6.109) become

$$s = (k + p)^2 = 2k \cdot p - Q^2 = 2k' \cdot p', \text{ and so on.}$$

Repeat the derivation of (6.113) and show that  $\overline{|\mathcal{M}_1|^2}, \overline{|\mathcal{M}_2|^2}$  are unchanged but that the interference contribution becomes  $4e^4 Q^2 t/su$ . Use (6.24).

**6.20** At high energy, the dominant contribution to  $\sigma$  comes from

$$\overline{|\mathcal{M}|^2} \approx 2e^4 \left( \frac{-s}{u - m^2} \right) \approx 4e^4 \left( \frac{2m^2}{s} + 1 + \cos \theta \right)^{-1}$$

and the  $\cos \theta$  integration leads to the  $\log(s/m^2)$  behavior.

**6.23** See Aitchison and Hey (1982), Chapter 2, Section 10.

## CHAPTER 8

**8.1** Revision. For further discussion, see Section 7.1.

**8.4** For a spherically symmetric potential, we can perform the angular integration in (8.3) and obtain

$$F = 2\pi \int \rho(r) \left( \frac{e^{iqr} - e^{-iqr}}{iqr} \right) r^2 dr.$$

Substitution of  $\rho = Ae^{-mr}$  and straightforward integration yield the result.

**8.5** We might expect the most general form (for  $x = 0$ ) to be

$$\begin{aligned} J^\mu &= e\bar{u}(p') (\gamma^\mu K_1 + i\sigma^{\mu\nu} (p' - p)_\nu K_2 + i\sigma^{\mu\nu} (p' + p)_\nu K_3 \\ &\quad + (p' - p)^\mu K_4 + (p' + p)^\mu K_5) u(p) \end{aligned}$$

where  $K_i \equiv K_i(q^2)$ . But using the Gordon decomposition, (6.7), we can reexpress the  $(p' + p)^\mu$  terms as linear combinations of the  $\gamma^\mu$  and  $\sigma^{\mu\nu}(p' - p)_\nu$  terms. Thus, the most general form reduces to

$$J^\mu = e\bar{u}(p') \left( \gamma^\mu F_1 + \frac{i\kappa}{2M} F_2 \sigma^{\mu\nu} q_\nu + q^\mu F_3 \right) u(p) e^{iq \cdot x}.$$

Current conservation

$$q_\mu J^\mu = e\bar{u}(p') \left( q F_1 + \frac{i\kappa}{2M} F_2 q_\mu \sigma^{\mu\nu} q_\nu + q^2 F_3 \right) u(p) = 0$$

implies  $F_3 = 0$ , as the first term vanishes by virtue of the Dirac equation, and the second vanishes since  $\sigma^{\mu\nu}$  is antisymmetric.

**8.6** On squaring  $p' = p + q$ , we have

$$M^2 = M^2 + 2p \cdot q + q^2,$$

so  $p \cdot q = -q^2/2$  is not an independent scalar variable.

**8.7** Equation (8.18) follows from (8.13) on using the Gordon decomposition, (6.7). In the Breit frame  $p^\mu = (E, \mathbf{p})$  and  $p'^\mu = (E, -\mathbf{p})$ . Therefore, (8.18) gives

$$\rho \equiv J^0 = e\bar{u}(p') \left( \gamma^0(F_1 + \kappa F_2) - \frac{E}{M}\kappa F_2 \right) u(p).$$

But in this frame,

$$\bar{u}\gamma^0 u = 2M \quad \text{and} \quad \bar{u}u = 2E$$

with only states  $\lambda = -\lambda'$  contributing. Thus,

$$p = 2Me \left[ F_1 + \left( 1 - \frac{E^2}{M^2} \right) \kappa F_2 \right] = 2MeG_E$$

using (8.16) and noting  $q^2 = 4\mathbf{p}^2$ . Similarly,

$$\mathbf{J} = e\bar{u}(p')\gamma u(p)G_M$$

in the Breit frame.

**8.9** See Chapter 6;  $L_{\mu\nu}$  is the product of two currents summed and averaged over spins. Use current conservation or check directly using the explicit form (6.25).

**8.10** Using (8.24) and (8.26), we have

$$-W_1 q^\mu + \frac{W_2}{M^2}(p \cdot q)p^\mu + \frac{W_4}{M^2}q^2 q^\mu + \frac{W_5}{M^2}(q^2 p^\mu + (p \cdot q)q^\mu) = 0.$$

The coefficients of  $q^\mu$  and  $p^\mu$  must vanish separately.

**8.11**  $q^2 \leq 0$  and  $\nu \geq 0$ , so  $x \geq 0$ .  $W^2 \geq M^2$ , and so  $x \leq 1$  from (8.29).  $y$  is an invariant variable, so evaluate in the target rest frame. We have  $y = 1 - (E'/E)$ , and hence  $0 \leq y \leq 1$ .

**8.15** Substitute (8.27) into (8.52). For  $\lambda = 0$ , for example,

$$\sigma_L = \frac{4\pi^2\alpha}{K} \left( -\epsilon_0^\mu \epsilon_0^\nu g_{\mu\nu} W_1 + \epsilon_0^\mu \epsilon_0^\nu p_\mu p_\nu \frac{W_2}{M^2} \right),$$

since  $\epsilon \cdot q = 0$  (see Exercise 8.14). Evaluate in the laboratory frame using (8.50).

**8.16** Solve (8.53) and (8.54) for  $W_{1,2}$  and substitute into (8.34).

**8.17** The poles at  $q^2 = 0$  in (8.27) cannot be real but must be an artifact of the way we have written  $W_{\mu\nu}$ . To remove the leading pole, we must have

$$q^2 W_1 + \frac{(p \cdot q)^2}{M^2} W_2 \rightarrow 0 \quad \text{as } q^2 \rightarrow 0$$

or

$$W_2 \rightarrow -\frac{q^2}{\nu^2} W_1 + O(q^4) \quad \text{as } q^2 \rightarrow 0.$$

But  $W_1$  can approach a constant as  $q^2 \rightarrow 0$ , and so  $W_2 \rightarrow 0$ . Hence,  $\sigma_L \rightarrow 0$ , as it must in the limit of real photons.

## CHAPTER 9

### 9.3

$$\hat{s} = (k + xp)^2 \simeq x(2kp) \simeq xs,$$

$$\hat{t} = (k - k')^2 = t,$$

$$\hat{u} = (k' - xp)^2 \simeq xu.$$

Use (6.30) together with (4.35) and (4.45) to show that

$$\frac{d\sigma}{dt} = \frac{2\pi\alpha^2 e_i^2}{\hat{t}^2} \left( \frac{\hat{s}^2 + \hat{u}^2}{\hat{t}^2} \right).$$

Equation (9.18) then follows upon using

$$-\frac{t}{s+u} = \frac{Q^2}{2M\nu} = x.$$

To derive (9.19), first verify that (8.31) may be written

$$\begin{aligned} (L^e)^{\mu\nu} W_{\mu\nu} &= -2tW_1 - su \frac{W_2}{M^2} \\ &= \frac{2}{M(s+u)} [(s+u)^2 xF_1 - usF_2]. \end{aligned}$$

Equation (9.19) follows on inserting this expression into (8.35) and using

$$d\Omega dE' = 2\pi d(\cos\theta) dE' = \frac{4\pi M^2}{su} dt \left( -\frac{1}{2M} du \right).$$

Here, we have used the laboratory kinematics of Section 6.8,

$$s = 2ME, \quad u = -2ME', \quad t = -Q^2 = -4EE' \sin^2 \frac{\theta}{2}.$$

- 9.4** Equation (9.21) follows on using  $Q^2 = 4EE' \sin^2 \frac{\theta}{2}$  and  $d\nu = -dE'$ . Show that, in the laboratory frame,

$$\sin^2 \frac{\theta}{2} = xy \frac{M}{2E}, \quad \cos^2 \frac{\theta}{2} = \frac{E}{E'} \left(1 - y - \frac{Mxy}{2E}\right).$$

Insert these expressions into (8.34) and obtain

$$\frac{d\sigma}{dx dy} = \frac{8ME\pi\alpha^2}{Q^4} \left[ xy^2 F_1 + \left(1 - y - \frac{Mxy}{2E}\right) F_2 \right].$$

Equation (9.23) then follows on verifying that

$$M\nu_{\max} x^2 y^2 = \frac{Q^4}{4ME}$$

in the laboratory frame (where  $\nu_{\max} = E$ ).

- 9.5** In the deep inelastic limit, the above equation for  $d\sigma/dx dy$  becomes

$$\frac{d\sigma}{dx dy} = \frac{4\pi s\alpha^2}{Q^4} \left\{ \frac{y^2}{2} + (1-y) \right\} F_2,$$

since  $s = 2ME$  and  $2xF_1 = F_2$ .

- 9.7** In the  $\nu, Q^2 \rightarrow \infty$  limit, (8.54) and (8.53) imply

$$\frac{\sigma_L}{\sigma_T} \approx \frac{\nu^2 W_2 - Q^2 W_1}{Q^2 W_1} = \frac{(F_2/2x) - F_1}{F_1} \rightarrow 0.$$

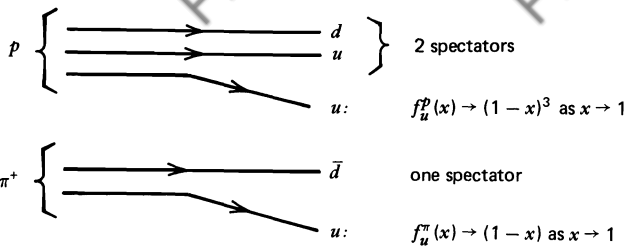
- 9.9** This result is even more obvious using (9.32).

- 9.10** There is experimental evidence that  $\nu W_2 \rightarrow \text{constant}$  as  $x \rightarrow 0$ . Then, (9.13) requires that  $f_i(x) \sim 1/x$  as  $x \rightarrow 0$ . Let us therefore answer the question in reverse. From (8.53), (9.13), (9.14), and (8.48), we have, for fixed  $Q^2$  and  $\nu \rightarrow \infty$ ,

$$\begin{aligned} \sigma_T &= \frac{4\pi^2\alpha}{MK} F_1 = \frac{4\pi^2\alpha}{M\nu} \frac{1}{2x} \sum_i e_i^2 x f_i(x) \\ &\sim \frac{4\pi^2\alpha}{Q^2} \sum_i e_i^2 \end{aligned}$$

if  $f_i(x) \sim 1/x$  as  $x \rightarrow 0$ . That is,  $\sigma_T$  is independent of  $\nu$  and approaches a constant at high energies and fixed  $Q^2$ .

- 9.11** The more spectators that share the initial momentum, the smaller is the chance of producing a parton with a large fraction of the momentum.



## CHAPTER 10

**10.1** Equations (10.3) and (10.4) follow from (8.53) and (8.54) with  $K \simeq \nu$ .

**10.2** For a  $\gamma^*$  with polarization vector  $\epsilon_\mu$  interacting with a quark of charge  $ee_i$ ,

$$-i\mathcal{M} = \bar{u}(p')(-iee_i\gamma^\mu)u(p)\epsilon_\mu.$$

Thus, neglecting the mass of the quark, we have

$$|\mathcal{M}|^2 = \frac{1}{4}2e_i^2e^2 \text{Tr}(\not{p'}\not{p}) = 2e_i^2e^2 p \cdot q,$$

using (6.93). From (10.13),

$$\begin{aligned} F\hat{\sigma}_T &= |\mathcal{M}|^2 2\pi \int d^3p' dp'_0 \delta^4(p' - p - q) \theta(p'_0) \delta(p'^2) \\ &= 2\pi |\mathcal{M}|^2 \delta((p + q)^2) = 8\pi^2 \alpha e_i^2 \delta(1 - z). \end{aligned}$$

**10.3**

$$q = (q_0; 0, 0, k), \quad q_2 = (k'; k' \sin \theta, 0, k' \cos \theta),$$

$$q_1 = (k; 0, 0, -k), \quad g = (k'; -k' \sin \theta, 0, -k' \cos \theta).$$

Equations (10.20)–(10.23) follow from

$$\hat{s} = (q + q_1)^2 = (q_2 + g)^2,$$

$$\hat{t} = (q - q_2)^2 = (g - q_1)^2, \quad \hat{u} = (q_1 - q_2)^2,$$

$$-\hat{t} - \hat{u} = Q^2 + 2k'q_0 + 2kk' = Q^2 + 4k'^2 = Q^2 + \hat{s},$$

where we have used  $q_0 = 2k' - k$  (energy conservation). From (10.20)–(10.22), we have

$$\hat{s}\hat{t}\hat{u} = 4k'^2(2kk')^2 \sin^2 \theta = (4kk')^2 p_T^2$$

$$= (\hat{t} + \hat{u})^2 p_T^2 = (\hat{s} + Q^2)^2 p_T^2.$$

If  $-\hat{t} \ll \hat{s}$ , then  $-\hat{u} = \hat{s} + Q^2$ , and hence (10.25) follows. Finally,

$$dp_T^2 = k'^2 d(\sin^2 \theta) = 2k'^2 \sin \theta \cos \theta d\theta$$

$$\approx \frac{\hat{s}}{2} d(\cos \theta) \quad \text{for } \cos \theta \simeq 1.$$

**10.4** Adopting convention (8.48), the flux in the laboratory frame is

$$F = 4m_q K = 4m_q \left( q_0 - \frac{Q^2}{2m_q} \right) = 4m_q q_0 - 2Q^2,$$

where  $\gamma^*$  has  $q = (q_0, 0, 0, k_L)$ . But

$$\hat{s} = (m_q + q_0)^2 - k_L^2 = 2m_q q_0 - Q^2,$$

and so  $F = 2\hat{s}$ . Returning to the center-of-mass frame, (4.29) becomes

$$\frac{d\sigma}{d\Omega} = \frac{1}{64\pi^2 \hat{s}} |\mathcal{M}|^2,$$

and (10.27) follows on using (10.26).

### 10.5

$$(p_T^2)_{\max} = k'^2 = \frac{\hat{s}}{4},$$

see (10.20). Substitute for  $\hat{s}$  using (10.29).

**10.6** The  $\log Q^2$  term originates from the  $p_T^{-2}$  behavior of  $d\hat{\sigma}/dp_T^2$ , see (10.32) and (10.33). The  $p_T^{-2}$  results from the square of the propagator  $t^{-2} \sim p_T^{-4}$  and a helicity suppression factor  $(\sin \frac{1}{2}\theta)^2 \sim \theta^2 \sim p_T^2$ . In the relativistic limit, the transition  $q_L \rightarrow \text{gluon} + q_L$  is forbidden at  $\theta = 0$  by angular momentum conservation as real spin-1 gluons flip  $q_L$  to  $q_R$ .

### 10.7

$$q(x, Q^2) \sim \int^{Q^2} dp_T^2 \frac{\alpha_s(p_T^2)}{p_T^2} \sim \int \frac{d \log p_T^2}{\log p_T^2} \sim \log(\log Q^2)$$

and so

$$\frac{d}{d \log Q^2} q(x, Q^2) \sim \frac{1}{\log Q^2} \sim \alpha_s(Q^2);$$

and, on following through the derivation, we recover (10.37) with  $\alpha_s \rightarrow \alpha_s(Q^2)$ .

**10.8** The color factor  $= (\frac{1}{2})^1 (3 \times 3 - 1)/8 = \frac{1}{2}$ . The first factor recovers the conventional definition of  $\alpha_s$ , see (10.19); the denominator averages over the eight initial gluon colors; and the numerator sums over the final  $q\bar{q}$  color states (excluding the colorless combination, as the initial  $\gamma^*g$  state is colored).

**10.9** Follow the method used in Exercise 6.19. The terms in (10.38) correspond to  $|\mathcal{M}_1|^2$ ,  $|\mathcal{M}_2|^2$ , and the interference contribution, respectively. Equation (10.41) follows upon replacing (10.17) with (10.38) and retracing the steps to (10.31).

**10.10** Either repeat the calculation of Section 10.4 reordering q and g in the final state of  $\gamma^*q \rightarrow gq$ , or use (10.31) and (10.56). To calculate  $P_{gg}$ , we need to study the three-gluon vertex either directly or in, say,  $\gamma^*g \rightarrow q\bar{q}g$  [see, e.g., Altarelli (1978, 1982)].

**10.12** The second term in (10.42) does not contribute to the evolution of  $q_{NS}$ . On the contrary, the flavor singlet structure function contains quarks and gluons, and we have coupled evolution equations of the form

$$\frac{d}{d \log Q^2} \begin{bmatrix} q_S(x) \\ g(x) \end{bmatrix} = \frac{\alpha_s}{2\pi} \int_x^1 \frac{dy}{y} \begin{bmatrix} P_{qq} & 2n_f P_{qg} \\ P_{gq} & P_{gg} \end{bmatrix} \begin{bmatrix} q_S(y) \\ g(y) \end{bmatrix}.$$

**10.13 and 10.14** See, for example, Altarelli (1978, 1982).

**10.15**  $P_{qq}(z)$  is related to the probability that a quark emits a quark with momentum fraction  $z$  and a gluon with momentum fraction  $(1 - z)$ ; therefore,  $P_{qq}(z) = P_{gq}(1 - z)$ .

**10.16** Multiply both sides of (10.37) by  $x^{n-1}$  and integrate over  $x$ :

$$\frac{d}{d \log Q^2} \int_0^1 x^{n-1} q(x) dx = \frac{\alpha_s}{2\pi} \int_0^1 y^{n-1} q(y) dy \int_0^1 z^{n-1} P_{qq}(z) dz$$

using  $x = zy$ . Denoting the  $(n - 1)$ th moment of  $q(x)$  by  $M_n$ , this becomes

$$\frac{d}{d \log Q^2} M_n = \frac{A_n}{\log Q^2} M_n.$$

The solution is

$$M_n \sim (\log Q^2)^{A_n}.$$

## CHAPTER 11

### 11.1

$$\langle z \rangle = \int_0^1 z D_q^h(z) dz = N \int_0^1 (1 - z)^n dz = \frac{N}{n + 1}.$$

$$n_h \propto N \int_{2m_h}^1 \frac{dz}{z} + \dots \propto N \log\left(\frac{Q}{2m_h}\right) + \dots,$$

where ... represent terms which do not increase with  $Q$ .

**11.2, 11.3, and 11.4** See Close (1979), Chapter 12, Section 2.

**11.5** Subtract eqs. (11.18),

$$x_{\bar{q}}^2 + x_q^2 - x_g^2 = 2x_L x_q.$$

Square, and eliminate  $x_L^2$  in favor of  $x_T^2$ ,

$$\begin{aligned} 4x_q^2 x_T^2 &= 4x_q^2 x_{\bar{q}}^2 - (x_q^2 + x_{\bar{q}}^2 - x_g^2)^2 \\ &= ((x_q + x_{\bar{q}})^2 - x_g^2)(x_g^2 - (x_q - x_{\bar{q}})^2) \\ &= 16(1 - x_q)(1 - x_{\bar{q}})(1 - x_g). \end{aligned}$$

Each of the last two steps uses the identity  $a^2 - b^2 = (a + b)(a - b)$ ; also use (11.17). To obtain (11.20), start with  $x_{\bar{q}} \sin \theta = x_T$ , see Fig. 11.7. Square, and use (11.19) and (11.17),

$$\begin{aligned} \tfrac{1}{4}x_q^2 x_{\bar{q}}^2 \sin^2 \theta &= (1 - x_q)(1 - x_{\bar{q}})(x_q + x_{\bar{q}} - 1) \\ &= -(1 - x_q - x_{\bar{q}} + \tfrac{1}{2}x_q x_{\bar{q}})^2 + \tfrac{1}{4}x_q^2 x_{\bar{q}}^2. \end{aligned}$$

Using  $1 - \sin^2 \theta = \cos^2 \theta$ , we have

$$1 - x_q - x_{\bar{q}} + \tfrac{1}{2}x_q x_{\bar{q}} = \tfrac{1}{2}x_q x_{\bar{q}} \cos \theta.$$

**11.6** Use (11.30) and  $\theta \approx 2p_T/Q = x_T$ .

**11.7** See, for example, Cutler and Sivers (1978) *Phys. Rev.* **D17**, 196, where the diagrams are enumerated and evaluated in the appendix.

**11.8** See, for example, Berman et al. (1971) *Phys. Rev.* **D4**, 3388, especially Appendix B.

**11.9** When  $Q^2/s \approx 0$ ,  $x \approx y \approx 0$  and sea quarks dominate, and there is no difference between  $\pi^\pm C$ . When  $Q^2/s \approx 1$ ,  $x \approx y \approx 1$  and valence quarks dominate. Thus,

$$\frac{\sigma(\pi^+ C)}{\sigma(\pi^- C)} = \frac{e_d^2 f_d^{\pi^+} f_d^C}{e_u^2 f_u^{\pi^-} f_u^C} = \frac{e_d^2}{e_u^2} = \frac{1}{4},$$

since  $f_d^{\pi^+} = f_u^{\pi^-}$  and the isoscalar C target has equal numbers of u and d quarks.

**11.10** See, for example, Halzen and Scott (1978) *Phys. Rev.* **D18**, 3378.

## CHAPTER 12

**12.1**  $\tau^- \rightarrow e^- \bar{\nu}_e \nu_\tau$  or  $\mu^- \bar{\nu}_\mu \nu_\tau$  or  $\nu_\tau + \text{hadrons}$ .  $\nu_\tau$  is the tau neutrino (analogous to  $\nu_e$  and  $\nu_\mu$ ); the lepton numbers  $L_e$ ,  $L_\mu$ , and  $L_\tau$  are separately conserved.

**12.2**  $\bar{u}_e \gamma^\mu \tfrac{1}{2}(1 - \gamma^5) u_\nu = \bar{u}_e \tfrac{1}{2}(1 + \gamma^5) \gamma^\mu u_\nu$ , and use (6.36). See Exercise 5.15.

**12.3** Use the Feynman rules of Chapter 6:  $u_e$  describes an ingoing  $e^-$  or an outgoing  $e^+$ .

## 372 Answers and Comments on the Exercises

**12.4** The  $I = 1$  states of  $^{14}\text{O}$  and  $^{14}\text{N}^*$  are  $|\text{pp}\rangle$  and  $\sqrt{\frac{1}{2}}(|\text{np}\rangle + |\text{pn}\rangle)$ , respectively. Each proton can decay, so the  $^{14}\text{O} \rightarrow ^{14}\text{N}^*$  amplitude contains the factor  $2\sqrt{\frac{1}{2}}$ .

**12.5** For a detailed discussion of how to obtain  $G$  from data on lifetimes of  $\beta$ -emitters, see, for example, Källén (1964), Gasiorowicz (1967), or Commins (1973).

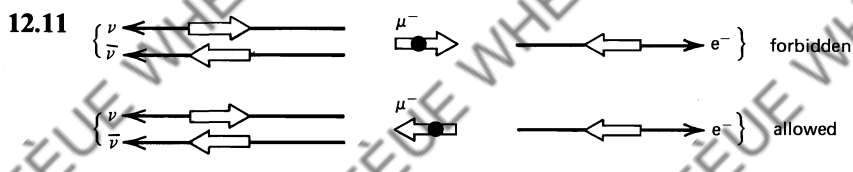
**12.6** Using (12.15), we obtain  $M_W^2 = \sqrt{2}e^2/8G \approx (37.3 \text{ GeV})^2$ . In the standard model with  $\sin^2 \theta_W = \frac{1}{4}$ , we have  $M_W = 2 \times 37.3 \text{ GeV} = 74.6 \text{ GeV}$ .

**12.7** Use the trace theorems of Section 6.4. The presence of  $\gamma^5$  can be taken care of by using (6.23). An elegant derivation of (12.28) is given by Bjorken and Drell (1964), page 262. Equation (12.29) follows directly from (12.27) and (12.28).

**12.8**  $\int d^3k d\omega \theta(\omega) \delta(\omega^2 - |\mathbf{k}|^2) = \int d^3k/2\omega$ , with  $\omega^2 = |\mathbf{k}|^2$ , see Solution 6.7.

**12.9** Use (12.29).

**12.10**  $2\mathbf{k} \cdot \mathbf{p}' \approx (\mathbf{k} + \mathbf{p}')^2 = (\mathbf{p} - \mathbf{k}')^2 = m^2 - 2\mathbf{p} \cdot \mathbf{k}'$ .



**12.12**

$$\frac{\tau(\tau \rightarrow e\nu\bar{\nu})}{\tau(\mu \rightarrow e\nu\bar{\nu})} = \left(\frac{m_\mu}{m_\tau}\right)^5 \approx 7 \times 10^{-7}$$

using (12.42). Thus,

$$\tau \text{ lifetime} = (2.2 \times 10^{-6})(7 \times 10^{-7})^{\frac{1}{5}} = 3 \times 10^{-13} \text{ sec}$$

$$(\tau \rightarrow e) : (\tau \rightarrow \mu) : (\tau \rightarrow \text{hadrons}) = 1 : 1 : 3,$$

because of two lepton versus three ( $u\bar{d}$ ) color decay modes.

**12.13** The result is that  $f_K \approx f_\pi$ .

**12.14** For a point interaction,  $s$  is the only dimensional variable. As  $\sigma$  is proportional to  $G^2$ , the product  $G^2 s$  is the only combination with the dimensions of a cross section. But a point interaction is an  $s$ -wave ( $l = 0$ ) process for which  $\sigma \leq \text{constant}/s$ , and so this simple approach must fail when  $s \sim \frac{1}{G} \sim 10^5 \text{ GeV}^2$ .

**12.15** Use  $s \approx 2m_e E_\nu$  and (12.60).

**12.17** Note the similarity to the nuclear  $\beta$ -decay rate, Section 12.3.

**12.18** To obtain the factor  $\frac{5}{18}$ , use (9.32) and (12.75), and neglect strange quarks:

$$\frac{F_2^{ep} + F_2^{en}}{F_2^{vp} + F_2^{vn}} = \frac{\frac{4}{9}(u + \bar{u}) + \frac{1}{9}(d + \bar{d}) + \frac{1}{9}(u + \bar{u}) + \frac{4}{9}(d + \bar{d})}{2(u + \bar{u} + d + \bar{d})} = \frac{5}{18}.$$

**12.21** Draw quark diagrams and identify the Cabibbo-favored and Cabibbo-suppressed vertices. The amplitudes are in the ratio  $\cos^2 \theta_c : \sin \theta_c \cos \theta_c : \sin^2 \theta_c$ .

**12.22** Use the  $(\Delta m)^5$  rule of Exercise 12.17. To determine  $\tau(D^0)$ , estimate the leptonic branching ratio as was done for the  $\tau$ -lepton in Exercise 12.12.

## CHAPTER 13

### 13.2

$$|\mathcal{M}|^2 = \frac{g_X^2}{4} \left[ \frac{1}{3} \sum_{\lambda} \epsilon_{\mu}^{(\lambda)} \epsilon_{\nu}^{(\lambda)*} \right] \left[ (c_V^2 + c_A^2) T_1^{\mu\nu} - 2c_V c_A T_2^{\mu\nu} \right]$$

where the first term in brackets is the average over the three helicity states of the X boson and the second brackets gives the sum over the fermion spin states performed as in (6.20), where  $T_1$  and  $T_2$  are the traces

$$T_1^{\mu\nu} = \text{Tr}(\gamma^{\mu} k \gamma^{\nu} k'), \quad T_2^{\mu\nu} = \text{Tr}(\gamma^5 \gamma^{\mu} k \gamma^{\nu} k').$$

We denote the X,  $f_1, \bar{f}_2$  four-momenta by  $q, k, k'$ , respectively. From (6.93) and (6.23), we see that the  $c_V c_A$  term vanishes; the polarization sum is symmetric under  $\mu \leftrightarrow \nu$ , and  $T_2$  is antisymmetric. In the X rest frame,

$$q = (M_X; 0, 0, 0), \quad k = \frac{1}{2} M_X (1; 0, 0, 1), \quad k' = \frac{1}{2} M_X (1; 0, 0, -1);$$

and using (6.25), we find

$$-g_{\mu\nu} T_1^{\mu\nu} = 4M_X^2, \quad q_{\mu} q_{\nu} T_1^{\mu\nu} = 0.$$

Finally, from (4.37), we have

$$\Gamma(X \rightarrow f_1 \bar{f}_2) = \frac{1}{64\pi^2 M_X} \int |\mathcal{M}|^2 d\Omega = \frac{1}{16\pi M_X} \frac{g_X^2}{12} (c_V^2 + c_A^2) 4M_X^2.$$

Note that if we were to consider the different polarization states,  $\epsilon^{(\lambda)}$ , separately, then  $T_2$  does not vanish. We find the widths

$$\Gamma^{(\pm)} \propto (c_V^2 + c_A^2)(1 + \cos^2 \theta) \pm 2c_V c_A 2 \cos \theta$$

$$\Gamma^{(0)} \propto (c_V^2 + c_A^2) 2 \sin^2 \theta$$

where  $k = \frac{1}{2} M_X (1; \sin \theta, 0, \cos \theta)$ . Check that these results embody angular momentum conservation for, say,  $W^+ \rightarrow e^+ \nu$ .

**13.3** Substitute  $c_V = c_A = \frac{1}{2}$ ,  $M_X = M_Z$ , and  $g_X = g/\cos\theta_W$  into (13.43). Calculate  $g$  from (12.15) with  $G = 1.166 \times 10^{-5} \text{ GeV}^{-2}$  and  $M_W = M_Z \cos\theta_W$ , and hence show that  $\Gamma(Z \rightarrow \nu\bar{\nu}) = 159 \text{ MeV}$ .

**13.4** Use Table 13.2 to calculate  $c_V^2 + c_A^2$ ; for the  $q\bar{q}$  modes, include a factor 3 for color. With three generations,  $\Gamma(Z) = 2.5 \text{ GeV}$  (neglecting fermion masses).

### 13.5

$$\Gamma(W^+ \rightarrow e^+ \nu) = \frac{g^2 M_W}{48\pi} = \frac{G}{\sqrt{2}} \frac{M_W^3}{6\pi} \simeq 224 \text{ MeV}.$$

**13.7** In this limit, the propagator is  $i g_{\mu\nu}/M_Z^2$ ; use (13.35).

**13.9** For a derivation of the Fierz theorem, see, for example, Itzykson and Zuber (1980) or Bailin (1982).

### 13.10

$$R_\mu \simeq \frac{1}{8} \left( GM_Z^3 / \Gamma_Z e^2 \right)^2 = 173.$$

**13.11**  $R_u = 3(10/9) R_\mu$  and  $R_d = 3(13/9) R_\mu$ . With three generations,

$$R(\text{hadrons}) \simeq 3(R_u + R_d) \simeq 4000.$$

## CHAPTER 14

**14.2** Substitute (14.8) into (14.4) with  $\phi = \psi, \bar{\psi}$ , respectively. For  $\phi = \bar{\psi}$ , we first rewrite the Lagrangian density (14.8) as

$$\mathcal{L} = -i(\partial^\mu \bar{\psi}) \gamma_\mu \psi - m\psi \bar{\psi}.$$

This leaves the action,  $\int \mathcal{L} d^4x$ , unchanged, as can be verified by partial integration. On substituting into (14.4), we obtain the Dirac equation for  $\psi$ , (5.7).

### 14.3 and 14.4

$$\begin{aligned} \frac{\partial \mathcal{L}}{\partial(\partial_\mu A_\nu)} &= -\frac{1}{4} \frac{\partial}{\partial(\partial_\mu A_\nu)} \left( (\partial_\alpha A_\beta - \partial_\beta A_\alpha)(\partial^\alpha A^\beta - \partial^\beta A^\alpha) \right) \\ &= -\frac{1}{2} g^{\alpha\alpha} g^{\beta\beta} \frac{\partial}{\partial(\partial_\mu A_\nu)} \left( (\partial_\alpha A_\beta)^2 - (\partial_\beta A_\alpha)(\partial_\alpha A_\beta) \right) \\ &= -\partial^\mu A^\nu + \partial^\nu A^\mu = -F^{\mu\nu}, \\ \frac{\partial \mathcal{L}}{\partial A_\nu} &= -j^\nu + m^2 A^\nu. \end{aligned}$$

**14.8**  $U^\dagger U = I$  implies  $(\det U)^*(\det U) = 1$ . Also, if we write  $U_{ij} = \delta_{ij} + \epsilon_{ij}$ , then  $\det U = 1 + \text{Tr}(\epsilon) + O(\epsilon^2)$ . Finally, for infinitesimal  $\alpha_a$ ,  $U^\dagger = U^{-1}$  gives

$$1 - i\alpha_a^* T_a^\dagger = 1 - i\alpha_a T_a.$$

**14.9** The conventional notation is  $T_a \equiv \lambda_a/2$ ; compare (14.32) with (2.44). Just as for Pauli matrices,  $\text{Tr}(\lambda_a \lambda_b) = 2\delta_{ab}$ , which together with (2.44) gives

$$\text{Tr}(\lambda_c [\lambda_a, \lambda_b]) = 4if_{abc}.$$

It is now easy to show that  $f_{abc}$  is totally antisymmetric. Antisymmetry in  $a, b$  is obvious. For the pair  $b, c$ , we have

$$4if_{acb} = \text{Tr}(\lambda_b [\lambda_a, \lambda_c]) = -\text{Tr}(\lambda_c [\lambda_a, \lambda_b]) = -4if_{abc}$$

since  $\text{Tr}(ABC) = \text{Tr}(CAB)$ .

**14.10** In QED, the field strength tensor, (14.27), can be introduced by

$$[D_\mu, D_\nu] = -ieF_{\mu\nu},$$

where  $D_\mu$  is the covariant derivative (14.24). This construction is true for any gauge group [Itzykson and Zuber (1980)]. For QCD,

$$[D_\mu, D_\nu] = igT_a G_{\mu\nu}^a.$$

Substituting (14.38) into the left-hand side yields expression (14.40) for  $G_{\mu\nu}^a$ . Now under a gauge transformation,

$$\psi \rightarrow e^{i\alpha_a(x)T_a}\psi \equiv U\psi,$$

$D_\mu \rightarrow UD_\mu U^{-1}$ , and so  $G_{\mu\nu} \rightarrow UG_{\mu\nu}U^{-1}$ . Thus, the gauge invariant quantity [see (14.39)] is

$$\text{Tr}(G_{\mu\nu}G^{\mu\nu}) \rightarrow \text{Tr}(UG_{\mu\nu}G^{\mu\nu}U^{-1}) = \text{Tr}(G_{\mu\nu}G^{\mu\nu}).$$

**14.11** Substitute (14.40) into (14.39) and isolate the terms containing the three gluon fields. After appropriately relabeling the dummy indices in the different terms, we find

$$(i\mathcal{L})_{3g} = -\frac{g}{2}f_{abc}(g_{\mu\nu}p_{1\lambda} - g_{\lambda\mu}p_{1\nu})G_a^\mu G_b^\nu G_c^\lambda.$$

We have used  $i\partial_\mu G_a^\mu = p_{1\mu}G_a^\mu$ . We sum over all possible orderings of the gluons, bearing in mind that the three-gluon vertex must be completely symmetric. As  $f_{abc}$  is totally antisymmetric, we must make the factor in brackets totally antisymmetric.

**14.13** The relevant term of the Lagrangian is [see (14.65) and (14.74)]

$$\begin{aligned} \tfrac{1}{2}|igT_k W_k \phi|^2 &= \tfrac{1}{2}|ig(-i\epsilon_{ijk})W_k \phi_j|^2 \\ &= \tfrac{1}{2}g^2 v^2 \epsilon_{i3k} \epsilon_{i3l} W_k W_l = \tfrac{1}{2}g^2 v^2 (W_1^2 + W_2^2), \end{aligned}$$

using  $\phi_j = v\delta_{j3}$ . Two bosons acquire mass  $gv$ , and the third remains massless.

**CHAPTER 15**

**15.2** Use (15.18) and the solution to Exercise 12.6.

**15.3** The relevant term in the Lagrangian is

$$\left| \frac{g}{\sqrt{2}} (T^+ W_\mu^+ + T^- W_\mu^-) \phi_0 + \left( g T^3 W_\mu^3 + \frac{g'}{2} Y B_\mu \right) \phi_0 \right|^2.$$

$$M_W^2 = \frac{g^2}{2} \phi_0^\dagger (T^+ T^- + T^- T^+) \phi_0 = \frac{g^2 v^2}{2} [T(T+1) - (T^3)^2] = 4g^2 v^2,$$

since  $T = 3$  and  $T^3 = 2$ . Also, following (15.19),

$$\frac{1}{2} M_Z^2 Z_\mu^2 = \frac{v^2}{2} 4(g W_\mu^3 - g' B_\mu)^2 = \frac{2g^2 v^2}{\cos^2 \theta_W} Z_\mu^2.$$

**15.8**

$$Q_X = \frac{4}{3}, Q_Y = \frac{1}{3}.$$

**15.9** Investigate (15.54) for the full  $SU(5)$  group and compare with (15.53).

# Supplementary Reading

## Chapter 1

Read the introductory chapters in Bransden, Evans, and Major (1973), Cheng and O'Neill (1979), Gasiorowicz (1967), Muirhead (1965), Perl (1974), and Perkins (1982). Also see articles by Adams, Peierls, and Wilkinson in Mulvey (1981), also Fabjan and Ludlam (1982), Harari (1978), and Kleinknecht (1982).

## Chapter 2

*Group Theory:* Carruthers (1966), Georgi (1982), Hammermesh (1963), Lipkin (1966, 1973), Schiff (1955), and Wybourne (1974). *Quarks:* Close (1979), Feynman (1972), Leader and Predazzi (1982), Lipkin (1973), and Rosner (1974).

## Chapter 3

Aitchison (1972), Aitchison and Hey (1982), Bjorken and Drell (1964), and Feynman (1961). *Perturbation Theory:* Merzbacher (1961) and Messiah (1962). *Relativistic Kinematics:* Byckling and Kajantie (1973) and Martin and Spearman (1970).

## Chapter 4

Aitchison (1972), Aitchison and Hey (1982), and Feynman (1961). *Cross sections:* Martin and Spearman (1970), Pilkuhn (1967) and Scadron (1979).

## Chapter 5

Aitchison (1972), Bethe and Jackiw (1968), Bjorken and Drell (1964), Gasiorowicz (1967), and Sakurai (1967).

## Chapter 6

Aitchison (1972), Aitchison and Hey (1982), Bjorken and Drell (1964), Feynman (1961, 1962), Gasiorowicz (1967), Källén (1972), Sakurai (1967), and Scadron (1979).

### **Chapter 7**

Bjorken and Drell (1964), Gastmans (1975), Gasiorowicz (1967), Feynman (1962), Itzykson and Zuber (1980), Jauch and Rohrlich (1976), Källén (1972), Lautrup (1975), Lee (1980), Lurie (1968), Mandl (1966), Ramond (1981), Sakurai (1967), and Scadron (1979). *Tests of QED*: Cheng and O'Neill (1979) and Perkins (1982). *QCD*: Aitchison and Hey (1982) and Field (1979).

### **Chapter 8**

Close (1979), Feynman (1972), Gilman (1972), Llewellyn Smith (1972), Perl (1974), and West (1975). *Nonrelativistic Form Factors*: Bethe and Jackiw (1968).

### **Chapter 9**

Close (1979), Feynman (1972), Leader and Predazzi (1982), Perl (1974), and Perkins (1982).

### **Chapters 10 and 11**

Aitchison and Hey (1982), Altarelli (1978, 1982), Collins and Martin (1984), Ellis and Sachrajda (1979), Field (1979), Kogut and Susskind (1973), Mess and Wiik (1983), Pennington (1983), Reya (1981), Söding and Wolf (1981), Wiik and Wolf (1979), and Wilczek (1982).

### **Chapter 12**

Bailin (1982), Bjorken and Drell (1964), Commins (1973), Feynman (1972), Gaillard and Maiani (1979), Gasiorowicz (1967), Harari (1978), Källén (1964), Maiani (1976), Marshak (1969), Muirhead (1965), Okun (1982), Perkins (1982), Pilkuhn (1979), and Steinberger (1976).

### **Chapter 13**

Bailin (1982), Bilenky and Hosek (1982), Gaillard and Maiani (1979), Ellis et al. (1982), Harari (1978), Hung and Sakurai (1981), Maiani (1976), and Weinberg (1974).

### **Chapter 14**

Abers and Lee (1973), Aitchison (1982), Aitchison and Hey (1982), Bailin (1982), Beg and Sirlin (1974), Bernstein (1974), Feynman (1977), Fritzsch and Minkowski (1981), Gaillard and Maiani (1979), Gastmans (1975), 't Hooft and Veltman

(1973), Iliopoulos (1976), Maiani (1976), Okun (1982), Politzer (1975), Ramond (1981), Taylor (1976), and Weinberg (1974).

### Chapter 15

Same as Chapters 13 and 14. Also Dolgov and Zeldovich (1981), Ellis (1982), Ellis and Salam in Mulvey (1981), Langacker (1981), Llewellyn Smith (1974), Steigman (1979), and Weinberg (1977).

**10202**

# References

- Abers, E., and Lee, B. W. (1973) "Gauge Theories." *Phys. Rep.* **9C**, 1.
- Aitchison, I. J. R. (1972) *Relativistic Quantum Mechanics*. Macmillan, London.
- Aitchison, I. J. R. (1982) *An Informal Introduction to Gauge Field Theories*. Cambridge University Press, Cambridge, England.
- Aitchison, I. J. R., and Hey, A. J. G. (1982) *Gauge Theories in Particle Physics*. Adam Hilger Ltd., Bristol.
- Altarelli, G. (1978) In *New Phenomena in Lepton-Hadron Physics*. NATO Advanced Study Series, Series B, Vol. 49. Plenum Press, New York.
- Altarelli, G. (1982) "Partons in Quantum Chromodynamics." *Phys. Rep.* **81C**, 1.
- Bailin, D. (1982) *Weak Interactions*. Adam Hilger Ltd., Bristol.
- Beg, M. A., and Sirlin, A. (1974) "Gauge Theories of Weak Interactions." *Ann. Rev. Nucl. Sci.* **24**, 379.
- Bernstein, J. (1974) "Spontaneous Symmetry Breaking, Gauge Theories and All That." *Rev. Mod. Phys.* **46**, 7.
- Bethe, H. A., and Jackiw, R. (1968) *Intermediate Quantum Mechanics*. Benjamin, Reading, Mass.
- Bethe, H. A., and Salpeter, E. E. (1957) *Quantum Mechanics of One and Two Electron Atoms*. Academic Press, New York.
- Bilenky, S. M., and Hosek, J. (1982) "Glashow-Weinberg-Salam Theory of Electroweak Interactions and the Neutral Currents." *Phys. Rep.* **90C**, 73.
- Bjorken, J. D., and Drell, S. D. (1964) *Relativistic Quantum Mechanics*. McGraw-Hill, New York.
- Bransden, B. H., Evans, D., and Major, J. V. (1973) *The Fundamental Particles*. Van Nostrand Reinhold, London.
- Byckling, E., and Kajantie, K. (1973) *Particle Kinematics*. Wiley, New York.
- Carruthers, P. (1966) *Introduction to Unitary Symmetries*. Wiley-Interscience, New York.
- Cheng, D. C., and O'Neill, G. K. (1979) *Elementary Particle Physics*. Addison Wesley, Reading, Mass.
- Close, F. E. (1979) *An Introduction to Quarks and Partons*. Academic Press, London.
- Collins, P. D. B., and Martin A. D. (1984) *Hadron Interactions*. Adam Hilger Ltd., Bristol.
- Commins, E. D. (1973) *Weak Interactions*. McGraw-Hill, New York.
- Dokshitzer, Y. L., Dyakonov, D. I., and Trojan, S. I. (1980) "Hard Processes in Quantum Chromodynamics." *Phys. Rep.* **58C**, 269.
- Dolgov, A. D., and Zeldovich, Ya. B. (1981) "Cosmology and Elementary Particles." *Rev. Mod. Phys.* **53**, 1.

- Ellis, J. (1982) "Grand Unified Theories in Cosmology." *Phil. Trans. Roy. Soc. London*, **A307**, 21.
- Ellis, J., Gaillard, M. K., Girardi, G., and Sorba, P. (1982) "Physics of Intermediate Vector Bosons." *Ann. Rev. Nucl. Particle Sci.* **32**, 443.
- Ellis, J., and Sachrajda, C. T. (1979) In *Quarks and Leptons*. NATO Advanced Study Series, Series B, *Physics*, Vol. 61. Plenum Press, New York.
- Fabjan, C. W., and Ludlam, T. (1982) "Calorimetry in High-Energy Physics." *Ann. Rev. Nucl. Particle Sci.* **32**, 335.
- Feynman, R. P. (1961) *The Theory of Fundamental Processes*. Benjamin, New York.
- Feynman, R. P. (1962) *Quantum Electrodynamics*. Benjamin, New York.
- Feynman, R. P. (1963) *The Feynman Lectures on Physics*. Addison Wesley, Reading, Mass.
- Feynman, R. P. (1972) *Photon-Hadron Interactions*. Benjamin, New York.
- Feynman, R. P. (1977) In *Weak and Electromagnetic Interactions at High Energies*. Les Houches Session 29. North-Holland, Amsterdam.
- Field, R. D. (1979) In *Quantum Flavordynamics, Quantum Chromodynamics and Unified Theories*. NATO Advanced Study Series, Series B, *Physics*, Vol. 54. Plenum Press, New York.
- Fritsch, H., and Minkowski, P. (1981) "Flavordynamics of Quarks and Leptons." *Phys. Rep.* **73C**, 67.
- Gaillard, M. K., and Maiani, L. (1979) In *Quarks and Leptons*. NATO Advanced Study Series, Series B, *Physics*, Vol. 61. Plenum Press, New York.
- Gasiorowicz, S. (1967) *Elementary Particle Physics*. Wiley, New York.
- Gastmans, R. (1975) In *Weak and Electromagnetic Interactions at High Energies*.
- NATO Advanced Study Series, Series B, *Physics*, Vol. 13a, Plenum Press, New York.
- Georgi, H. (1982) *Lie Algebras in Particle Physics*. Benjamin-Cummings, Reading, Mass.
- Gilman, F. J. (1972) "Photoproduction and Electroproduction." *Phys. Rep.* **4C**, 95.
- Goldstein, H. (1977) *Classical Mechanics*. Addison Wesley, Reading, Mass.
- Halliday, D., and Resnick, R. (1970) *Fundamentals of Physics*. Wiley, New York.
- Hamermesh, M. (1963) *Group Theory*. Addison Wesley, Reading, Mass.
- Harari, H. (1978) "Quarks and Leptons." *Phys. Rep.* **42C**, 235.
- Hung, P. Q., and Sakurai, J. J. (1981) "The Structure of Neutral Currents." *Ann. Rev. Nucl. Particle Sci.* **31**, 375.
- Iliopoulos, J. (1977) "An Introduction to Gauge Theories." Proceedings of the 1977 CERN School of Physics, CERN Report 77-18. CERN, Geneva.
- Itzykson, C., and Zuber, J. B. (1980) *Quantum Field Theory*. McGraw-Hill, New York.
- Jauch, J. M., and Rohrlich, F. (1976) *Theory of Photons and Electrons*. Springer-Verlag, Berlin.
- Källén, G. (1964) *Elementary Particle Physics*. Addison Wesley, Reading, Mass.
- Källén, G. (1972) *Quantum Electrodynamics*. Addison Wesley, Reading, Mass.
- Kim, J. E., Langacker, P., Levine, M., and Williams, H. H. (1981) "A Theoretical and Experimental Review of Neutral Currents." *Rev. Mod. Phys.* **53**, 211.

- Kleinknecht, K. (1982) "Particle Detectors." *Phys. Rep.* **84C**, 85.
- Kogut, J., and Susskind, L. (1973) "The Parton Picture of Elementary Particles." *Phys. Rep.* **8C**, 75.
- Langacker, P. (1981) "Grand Unified Theories and Proton Decay." *Phys. Rep.* **72C**, 185.
- Lautrup, B. (1975) In *Weak and Electromagnetic Interactions at High Energies*. NATO Advanced Study Series, Series B, *Physics*, Vol. 13a. Plenum Press, New York.
- Leader, E., and Predazzi, E. (1982) *Gauge Theories and the New Physics*. Cambridge University Press, Cambridge, England.
- Lee, T. D. (1980) *Particle Physics and Introduction to Field Theory*. Harwood Academic Publishers, Chur.
- Lipkin, H. (1966) *Lie Groups for Pedestrians*. North-Holland, Amsterdam.
- Lipkin, H. (1973) "Quark Models for Pedestrians." *Phys. Rep.* **18C**, 175.
- Llewellyn Smith, C. H. (1972) "Neutrino Interactions at Accelerators." *Phys. Rep.* **3C**, 261.
- Llewellyn Smith, C. H. (1974) In *Phenomenology of Particles at High Energy*. Academic Press, New York.
- Lurie, D. (1968) *Particles and Fields*. Wiley-Interscience, New York.
- Maiani, L. (1976) "An Elementary Introduction to Yang-Mills Theories and to their Applications to the Weak and Electromagnetic Interactions." Proceedings of the 1976 CERN School of Physics, CERN Report 76-20, CERN, Geneva.
- Mandl, F. (1966) *Introduction to Quantum Field Theory*. Wiley-Interscience, New York.
- Marshak, R. E., Riazuddin, and Ryan, C. P. (1969) *Theory of Weak Interactions in Particle Physics*. Wiley-Interscience, New York.
- Martin, A. D., and Spearman, T. D. (1970) *Elementary Particle Theory*. North-Holland, Amsterdam.
- Merzbacher, E. (1961) *Quantum Mechanics*. Wiley, New York.
- Mess, K. H., and Wiik, B. H. (1983) In *Gauge Theories in High Energy Physics*. Les Houches Summer School Proc., 37.
- Messiah, A. (1962) *Quantum Mechanics*. North-Holland, Amsterdam.
- Muirhead, H. (1965) *The Physics of Elementary Particles*. Pergamon, London.
- Mulvey, J. H. (1981) *The Nature of Matter*. Clarendon, Oxford.
- Okun, L. B. (1982) Leptons and Quarks. North-Holland, Amsterdam.
- Omnès, R. (1970) *Introduction to Particle Physics*. Wiley, New York.
- Pennington, M. R. (1983) "Cornerstones of QCD." *Rep. Prog. Phys.* **46**, 393.
- Perkins, D. H. (1982) *Introduction to High Energy Physics*. Addison Wesley, Reading, Mass.
- Perl, M. (1974) *High Energy Hadron Physics*. Wiley-Interscience, New York.
- Pilkuhn, H. (1967) *The Interactions of Hadrons*. North-Holland, Amsterdam.
- Pilkuhn, H. (1979) *Relativistic Particle Physics*. Springer-Verlag, New York.
- Politzer, H. D. (1974) "Quantum Chromodynamics." *Phys. Rep.* **14C**, 129.
- Ramond, P. (1981) *Field Theory, A Modern Primer*. Benjamin-Cummings, Reading, Mass.
- Reya, E. (1981) "Perturbative Quantum Chromodynamics." *Phys. Rep.* **69C**, 195.
- Rose, M. E. (1957) *Elementary Theory of Angular Momentum*. Wiley, New York.
- Rosner, J. (1974) "Classification and Decays of Resonant Particles." *Phys. Rep.* **11C**, 193.

- Sakurai, J. J. (1967) *Advanced Quantum Mechanics*. Addison Wesley, Reading, Mass.
- Scadron, M. D. (1979) *Advanced Quantum Theory*. Springer-Verlag, New York.
- Schiff, L. I. (1955) *Quantum Mechanics*. Third edition. McGraw-Hill, New York.
- Söding, P., and Wolf, G. (1981) "Experimental Evidence on QCD." *Ann. Rev. Nucl. Particle Sci.* **31**, 231.
- Steigman, G. (1979) "Cosmology Confronts Particle Physics." *Ann. Rev. Nucl. Sci.* **29**, 313.
- Steinberger, J. (1976) "Neutrino Interactions." Proceedings of the 1976 CERN School of Physics, CERN Report 76-20, CERN, Geneva.
- Taylor, J. C. (1976) *Gauge Theories of Weak Interactions*. Cambridge University Press, Cambridge, England.
- 't Hooft, G., and Veltman, M. (1973) "Diagrammar." CERN Report 73-9, CERN, Geneva.
- Weinberg, S. (1974) "Recent Progress in the Gauge Theories of the Weak, Electromagnetic and Strong Interactions." *Rev. Mod. Phys.* **46**, 255.
- Weinberg, S. (1977) *The First Three Minutes*. A. Deutsch and Fontana, London.
- West, G. B. (1975) "Electron Scattering from Atoms, Nuclei, Nucleons." *Phys. Rep.* **18C**, 264.
- Wiik, B. H., and Wolf, G. (1979) *Electron-Positron Interactions*. Springer Tracts in Modern Physics 86, Springer-Verlag, Berlin.
- Wilczek, F. (1982) "Quantum Chromodynamics: The Modern Theory of the Strong Interaction." *Ann. Rev. Nucl. Particle Sci.* **32**, 177.
- Wybourne, B. G. (1974) *Classical Groups for Physicists*. Wiley, New York.

# Index

Page numbers in **boldface** type refer to principle information.

- Abelian gauge symmetry, 316
- Accelerator, 28
- Acollinearity distribution, 242
- Adjoint equation, 102
- Adjoint spinor, 103
- Algebra, *see* Lie algebra
- Alpha:
  - $\alpha$  of QED, 12, 168
  - $\alpha_s$  of QCD, 15, 171
- Altarelli-Parisi equation, 215, 220
- Altarelli-Parisi functions, *see* Splitting functions
- Amplitude, *see* Invariant amplitude
- Angular momentum, 37
  - orbital, 37
  - spin, 105
  - total, 106
- Angular momentum operator, 37
- Anomalous magnetic moment, 161
  - of electron and muon, 162
  - interaction, 160
  - of nucleons, 55, 64, 176
- Anomaly, 285
- Anticommutation of  $\gamma$ -matrices, 102
- Antineutrino, 3, 114
- Antiparticle, 3, 70, 76
  - of Dirac particle, 107
  - isospin for, 42
  - as negative energy state, 77, 108
- Antiquark structure function, 198, 275
- Antiumitary operator, 41
- Associated production, 27, 44
- Asymmetry:
  - in  $e^+e^- \rightarrow \mu^+\mu^-$ , 305
  - of longitudinally polarized electrons, 309
- Asymptotic freedom, 12, 170, 346
- Axial vector, 112
- b quark, 27, 62, 286
- Background radiation, 352
- Bare charge, 164
- Baryon, 2, 4
  - masses, 65
  - number, 3
- number conservation, 23, 349, 353
- in quark model, 54, 63
- Baryon-to-photon ratio, 353
- $\beta$  decay, 252
  - Fermi constant of, 253, 264
  - Fermi theory of, 253
  - in nuclei, 258
  - V-A theory of, 252
- Bhabha scattering, 129
- Big Bang model, 352
- Bilinear covariants, 111
- Bjorken scaling, 188, 192
  - x-variable, 192
- Bohm-Aharonov effect, 317
- Boson, 2
- Breit frame, 177
- Breit-Wigner resonance, 50, 306
- Bremsstrahlung, 19
- Bubble chamber, 31
- Bunches, 30
- c quark, 27, 57, 280
- Cabibbo angle, 279
- Cabibbo-favored and -suppressed transitions, 281
- Callan-Gross relation, 196
- Calorimeter, 32
- Cascade decays, 286
- Casimir operator, 37
- Center-of-mass frame, 73
- Cerenkov light, 32

- Channel, 95  
 Charge:  
     color, 5  
     conservation of, 315, 334  
     definition of, 3  
     electromagnetic, 12, 85  
     quantization, 352  
     renormalization, 157  
     screening, 9, 11, 158, 163, 167, 347.  
     weak, 23, 255, 257  
 Charge conjugate spinors, 109, 288, 368  
 Charge conjugation, 41, 108, 288  
     invariance, 110  
 Charge-current density, 76, 103  
 Charged current interaction, 256, 298  
     in Cabibbo theory, 300  
     in electroweak theory, 332  
     neutrino-electron scattering, 267  
 Charged weak current, 255  
 Charge radius, 175  
     of nucleon, 179  
 Charge raising (lowering) weak current, 256, 293  
 Charm, 57, 282  
     quantum number, 58  
 Charmed:  
     baryons, 62  
     c quark, 27, 57, 280  
     mesons, 57, 59  
     particle decay, 59, 282  
     particle lifetime, 283  
 Charmonium, 59  
     potential, 61  
 Chirality, 116  
 Chiral representation, 115  
 Circular polarization, 135  
 Classical radius, 14  
 Clebsch-Gordan coefficients, 40  
 Cloud chamber, 31  
 Collider, 30, 308  
 Collinear divergence, 243  
 Color, 5  
     charge, 8  
     confinement of, 6, 19  
     factor, 67, 211  
     screening, 9, 168  
     singlet, 5, 53, 67  
     SU(3) of, 43, 317  
 Colored quarks, 5  
 Color multiplets, 5  
     of gluons, 43, 317  
     of quarks, 43, 317  
 Completeness relation:  
     for Dirac spinors, 111, 361  
     for polarization vectors, 135, 139, 185  
 Compton scattering, 141  
     for massive photon, 144, 213  
     QCD analogue of, 210  
 Compton wavelength, 14  
 Confinement, 6, 19  
 Conservation:  
     of angular momentum, 37  
     of baryon number, 23, 349, 353  
     of charge, 315  
     of lepton number, 3, 4, 251  
 Conservation law, 37, 41, 314  
 Conserved current:  
     for Dirac particles, 102  
     for spinless particles, 74  
 Conserved quantum number, 4, 37, 41, 315  
 Conserved vector current hypothesis, 258  
 Constants of motion, 37  
 Constituent quark, 64  
 Contact term, 319  
 Continuity equation, 71, 74, 103  
 Cosmology, 352  
 Cosmic rays, 30  
 Coulomb gauge, 134  
 Coulomb potential, 158  
 Counting rules, 200, 368  
 Coupling:  
     electromagnetic, 12, 84, 117, 168  
     first introduction of, 15  
     quark-gluon, 15, 171, 320  
     running, 9, 169, 347  
     strong, 16, 169  
     three gluons, 320  
     weak, 23, 253, 296, 333  
 Covariance, 73  
 Covariant (contravariant), 73  
 Covariant derivative, 316  
     for  $SU(2) \times U(1)$ , 316, 328  
     for  $SU(3)$ , 318  
 Covariant parton model, 193  
 Covariant scalar product, 73  
 CP, 255, 287  
     eigenstates, 290  
     transformation, 41, 255, 288  
     violation, 287, 289, 353  
 Crossed channel, 95  
 Crossing, 93  
     examples of, 124, 129, 145, 269  
 Cross section, 89, 90  
     for Compton scattering, 141, 144, 213  
     for deep inelastic scattering, 182  
     for Drell-Yan process, 249  
     for  $e^+ e^- \rightarrow e^+ e^-$ , 129

- for  $e^+ e^- \rightarrow \mu^+ \mu^-$ , 125, 307  
 for  $e^+ e^- \rightarrow q\bar{q}$ , 228  
 for  $e^+ e^- \rightarrow q\bar{q}g$ , 237, 239  
 for  $e^+ e^- \rightarrow Z \rightarrow q\bar{q}$ , 308  
 for electron-proton scattering, 177, 183  
 for electron-quark scattering, 129  
 for  $e^- \mu^+ \rightarrow e^- \mu^+$ , 123  
 for  $\gamma^* g \rightarrow q\bar{q}$ , 219  
 for  $\gamma^* q \rightarrow qg$ , 213  
 general formula for, 91  
 for neutrino-electron scattering, 268, 302, 342  
 for neutrino-quark scattering, 271, 273  
 for pair annihilation, 145  
 for quark-anti-quark scattering, 129  
 for scattering of spinless particles, 91  
 for virtual photon-proton scattering, 184, 208
- Cross section summary, 129, 183
- Current, *see* Electromagnetic current; Weak current
- Current conservation, 75, 103
- Current-current interaction, 87, 119, 252, 256, 277, 281, 298
- Cyclotron, 28
- D'Alembertian operator, 74
- Decay rate, 92
  - for  $\beta$  decay, 260
  - for D-mesons, 59, 283
  - general formula for, 92, 301, 373
  - for K-mesons, 267, 290
  - for  $K \rightarrow \mu\mu$ , 280, 282
  - for  $K \rightarrow \mu\nu, \bar{\nu}\mu$ , 267, 280
  - for  $K^+ \rightarrow \pi^+ e^+ e^-$ , 276
  - for  $K \rightarrow \pi^0 \bar{\nu}\nu$ , 276, 280, 283
  - for  $\mu$  decay, 263
  - for  $\pi$  decay, 266
  - for  $\pi \rightarrow \mu\nu, \bar{\nu}\mu$ , 251, 255, 264, 266, 280
  - for  $\pi \rightarrow \pi^0 \bar{\nu}\nu$ , 272, 280
  - proton, 351
  - for  $\tau$  meson, 264
  - for W, Z bosons, 301, 373
- Decuplet representation, 51
- Deep inelastic scattering, 17, 172, 179
  - cross section, 182
  - kinematics, 181
  - lepton scattering, 17, 172, 179
  - neutrino scattering, 273
  - structure functions, 181
- Delta ( $\Delta$ ) resonance, 4, 22, 53, 66
- Density of states, 80, 89
- “Desert” of grand unified theories, 354
- Detector, 30
- Differential cross section, 90, 91
- Dipole magnet, 29
- Dirac equation, 100
  - adjoint, 102
  - charge conjugate, 108
  - Lorentz covariance of, 102, 112
  - nonrelativistic limit of, 106
  - plane-wave solutions of, 104
- Dirac matrices, 102, 111
- Dirac moment, 107
- Dirac-Pauli representation, 101, 111
- Dirac sea, 76
- Dirac spinors, 104
- Direct photons, 247
- Divergences, 156, 321, 342
  - collinear, 243
  - infrared, 171, 243
- $d^i$  matrices, *see* Rotation matrices  $d^i(\theta)$
- D-meson, 58
  - decays, 59, 283
- Down quark, 3
- Drell-Yan process, 247
- Drift chamber, 31
- Early universe, 352
- Electric form factor, 172, 175, 177, 210
- Electrodynamics:
  - for spinless particles, 84
  - for spin 1/2 particles, 117
- Electromagnetic coupling, 12, 168
  - minimal substitution for, 84, 316
- Electromagnetic current, 76, 103
  - conservation, 75, 315
  - for Dirac particle, 103
  - Gordon decomposition of, 118
  - for spinless particle, 74
- Electromagnetic decays, *see* Radiative decays
- Electromagnetic field, 84, 133
  - as gauge field, 316
- Electromagnetic force, 1
- Electromagnetic interaction, 84, 103, 316
- Electromagnetic potential, 84
- Electron, 3
  - magnetic moment, 107, 162
  - number conservation, 3, 4, 251
  - propagator, 136, 146
  - spectrum in  $\beta$  decay, 260
  - spinor, 101
- Electron-muon scattering, 123
  - for spinless particles, 86
- Electron-positron annihilation, 18, 226
  - into hadrons, 226, 228
  - heavy quark production in, 226, 234
  - into jets, 19, 230, 234, 240

- Electron-positron annihilation (*Continued*)  
 into muon pairs, 125, 226, 307  
 parton model of, 226, 230  
 R factor and color, 228, 243
- Electron-positron collider, 18, 226, 308
- Electron scattering, 119, 129  
 deep inelastic, 172, 179, 181  
 by external potential, 152, 173  
 off muons, 123  
 off neutrinos, 267, 302, 342  
 off protons, 175  
 off quarks, 129, 310
- Electroweak interaction, 292, 296, 331
- Electroweak interference:  
 in atomic transitions, 308  
 in  $e^+ e^- \rightarrow \mu^+ \mu^-$ , 305  
 in electron scattering, 308
- Emulsion, 31
- Energy-momentum sum rule, 202
- Equivalent photon approximation, 225
- Eta ( $\eta$ ) meson, 48  
 charmed ( $\eta_c$ ), 59, 61  
 quark content of, 48
- Euler-Lagrange equation, 312
- Evolution equation, 217, 220
- Exchange force, 7
- External line, 149
- Family, 27, 349. *See also* Generation
- Fermi constant G, 253, 264  
 relation to weak boson coupling, 257, 298
- Fermi's Golden Rule, 80
- Fermi statistics, 5
- Fermi theory, 253
- Fermion, 2
- Feynman diagram, 8, 87, 149
- Feynman gauge, 138
- Feynman propagator, 138
- Feynman rules:  
 for electroweak interactions, 299  
 introduction of, 8, 88  
 from Lagrangian, 313  
 for loops, 149, 155  
 for QCD, 211, 320  
 for spinless particles, 88, 150  
 table for QED, 149
- Feynman-Stückelberg interpretation, 77, 82
- Field strength, 102, 133, 317, 319, 375
- Field theory, 313
- Fierz reordering, 303
- Fine structure constant, 13
- Finite group, 41
- Flash chamber, 31
- Flavor, 24
- Flux, 71, 89, 91
- Flux factor, 89  
 of virtual photon, 185, 213
- F-meson, 59, 283
- Form factors, 172  
 $F_1$  and  $F_2$ , 176  
 Fourier transform of, 173  
 $G_E$  and  $G_M$ , 177, 372  
 of neutron, 176  
 of proton, 175  
 $W_1$  and  $W_2$ , 181
- Four fermion interaction, 253
- Four-momentum, 72  
 transfer, 87, 119, 173
- Four-vector, 72  
 current, 75, 76, 103  
 potential, 84, 133
- Fragmentation function, 230
- Free-particle spinor, 104
- Fundamental representation, 39
- G, *see* Fermi constant G
- Gamma matrices, 102  
 anticommutation relations, 102  
 and charge conjugation, 109, 288, 361  
 $\gamma_5$ -matrix, 111, 114  
 properties, 123  
 standard representation, 101, 111  
 trace theorems, 123, 261  
 Weyl representation, 101
- Gauge, 311  
 boson, 3, 316, 350  
 field, 316, 318, 328  
 transformation, 133, 314, 316, 317, 328, 332
- Gauge symmetry, 315  
 breaking, 321, 324, 327  
 global, 315  
 hidden, 321  
 local, 316  
 nonAbelian, 317
- Gauge theory, 311  
 electroweak, 332  
 grand unified, 344  
 QCD, 317  
 QED, 316
- Geiger counter, 31
- Gell-Mann matrices, 43, 356, 375
- Gell-Mann-Nishijima scheme, 44
- Generation, 349
- Generator, 37, 43
- g factors, 107, 161

- Ghost particles, 170  
GIM mechanism, 57, 282  
Global gauge symmetry, 315  
Gluons, 3, 8, 202  
    bremsstrahlung of, 205, 210, 237  
    color octet of, 8, 67  
    constituents of proton, 202  
    coupling to quarks, 205, 320  
    emission of, 206, 210, 237  
    jets of, 206, 214, 241  
    self interaction of, 205, 320, 375  
Golden Rule, 80  
Goldstone boson, 325  
Goldstone theorem, 325  
Gordon decomposition, 118  
Grand unification, 344  
    scale, 345, 348  
Gravity, 27, 348  
Green's function, 145  
Group theory, 35  
Gyromagnetic ratio, *see* g factors
- Hadrons:  
    definition of, 2  
    masses of, 63  
    quark model of, 45  
    structure of, 172  
    weak current of, 252, 272  
Heaviside-Lorentz units, 133  
Heavy quark, 27, 57, 285  
    production in  $e^+e^-$  annihilation, 234  
    *see also* b quark; c quark; Top quark
- Helicity, 106  
    eigenspinor, 106, 361  
    of electrons, 126  
    in leptonic decays, 264, 267, 372  
    in lepton scattering, 128  
    of neutrinos, 114  
    of photons, 132, 134  
    in V-A theory, 255
- Helicity conservation, 126, 270
- Helium abundance, 353
- Hermitian operator, 36
- Hidden symmetry, 321, 323
- Higgs bosons, 327, 334, 340
- Higgs doublet, 334
- Higgs mechanism, 326, 329
- Higher order corrections, 126, 154, 206
- Hole theory, 76
- Hypercharge, 46, 58. *See also* Weak hypercharge
- Hyperfine splitting in QCD, 65
- Hyperons:  
    discovery of, 26, 44, 53
- magnetic moments of, 64  
masses of, 66
- Ideal mixing, 49
- Identical fermions, 149
- Impulse approximation, 193, 245
- Incoherent scattering, 193, 245
- Inelastic scattering:  
    deep, 17, 172, 179  
    of longitudinally polarized electrons, 309
- Infinite momentum frame, 193
- Infrared divergence, 171, 243
- Infrared slavery, 19
- Instantaneous Coulomb interaction, 141
- Interaction vertex, 25, 82. *See also* Vertex factor
- Intermediate vector bosons, *see* Weak bosons (W and Z)
- Internal line, 149
- Intrinsic angular momentum, *see* Spin
- Intrinsic parity, *see* Parity
- Invariant amplitude, 87  
    cross section in terms of, 90  
    decay rate in terms of, 92
- Invariant variables, 94
- Irreducible representation, 38
- Isospin, 33  
    conservation of, 33  
    invariance of nuclear forces, 34  
    matrices, 42  
    multiplets, 42, 47  
    in 2-nucleon systems, 33  
    weak, *see* Weak isospin
- Jets:  
    definition of, 19, 214, 242  
    in electron-positron collisions, 19, 230, 234, 240  
    gluon, 205, 213, 241  
    quark, 19, 230
- $K_L$ ,  $K_S$  mesons, *see* Neutral kaons
- Kaluza-Klein theory, 354
- Kinematics:  
    of deep inelastic scattering, 181  
    invariant, 94  
    laboratory frame, 130
- Kinoshita, Lee, Nauenberg theorem, 244
- Klein-Gordon equation, 74
- $K$ -meson, 27  
    decays, 252, 276, 280  
    decay constant  $f_K$ , 267  
    neutral, *see* Neutral kaons

## 390 Index

- K-meson (*Continued*)  
  quark content of, 48  
  *see also* Decay rate  
Kobayashi-Maskawa matrix, 286  
Kurie plot, 260
- Laboratory frame, 73  
  kinematics, 130
- Lagrangian, 311  
  for Dirac equation, 312, 374  
  for Klein-Gordon equation, 312  
  for Maxwell equations, 312, 374  
  for QCD, 319  
  for QED, 317  
  for Weinberg-Salam model, 341
- Lambda ( $\Lambda$ ) hyperon, 44, 53, 64  
  charmed, 63, 66  
  magnetic moment of, 64  
  quark content of, 53
- $\lambda$ -matrices for SU(3), 43, 318, 356, 375
- Lambda ( $\Lambda$ ) of QCD, 170
- Lamb shift, 158
- Large transverse momentum, 18, 214, 246  
  in deep inelastic scattering, 207, 214, 246  
  in  $e^-e^+$  annihilation, 240, 242, 247  
  in  $\gamma\gamma$  collisions, 247  
  in hadronic interaction, 18, 246  
  in photoproduction, 246
- Left-handed states, 114  
  neutrinos, 115
- Leptonic decay:  
  non-, 252  
  semi-, 252  
  of vector mesons, 61
- Leptons:  
  definition of, 2, 3  
  families, 27, 349  
  number, 3, 4, 251  
  pair production of, 248  
  table of, 27  
  weak current of, 255, 293
- Lepton tensor, 122
- Leptoproduction of hadrons, 233, 243
- Leptoquark, 350
- Lie algebra, 37
- Lie group, 35. *See also* SU entries
- Lifetime, 50, 92, 251
- Linear accelerator, 28
- Local gauge symmetry, 316
- Longitudinal photon, 140, 186
- Loop, 154  
  diagrams, 155, 244  
  momenta, 149, 155
- Lorentz condition, 133
- Lorentz covariance, 72
- Lorentz invariant phase space (LIPS), 91
- Lorentz transformation, 35, 72  
  and Dirac's equation, 112
- Majorana neutrinos, 116
- Magnetic dipole transition, 57
- Magnetic form factor, 177
- Magnetic moment, 107, 119  
  anomalous, 161  
  of baryons, 55, 64, 176  
  of Dirac particles, 107, 162  
  interaction, 119, 132  
  operator, 55, 107  
  of quarks, 55, 64
- Mandelstam plot, 95
- Mandelstam variables, 94
- Mass:  
  of fermions, 334, 338  
  of gauge bosons, 335  
  of hadrons in quark model, 63
- Mass generation, 323, 326, 334, 338
- Massive gauge bosons, 24, 257, 320, 327, 336
- Massive neutrinos, 116
- Mass matrix, 336
- Mass-shell, 73, 88
- Matter-antimatter asymmetry, 353
- Maxwell's equations, 132  
  covariant form of, 132  
  and gauge invariance, 133  
  and Lagrangian formalism, 312, 374
- Mean square radius, 175, 179
- Mesons:  
  color singlets, 4, 6  
  definition of, 2  
  masses of, 65  
  pseudoscalar, 48  
  in quark model, 46, 48, 59  
  tensor, 49  
  vector, 49
- Metric tensor, 73
- Minimal substitution, 84, 316
- Missing momentum, 203
- Mixed symmetry state, 51
- Mixing:  
  Cabibbo, 279, 283  
  ideal, 49  
  Kobayashi-Maskawa, 283, 286  
  of neutral kaons, 290, 291  
  octet-singlet, 49  
  of photon and Z boson, 296  
  Möller scattering, 119, 129